Multinuclear complexes with 2,6-dipicolinoylbis(*N,N*-dialkylthioureas)

Department of Biology, Chemistry and Pharmacy
Freie Universität Berlin
PhD Dissertation

Jecob Jegathesh Jesudas
Berlin, June 2013

1. Supervisor: Prof. Dr. Ulrich Abram

2. Supervisor: Prof. Dr. Christian Müller

Date of defense: 26-07-2013.

Acknowledgment

I would like to express my sincere gratitude to my supervisor, Prof. Dr. Ulrich Abram, for his guidance, encouragement and continuous support throughout the course of this work.

Special thanks to Prof. Dr. Christian Müller for being my second supervisor.

My sincere appreciation is extended to Dr. Adelheid Hagenbach for her constructive crystallographic discussions and X-ray measurements. I wish to thank Dr. Nguyen Hung Huy and Dr. Axel Rodenstein for their support and advice at the beginning of my research. I express my thanks to Prof. Dr. Victor M. Deflon and his working group for their help and support throughout my stay in Sao Carlos, Brazil. I would like to thank Prof. Dr. Reinhard Kirmse for the magnetic susceptibility measurements and Prof. Dr. Robert Bittl for the measurement of W-band EPR spectra.

I am very grateful for the friendship of my colleagues in the working group of Prof. Abram, Jacqueline Grewe, Detlef Wille, Juan C. Gomez, Philip Schweighöfer, Christelle Noufele, Lars Kirsten, Samundeeswari M. Balasekaran, Pham Thang, Janine Ackermann, and my Brazilian colleagues Pedro I. da S. Maia, Andre G. de A. Fernandes, Sailer S. dos Santos, Rafaela Pesci, Barbara Tirloni, Vania D. Schwade, Murilo Carroccia, Melina de A. Mello, Roberta Cargnelutti, and all the former members of the working group with whom I enjoyed the wonderful, unforgettable and friendly working environment during the 4-year period.

I gratefully acknowledge the scholarship of the Center of Supramolecular Interactions (CSI) for part of my research project. I would also like to thank the Institute of Chemistry and Biochemistry of the Freie Universität Berlin, the analytical services and particularly Mrs. Doris Plewinsky for the elemental analyses. I would like to thank my project students, Aref Takiden, Dominik Wessels, Hendrik Reuter and Kai Sonderhof for their enthusiasm and hard work.

I would like to express my appreciation to my wife, Vinotha Judy Thambipillai. Her love, support and patience are the greatest encouragement. Lots of kisses and hugs to my little son Asthigan Antony Jesudas, with whom I enjoy the evenings after the stressful working days. My thanks are extended to all my relatives and friends for their help and support all the time.

Finally, this work is dedicated to my loving parents, Antony Wilfred Jesudas and Mary Antonita Jesudas, whose unconditional love, encouragement and support have been the source of inspiration to achieve every goal in my life.

Table of contents

Abbreviations

Bu	Butyl
Calcd.	Calculated
d	Doublet
Et	Ethyl
IR	Infrared
m	Medium
Me	Methyl
MS	Mass Spectrometry
NBu_4	Tetrabutylammonium
NEt_3	Triethylamine
NMR	Nuclear Magnetic Resonance
Ph	Phenyl
s	Singlet
st	Strong
t	Triplet
temp.	Temperature
THF	Tetrahydrofuran
w	Weak

Abstract

This thesis contains synthesis and structural characterization of new classes of multinuclear complexes with pentadentate 2,6-dipicolinoylbis(*N,N*-dialkylthioureas). Three types of complexes regarding to the metal combinations were synthesized: (1) Trinuclear $[M^{II}Ln^{III}M^{II}]$ systems with lanthanide (Ln^{3+}) and transition metal (M^{2+}) ions, (2) Trinuclear $[(Mb)^{II}(Ma)^{II}(Mb)^{II}]$ systems with alkaline earth metal (Ma^{2+}) and transition metal (Mb^{2+}) ions and (3) Bi- and tetranuclear oxidorhenium(V) complexes with additional guest metal cations ($M1^{+}$), where M1 = K^{+}, Rb^{+}, Cs^{+} or Tl^{+}.

Introduction

Introduction

The coordination chemistry of *N,N*-dialkyl-*N*'-benzoylthioureas (**1**) with transition metals has constantly been studied during the last decades.[1-7] They are versatile ligands and show different kinds of coordination modes with a considerable number of transition metals. They are able to coordinate as either *O,S*-bidentate (**2**, **3**) or *S*-monodentate (**4**, **5**) ligands. In addition to that, the possibility of deprotonation allows them to act as either monoanionic (**2**, **4**) or neutral (**3**, **5**) ligands. *N*-benzoylthioureas are good chelating ligands for transition metal ions and are found to be effective extractants for liquid-liquid extraction of transition metal ions.[3, 8]

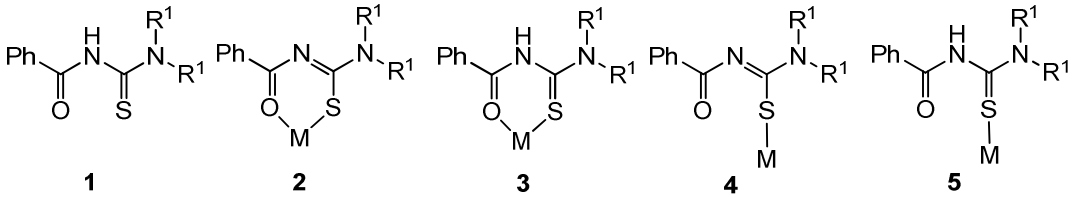

1 **2** **3** **4** **5**

R^1 = Me, Et, Pr, iPr R^1-R^1 = -$(CH_2)_5$-, -$(CH_2)_4$-, -$(CH_2)_2$-O-$(CH_2)_2$-

Most of the structurally characterized mononuclear complexes show a bidentate *O,S*-monoanionic coordination of the ligand.[9-12] Moreover, *cis* square-planar geometry (**6**) is observed in the complexes of Ni^{2+}, Pd^{2+}, Pt^{2+}, Cu^{2+}, Zn^{2+} and Cd^{2+}.[13-17] Complexes with facial octahedral coordination (**7**) are reported with Co^{3+}, Tc^{3+}, Ru^{3+} and Rh^{3+}.[18-21] However, monodentate and neutral coordination of the ligand via the sulfur donor atom (**5**) was also reported for Pt^{2+}, Au^{+} and Ag^{+}.[22-24]

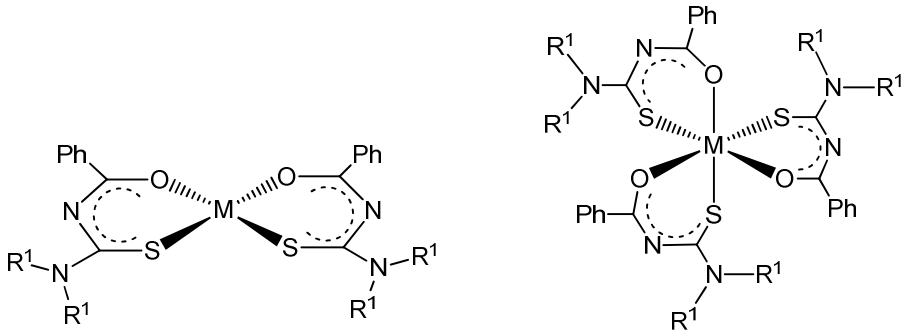

6 **7**

R^1 = Et, Pr or Ph

Coordination mode of the ligand, coordination number of the metal, coordination geometry and overall charge of the complexes depend mostly on the transition metal applied.

A significant number of bi- and trinuclear transition metal complexes with extended tetraalkyl isophthaloylbis(thioureas) (**8**) have also been synthesized and structurally characterized. Binuclear bis-chelates (**9**) have been published with Cu^{2+}, Ni^{2+}, Zn^{2+}, Co^{2+}, Cd^{2+}, Pt^{2+} and Pd^{2+} metal ions.[25-31] In addition to that, a binuclear tris-chelate exists with In^{3+}.[32] Moreover, trinuclear complexes (**10**) are also reported with the related terephthaloyl derivative.[25, 27-28, 33]

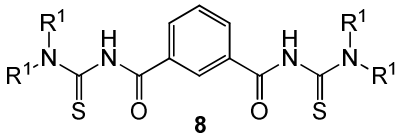

8

R^1 = Et, iBu, nBu

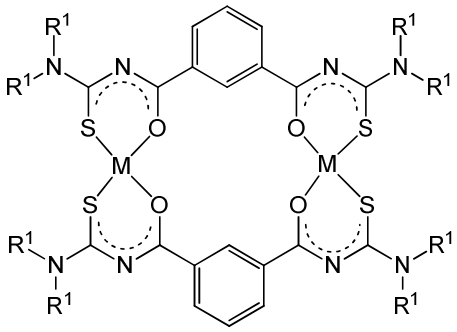

9

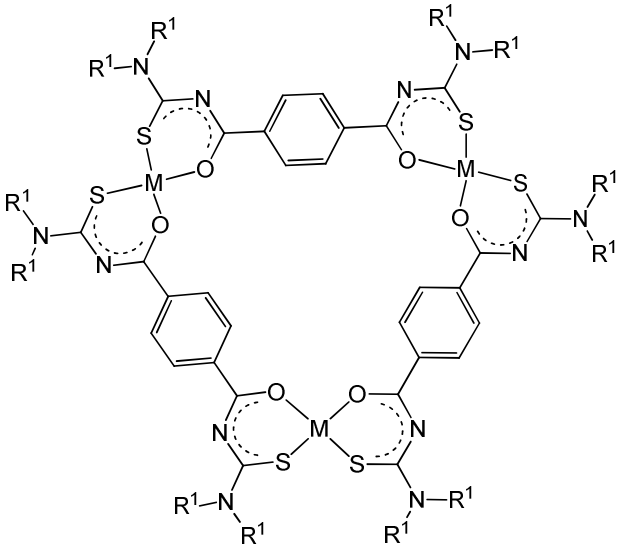

10

N,N-Dialkyl-*N*'-benzoylthioureas are known to be efficient ligand systems in rhenium and technetium complexes with the metals in different oxidation states. ^{99m}Tc, ^{186}Re and ^{188}Re are important radionuclides and have almost perfect physical properties for the application in nuclear medicine.[34-36] Coordination chemistry of rhenium and technetium with thioureas has repeatedly been investigated due to the continuous need of efficient ligand systems for the application in radiopharmacy.[37-39] Particularly, stable oxidorhenium(V) and oxidotechnetium(V) complexes with *N,N*-dialkyl-*N*'-aroylthioureas have successfully been

synthesized and structurally characterized (**10, 11**).[21, 40-41] The methoxido oxidorhenium(V) (**11**) complexes undergo dimerization under formation of oxo-bridges.

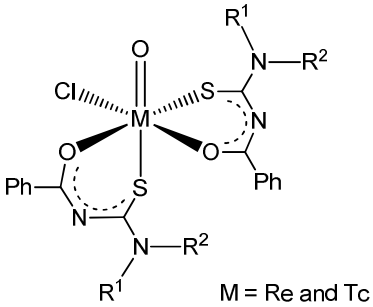

M = Re and Tc

10

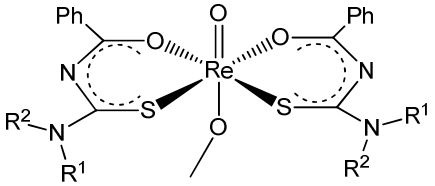

11

$R^1 = R^2$ = Et or Ph and R^1 = Me, R^2 = Ph

Introduction of a nitrogen donor to the bidentate ligand (**8**) produces a new class of ligand (**12**),[11] which could favor the coordination of an additional metal ion to the *O,N,O* moiety. Despite the early introduction of the multidentate ligand (**12**) (R^1 = Et) with an Ag^+ polymeric complex in the year 2000[42], there are no other metal complexes reported until now. Due to the presence of hard (*N, O*) and soft (*S*) donor atoms in the ligand, coordination of different combinations of metal ions is possible.

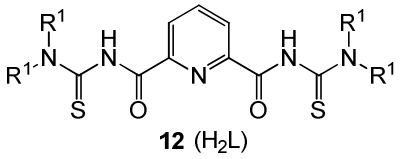

12 (H_2L)

R^1 = Et or R^1-R^1 = -$(CH_2)_2$-O-$(CH_2)_2$-

This thesis introduces three types of novel mixed metal complexes with 2,6-dipicolinoylbis(*N,N*-dialkylthioureas) (H_2L) (**12**).

1) Trinuclear, transition metal – lanthanide complexes of the type $M^{II}Ln^{III}M^{II}$ (where M = Co, Ni, Mn, Cu or Zn and Ln = Ce, Nd, Sm, Gd, Dy, Er or Yb).
2) Trinuclear, transition metal - alkaline earth metal complexes of the type $Ma^{II}Mb^{II}Ma^{II}$ (where Ma = Mn, Co or Ni and Mb = Ba, Sr or Ca).
3) Bi- and tetranuclear oxidorhenium(V) complexes with a guest metal ion M^1 (where M^1 = K, Rb, Cs or Tl).

Syntheses of such mixed-metal complexes are necessary to understand and analyze intermolecular and intramolecular metal-metal interactions. Complexes of the type $M^{II}Ln^{III}M^{II}$

might be used to study magnetic interactions between metals in a 3d-4f-3d system. Due to the high number of unpaired electrons and extremely complicated magnetic behavior of Ln^{III} metal ions, studies of magnetic interactions between the metal ions in such complexes is not an easy task. Several complexes containing 3d-4f-3d systems with various organic ligands have been synthesis in order to analyze the magnetic interactions between metals.[43-46]

Linear trinuclear complexes of the type $Mb^{II}Ma^{II}Mb^{II}$ (where Ma = Ba, Sr or Ca and Mb = Mn, Co or Ni) with a multidentate organic ligand are new to the coordination chemistry of these metal ions. Even binuclear mixed-metal complexes with transition metal ions and alkaline earth metal ions are not well known.[47] However, the role of such mixed metal complexes as catalyst in biological systems is a research field of permanent interest. The important role of the Mn_4Ca clusters in the oxidation of water during the photosynthesis has repeatedly been investigated.[48-50] A structural model of the oxygen evolving Mn_4Ca cluster has been presented having Mn-Ca distances of 3.4 Å.[51] Synthetic and structural studies of such mixed-metal complexes might contribute to a better understanding of the catalytic processes in our biological systems. In addition to that, such multinuclear complexes could also be applied as building blocks for supramolecular assemblies in order to study intermolecular metal-metal interactions.[52]

The third type of complexes has been studied exclusively with oxidorhenium(V) cores. A similar type of bi- and tetranuclear oxidorhenium(V) complexes with tetraalkylisophthaloylbis(thiourea) (**8**) ligands has recently been reported.[53] Dimerization of the binuclear oxidorhenium(V) complexes via the formation of oxo bridges between oxidorhenium(V) moieties leads to tetranuclear oxidorhenium(V) complexes. The reported tetranuclear oxidorhenium(V) cage possesses a big cavity in its center with a diameter of around 6.5 Å. The similar cage formation with 2,6-dipicolinoylbis(*N,N*-dialkylthioureas) (**12**) favor the capture of metal cations, such as K^+, Rb^+, Cs^+ or Tl^+, in the corresponding void. The presence of additional *N* donor atoms from the pyridine rings increases the stability of the captured metal cations. The coordination chemistry and the host-guest chemistry of the tetranuclear oxidorhenium(V) cage complexes with the above metal cations are reported in this thesis. Interestingly, a metal-metal exchange inside the cage is observed. This exchange depends on the size of the metal cation, in a way that the bigger cations are more stable inside the cage than smaller ones and shows a stability of the host-guest compounds in the order $Cs^+ > Rb^+ = Tl^+ > K^+$.

Chapter 1

2,6-Dipicolinoylbis(*N,N*-dialkylthioureas)

2,6-Dipicolinoylbis(*N,N*-dialkylthioureas)

Thiourea derivatives such as benzoylthioureas (**1**) or isophthaloylbis(thioureas) (**8**) are synthesized from benzoyl chloride or isophthaloyl dichloride, NH_4SCN and appropriate amines (Scheme 1.1).[3] However, a pre-synthesis of appropriate *N,N*-dialkylthioureas is recommended for the synthesis of 2,6-dipicolinoylbis(*N,N*-dialkylthioureas) (H_2L).[42] The general method using NH_4SCN and appropriate amines gives low yields with pyridine-2,6-dicarbonyl dichloride, while the pre-synthesis of thioureas and a following coupling reactions with pyridine-2,6-dicarbonyl dichloride increases the yields significantly.

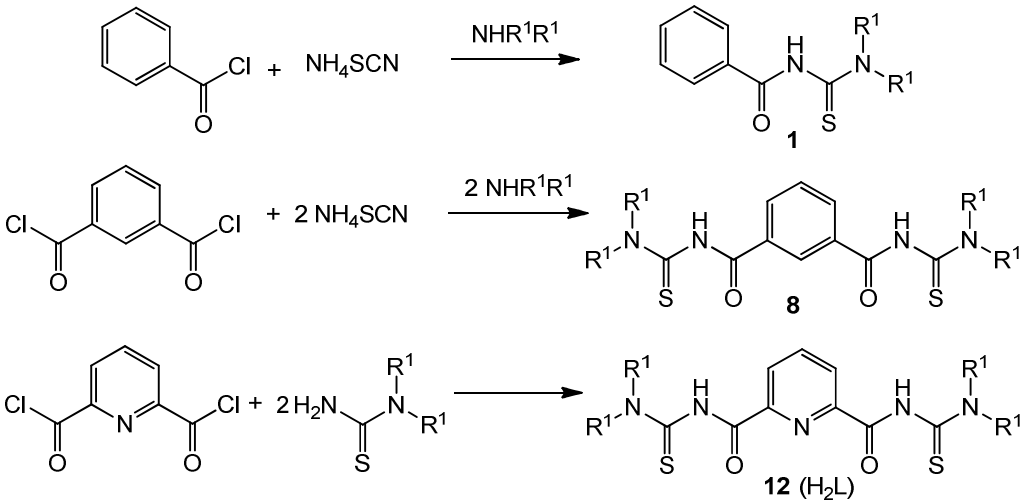

Scheme 1.1 Synthesis of benzoylthioureas (**1**), isophthaloylbis(thioureas) (**8**) and 2,6-dipicolinoylbis (*N,N*-dialkylthioureas) (H_2L).

1.1 Synthesis of *N,N*-dialkylthioureas

The synthesis of asymmetric thioureas was first reported by *Hartmann* et al. starting from ethyl chloroformate, KSCN and secondary amines via formation of *N,N*-dialkyl-*N*'-ethoxycarbonate thioureas (**13**) (Scheme 1.2).[54] From this procedure, the *N,N*-dialkylthioureas (**14**) can be obtained as colorless crystalline products in 55 – 60 % yields. IR spectra of thioureas show a combination of stretching vibrations of C=S and C-N moieties at 1627, 1517 and 1359 cm^{-1}, and two NH_2 stretching vibrations at 3375 and 3298 cm^{-1}. The ^1H NMR spectra show broad singlets at 5.85 ppm for the *N,N*-diethylthiourea (**14a**) and at 5.78 ppm for the *N*-morpholinethiourea (**14b**), which can be assigned to the NH_2 group. The aliphatic protons of *N,N*-diethylthiourea (**14a**) appear at 1.19 ppm and 3.65 ppm. A broad multiplet at 3.74 ppm in the spectrum of *N*-morpholinethiourea (**14b**) can be assigned to the methylene protons of morpholine ring.

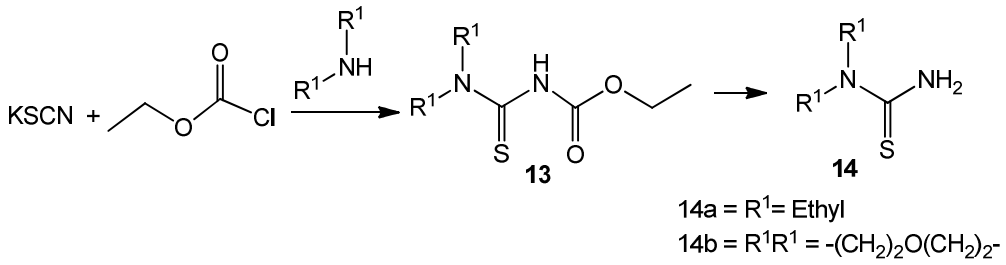

Scheme 1.2 Synthesis of *N,N*-dialkylthioureas (**16**).[54]

1.2 Synthesis of 2,6-dipicolinoylbis(*N,N*-dialkylthioureas)

The synthesis of 2,6-dipicolinoylbis(*N,N*-dialkylthioureas) was slightly modified from a previously reported synthesis.[42] A considerable increase in the yield to 90-95% can be obtained when the reaction is carried out in THF, instead of in acetone. Coupling reactions of *N,N*-dialkylthioureas (**14**) with pyridine-2,6-dicarbonyl dichloride in dry THF in the presence of an excess of triethylamine give the multidentate 2,6-dipicolinoylbis(thiourea) ligands H_2L^a and H_2L^b (Scheme 1.3). The pale yellow products are readily soluble in CH_2Cl_2 and $CHCl_3$ and partially soluble in MeOH and acetone. The crude products could be purified by recrystallization from a solvent mixture of CH_2Cl_2/EtOH (2:1). Weak IR absorptions at 3273 cm^{-1} for H_2L^a and at 3360 cm^{-1} for H_2L^b can be assigned to the stretching vibration of the NH group and intense IR absorptions at 1687 cm^{-1} for H_2L^a and at 1711 cm^{-1} for H_2L^b are due to the stretching vibration of the C=O groups.

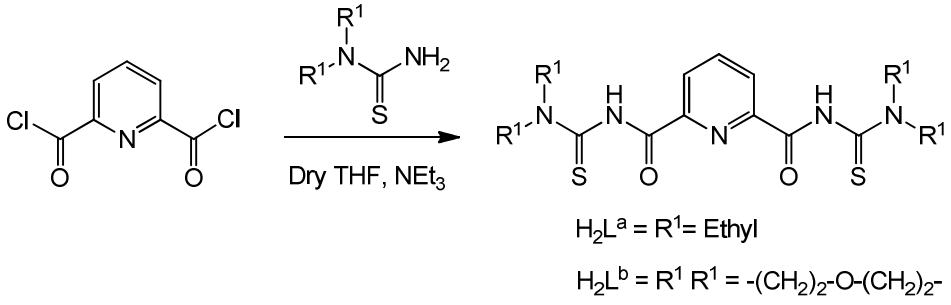

Scheme 1.3 Synthesis of 2,6-dipicolinoylbis(*N,N*-dialkylthioureas) H_2L^a and H_2L^b

^{1}H NMR spectra show sharp singlets at 9.91 ppm for H_2L^a and at 10.10 ppm for H_2L^b, which are assigned to NH protons. Moreover, in the case of H_2L^a, a broad signal at 1.33 ppm instead of a well resolved triplet can be assigned to the methyl protons, and two broad signals at 3.65 and 4.02 ppm instead of a well resolved quartet are due to the methylene protons. This is due to a hindered rotation around the C-NR^1R^2 bonds and has already been reported previously for

other *N,N*-dialkyl-*N'*-benzoylthioureas.[55-58] The ^{1}H NMR spectrum of H_2L^b shows a broad mutiplet in the range of 3.60 – 4.40 ppm which corresponds to the morpholine CH_2 groups. Single crystals of H_2L^a were obtained by slow evaporation of a CH_2Cl_2/EtOH (2:1) mixture. The molecular structure of H_2L^a (Fig. 1.1) was determined by X-ray diffraction. Selected bond lengths and angles are summarized in Table 1.1.

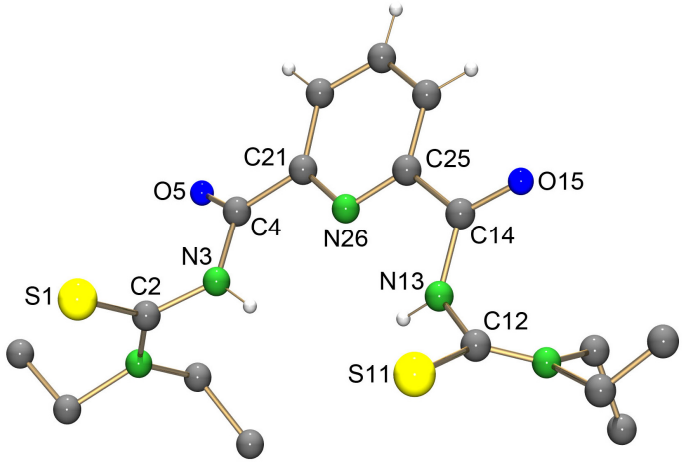

Figure 1.1 Molecular structure of H_2L^a. Hydrogen atoms of ethyl groups are omitted for clarity.

Table 1.1 Selected bond lengths and angles in H_2L^a.

Bond lengths (Å)					
S1–C2	1.669(4)	C2–N3	1.427(5)	N3–C4	1.340(5)
C4–O5	1.223(5)	S11–C12	1.662(5)	C12–N13	1.423(5)
N13–C14	1.360(5)	C14–O15	1.209(5)		
Angles (°)					
S1–C2–N3	117.6(3)	C2–N3–C4	122.2(3)	N3–C4–O5	123.9(4)
S11–C12–N13	117.3(3)	C12–N13–C14	121.8(3)	N13–C14–O15	124.6(4)

The crystal structure of H_2L^a is calculated in the monoclinic space group Cc and two molecules, which are perpendicular to each other, are seen in the asymmetric unit. Inter-molecular hydrogen bonds between NH protons of one molecule and the carbonyl oxygen of the adjacent molecule are observed. A discussion of the bond lengths and angles of the potentially chelating parts of H_2L^a, which are S1–C2–N3–C4–O5 and S11–C12–N13–C14–O15, is important to understand the coordination with metal ions. The carbonyl bond lengths C4–O5 and C14–O15 are 1.223(5) and 1.209(5) Å respectively. The thiocarbonyl bond lengths S1–C2 and S11–C12 are 1.669(4) and 1.662(5) Å respectively. They are within the

expected range of C=O and C=S double bonds. The N3–C4 and N13–C14 bond lengths are 1.340(5) and 1.360(5) Å respectively and they reflect a partial double bond character. All the bond lengths and angles agree with the values previously reported for similar aroylthiourea derivatives.[59]

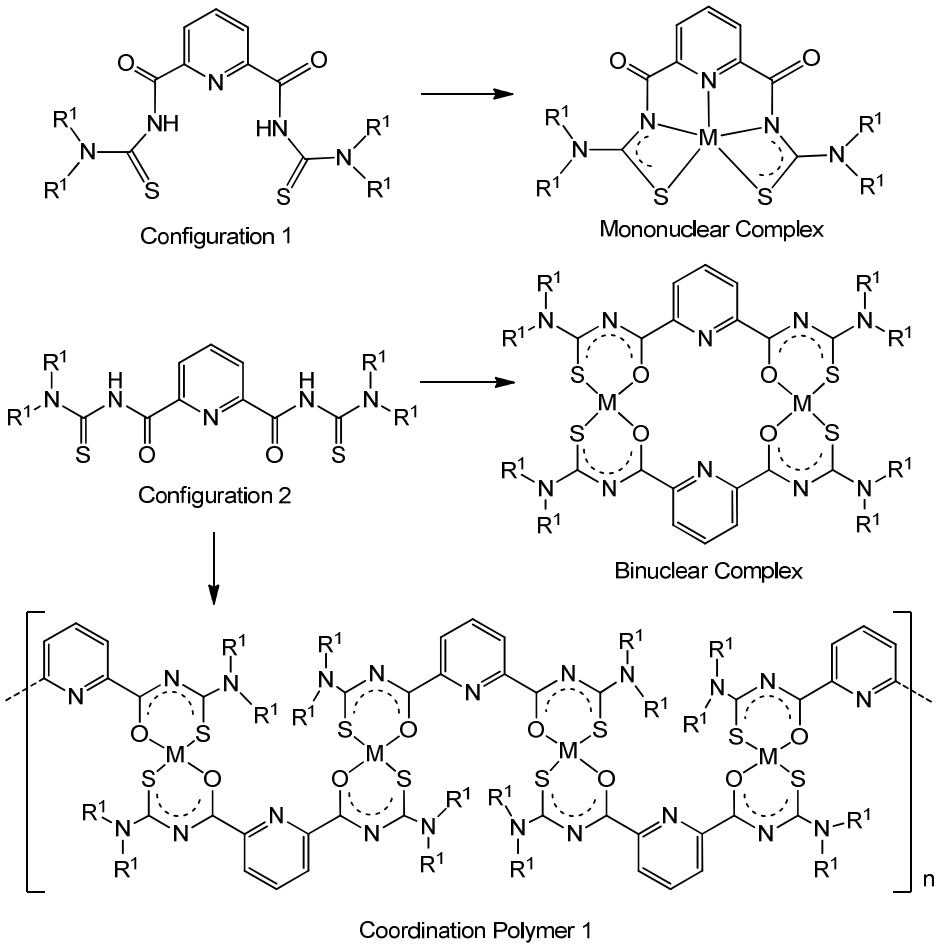

Chart 1.1 Expected configurations (configuration 1 and 2) and possible coordination modes of H_2L.

Due to the free rotations around the bonds C2–N3, N3–C4, C4–C21, C12–N13, N13–C14 and C14–C25, different configurations of the ligand are possible. This may leads to a high flexibility of the ligand to form different coordination patterns (Chart 1.1 and 1.2). A mononuclear complex with a M^{2+} ion is possible with the configuration 1. In this case, the carbonyl oxygens are not participated in the coordination and the complex shows a pentadentate *S, N, N, N, S* coordination of the ligand. The configuration 2 might be the sterically most accepted one for binuclear complexes. *Cis* coordination of the ligand might form binuclear complexes of two M^{2+} ions, where each coordinates to the *S,O* moieties of both ligands. In this case coordination of an additional metal ion in the middle position is

favored due to the presence of four carbonyl oxygen and two pyridine nitrogen donor atoms. This leads to a trinuclear complex and this is the main focus of this thesis and discussed in detail in following Chapters. *Trans* chelates of the similar configuration of the ligands leads to the polymerization and forms coordination polymers (Chart 1.1). However the sterical hindering of the alkyl rest of the amine group might obstruct the formation of the polymers. Similar coordination polymers with tetraalkylisophthaloylbis(thioureas) have recently been reported.[32]

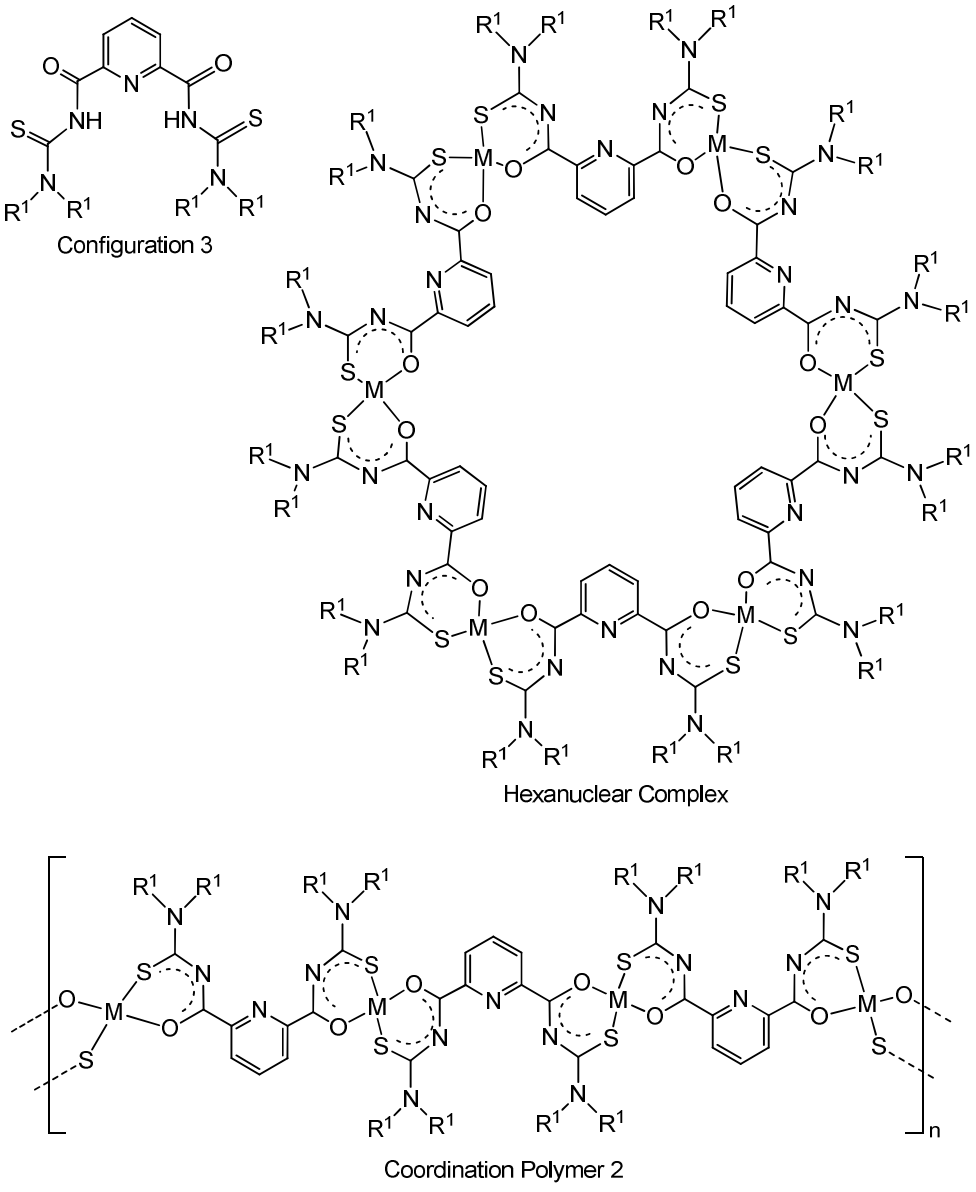

Chart 1.2 Expected configurations (configuration 3) and possible coordination modes of H_2L.

The configuration 3 is formed by the 180 ° rotations of the C4–C21 and C14–C25 bonds of configuration 2. The possible *cis* and *trans* coordinations of *S,O* moieties to the M^{2+} ions might forms different kinds of multinuclear complexes. The *cis* coordination of the aroylthiourea moieties results in a hexanuclear complex and *trans* coordination of the ligands form the coordination polymer 2 (Chart 1.2). The coordination polymer 2 seems to be sterically more favored than the coordination polymer 1. The reason may be the alkyl rests of the chelating parts, which are directed to opposite sides in the coordination polymer 2, but point to the same sides in the case of coordination polymer 1.

There are more other coordination modes possible if the monodentate *S* coordination and the bidentate *S,N* coordination are taken into account. They are omitted due to the irrelevance to the current work.

Chapter 2

Trinuclear mixed-metal complexes of lanthanides and transition metals with 2,6-dipicolinoylbis(*N*,*N*-dialkylthioureas)

Trinuclear mixed-metal complexes of lanthanides and transition metals with 2,6-dipicolinoylbis(*N,N*-dialkylthioureas)

The coordination chemistry of 2,6-dipicolinoylbis(*N,N*-dialkylthiourea) ligands is only less studied. Surprisingly, there is up to now only one structurally characterized metal complex with this ligand system.[42] In this Ag^I complex, two neutral 2,6-dipicolinoylbis(*N,N*-diethylthioureas) are coordinated to two Ag^I centers via their *S* donor atoms. Two of this $[Ag_2(H_2L^a)_2]^{2+}$ subunits are connected by another neutral ligand through a μ_2-coordination of the *S* donor atoms. This coordination mode results in a coordination polymer with tetrahedrally coordinated Ag^I atoms (**14**) (Chart 2.1). In addition to this structural report of the Ag complex, there exists an investigation on the thermochemical properties of this ligand.[60] The enthalpy of combustion ($-\Delta_c U°_m$) of H_2L^a in oxygen gas was found to be 11027.1 ± 5.2 kJ·mol^{-1} at 298.15 K and the standard molar enthalpy of formation ($-\Delta_f H°_m$) of H_2L^a in crystalline state was derived to be 425.2 ± 5.6 kJ·mol^{-1}.

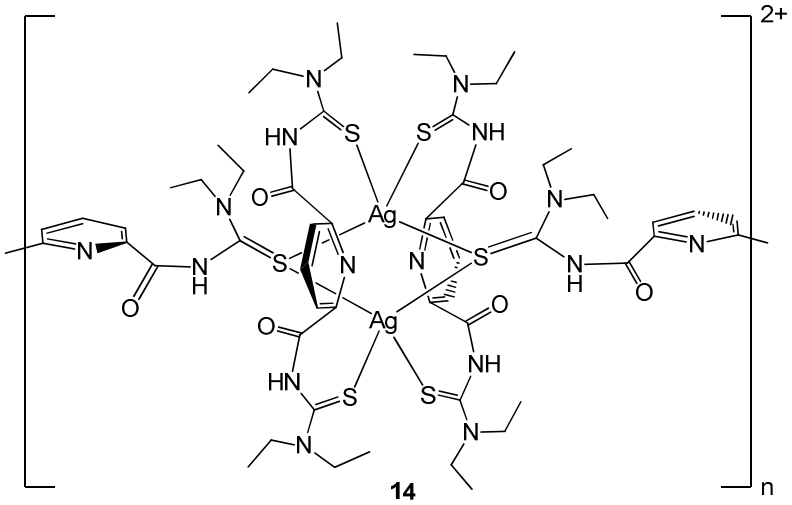

14

Chart 2.1 Previously reported coordination polymer of H_2L^a with Ag^I.[42]

More studies have been done with a similar ligand system 2,6-di(acetoacetyl)pyridine. Structural and magnetic studies of series of linear trinuclear mixed-metal complexes of the type $M^{II}Ln^{III}M^{II}$ with this system were reported by *ohba* et al.[46] The complexes were synthesized by one-pot reactions between $Ln(NO_3)_3$ (where Ln = La – Lu, except Pm), $M(NO_3)_2$ (where M = Ni, Cu or Zn) and 2,6-di(acetoacetyl)pyridine in MeOH (Scheme 2.1). Expectedly, 2,6-dipicolinoylbis(*N,N*-dialkylthioureas) (H_2L) should react in a similar way and form trinuclear complexes. In addition to the potentially multidentate nature of the ligand, the

presence of the 'soft' donor atom (*S*) and two differently 'hard' donor atoms (*O*) and (*N*) should make this ligand flexible in the sense to accept 'soft' and 'hard' metal ions simultaneously. Moreover, such trinuclear complexes containing different metal ions may offer the opportunity for the synthesis of molecular magnets or building blocks for supramolecular assemblies.

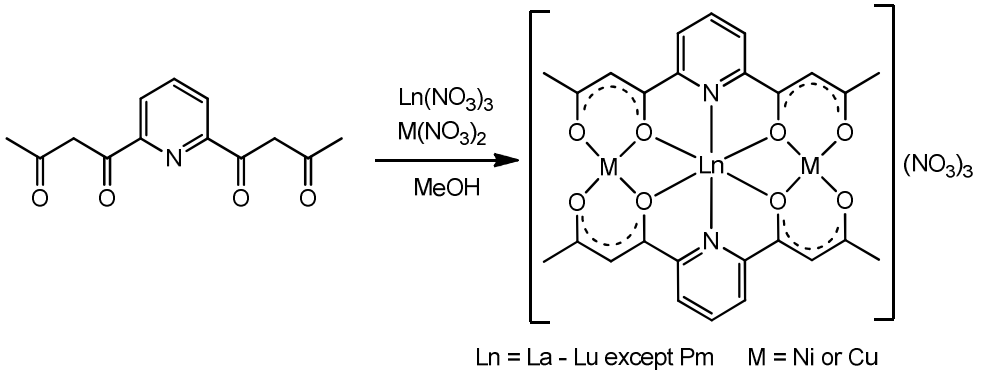

Scheme 2.1 Previously reported trinuclear complexes of type $M^{II}Ln^{III}M^{II}$.[45-46]

More interestingly, in addition to the coordination chemistry, design and synthesis of new heteronuclear complexes are necessary to analyze the magnetic interactions between different metal ions. This leads to a better understanding of molecular based magnetic materials. Unfortunately, due to the weak d-f interactions and large anisotropic effects of lanthanide ions, the magnetic interactions involved in d-f systems are not easy to understand.[61-64] Since Gd^{III} has no first order orbital angular momentum and the highest spin quantum number ($S = 7/2$), most of the d-f systems are reported with Gd^{III}.[43-44, 65-69] Surprisingly, ferromagnetic interactions between the adjacent Cu^{II} and Gd^{III} ions in a non-linear, trinuclear $Cu^{II}Gd^{III}Cu^{II}$ complex were first reported in 1985 by *Bencini* et al.[70] Furthermore, *Kahn* et al. suggested that the magnetic nature in the Cu^{II}–Ln^{III} pair is apparently antiferromagnetic for the Ln ions with $4f^{1}$–$4f^{6}$ configurations, whereas it is ferromagnetic for the Ln ions with $4f^{8}$–$4f^{13}$ configurations.[43, 66] Among the reported heteronuclear complexes containing transition metal (M^{II}) and lanthanide (Ln^{III}) ions, a considerable number of trinuclear complexes in the form of $M^{II}Ln^{III}M^{II}$ is published. Magnetic interactions between Ln^{III} and Cu^{II} ions in the $Cu^{II}Ln^{III}Cu^{II}$ trinuclear core have been analyzed in more detail compared to the other transition metals in similar systems.[70-78] For the lanthanide series of linear $Cu^{II}Ln^{III}Cu^{II}$ complexes (where Ln = La – Lu, except Pm) derived from chelating 2,6-di(acetoacetyl) pyridine ligand mentioned above, the results are in a good agreement with the predictions of

Kahn.[46] Furthermore, a number of studies have been reported on the synthesis, structural and magnetic properties of trinuclear $Ni^{II}Ln^{III}Ni^{II}$ complexes as well. In addition to the ferromagnetic interactions between Ni^{II} and Gd^{III} in the $Ni^{II}Gd^{III}Ni^{II}$ trinuclear system, magnetic interactions between Ni^{II} and other lanthanide ions such as La^{III}, Nd^{III}, Eu^{III}, Tb^{III}, Dy^{III} or Yb^{III} in trinuclear systems have also been reported.[79-85]

Some systematic studies of structure and magnetic data of $Ni^{II}Ln^{III}Ni^{II}$ systems covering the whole lanthanide series have also been reported.[45, 86-87] *Shiga* et al. reported magnetic interactions between Ni^{II} and Ln^{III} in linear trinuclear $Ni^{II}Ln^{III}Ni^{II}$ complexes with the 2,6-di(acetoacetyl)pyridine ligand for the whole series of Ln^{III} ions.[45] Trinuclear $Co^{II}Ln^{III}Co^{II}$ complexes are structurally as well as magnetically not been well explored. Especially, an evaluation of magnetic interactions between Co^{II} and Ln^{III} is extremely complicate due to the high magnetic anisotropy of Co^{II} ions. However, ferromagnetic interaction between Gd^{III} and Co^{II} in a linear trinuclear $Co^{II}Gd^{III}Co^{II}$ system and antiferromagnetic interaction between La^{III} and Co^{II} in a linear trinuclear $Co^{II}La^{III}Co^{II}$ system have previously been reported with different kinds of chelating ligand systems.[88-91]

Magnetic interactions between d and f metal ions are not clearly understood in all reported heteronuclear d-f complexes due to the presence of indefinable microscopic magnetic mechanisms for the interactions between the metal centers. Until now, no specific theoretical calculations are available, which give a clear view and a better understanding of such magnetic interactions. In order to study the magnetic interactions of 3d-4f complexes more in detail and systematically, the introduction of new heteronuclear systems with different chelating ligand systems are necessary.

In this Chapter, synthesis and structural studies of trinuclear $M^{II}Ln^{III}M^{II}$ complexes (where Ln = Ce, Nd, Sm, Gd, Dy, Er or Yb and M = Co, Ni, Mn, Cu or Zn) with the novel bridging 2,6-dipicolinoylbis(*N,N*-diethylthiourea) ligand system are reported. Warm solutions of two equivalents of H_2L^a and one equivalent of $LnCl_3$ (Ln = Ce, Nd, Sm, Gd, Dy, Er or Yb) in MeOH react rapidly with two equivalents of $M(CH_3COO)_2 \cdot nH_2O$ (M = Co, Ni, Mn, Cu or Zn) in the presence of a supporting base such as Et_3N (Scheme 2.2). In most of the cases, the structural analysis of the products confirm the coordination of two doubly deprotonated ligands to one Ln^{III} and two M^{II} centers (**15**) (Scheme 2.2a). Expectedly, the lanthanide metal ion coordinates exclusively to the diacylpyridine moiety via *O,N,O* donors and the transition metals coordinate to the aroylthiourea moieties via *S, O* donors. The remaining three positive charges of the trinuclear complexes are compensated by chlorido and/or methanolato and/or

bridging and chelating acetato co-ligands. The complete struct ures of the complexes including co-ligands are discussed in each subchapter in detail.

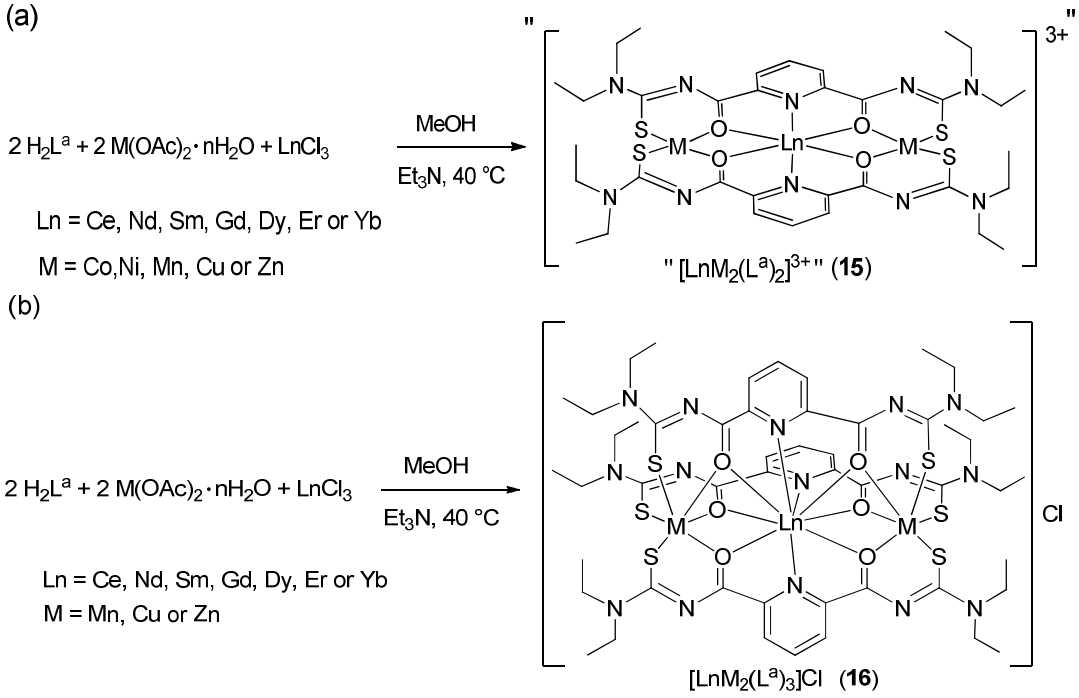

Scheme 2.2 Synthesis of trinuclear complexes of H_2L^a with lanthanides (III) and transition metals (II)

In some cases, e.g. with the transition metals Mn, Cu and Zn, such reactions give a second product (Scheme 2.2b). The structural analysis of these products reveals coordination of three doubly deprotonated ligands with one Ln^{III} and two M^{II} metal centers (**16**). In this case, the cationic complexes precipitate as chloride salts. This kind of trinuclear complexes with three ligands has not been obtained with Ni^{2+} or Co^{2+}. Colors, individual compositions and yields of the major products are given in Table 2.1. The details about the minor products in each case are discussed in the corresponding subchapters.

Table 2.1 Colors of the precipitates or the reaction mixtures, composition and yields of $M^{II}Ln^{III}M^{II}$.

	Mn^{2+}	Ni^{2+}	Co^{2+}	Cu^{2+}	Zn^{2+}
Ce^{3+}	Orange precipitate $[CeMn_2(L^a)_3]Cl$	Brown precipitate $[CeNi_2(L^a)_2(\mu\text{-}OAc)_2(OAc)]$	Green precipitate $[CeCo_2(L^a)_2(\mu\text{-}OAc)_2Cl]$	Green precipitate $[CeCu_2(L^a)_2(\mu\text{-}OAc)_2(OAc)]$	Yellow precipitate $[CeZn_2(L^a)_2(\mu\text{-}OAc)_2(OAc)]$
Nd^{3+}	Orange precipitate $[NdMn_2(L^a)_3]Cl$	Brown precipitate $[NdNi_2(L^a)_2(\mu\text{-}OAc)_2(OAc)]$	Green precipitate $[NdCo_2(L^a)_2(\mu\text{-}OAc)_2Cl]$	Green precipitate $[NdCu_2(L^a)_2(\mu\text{-}OAc)_2(OAc)]$	Colorless precipitate $[NdZn_2(L^a)_2(\mu\text{-}OAc)_2(OAc)]$
Sm^{3+}	Orange precipitate $[SmMn_2(L^a)_3]Cl$	Brown precipitate $[SmNi_2(L^a)_2(\mu\text{-}OAc)_2Cl]$	Green precipitate $[SmCo_2(L^a)_2(\mu\text{-}OAc)_2Cl]$	Brown precipitate $[SmCu_2(L^a)_2(\mu\text{-}OAc)_2(OAc)]$	Colorless precipitate $[SmZn_2(L^a)_2(\mu\text{-}OAc)_2(OAc)]$
Gd^{3+}	Orange precipitate $[GdMn_2(L^a)_3]Cl$	Brown precipitate $[GdNi_2(L^a)_2(\mu\text{-}OAc)_2Cl]$	Green precipitate $[GdCo_2(L^a)_2(\mu\text{-}OAc)_2(OAc)]$	Green precipitate $[GdCu_2(L^a)_2(\mu\text{-}OAc)_2)OAc)]$	Yellow precipitate $[GdZn_2(L^a)_2(\mu\text{-}OAc)_2(OAc)]$
Dy^{3+}	Orange precipitate $[DyMn_2(L^a)_3]Cl$	Brown solution Crystalized by over-layering with diethylether $[DyNi_2(L^a)_2(\mu\text{-}OAc)_2Cl]$	Red solution Crystalized by over-layering with diethylether $[DyCo_2(L^a)_2(\mu\text{-}OAc)_2Cl]$	Green solution Crystalized by slow evaporation $[DyCu_2(L^a)_2(\mu\text{-}OAc)_2(OAc)]$	Colorless precipitate $[DyZn_2(L^a)_2(\mu\text{-}OAc)_2(OAc)]$
Er^{3+}	Orange precipitate $[ErMn_2(L^a)_3]Cl$	Brown solution Crystalized by over-layering with diethylether $[ErNi_2(L^a)_2(\mu\text{-}OAc)_2Cl]$	Green solution Crystalized by over-layering with diethylether $[ErCo_2(L^a)_2(\mu\text{-}OAc)_2Cl]$	Green solution Crystalized by slow evaporation $[ErCu_2(L^a)_3]Cl$	Colorless precipitate $[ErZn_2(L^a)_3]Cl$
Yb^{3+}	Orange precipitate $[YbMn_2(L^a)_3]Cl$	Brown solution Crystalized by over-layering with diethylether $[YbNi_2(L^a)_2(\mu\text{-}OAc)_2Cl]$	Green solution Crystalized by over-layering with diethylether $[YbCo_2(L^a)_2(\mu\text{-}OAc)_2Cl]$	Green solution Crystalized by slow evaporation $[YbCu_2(L^a)_3]Cl$	Colorless precipitate $[YbZn_2(L^a)_3]Cl$

In most of the cases, solid precipitates could be collected in relatively high yields after 30 minutes directly from the reaction mixtures. These precipitates are readily soluble in CH_2Cl_2 and most of them, could be crystalized by slow evaporation of CH_2Cl_2/MeOH (1:1) mixtures. In the other cases the products could be isolated either by slow evaporation of the reaction mixtures or by over-layering of the reaction mixtures with diethylether. The colors of the complexes depend on the metal ions combined. Details are given in Table 2.1. IR spectra of the complexes generally show a strong absorption band between 1585 and 1593 cm^{-1}, which is assigned to the $\nu_{C=O}$ stretching vibration of the thiourea ligand. They appear in the spectrum of H_2L^a at 1687 cm^{-1}. The absence of NH bands in the spectra of the complexes confirms the deprotonation of the chelating ligand. The measurement of mass spectra was possible in CH_2Cl_2 solution, and they generally show peaks which can be assigned to ions of $[LnM_2(L^a)_2(X)_2]^+$ (where X = CH_3COO^-, Cl^- or CH_3O^-) or $[LnM_2(L^a)_3]^+$ which confirms the presence of one lanthanide and two transition metal ions with two or three each doubly deprotonated ligands. The details of mass spectra are discussed in the subchapters.

2.1 Complexes of lanthanides and cobalt [$Co^{II}Ln^{III}Co^{II}$]

Trinuclear systems having $Co^{II}Ln^{III}Co^{II}$ units are structurally as well as magnetically not well explored. Only two linear trinuclear systems, containing $Co^{II}Gd^{III}Co^{II}$ and $Co^{II}La^{III}Co^{II}$ units, have recently been reported (Chart 2.2). The first one shows the coordination of two planar 2,6-di(acetoacetyl)pyridine ligands to a trinuclear $Co^{II}Ln^{III}Co^{II}$ system (**17**). Each ligand is doubly deprotonated and the complex is crystallized as $[Cr(CN)_6]^{3-}$ salt.[89] The second complex is with phosphorous based trishydrazone derivatives (**18**). Two of the trianionic multidentate ligands coordinate to the trinuclear system. The complex is neutralized by a nitrate anion.[90]

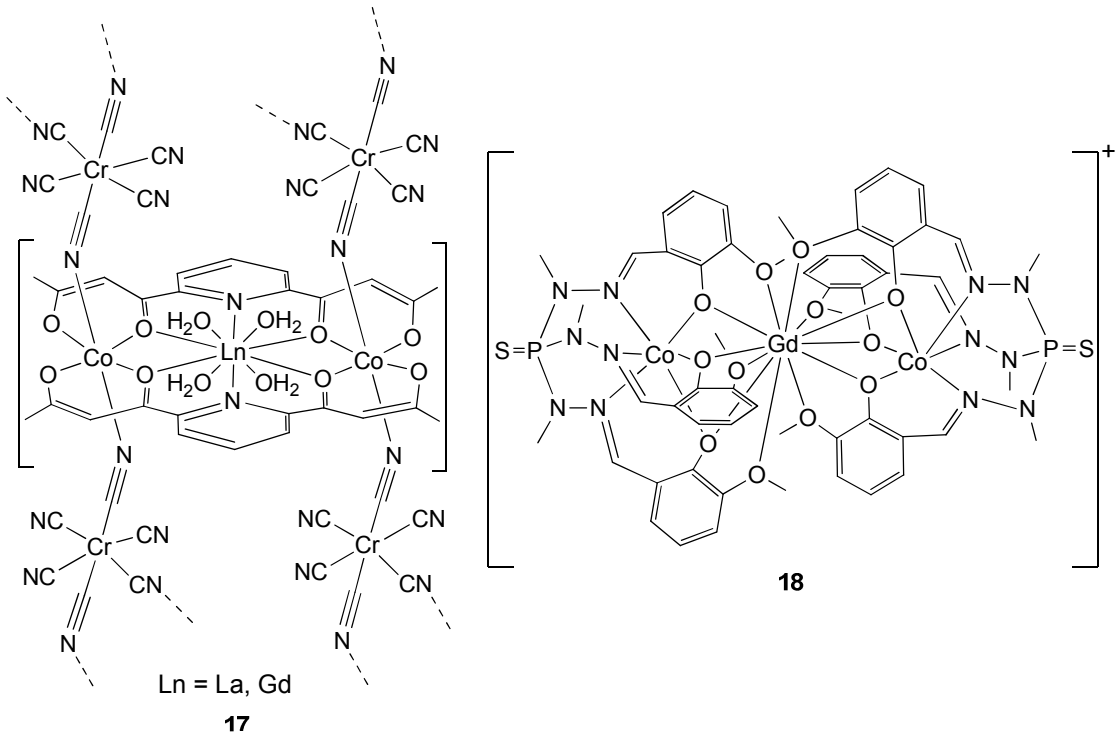

Chart 2.2 Previously reported linear trinuclear $Co^{II}Ln^{III}Co^{II}$ complexes.[89-90]

Two equivalents of the multidentate H_2L^a ligand react rapidly with one equivalent of $LnCl_3$ (where Ln = Ce, Nd, Sm, Gd, Dy, Er or Yb) and two equivalents of $Co(OAc)_2{\cdot}4H_2O$ in MeOH at 40 °C in the presence of Et_3N. They form complexes of the compositions $[LnCo_2(L^a)_2(\mu\text{-}OAc)_2Cl]$ (**19**) or $[GdCo_2(L^a)_2(\mu\text{-}OAc)_2(OAc)]$ (**20**) following the general procedure given in Scheme 2.3. The colors of such reaction mixtures turn immediately to either dark green (Ln = Ce, Nd, Sm or Gd) or dark red (Ln = Dy, Er or Yb) after the addition of the supporting base. Stable green precipitates were collected in high yields after 30 minutes in the cases of Ln = Ce, Nd, Sm and Gd. The precipitates are readily soluble in CH_2Cl_2 and

were recrystallized by slow evaporation of CH_2Cl_2/MeOH (1:1) mixtures. Slow evaporation of the reaction mixtures gave single crystals in high yields in the cases of Ln = Dy, Er and Yb. In all combinations, the obtained crystals were stable and suitable for X-ray analysis. Mass spectra of all complexes show as main peak $[LnCo_2(L^a)_2(\mu\text{-}OAc)_2]^+$, which confirms the formation of products with each two doubly deprotonated ligands, two Co^{2+} and one Ln^{3+} ions along with two bridging acetato ligands.

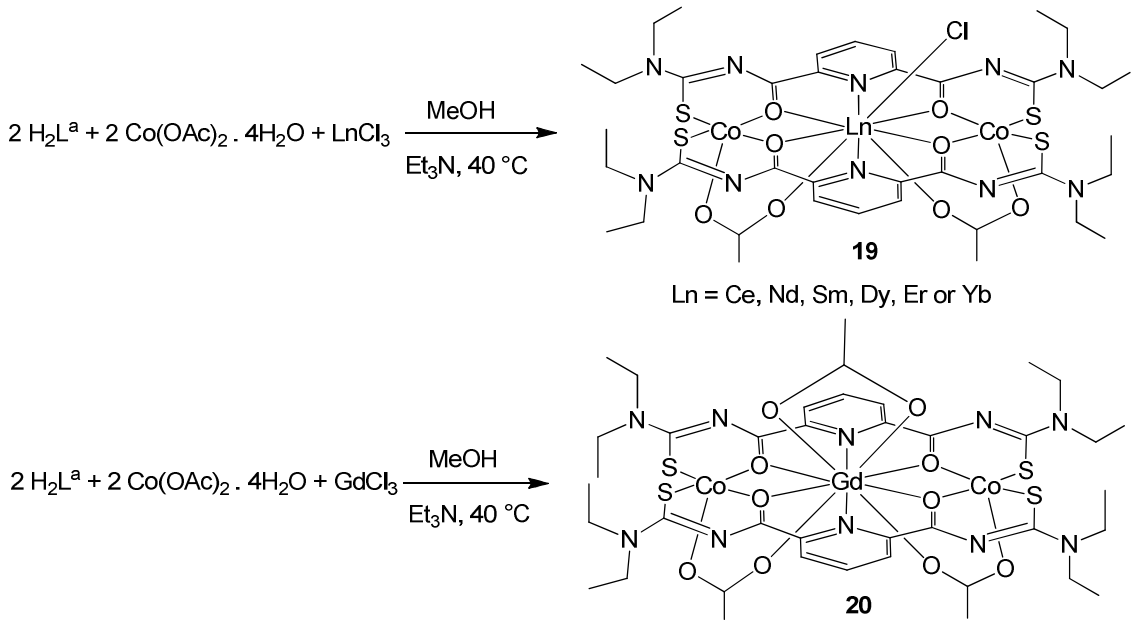

Scheme 2.3 Synthesis of trinuclear complexes with lanthanides and cobalt.

The molecular structures of the products were studied by single crystal X-ray diffraction. All complexes crystallize in the monoclinic crystal system with *C2/c* as space group with one half of the molecule in the asymmetric unit. The complete molecule is generated by a C_2 rotation axis which is perpendicular to the thioureato ligand plane and passes through the central lanthanide ion. In all structures, the Co^{2+} ions are equatorially coordinated by two bidentate *N*-arylthiourea sites via the *S* and *O* donor atoms. Square pyramidal coordination geometry of Co^{2+} is completed by the axial coordination of an oxygen atom of the bridging acetato ligand. The lanthanide metal ions coordinate with the tridentate 2,6-dipicolinoyl moieties of both ligands via the *N* donor atoms of pyridine rings and the *O* donor atoms of both carbonyl groups. All structures reveal two acetato bridges, where each bridge is between the terminal Co^{2+} and central Ln^{3+} ions. The molecular structures with Ce, Nd, Sm, Dy, Er and Yb show the coordination of an additional chlorido ligand to the Ln ion, which finally has a coordination number of 9 (Figure 2.1). The structure with Gd differs from the others by the

replacement of the central chlorido ligand by a chelating acetato ligand and shows the coordination number of 10 for the Gd atom (Figure 2.2). Ionic radii of lanthanides steadily decrease from Ce^{3+} to Yb^{3+} which is known as lanthanide contraction (Table 2.2).

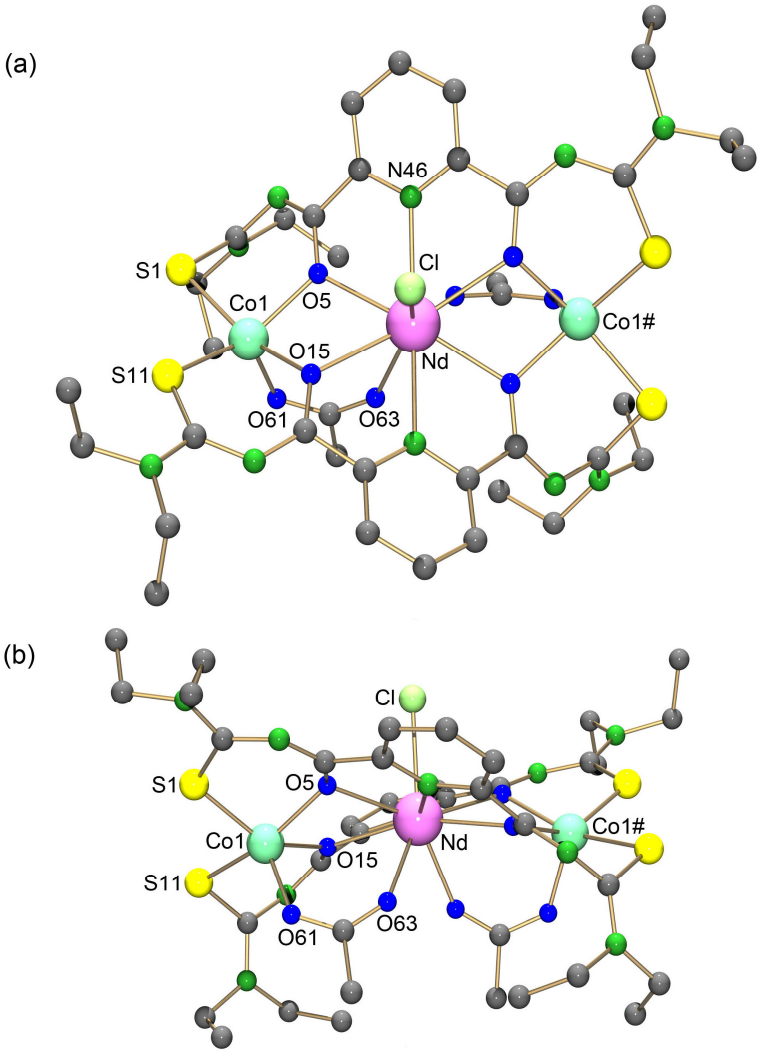

Figure 2.1 Molecular structure of $[NdCo_2(L^a)_2(\mu\text{-}OAc)_2Cl]$. (a) View perpendicular to the plane of the thioureato ligands. (b) View parallel to the plane of the thioureato ligands. Hydrogen atoms are omitted for clarity. Labeling of symmetry related atoms see Figure 2.3.

In the case of the isostructural complexes, the distance between the lanthanide and cobalt ions is also decreasing from Ce to Er and can be explained by the lanthanide contraction. The structure with Gd is an exception and has a Gd–Co distance of 3.621(2) Å, which does not fit with the decreasing value and can be explained by its different structure. The angle between Co1–Ln–Co1# is slightly increasing from Ce to Dy from 166.37(2) to 167.18(2) °. The structure with Gd has a Co1–Gd–Co1# angle of 163.14(2) °.

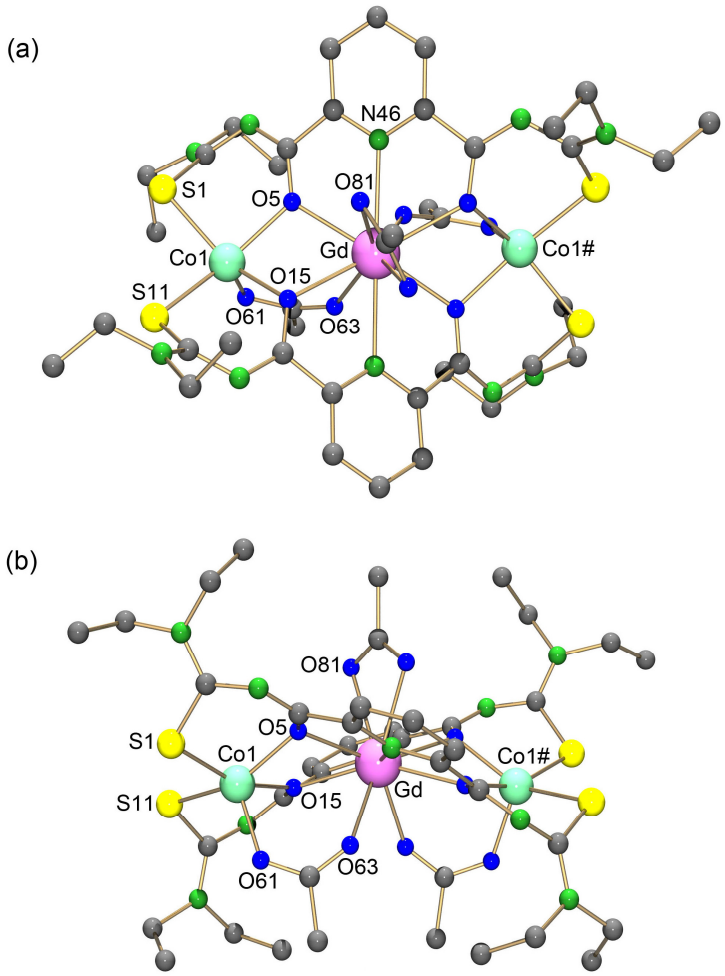

Figure 2.2 Molecular structure of $[GdCo_2(L^a)_2(\mu\text{-}OAc)_2(OAc)]$. (a) View perpendicular to the plane of the thioureato ligands. (b) View parallel to the plane of the thioureato ligands. Hydrogen atoms are omitted for clarity. Labeling of symmetry related atoms see Figure 2.3.

Table 2.2 Ionic radii of lanthanides and Ln–Co1 distances and Co1–Ln–Co1# angles in the $[Co^{II}Ln^{III}Co^{II}]$ complexes.

Ln	Ionic radius of Ln^{3+} (Å)	Ln–Co1 Distance (Å)	Co1–Ln–Co1# Angle (°)
Ce	1.03	3.678(1)	166.37(2)
Nd	1.00	3.666(2)	166.40(2)
Sm	0.96	3.663(1)	166.64(3)
Gd	0.94	3.621(2)	163.14(2)
Dy	0.91	3.655(2)	167.10(3)
Er	0.88	3.642(1)	167.00(2)
Yb	0.86	3.646(2)	167.18(2)

The Ln–Co distances are in the range of 3.621(2) – 3.678(1) Å and the Co–Co distances are in the range of 7.242(2) – 7.356(2) Å. A previously reported binuclear Co(II) complex with isopththaloylbisthiourea ligand has a Co–Co distance of 7.249(3) Å.[30]

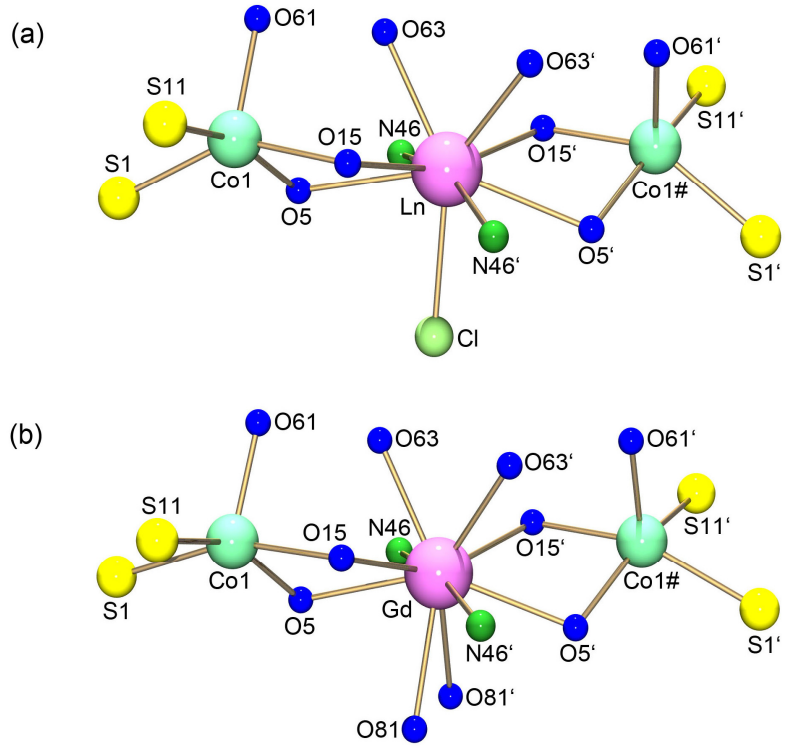

Figure 2.3 Coordination patterns of the metal ions in the $Co^{II}Ln^{III}Co^{II}$ complexes (a) in $[LnCo_2(L^a)_2(\mu\text{-}OAc)_2Cl]$ (b) in $[GdCo_2(L^a)_2(\mu\text{-}OAc)_2(OAc)]$. Symmetry related atoms are produced by a C_2 rotation axis.

The coordination spheres of the metal complexes are shown in Figure 2.3. The equatorial Co–S bonds and Co–O bonds are in the ranges of 2.290(2) – 2.401(2) Å and 2.043(3) – 2.104(2) Å respectively (Table 2.3). Both are in the normal range of Co–S and Co–O bonds in previously reported binuclear Co^{II} complexes.[30] The axial Co–O61 bond between Co and the axial O donor of the acetate-bridge is in the range of 1.981(3) –1.998(4) Å. The equatorial Ln–O5 and Ln–O15 bonds are much longer. They fall in the range between of 2.359(3) and 2.490(4) Å and 2.515(3) – 2.607(4) Å respectively. The Ln–N46 bonds are in the range of 2.554(4) – 2.652(4) Å (Table 2.3). Similar Ln–O and Ln–N equatorial bond lengths are observed in the trinuclear $Cu^{II}Ln^{III}Cu^{II}$ and $Ni^{II}Ln^{III}Ni^{II}$ complexes with the 2,6-di(acetoacetyl)pyridine ligand, where the central Ln ion is coordinated similarly to the 2,6-dipicolinoyl site.[45-46]

Table 2.3 Selected bond lengths (Å) in $Co^{II}Ln^{III}Co^{II}$ complexes.

	Ce	Nd	Sm	Gd	Dy	Er	Yb
Ln–O5	2.490(4)	2.458(3)	2.444(3)	2.407(2)	2.401(4)	2.379(2)	2.359(3)
Ln–O15	2.607(4)	2.587(2)	2.572(4)	2.515(3)	2.551(4)	2.558(2)	2.570(3)
Ln–N46	2.652(4)	2.628(3)	2.616(4)	2.600(3)	2.561(4)	2.557(3)	2.554(4)
Ln–Cl	2.761(2)	2.725(1)	2.702(2)	-	2.646(2)	2.624(1)	2.600(2)
Ln–O63	2.455(4)	2.422(3)	2.392(4)	2.415(3)	2.337(4)	2.311(2)	2.279(3)
Ln–O81	-	-	-	2.561(3)	-	-	-
Co1–S1	2.401(2)	2.397(1)	2.392(2)	2.354(1)	2.291(2)	2.293(1)	2.375(2)
Co1–S11	2.292(2)	2.293(1)	2.290(2)	2.354(1)	2.381(2)	2.376(1)	2.302(2)
Co1–O5	2.055(4)	2.060(2)	2.059(4)	2.071(2)	2.068(4)	2.063(2)	2.084(3)
Co1–O15	2.099(4)	2.087(3)	2.084(3)	2.104(2)	2.065(4)	2.070(2)	2.043(3)
Co1–O61	1.983(5)	1.987(3)	1.998(4)	1.981(3)	1.995(4)	1.993(3)	1.987(4)

Synthesis, structural and X-band EPR analysis of binuclear Cu^{II} and Co^{II} complexes with isophthaloylbis(thiourea) ligand systems (Chart 2.3) have been reported by *Kirmse* et.al.[30-31] The intramolecular metal-metal distances in the complexes are 7.704 Å for the Cu^{II} complex (**21**) and 7.249 Å for the Co^{II} complex (**22**). Since Cu^{II} is the classical candidate for EPR studies on metals, and the spectra of the Cu^{II} complexes are well studied and understood. Due to the very short spin-lattice relaxation time of Co^{II}, no EPR signals can be detected for Co^{II} complexes at room temperature. However, EPR signals of Co^{II} complexes in $CHCl_3$/toluene solutions can be seen at the temperature range of 4.2 K – 120 K.[30] Even though, a complete interpretation of the EPR signals of the binuclear Co^{II} complexes have not yet been reported.[30]

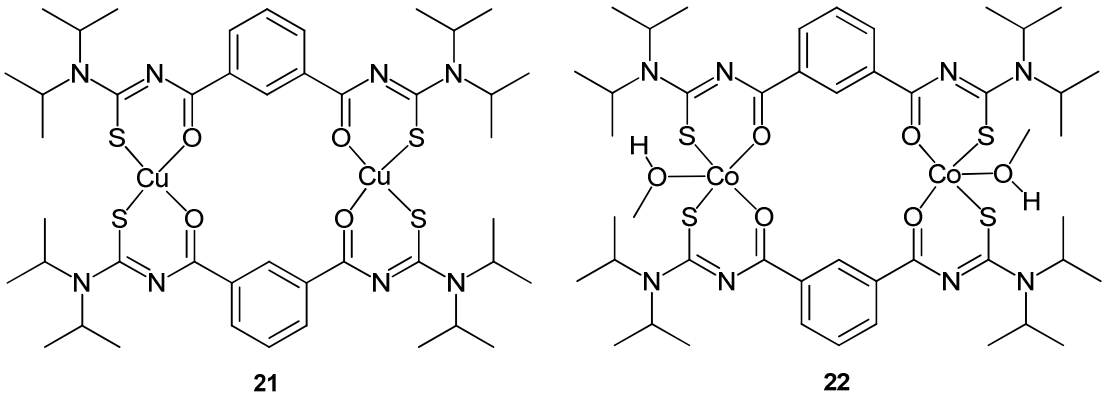

Chart 2.3 Binuclear complexes of Cu(II) and Co(II) previously analyzed by EPR spectroscopy.[30]

Expectedly, trinuclear complexes of the type $Co^{II}Ln^{III}Co^{II}$ should give more complicated EPR spectra due to the presence of the paramagnetic Ln^{III} ions and their interactions with the two Co^{II} ions, which are separated in an averaged distance of 3.7 Å. The complexes $Co^{II}Ln^{III}Co^{II}$, where Ln = Ce, Gd, Er or Yb, were also analyzed by W-band EPR spectroscopy at 5 K. The recorded spectra of $[CeCo_2(L^a)_2(\mu\text{-}OAc)_2Cl]$ and $[ErCo_2(L^a)_2(\mu\text{-}OAc)_2Cl]$ are similar to the background, while the $[GdCo_2(L^a)_2(\mu\text{-}OAc)_2(OAc)]$ and $[YbCo_2(L^a)_2(\mu\text{-}OAc)_2Cl]$ complexes show EPR signals at 5K. Their spectra are depicted in Figure 2.4. Interestingly, the spectrum of $[GdCo_2(L^a)_2(\mu\text{-}OAc)_2(OAc)]$ shows a number of complicated couplings. An interpretation of the complicated EPR signal of the $[GdCo_2(L^a)_2(\mu\text{-}OAc)_2(OAc)]$ complex, however, is not possible on the basis of the available solution spectra.

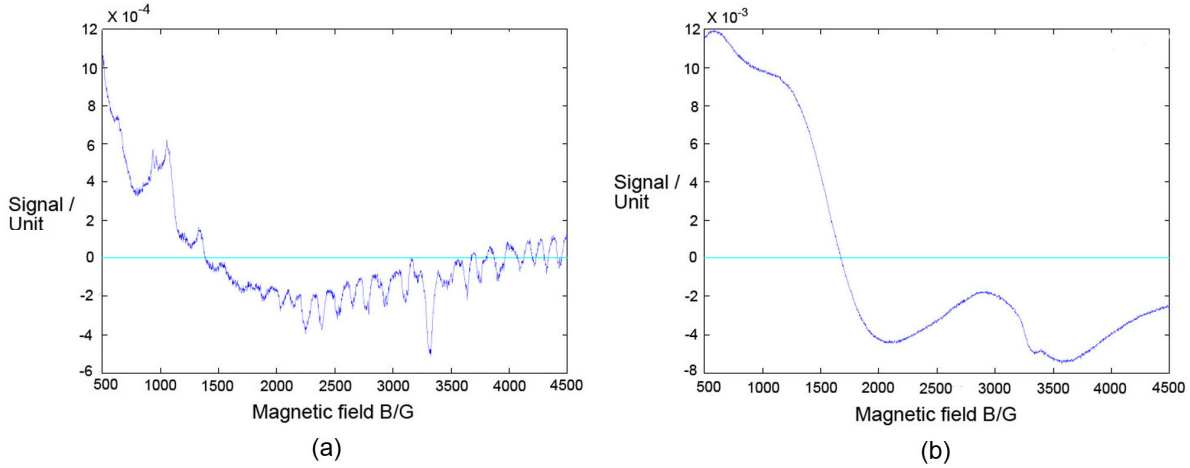

Figure 2.4 W-band (94 GHz) EPR spectra of (a) $[GdCo_2(L^a)_2(\mu\text{-}OAc)_2(OAc)]$ and (b) $[YbCo_2(L^a)_2(\mu\text{-}OAc)_2Cl]$ at 5 K in $CHCl_3$/toluene (1:1) mixture.

Cryomagnetic properties of the complexes were studied in the temperature range of 2-330 °K under an applied field of 1T. The magnetic interactions of the trinuclear $Co^{II}Ln^{III}Co^{II}$ system could be inspected from the temperature variation of the magnetic moment. Temperature dependencies of the magnetic moments of the complexes are shown in Figure 2.5. In the case of $[DyCo_2(L^a)_2(\mu\text{-}OAc)_2Cl]$, the observed value of the effective magnetic moment ($\mu_{eff(Observed)}$) is increasing with temperature from 11.41 to 12.89 μ_B and at room temperature it is 12.86 μ_B. Moreover, the complex $[YbCo_2(L^a)_2(\mu\text{-}OAc)_2Cl]$ shows an increase of the observed effective magnetic moment ($\mu_{eff(Observed)}$) from 6.49 μ_B at 2K to 8.04 μ_B at 330 K and at room temperature it is 8.05 μ_B.

With increasing temperature, the complex $[GdCo_2(L^a)_2(\mu\text{-}OAc)_2(OAc)]$ shows a slight decrease of $\mu_{eff(Observed)}$ from 11.66 μ_B at 9 K to 10.70 μ_B at 330 K. The observed effective

magnetic moments of the complexes with Ce, Nd, Sm and Er initially increase with the temperature and then they decrease. It is difficult to analyze the temperature dependence of magnetic moments in complexes which contain Co^{II} ions due to their intrinsic complicated magnetic properties.[89-90] Ferromagnetic interactions are suggested for $[GdCo_2(L^a)_2(\mu\text{-}OAc)_2(OAc)]$ complex judged from the increasing magnetic moment at low temperatures. Antiferromagnetic interactions are observed for the complexes $[DyCo_2(L^a)_2(\mu\text{-}OAc)_2Cl]$ and $[YbCo_2(L^a)_2(\mu\text{-}OAc)_2Cl]$ as the magnetic moment deceases with low temperature. The magnetism in the trinuclear $Co^{II}Ln^{III}Co^{II}$ systems with Ce, Nd, Sm and Er are difficult to define. They show decreasing magnetic moments in lower temperatures and might have antiferromagnetic interactions. But the magnetism slightly decreases in higher temperatures and this is the nature of ferromagnetic interactions (Figure 2.5).

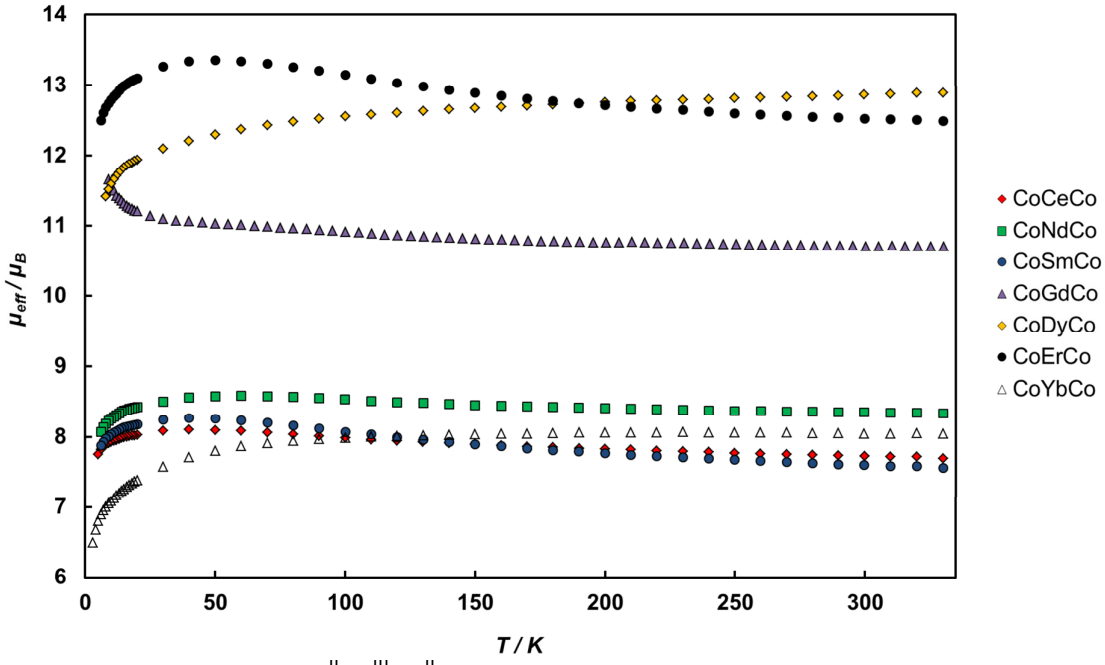

Figure 2.5 μ_{eff} vs T plot of $Co^{II}Ln^{III}Co^{II}$ complexes.

The theoretical magnetic moment of a trinuclear complex with magnetically isolated two Co^{II} ions and one Ln^{III} ion could be obtained by the substitution of Cu^{II} by Co^{II} in the equation reported by *Ohba* et al.[46]

$$\mu_{eff\,(\text{Calculated})} = [2[4S_{\text{Co}}(S_{\text{Co}}+1)] + g_J^2 J(J+1)]^{1/2} \qquad \mu_B \qquad ,(1)$$

where S_{Co} is the spin quantum number of Co^{II} and has the value of 3/2 and g_J is the Landé g factor of the ground *J* level of each Ln^{III} and is expressed as

$$g_J = \frac{3}{2} + \frac{S(S+1)-L(L+1)}{2J(J+1)} \quad , \qquad (2)$$

where *S*, *L* and *J* are spin, orbital and total angular moments for a specific Ln^{III} ion, respectively.

Equation 1 does not contain the magnetic interactions between adjacent trinuclear units, which were neglected because of significant metal-metal separations (≥ 8.06 Å). The obtained $\mu_{eff\,(\text{Calculated})}$ values are compared with the $\mu_{eff\,(\text{Observed})}$ values of complexes at room temperature and are summarized in Table 2.4.

Table 2.4 No. of *f* electrons, unpaired electrons in Ln^{3+}, *S*, *L*, *J*, g_J values of Ln^{3+} and μ_{eff} values of complexes

Ln	*f* electrons in Ln^{3+}	Unpaired electrons in Ln^{3+}	*S*	*L*	*J*	g_J	$\mu_{eff\,(\text{Calculated})}$ / μ_B	$\mu_{eff\,(\text{Observed})}$ at 300 K / μ_B
Ce	1	1	+1/2	+3	5/2	0.86	6.04	7.73
Nd	3	3	+3/2	+6	9/2	0.73	6.56	8.35
Sm	5	5	+5/2	+5	5/2	0.29	5.54	7.60
Gd	7	7	+7/2	0	7/2	2	9.64	10.71
Dy	9	5	+5/2	+5	15/2	1.33	11.97	12.86
Er	11	3	+3/2	+6	15/2	1.20	11.04	12.52
Yb	13	1	+1/2	+3	7/2	1.14	7.11	8.05

Interestingly, the observed values of effective magnetic moments are slightly higher than the calculated values in all cases. Figure 2.6 shows the comparison of the observed effective magnetic moment at 300K with the calculated values. A deviation in the magnetic moment is observed for all mixed-metal $Co^{II}Ln^{III}Co^{II}$ complexes. This deviation might be explained by the incorrect values of both calculated and observed magnetic moments. Probably the approximations applied in the equation used to the magnetic moment calculation might cause such deviations. In addition to that, the experimental errors during the measurement of observed magnetic moments could also cause such deviations. However the observations show the necessity of a more exact magnetic moment calculation method for trinuclear $Co^{II}Ln^{III}Co^{II}$ systems. Therefore, synthesis of more trinuclear $Co^{II}Ln^{III}Co^{II}$ complexes with different kinds of chelating ligand is necessary for improvements in magnetic moment calculation methods and for a better understanding of the magnetic chemistry of such complicated systems.

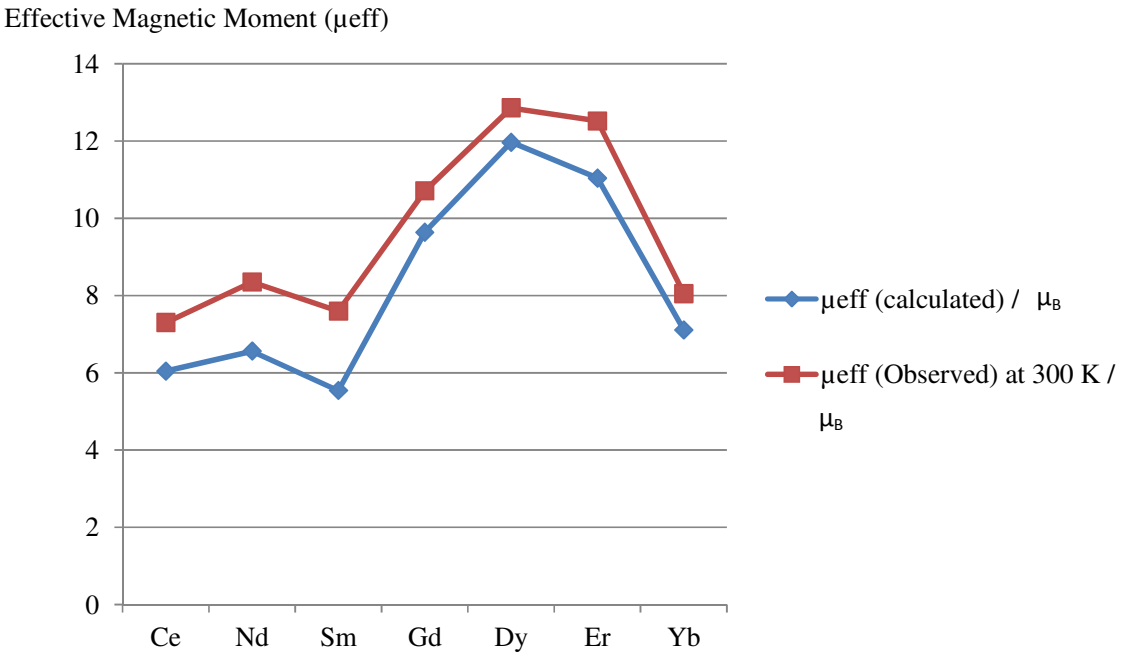

Figure 2.6 Comparison of calculated and observed μ_{eff} of $Co^{II}Ln^{III}Co^{II}$ complexes.

2.2 Complexes of lanthanides and nickel [$Ni^{II}Ln^{III}Ni^{II}$]

Synthesis of trinuclear $Ni^{II}Ln^{III}Ni^{II}$ complexes with different chelating ligand systems have been developed in last decade because of their application in the study of magnetic interactions between d and f block metal ions in a d/f/d system.

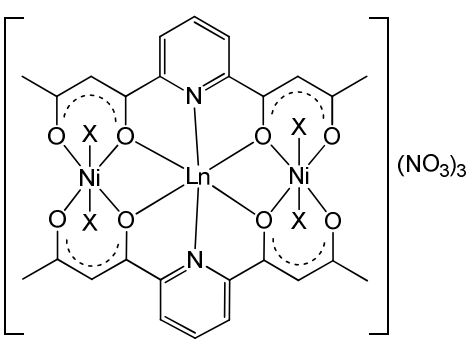

23

Ln = La - Lu, except Pm X = MeOH or H_2O

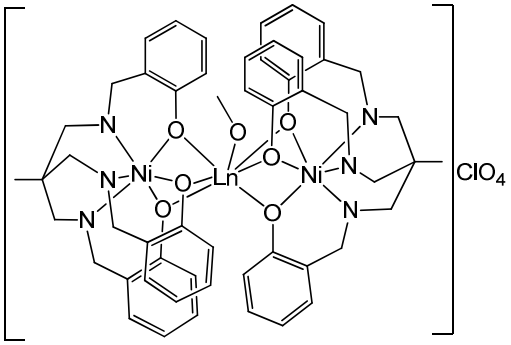

24

Ln = La, Pr, Nd, Gd, Dy, Ho, Er or Yb

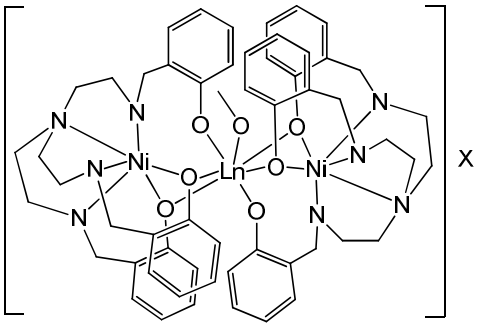

25

Ln = La - Lu, except Ce and Pm

X = $NO3^-$ or ClO_4^-

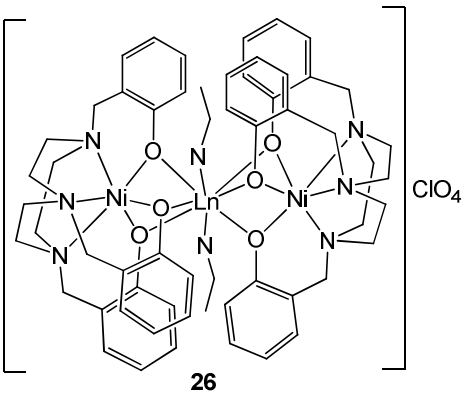

26

Ln = La, Nd, Gd, Dy or Yb

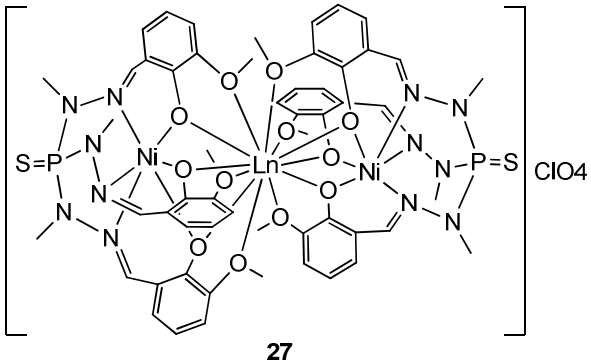

27

Ln = La - Er, except Pm

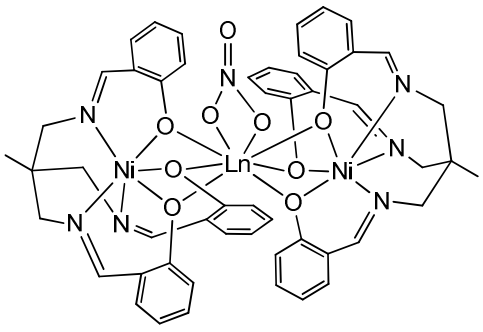

28

Ln = Eu, Gd, Tb or Dy

Chart 2.4 Previously reported trinuclear $Ni^{II}Ln^{III}Ni^{II}$ complexes.[45, 79, 82-83, 86-87]

Structural and magnetic studies on a series of linear trinuclear $Ni^{II}Ln^{III}Ni^{II}$ complexes (Ln = La–Lu, except Pm) with 2,6-di(acetoacetyl) pyridine ligand systems (**23**) were reported by *Shiga* et al (Chart 2.4).[45] It was a complete study including magnetic interactions between Ln^{3+} and Ni^{2+} ions in a linear trinuclear $Ni^{II}Ln^{III}Ni^{II}$ system with a chelating ligand. In addition to that, trinuclear $Ni^{II}Ln^{III}Ni^{II}$ systems with tris(2-hydroxybenzylamino) derivatives (**24**, **25** and **26**) and their magnetic properties have been reported by *Orvig* et al.(Chart 2.4)[79, 82, 86]. In the complexes **24**, **25** and **26** two trianionic ligands coordinated to one Ln^{3+} and two Ni^{2+} ions. The overall positive charge of the complexes is neutralized by either a nitrate or a perchlorate anion. In all complexes, the Ni atoms show the coordination number six. In addition to the phenolato *O* donor atoms of the ligand, the coordination of a methanol molecule to the Ln^{3+} ions is observed in complexes **24** and **25**. The additional coordination of two acetonitrile molecules to the Ln atom is observed in complex **26**. Complex **27** contains a phosphorous-based trishydrazone derivative. In this case, the Ln ions coordinate to the phenolato and methoxo *O* donor atoms of the ligands. The cationic complex is neutralized by a perchlorate anion[87]. Complex **28** is similar to complex **24**, but the coordination of a bidentate nitrato ligand to Ln^{3+} is observed[83]. The magnetic analyses of all the above-mentioned systems indicate antiferromagnetic interactions between Ln^{3+} and Ni^{2+} ions when the Ln ion is lighter than Gd^{3+} and a ferromagnetic behavior if Ln ion is heavier than Gd^{3+}. These observations are in a good agreement with the predictions of *Kahn*.

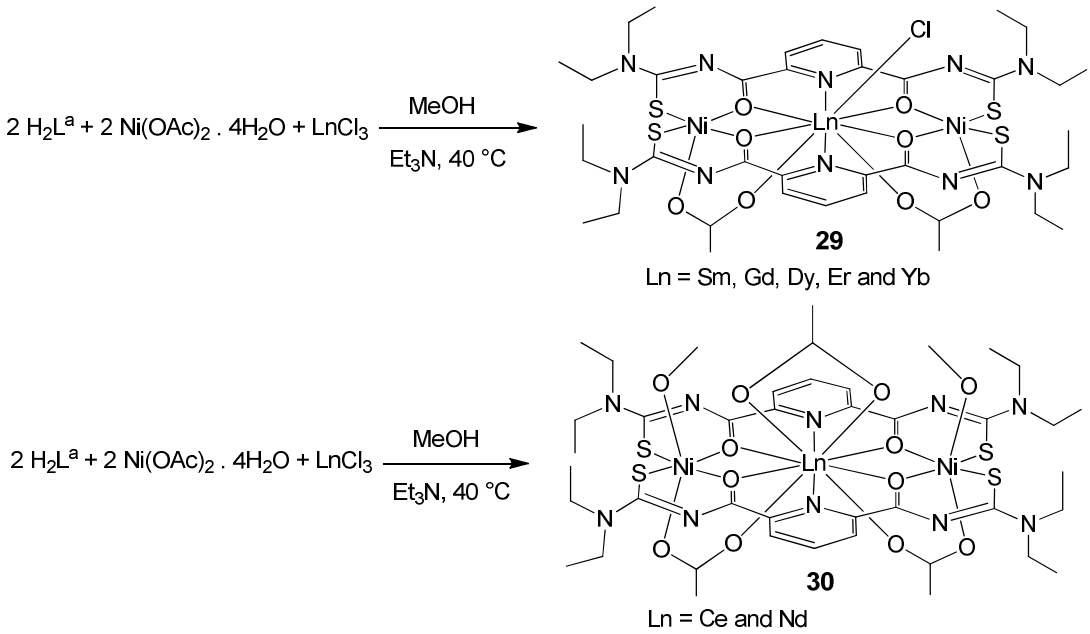

Scheme 2.4 Synthesis of trinuclear complexes with lanthanides (III) and nickel (II)

This chapter introduces novel trinuclear $Ni^{II}Ln^{III}Ni^{II}$ complexes with the multidentate ligand H_2L^a. Reactions of two equivalents of H_2L^a with two equivalents of $Ni(OAc)_2 \cdot 4H_2O$ and one equivalent of $LnCl_3$ (Ln = Ce, Nd, Sm, Gd, Dy, Er or Yb) in MeOH at 40 °C in the presence of Et_3N form trinuclear complexes of the general formula $[LnNi_2(L^a)_2(\mu\text{-}OAc)_2Cl]$ (**29**) or $[LnNi_2(L^a)_2(\mu\text{-}OAc)_2(OAc)]$ (**30**) (Scheme 2.4). The products were collected as precipitates after 30 minutes directly from the reaction mixtures in the cases of Ce, Nd, Sm and Gd. In the other cases, over-layering of the reaction mixtures with diethyl ether leads to crystallization of the products.

Preliminary analyses, such as IR spectroscopy of the products, confirm the deprotonation and chelate formation of the ligand. Over-layering of the reaction with diethyl ether lead to stable crystalline products in the cases of Ln = Dy, Er and Yb. All complexes are readily soluble in CH_2Cl_2 and single crystals suitable for X-ray analysis were obtained by slow evaporation of CH_2Cl_2/MeOH (1:1) mixture in the cases of Ln = Ce, Nd, and Gd. In the case of Ln = Sm, two types of crystalline products were obtained and were separated manually. The major product (green colored thin needles) was not suitable for X-ray analysis. However, the other analytical methods such as ESI mass spectroscopy and elemental analysis prove a complex of the composition $[SmNi_2(L^a)_2(\mu\text{-}OAc)_2Cl]$. The brown colored side product was suitable for X-ray analysis. The structure refinement shows the composition of $[SmNi_2(L^a)_2(\mu\text{-}OAc)(OAc)_2(MeOH)_2]$. Elemental analysis and ESI Mass spectra of isolated crystalline products of the Dy, Er and Yb complexes confirm the molecular formula of $[LnNi_2(L^a)_2(\mu\text{-}OAc)_2Cl]$. ESI Mass spectra of all compositions show main peaks corresponding to the $[LnNi_2(L^a)_2(\mu\text{-}OAc)_2]^+$ ions.

The molecular structures of the isostructural $[NdNi_2(L^a)_2(\mu\text{-}OAc)_2(OAc)(MeOH)_2]$ and $[CeNi_2(L^a)_2(\mu\text{-}OAc)_2(OAc)(MeOH)_2]$ complexes are presented in Figures 2.7a and 2.7b respectively. Each Ni atom coordinates equatorially to two bidentate *N*-arylthiourea sites via *S* and *O* donor atoms. The octahedral coordination spheres of the Ni atoms are each completed by an oxygen atom of the bridging acetato ligand and a solvent MeOH molecule. The Ln ions coordinate to two 2,6-dipicolinoyl moieties via *O,N,O* donor atoms. In addition to that, they coordinate to the *O* donor of two bridging acetato ligands and to a chelating acetato ligand. The coordination environments around the metal ions are illustrated in Figure 2.8. Selected bond lengths are summarized in Table 2.5.

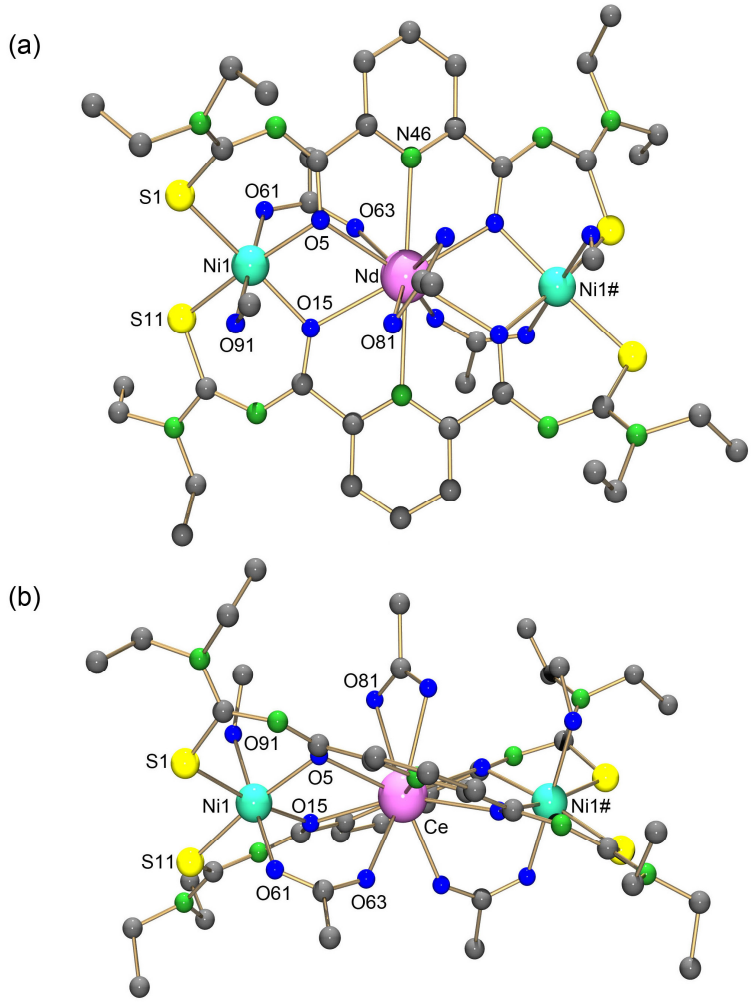

Figure 2.7 Molecular structures of $[LnNi_2(L^a)_2(\mu\text{-}OAc)_2(OAc)(MeOH)_2]$ (a) Ln = Nd, view perpendicular to the plane of the thioureato ligands. (b) Ln=Ce, view parallel to the plane of the thioureato ligands. Hydrogen atoms are omitted for clarity. Labeling of symmetry related atoms see Figure 2.8.

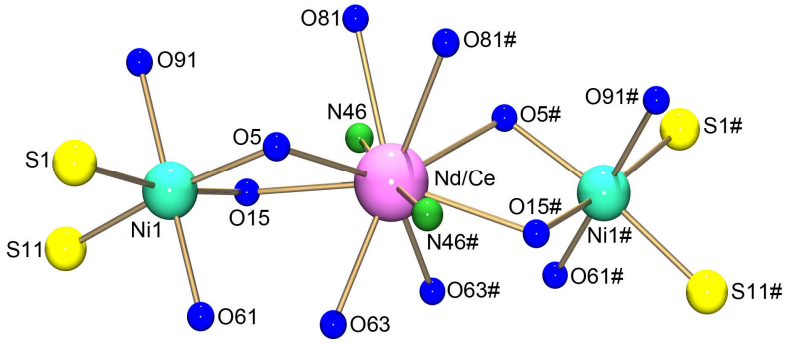

Figure 2.8 Coordination pattern of metal centers in $[LnNi_2(L^a)_2(\mu\text{-}OAc)_2(OAc)\ (MeOH)_2]$ where Ln = Nd or Ce. Symmetry related atoms are produced by a C_2 rotation axis.

Table 2.5 Selected bond lengths (Å) in $[LnNi_2(L^a)_2(\mu\text{-}OAc)_2(OAc)(MeOH)_2]$, where Ln = Nd or Ce.

	Nd/Ce		Nd/Ce
Ln–O5	2.568(3)/2.595(2)	Ln–O15	2.531(2)/2.549(2)
Ln–N46	2.634(3)/2.654(3)	Ln–O63	2.423(3)/2.458(2)
Ln–O81	2.570(3)/2.607(2)	Ni1–S1	2.384(2)/2.383((1)
Ni1–S11	2.338(1)/2.340(1)	Ni1–O5	2.081(2)/2.087(2)
Ni1–O15	2.045(3)/2.051(2)	Ni1–O61	2.062(3)/2.067(2)
Ni1–O91	2.142(3)/2.139(2)		

The equatorial Ni–O5/O15 bond lengths are in the range between 2.045(3) – 2.087(2) Å. The axial Ni–O61 bonds have the values of 2.062(3) Å and 2.067(2) Å and the Ni–O91 bonds are 2.142(3) Å and 2.139(2) Å. The Ni–S1/S11 bonds are in the range between 2.338(1) and 2.384(2) Å. The bond length values around the Ni ions show the presence of a distorted octahedral geometry. The lanthanide ions coordinate to the tridentate 2,6-dipicolynoyl moieties of both ligands via the *N* donor of pyridine rings and the *O* donors of both carbonyl groups. Coordination of two acetate bridges and one bidentate chelating acetato ligand are observed. The coordination number of the lanthanide ions in these cases is 10. The Ce–Ni distance is 3.661(1) Å and the Nd–Ni one is 3.650(1) Å. This may be due to the decrease of ionic radii from Ce^{3+} (1.03 Å) to Nd^{3+} (1.00 Å).

The structure of the complex $[GdNi_2(L^a)_2(\mu\text{-}OAc)_2Cl]$ (Figure 2.9) differs from those of the Ce and Nd complexes only by the replacement of central bidentate acetato ligand by a chlorido ligand. This results in the coordination number of 9 for the Gd atom. The coordination environments around the metal ions are illustrated in Figure 2.10. Selected bond lengths are summarized in Table 2.6. The distance between Gd and Ni is 3.603Å. The complex crystallizes in the monoclinic system and belongs to the space group *C2/c*. The C_2 symmetry axis goes through the Gd–Cl bond. Ni ions have the coordination number of 5 and show a distorted square pyramidal geometry. The axial Ni–O61 bond is 1.967(5) Å. The equatorial Ni–O5/O15 bonds are 2.025(4) and 2.022(4) Å. These are shorter than the equatorial Ni–S1/S11 bonds which are 2.279(2) and 2.379(2) Å respectively. The equatorial bond lengths of Gd^{3+} are 2.592(5) Å for Gd–N46 bond and 2.588(4) and 2.408(4) Å for Gd–O5 and Gd–O15 bonds. The axial Gd–Cl and Gd–O63 bond lengths are 2.649(3) and 2.343(4) Å.

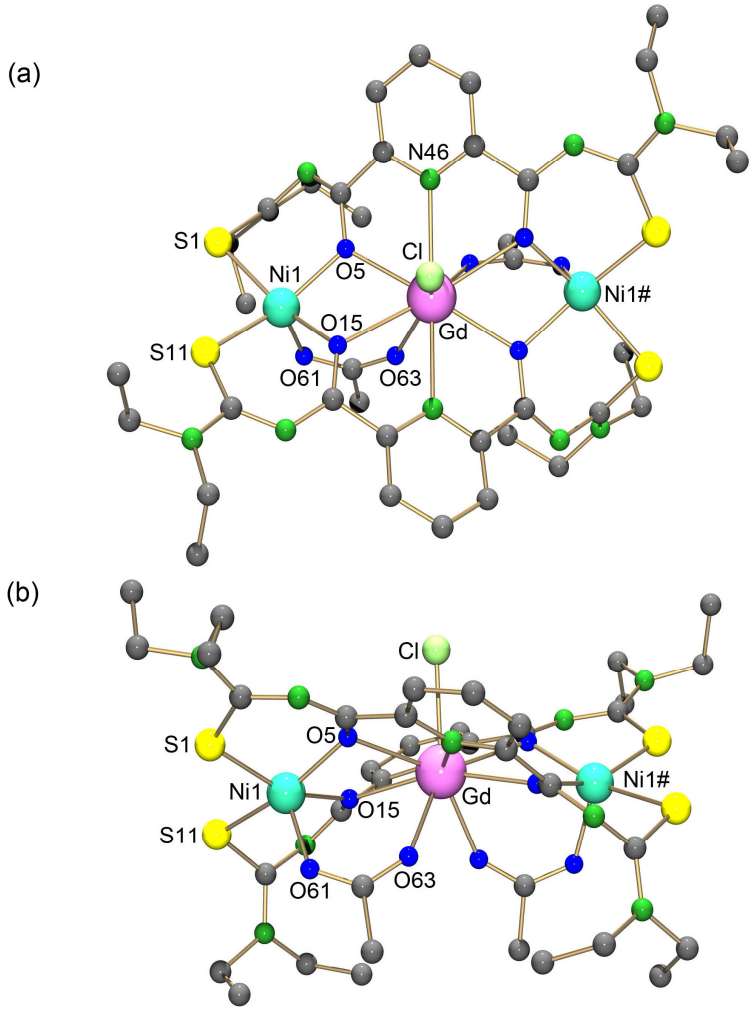

Figure 2.9 Molecular structure of $[GdNi_2(L^a)_2(\mu\text{-}OAc)_2Cl]$. (a) View perpendicular to the plane of the thioureato ligands. (b) View parallel to the plane of the thioureato ligands. Hydrogen atoms are omitted for clarity. Labeling of symmetry related atoms see Figure 2.10.

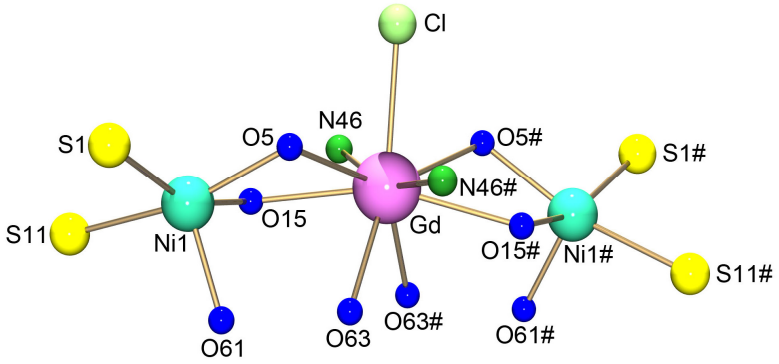

Figure 2.10 Coordination pattern of metal centers in $[GdNi_2(L^a)_2(\mu\text{-}OAc)_2Cl]$. Symmetry related atoms are produced by a C_2 rotation axis.

Table 2.6 Selected bond lengths (Å) in $[GdNi_2(L^a)_2(\mu\text{-}OAc)_2Cl]$.

Gd–O5	2.408(4)	Gd–O15	2.588(4)
Gd–N46	2.592(5)	Gd–O63	2.341(4)
Gd–Cl	2.649(3)	Ni1–S1	2.279(2)
Ni1–S11	2.379(2)	Ni1–O5	2.025(4)
Ni1–O15	2.022(4)	Ni1–O61	1.967(5)

The bond lengths of Gd^{3+} in the complex $[GdNi_2(L^a)_2(\mu\text{-}OAc)_2Cl]$ are in agreement with the lanthanide bond lengths observed in the similar type $[LnCo_2(L^a)_2(\mu\text{-}OAc)_2Cl]$ complexes (Table 2.3). A comparison of such bond lengths is appropriate because of the similar coordination environments around the lanthanide ions. It shows the gradual decrease of bond lengths of Ln^{3+} from Ce^{3+} to Yb^{3+} in each bond length category. This observation is in good agreement with the lanthanide contraction and it is independent of the transition metal ions.

The molecular structure of the nonsymmetric $[SmNi_2(L^a)_2(\mu\text{-}OAc)(OAc)_2(MeOH)_2]$ complex (Figure 2.11), differs from those of the other complexes. Along with the typical coordination mode of aroylthioureato ligand to the metals, a different kind of arrangement of the acetato ligands and solvent MeOH is observed. Instead of two acetato bridges, only one acetato bridge between Ni1 and Sm is established. Two more acetato ligands coordinate to Sm^{3+}, one as a bidentate chelating ligand and the other one as a monodentate ligand. This results in three different types of coordination of acetato ligands in one molecule. The structure shows two different coordination geometries of Ni atoms, where Ni1 is square pyramidal and Ni2 is octahedral. Ni2 coordinates axially to two MeOH ligands. Selected bond lengths of $[SmNi_2(L^a)_2(\mu\text{-}OAc)(OAc)_2(MeOH)_2]$ are summarized in Table 2.7. The bond lengths between the Sm atom and donor atoms of the ligand are in the similar range of those bonds observed previously in the Co complex $[SmCo_2(L^a)_2(\mu\text{-}OAc)_2Cl]$ (Table 2.3). The bond lengths between Sm atom and the *O* atoms of acetato ligands are also in the same range of those observed in other complexes.

The Ln–O5/O15 and Ln–N46/N56 bond lengths in all trinuclear $Ni^{II}Ln^{III}Ni^{II}$ complexes are in the ranges as were discussed previously for the trinuclear $Co^{II}Ln^{III}Co^{II}$ complexes in Chapter 2.2.1. This suggests that the basic coordination mode of the 2,6-dipicolinoyl moiety of the ligand to the central lanthanide atom is widely independent of the transition metal.

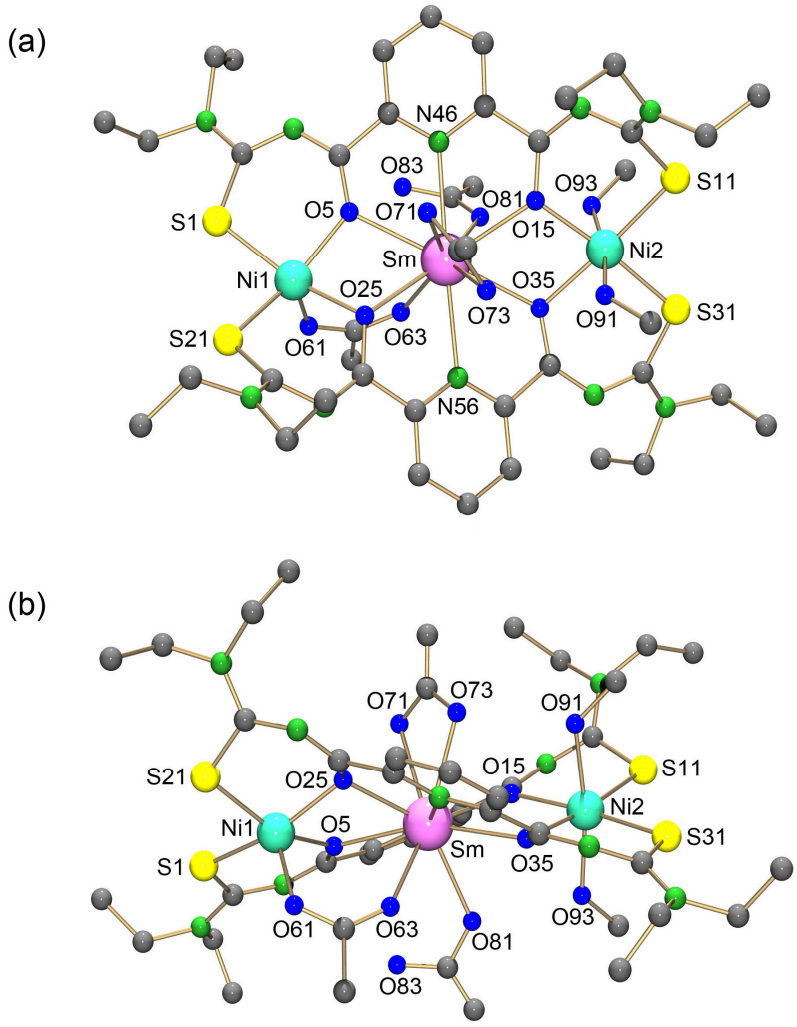

Figure 2.11 Molecular structure of $[SmNi_2(L^a)_2(\mu\text{-}OAc)(OAc)_2(MeOH)_2]$. (a) View perpendicular to the plane of the thioureato ligands. (b) View parallel to the plane of the thioureato ligands. Hydrogen atoms are omitted for clarity.

Table 2.7 Selected bond lengths (Å) in $[SmNi_2(L^a)_2(\mu\text{-}OAc)(OAc)_2(MeOH)_2]$.

Sm–O5/O15	2.502(8)/2.496(9)	Sm–O25/35	2.485(9)/2.532(9)
Sm–N46/N56	2.59(1)/2.63(1)	Sm–O71/73	2.59(1)/2.610(9)
Sm–O63	2.37(1)	Sm–O81	2.55(1)
Ni1–S1/S21	2.291(4)/2.322(5)	Ni2–S11/S31	2.370(5)/2.333(4)
Ni1–O5/O25	2.02(1)/2.069(8)	Ni2–O15/O35	2.054(8)/2.07(1)
Ni2–O91/O93	2.12(1)/2.10(1)	Ni1–O61	1.972(9)

The coordination polyhedra of the lanthanide ions belong to only two types in all crystallographically characterized complexes of type $LnM_2L_2X_3$ (Fig 2.10). The type of polyhedron depends on the coordination number. The lanthanide ions with the coordination number 9 show the polyhedron of Figure 2.12a and those with coordination number 10 shows the polyhedron of Figure 2.12b.

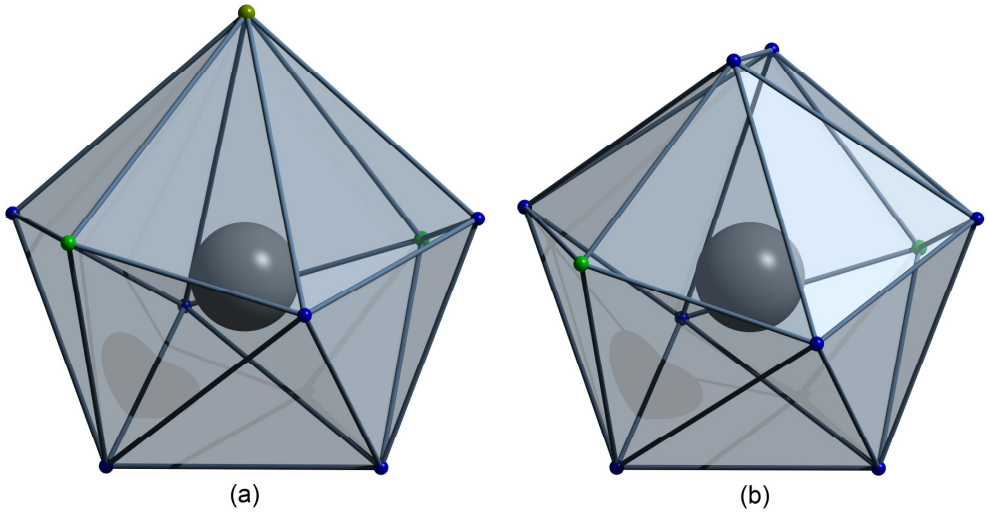

Figure 2.12 Coordination polyhedral of lanthanide centers in complexes of type $LnM_2L_2X_3$.

The equatorial coordination of four *O* and two *N* donor atoms from two dipicolinoyl moieties and the coordination of two *O* donor atoms from acetate ligands are common for all cases. This results in a fixed coordination number of 8 for all lanthanides. The apical monodentate coordination of the additional chlorido or acetato ligand results in the coordination number of 9 and produces the polyhedron of Figure 2.12(a). The apical bidentate coordination of acetato ligand results in the coordination number of 10 and shows the polyhedron of Figure 2.12(b). The complexes of higher coordination numbers are rare. Among them, the most probable polyhedron for the coordination number 9 is tricapped trigonal prism and the very common example for this kind is $[ReH_9]^{2-}$.[92-93] The coordination number 10 normally shows bicapped square antiprism or pentagonal prism.[94-95] The above discussed irregular polyhedra are uncommon for the coordination numbers of 9 and 10

2.3 Complexes of lanthanides and manganese [$Mn^{II}Ln^{III}Mn^{II}$]

There are only two previous reports on trinuclear complexes of the type $Mn^{II}Ln^{III}Mn^{II}$ (where Ln = Gd, Dy or Eu).[96-97] The first trinuclear $Mn^{II}Ln^{III}Mn^{II}$ complex is with a phosphorous based multidentate trishydrazone ligand. One 12-coordinate Ln^{3+} (where Ln = Eu, Gd or Dy) and two octahedral Mn^{2+} ions are present in these complexes (**31**). The Ln–Mn distances are in the range between 3.311 – 3.332 Å.[96] The second trinuclear $Mn^{II}Ln^{III}Mn^{II}$ complex is with a tetradentate Schiff base ligand and exists only with Gd^{3+} (**32**). The Gd–Mn distances in this case are 3.516 and 3.709 Å.[97] The magnetic properties of the above mentioned trinuclear $Mn^{II}Ln^{III}Mn^{II}$ complexes suggest the presence of weak ferromagnetic interactions between Ln^{3+} and Mn^{2+} ions.

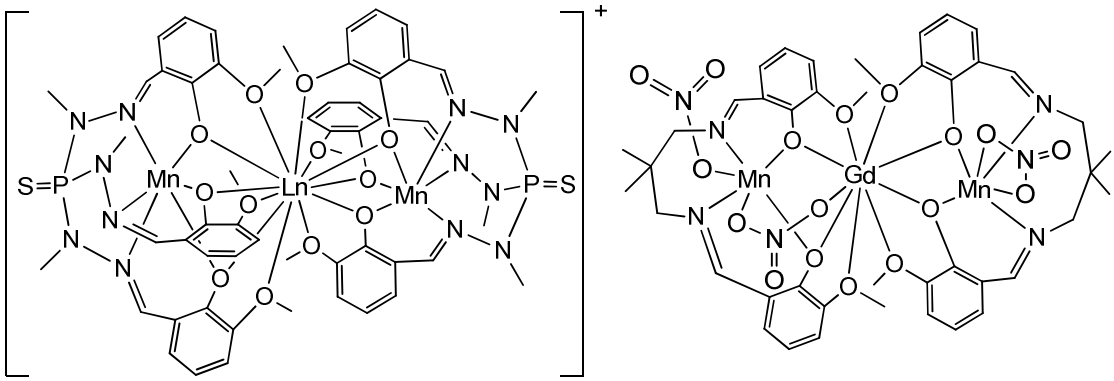

Chart 2.4 Previously reported trinuclear $Mn^{II}Ln^{III}Mn^{II}$ type complexes.[96-97]

This chapter introduces novel trinuclear $Mn^{II}Ln^{III}Mn^{II}$ complexes with the multidentate H_2L^a ligand. Two equivalents of H_2L^a react with one equivalent of $LnCl_3$ and two equivalents of $Mn(Oac)_2{\cdot}4H_2O$ in MeOH at 40 °C under formation of trinuclear complexes of the composition $[LnMn_2(L^a)_3]Cl$ (**33**) (Scheme 2.5). The products were isolated as orange-red precipitates and are readily soluble in CH_2Cl_2 and $CHCl_3$. The IR spectra of the complexes confirm the deprotonation of the ligands by the missing NH stretchings at 3273 cm^{-1}. The chelate formation of the ligands is confirmed by the shifts of the νC=O stretching vibrations from 1686 cm^{-1} in H_2L^a to a range between 1586 and 1591 cm^{-1} in the complexes. The ESI mass spectra of the products show their major peaks for ions of the composition $[LnMn_2(L^a)_3]^+$ and the elemental analysis values agree with the calculated values for

$[LnMn_2(L^a)_3]Cl$. The complexes were recrystallized from a variety of solvent mixtures in an attempt to grow crystals suitable for X-ray analysis, but no satisfactory crystals were obtained.

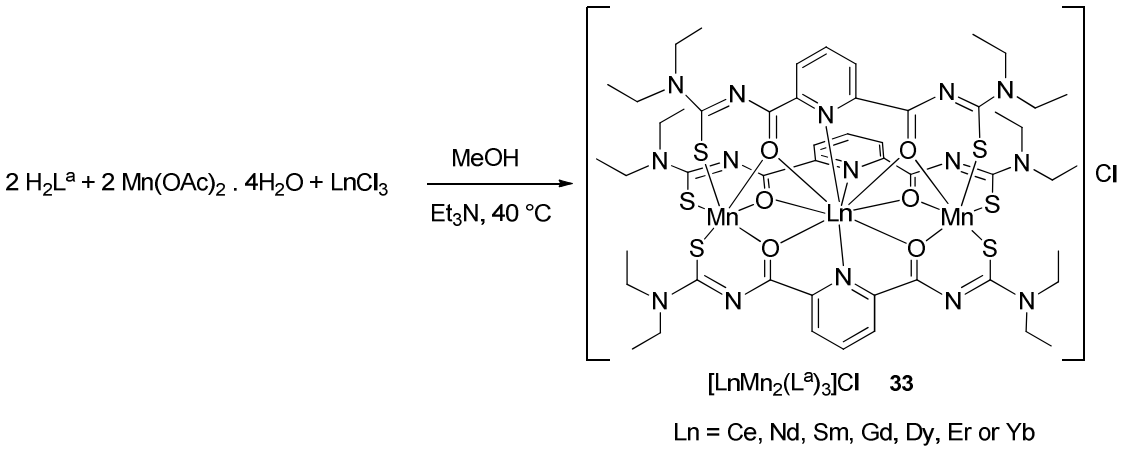

Scheme 2.5 Synthesis of trinuclear complexes with lanthanides (III) and manganese (II)

In addition to that, slow evaporation of the mother solutions in the cases of Ln = Gd and Ce gave single crystals suitable for X-ray crystallography. It shows the coordination of two ligands to one Ln^{III} and two Mn^{II} ions along with two bridging acetato ligands, which are considered as side products.

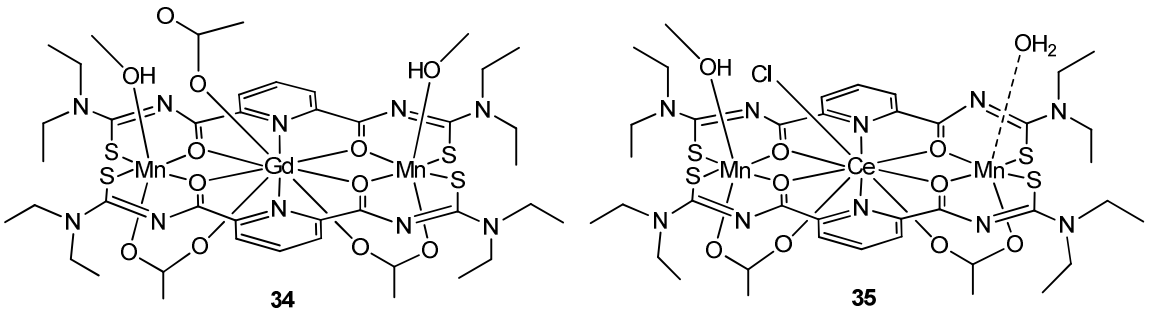

Chart 2.4 Structures of the side products obtained with Gd (**34**) and Ce (**35**).

The molecular structures of the complexes $[GdMn_2(L^a)_2(\mu\text{-}OAc)_2(OAc)(MeOH)_2]$ (**34**) and $[CeMn_2(L^a)_2(\mu\text{-}OAc)_2Cl(MeOH)(H_2O)]$ (**35**) are presented in Figures 2.13 and 2.14 respectively. Structural differences between the side products are observed in the coordination of the lanthanide, where Gd atom coordinates to a monodentate acetato ligand (Fig 2.13) and Ce atom coordinates to a chlorido ligand (Fig 2.15).

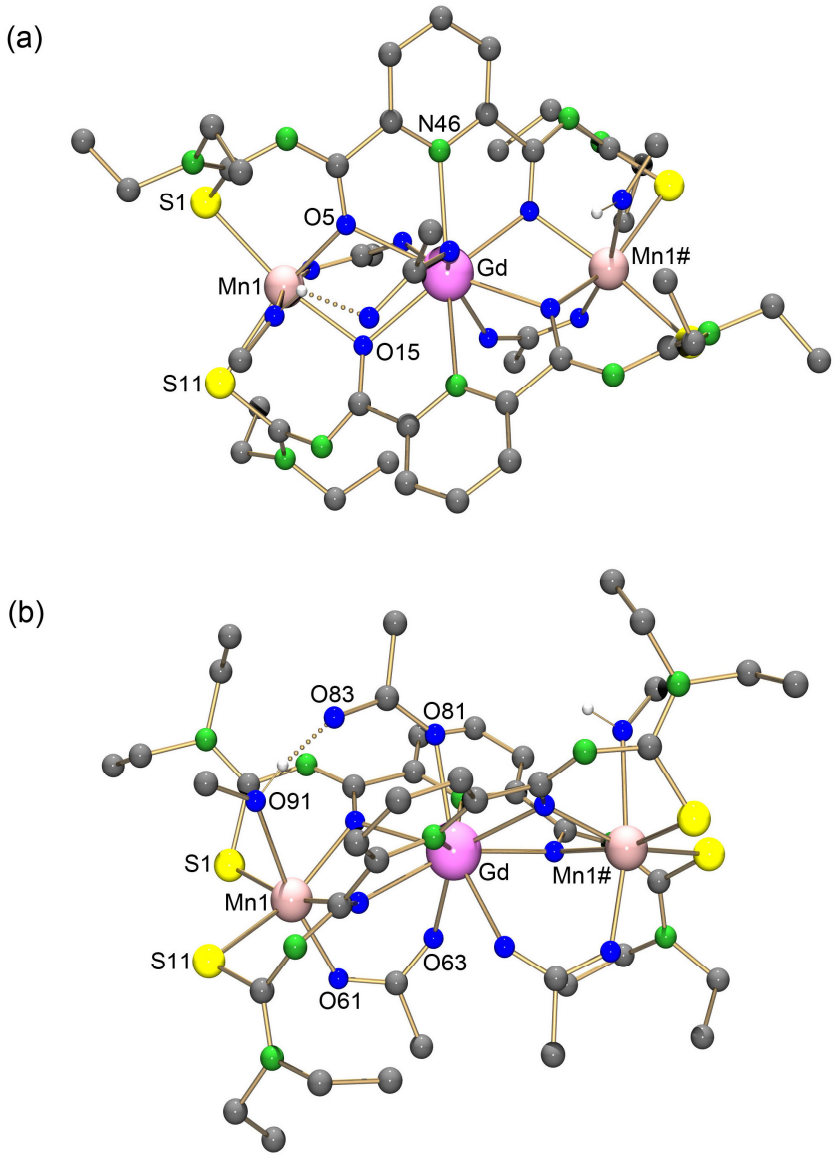

Figure 2.13 Molecular structure of $[GdMn_2(L^a)_2(\mu\text{-}OAc)_2(OAc)(MeOH)_2]$ (**34**). (a) View perpendicular to the plane of the thioureato ligands. (b) View parallel to the plane of the thioureato ligands. Hydrogen atoms are omitted for clarity. Labeling of symmetry related atoms see Figure 2.14.

The structure of the complex $[GdMn_2(L^a)_2(\mu\text{-}OAc)_2(OAc)(MeOH)_2]$ is axially symmetric (Figure 2.13) and the symmetry-related atoms are produced by a C_2 axis going through the Gd atom and is perpendicular to the thioureato ligand plane. In addition to the donor atoms of the organic ligands, the Gd atom coordinates to two *O* donors of the bridging acetato ligands and one *O* donor of the monodentate acetato ligand. Therefore, it shows the coordination number of 9 and belongs to the polyhedron in Figure 2.12(a).

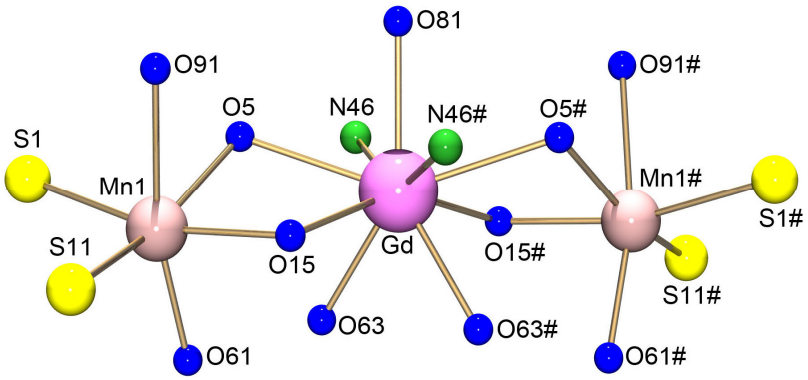

Figure 2.14 Coordination patterns of the metal centers in $[GdMn_2(L^a)_2(\mu\text{-}OAc)_2(OAc)(MeOH)_2]$. Symmetry related atoms are produced by a C_2 rotation axis.

Table 2.8 Selected bond lengths (Å) in $[GdMn_2(L^a)_2(\mu\text{-}OAc)_2(OAc)(MeOH)_2]$ (**34**).

Gd–O5	2.522(3)	Gd–O15	2.414(3)	Gd–N46	2.576(3)
Gd–O63	2.356(3)	Gd–O81	2.375(5)	Mn1–O61	2.081(4)
Mn1–S1	2.486(1)	Mn1–S11	2.515(2)	Mn1–O91	2.438(6)
Mn1–O5	2.144(3)	Mn1–O15	2.156(3)		
Hydrogen bonds					
D-H….A	d(D-H)	d(H…..A)	d(D…..A)	<(DHA)	
O91-H91…O83	0.93	1.82	2.52(1)	129.8	

Selected bond lengths of $[GdMn_2(L^a)_2(\mu\text{-}OAc)_2(OAc)(MeOH)_2]$ are summarized in Table 2.8. The bond lengths of Gd to the donor atoms of the ligands are in the range of bond lengths observed in the previously discussed Co and Ni complexes. The bond length of Gd–O63 is 2.356(3) Å and that of Gd–O81 is 2.375(5) Å. These are in the normal range of those observed in the previously discussed complexes with acetato ligand coordination (Chapter 2.1 and 2.2). The Mn atoms are symmetry-related. The Mn^{2+} ion coordinates equatorially to two aroylthioura moieties via *S* and *O* donors. The octahedral coordination geometry of the Mn ion is completed by the axial coordination of two *O* donor atoms. One is from the bridging acetato ligand and the other one is from MeOH. The equatorial Mn–O5/O15 bond lengths are 2.144(3) and 2.156(3) Å and Mn–S1/S11 bond lengths are 2.486(1) and 2.515(2) Å respectively. The axial Mn–O91 bond length is 2.438(6) Å. Therefore, the Mn^{2+} ion has a distorted octahedral geometry. An intramolecular hydrogen bond is presence between the hydrogen (H91) of the coordinated MeOH and the uncoordinated oxygen atom (O83) of the monodentate acetato ligand.

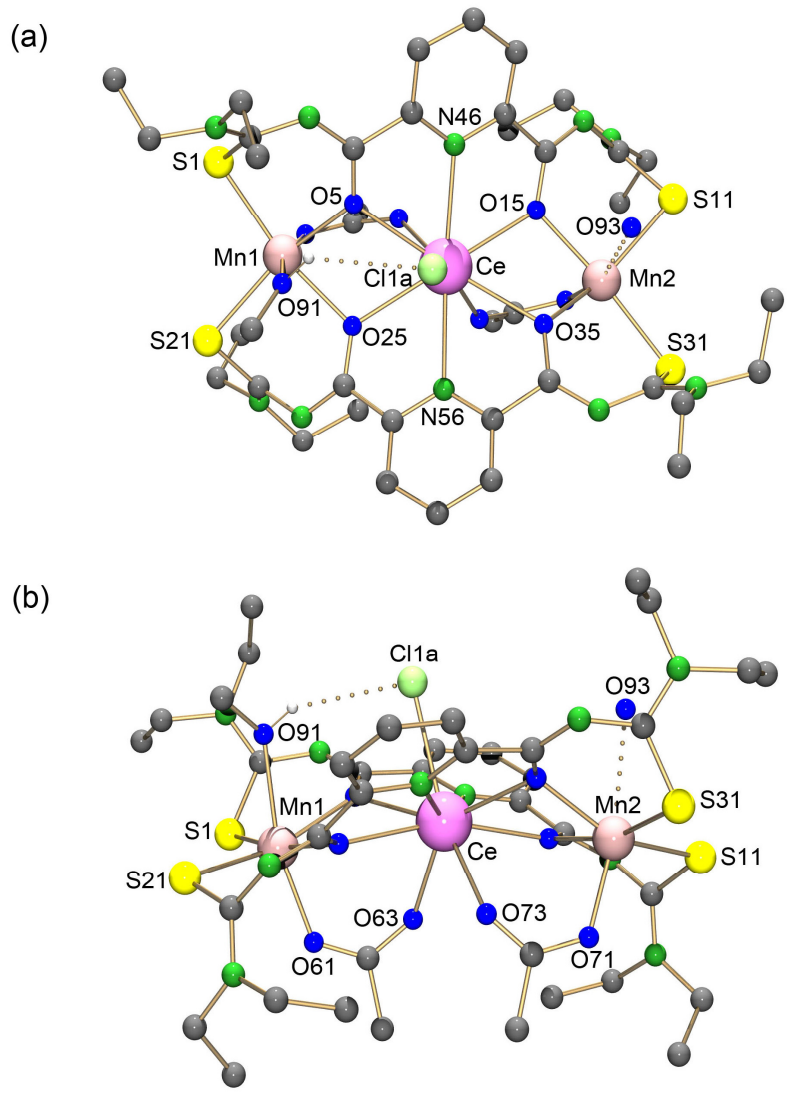

Figure 2.15 Molecular structure of $[CeMn_2(L^a)_2(\mu\text{-}OAc)_2Cl(MeOH)(H_2O)]$ (**35**). (a) View perpendicular to the plane of the thioureato ligands, (b) View parallel to the plane of the thioureato ligands. Hydrogen atoms are omitted for clarity. Labeling of symmetry related atoms see Figure 2.16.

The molecular structure of the complex $[CeMn_2(L^a)_2(\mu\text{-}OAc)_2Cl(MeOH)(H_2O)]$ is asymmetric (Figure 2.15). In addition to the thioureato ligands and two bridging acetato ligands, the Ce^{3+} ion coordinates to an apical chlorido ligand. This results in a 9-coordination number for Ce atom. Therefore the coordination polyhedron of Ce atom in this complex is similar to that of the Gd atom discussed above. The selected bond lengths of $[CeMn_2(L^a)_2(\mu\text{-}OAc)_2Cl(MeOH)(H_2O)]$ are summarized in Table 2.9. The bond lengths of the Ce atom to the donor atoms of the ligands are in the range of those observed in the previously discussed Co and Ni complexes. The bond lengths between Ce and the bridging acetato ligands are in the

typical range of those observed in previous chapters. Both Mn1 and Mn2 ions equatorially coordinate to two aroylthiourea moieties. The equatorial Mn–O bond lengths are in the range between 2.157(4) and 2.186(4) Å. The equatorial Mn–S bond lengths are in the range between 2.497(2) and 2.548(2) Å. The bond lengths between Mn atoms and donor atoms of the thioureato ligands are longer compared to the corresponding bond lengths between Co or Ni and donor atoms of the ligand.

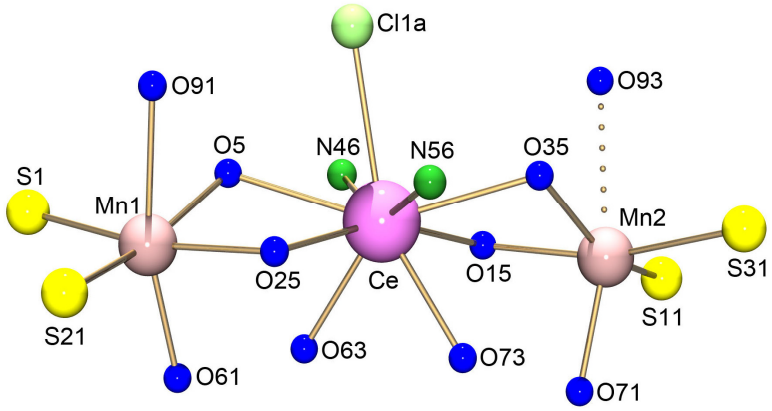

Figure 2.16 Coordination patterns of the metal centers in $[CeMn_2(L^a)_2(\mu\text{-}OAc)_2Cl(MeOH)(H_2O)]$. Symmetry related atoms are produced by a C_2 rotation axis.

Table 2.9 Selected bond lengths (Å) in $[CeMn_2(L^a)_2(\mu\text{-}OAc)_2Cl(MeOH)(H_2O)]$ (**30**).

Ce–O5	2.483(4)	Ce–O15	2.582(4)	Ce–O25	2.597(4)
Ce–O35	2.489(4)	Ce–N46	2.679(4)	Ce–N56	2.669(4)
Ce–O63	2.411(5)	Ce–O73	2.439(4)	Ce–Cl1a	2.903(4)
Mn1–S1	2.548(2)	Mn1–S21	2.501(2)	Mn2–S11	2.497(2)
Mn2–S31	2.526(2)	Mn1–O5	2.186(4)	Mn1–O25	2.157(4)
Mn2–O15	2.159(4)	Mn2–O35	2.157(4)	Mn1–O61	2.126(5)
Mn2–O71	2.086(5)	Mn1–O91	2.379(6)	Mn2–O93	2.867(6)
Hydrogen bonds					
D-H….A	d(D-H)	d(H…..A)	d(D…..A)	<(DHA)	
O91-H91…Cl1A	0.93	2.72	3.382(7)	128.6	

The octahedral geometry of Mn1 ion is completed by the axial coordination of the bridging acetato and MeOH ligands. The Mn2 ion axially coordinates a bridging acetato ligand. A water molecule is coordinated to the Mn2 ion from the opposite side of the bridging acetato ligand. The bond lengths between Mn and bridging acetato ligands, Mn1–O61 and Mn2–O71

are 2.126(5) and 2.086(5) Å respectively. The axial Mn1–O91 and Mn–O93 bond lengths are 2.379(6) Å and 2.867(6) Å respectively. The long Mn2–O93 bond should be regarded as a weak interaction. An intramolecular hydrogen bond is present. It is located between the hydrogen atom (H91) of the MeOH and the chlorido ligand.

W-band EPR spectra of the complexes $[GdMn_2(L^a)_3]Cl$ and $[YbMn_2(L^a)_3]Cl$ were measured in the solvent mixture of $CHCl_3$/toluene at 5 K. The spectra differ from the background and are presented in Figure 2.17. The expected number of unpaired electrons in the case of $[GdMn_2(L^a)_3]Cl$ complex is 17. There are 5 unpaired electrons each from Mn^{2+} ions and 7 from Gd^{3+} ion. In the case of complex $[YbMn_2(L^a)_3]Cl$, Yb^{3+} has one unpaired electron and two Mn^{2+} ions have together 10 unpaired electrons, which is a total of 11 unpaired electrons. Expectedly, they give complicated spectra with hyperfine couplings. But, the interpretation of the recorded spectra was not possible.

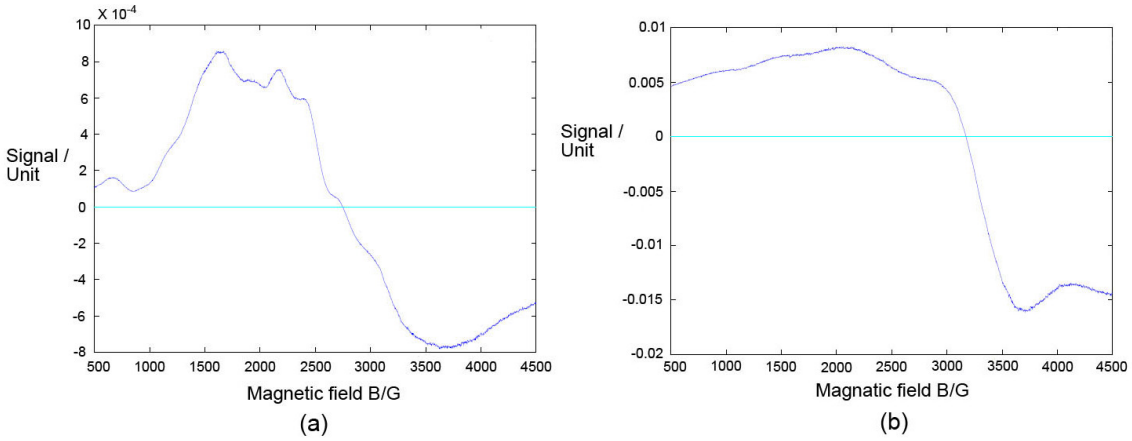

Figure 2.17 W-band (94 GHz) EPR Spectra of (a) $[GdMn_2(L^a)_3]Cl$ and (b) $[YbMn_2(L^a)_3]Cl$ complexes in $CHCl_3$/Toluene (1:1 mixture) at 5 K.

2.4 Complexes of lanthanides and copper [$Cu^{II}Ln^{III}Cu^{II}$]

Trinuclear $Cu^{II}Ln^{III}Cu^{II}$ systems have been continuously investigated on the basis of their magnetic interactions compared to those of with other transition metals ions such as Co^{2+}, Ni^{2+} and Mn^{2+}.[70] The reason may be the well-studied and well understood magnetic behavior of the Cu^{2+} ion which possesses a single unpaired electron. This leads to the understanding of the experimental results, much easier compared to the complexes with other transition metals with more complicated magnetic properties.[46, 72, 75, 78]

This chapter introduces novel trinuclear $Cu^{II}Ln^{III}Cu^{II}$ complexes with the multidentate ligand H_2L^a. A mixture of one equivalent $LnCl_3$ and two equivalents of $Cu(OAc)_2 \cdot H_2O$ reacts rapidly with two equivalents of H_2L^a in MeOH at 40 ° in the presence of Et_3N. Stable products precipitated directly from the reaction mixture. Reactions with Ce, Nd, Sm, Gd and Dy give trinuclear $Cu^{II}Ln^{III}Cu^{II}$ complexes of the composition $[LnCu_2(L^a)_2(\mu\text{-}OAc)_2(OAc)]$ (**36**), while with Er and Yb trinuclear $Cu^{II}Ln^{III}Cu^{II}$ complexes of the composition $[LnCu_2(L^a)_3]Cl$ (**37**) are formed (Scheme 2.6). The products were recrystallized from a variety of solvent mixtures in order to grow crystals suitable for X-ray analysis, but no satisfactory crystals were obtained.

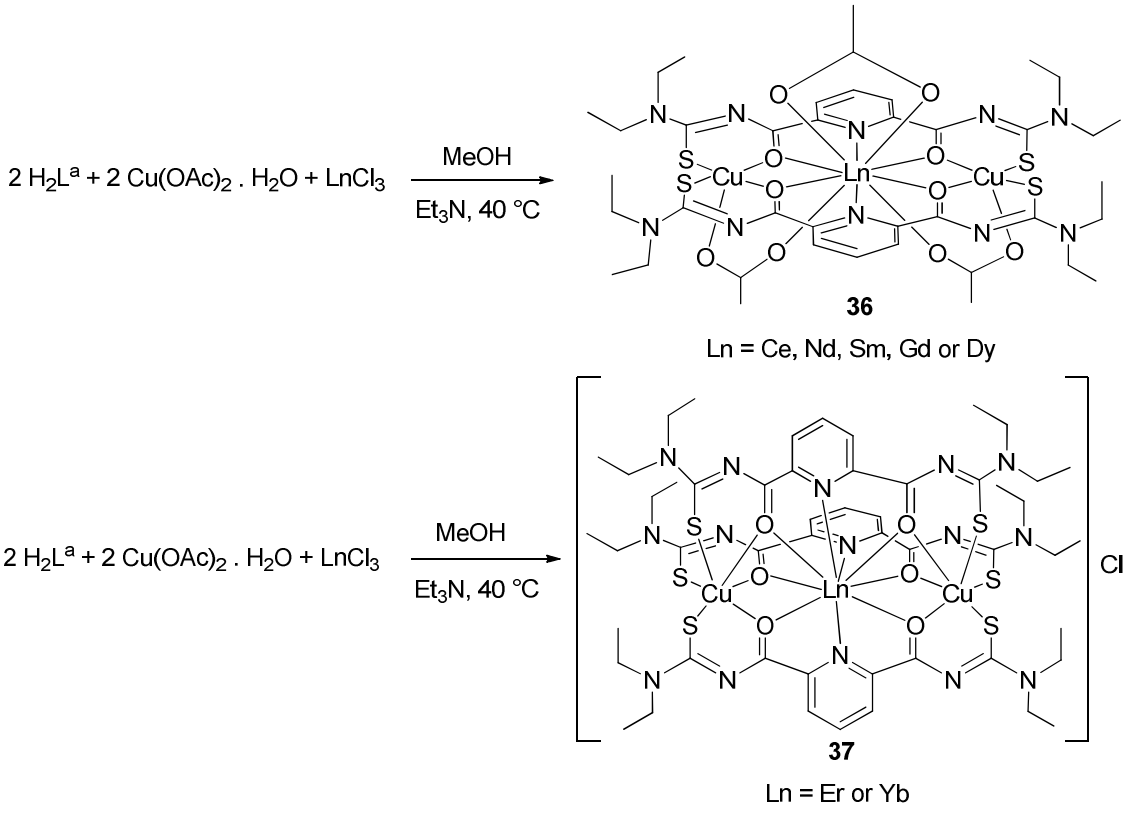

Scheme 2.6 Synthesis of trinuclear complexes with lanthanides (III) and copper (II)

IR spectroscopy shows the deprotonation and chelate formation of the thioureato ligands by the missing stretching vibration at 3273 cm^{-1} and the shifts of the $\nu_{C=O}$ vibrations of the thioureato ligands. The $\nu_{C=O}$ stretching vibrations are shifted from 1686 cm^{-1} in H_2L^a to a range between 1585 and 1590 cm^{-1} in the complexes. The ESI mass spectra show peaks corresponding to the molecular ions of the compositions $[LnCu_2(L^a)_2(\mu\text{-}OAc)_2]^+$ for Ln = Ce, Nd, Sm, Gd or Dy and $[LnCu_2(L^a)_3]^+$ for Ln = Er and Yb. Therefore the mass spectra confirm the formation of bis complexes in the cases of Ln = Ce, Nd, Sm, Gd and Dy and tris complexes in the cases of Ln = Er and Yb. The elemental analyses of the complexes confirm the composition of the complexes in each case.

Interestingly, in the case of Ln = Ce, slow evaporation of the mother solution gave a few single crystals of a side-product suitable for X-ray analysis. The molecular structure of this compound shows the formation of a complex of the composition $[CeCu_2(L^a)_2Cl_3]$. It is presented in Figure 2.18. The molecule is axially symmetric. The symmetry axis goes through the Ce–Cl1 bond and is perpendicular to the thioureato ligand plane.

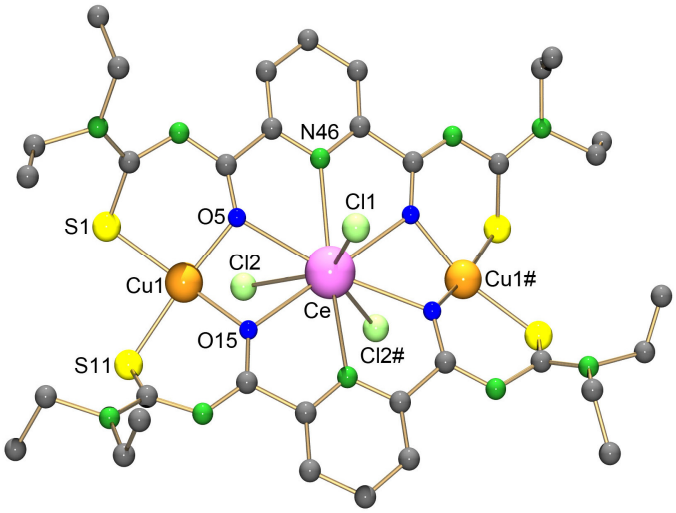

Figure 2.18 Molecular structure of $[CeCu_2(L^a)_2Cl_3]$. Hydrogen atoms are omitted for clarity. Labeling of symmetry related atoms see Figure 2.19.

In addition to the coordination of one Ce^{3+} ion and two Cu^{2+} ions to two thioureato ligands, the coordination of three chlorido ligands to the Ce atom is observed. Therefore, the cerium atom exhibits the coordination number nine. The coordination polyhedron is that of Figure 2.12a. Cu^{2+} ions are equatorially coordinated to two aroylthiourea moieties and show a square

planer coordination sphere. The coordination patterns of the metal ions are presented in Figure 2.19.

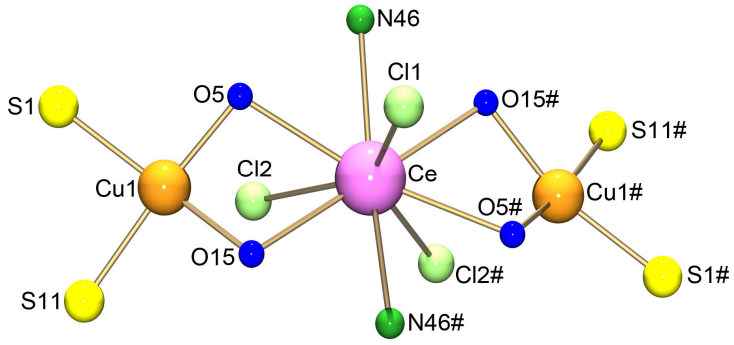

Figure 2.19 Coordination patterns of the metal ions in $[CeCu_2(L^a)_2Cl_3]$. Symmetry related atoms are produced by a C_2 rotation axis.

Table 2.10 Selected bond lengths (Å) in $[CeCu_2(L^a)_2Cl_3]$.

Ce–O5	2.54(1)	Ce–O15	2.62(1)	Ce–N46	2.67(2)
Ce–Cl1	2.81(1)	Ce–Cl2	2.915(6)	Cu1–O5	2.02(1)
Cu1–S1	2.278(6)	Cu1–S11	2.258(7)	Cu1–O15	1.98(1)

Selected bond lengths of the complex $[CeCu_2(L^a)_2Cl_3]$ are summarized in Table 2.10. The bond lengths of Ce atom to the donor atoms of the organic ligand are in the range of those observed in the previously discussed trinuclear complexes with Co (Table 2.3), Ni (Table 2.5) and Mn (Table 2.9). The Ce–Cl1 and Ce–Cl2 bond lengths are 2.81(1) and 2.915(6) Å respectively. The previously observed Ce–Cl bond lengths are 2.761(2) Å in the complex $[CeCo_2(L^a)_2(\mu\text{-}OAc)_2Cl]$ (Table 2.3) and 2.903(4) Å in the complex $[CeMn_2(L^a)_2(\mu\text{-}OAc)_2Cl(MeOH)(H_2O)]$ (Table 2.9). The equatorial Cu–S1/S11 and Cu–O5/O15 bond lengths are 2.278(6) / 2.258(7) Å and 2.02(1) / 1.98(1) Å respectively. These bond lengths are in the same range as observed for binuclear Cu complexes of isophthaloylbis(thiourea) ligands.[31] The Ce–Cu distance is 3.527(1) Å.

2.5 Complexes of lanthanides and zinc [$Zn^{II}Ln^{III}Zn^{II}$]

Trinuclear $Zn^{II}Ln^{III}Zn^{II}$ complexes (Ln = lanthanide, except Pm, Tm, Yb and Lu) with 2,6-di(acetoacetyl)pyridine ligands have previously been reported. The Zn^{2+} ion is diamagnetic. That's why no magnetic interactions are possible between Ln^{3+} and Zn^{2+} ions. Such compounds have been used as references in the studies of magnetic interactions between Ln^{3+} and M^{2+} in the analogous trinuclear $M^{II}Ln^{III}M^{II}$ (M = Cu and Ni) compounds.[45-46] In addition to that, a number of trinuclear $Zn^{II}Ln^{III}Zn^{II}$ systems with *N, N'*-bis(salicylidene) derivatives and their luminescence properties have been reported (Chart 2.5).[98-101]

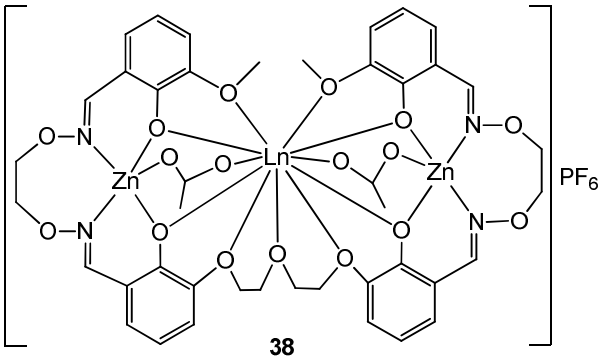

38

Ln = La, Ce, Pr, Nd, Sm, Eu or Gd

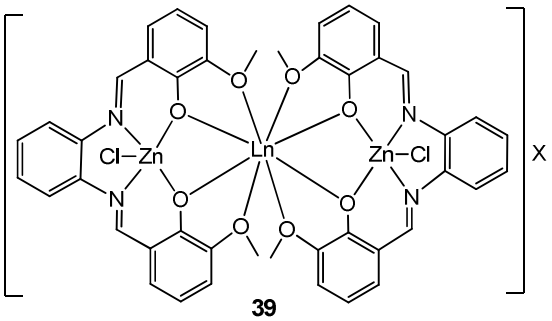

39

Ln = Nd, Eu, Gd, Tb or Dy X = CH_3COO^-, Cl^- or 1/2 $ZnCl_4^{2-}$

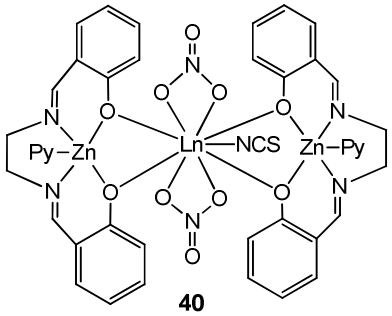

40

Ln = Nd, Gd, Er or Yb

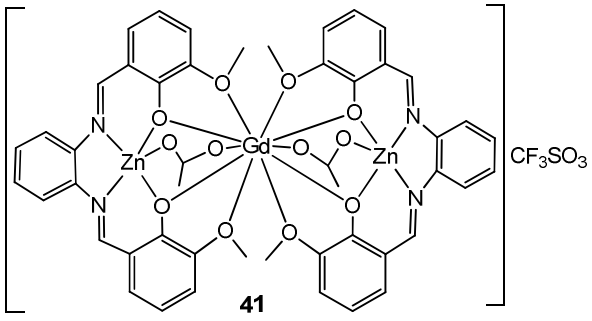

41

Chart 2.5 Previously reported trinuclear $Zn^{II}Ln^{III}Zn^{II}$ type complexes.[98-101]

The trinuclear complex (**38**) contains a tetraanionic *N, N'*bis(3-methoxysalicylidene) ligand. It has acetato bridges between Ln^{3+} and Zn^{2+} ions and the cationic complex is neutralized by a PF_6^- anion. The Ln atoms coordinate to 11 *O* donor atoms, two of them are from acetato bridges and 9 are from the organic ligands.[98] The trinuclear complex (**39**) contains two *N, N'*-bis(3-methoxysalicylidene)benzene-1,2-diamine ligands. A chlorido ligand completes the coordination sphere of Zn^{2+} and Ln^{3+} ion coordinated to 8 *O* donor atoms, 4 each from two ligands. This complex is neutralized either by acetato, chlorido or tetrachloridozincate(II) anions.[99] Two bianionic *N, N'*-bis(salicylidene)ethylenediamine ligands coordinate to two Zn^{2+} and one Ln^{3+} ions in the complex (**40**). The coordination of additional pyridine ligands to the Zn^{2+} ions is observed. In addition to that, nitrato and isothiocyanato ligands coordinate to the Ln^{3+} ion and compensate the total charge of the complex.[101] The complex (**41**) contains two *N, N'*-bis(3-methoxysalicylidene)benzene-1,2-diamine ligands which is the same ligand in the complex (**39**). Two acetato bridges between metal ions are observed and the complex is neutralized by a triflate anion.[100]

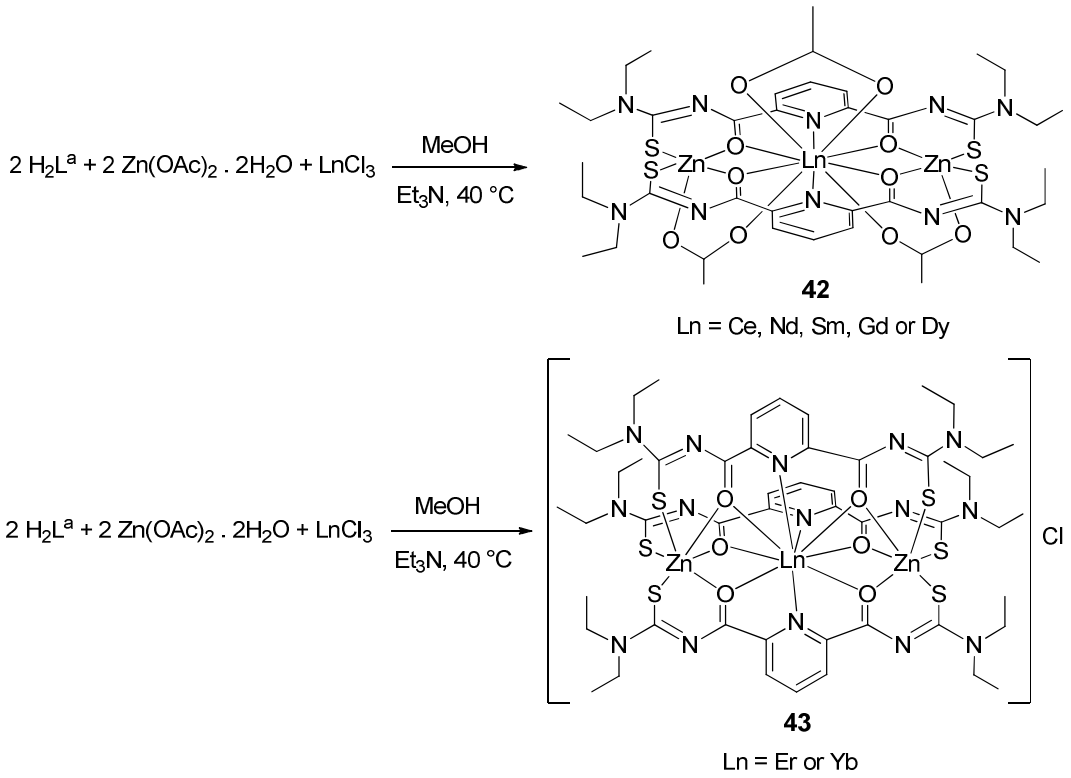

Scheme 2.7 Synthesis of trinuclear complexes with lanthanides (III) and zinc (II)

This chapter introduces novel trinuclear $Zn^{II}Ln^{III}Zn^{II}$ complexes with the H_2L^a ligand. Mixtures of one equivalent $LnCl_3$ and two equivalents of $Zn(OAc)_2{\cdot}2H_2O$ rapidly react with

three equivalents of H_2L^a in MeOH at 40 ° in the presence of Et_3N. Stable, solid products were collected directly from the reaction mixtures in high yields. Reactions with Ln = Ce, Nd, Sm, Gd or Dy give $Zn^{II}Ln^{III}Zn^{II}$ trinuclear complexes with two coordinated organic ligands. They have the composition of $[LnZn_2(L^a)_2(\mu\text{-}OAc)_2(OAc)]$ (**42**). Reactions with Ln = Er or Yb give $Zn^{II}Ln^{III}Zn^{II}$ complexes with three coordinated organic ligands and the composition $[LnZn_2(L^a)_3]Cl$ (**43**) (Scheme 2.7). Similar compositions of the complexes have been observed for the trinuclear $Cu^{II}Ln^{III}Cu^{II}$ analogs with the H_2L^a ligand. The products were recrystallized from various solvent mixtures in an attempt to grow single crystals suitable for X-ray analysis. Measurable single crystals were obtained only in the case of Gd from a CH_2Cl_2/MeOH (1:1) mixture.

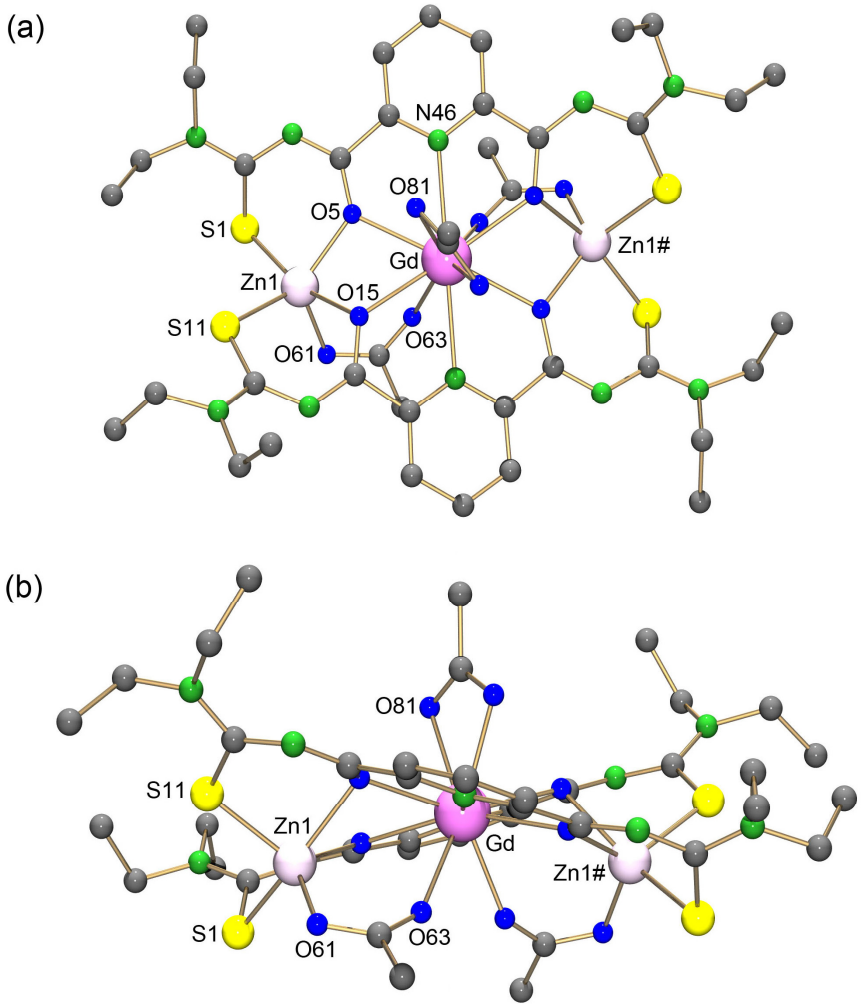

Figure 2.20 Molecular structure of $[GdZn_2(L^a)_2(\mu\text{-}OAc)_2(OAc)]$. (a) View perpendicular to the plane of the thioureato ligands. (b) View parallel to the plane of the thioureato ligands. Hydrogen atoms are omitted for clarity. Labeling of symmetry related atoms see Figure 2.21.

The deprotonation of the ligand is confirmed by the missing NH stretching frequencies at 3273 cm^{-1} in the IR spectra of the complexes. In addition to that, the IR spectra further confirm the chelate formation of the thioureato ligand through the shifts of the $\nu_{C=O}$ vibrations. The $\nu_{C=O}$ stretching vibrations are shifted from 1686 cm^{-1} in H_2L^a to a range between 1586 and 1590 cm^{-1} in the complexes. The ESI mass spectra show peaks corresponding to the molecular ions of the compositions $[LnZn_2(L^a)_2(\mu\text{-}OAc)_2]^+$ for Ln = Ce, Nd, Sm, Gd and Dy, and $[LnZn_2(L^a)_3]^+$ for Ln = Er and Yb. The products were further analyzed by elemental analysis and the results are in agreement with the complex compositions. The molecular structure of $[GdZn_2(L^a)_2(\mu\text{-}OAc)_2(OAc)]$ is presented in Figure 2.20. The crystal structure is calculated in the monoclinic space group C2/c. The symmetry related atoms are generated by a C_2 rotation axis. The C_2 symmetry axis goes through the Gd atom and is perpendicular to the thioureato ligand plane. The coordination patters of the metal centers are presented in Figure 2.21.

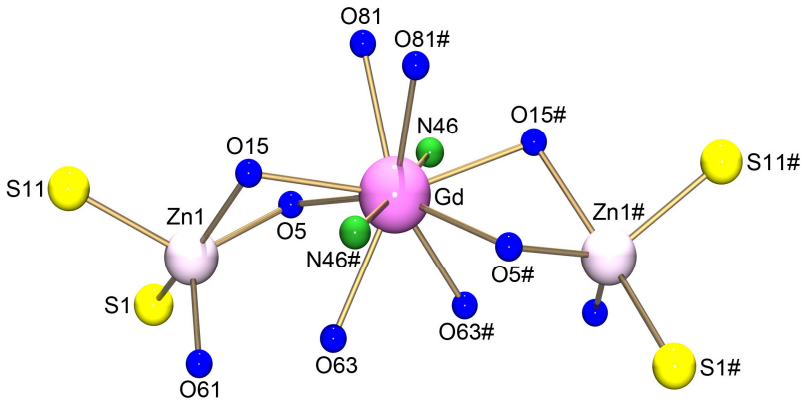

Figure 2.21 Coordination patterns of the metal centers in $[GdZn_2(L^a)_2(\mu\text{-}OAc)_2(OAc)]$. Symmetry related atoms are produced by a C_2 rotation axis.

Table 2.11 Selected bond lengths (Å) in $[GdZn_2(L^a)_2(\mu\text{-}OAc)_2(OAc)]$.

Gd–O5	2.486(4)	Gd–O15	2.495(4)	Gd–N46	2.628(4)
Gd–O63	2.426(4)	Gd–O81	2.454(4)	Zn1–O61	1.988(4)
Zn1–S1	2.341(2)	Zn1–S11	2.358(2)	Zn1–O15	2.268(4)
Zn1–O5	2.047(4)				

The Gd ion shows the typical coordination to the H_2L^a ligand. It coordinates to two 2,6-dipicolinoyl moieties via *O,N,O* donor atoms each. The coordination of two bridging acetato ligands between the Gd and Zn ions and an additional bidentate acetato ligand to the Gd ion

are observed. The Gd atom exhibits a coordination number of 10. The Zn^{2+} ions coordinate to two aroylthiourea moieties via *O,S* donor atoms and to an acetato bridge via *O* donor atom. Selected bonds in $[GdZn_2(L^a)_2(\mu\text{-}OAc)_2(OAc)]$ are summarized in Table 2.11. The Gd–O5/O15 and Gd–N46 bond lengths are 2.486(4)/2.495(4) Å and 2.684(4) Å respectively. The axial Gd–O63 and Gd–O81 bond lengths are 2.426(4) and 2.454(4) Å respectively. These are in the similar range of the corresponding bonds observed in other trinuclear complexes with bridging acetato ligands reported in the Chapters 2.1, 2.2 and 2.3. The Zn–S1/S11 and Zn–O5/O15 bonds are 2.341(2)/2.358(2) and 2.268(4)/2.047(4) Å respectively. The axial Zn–O61 bond is 1.988(4) Å. The Gd–Zn distance is 3.621(3) Å, a value, which has also been found for the Gd–Co distance in $[GdCo_2L^a{}_2(\mu\text{-}OAc)_2(OAc)]$. This is due to the equal ionic radius of 0.74 Å for both Co^{2+} and Zn^{2+}.

Chapter 3

Trinuclear mixed-metal complexes of alkaline earth metals and transition metals with 2,6-dipicolinoylbis(*N,N*-dialkylthioureas)

Trinuclear mixed-metal complexes of alkaline earth metals and transition metals with 2,6-dipicolinoylbis(*N,N*-dialkylthioureas)

Mixed metal complexes between transition metals and alkaline earth metals with chelating ligand systems are not well explored. A reason may be the difficulties to obtain suitable chelating ligand systems which can accept soft transition metals and hard alkaline earth metals simultaneously. The first trinuclear complex with alkaline earth metal (M^a) and transition metal (M^b) in the form of M^b-M^a-M^b was reported by *Costes* et al. in 1997.[102] Two bianionic salicylaldiminato derivatives form a trinuclear complex with two Ni^{2+} and one Ba^{2+} ions (**44**). The complex was crystallized with two perchlorate counterions. In addition to that, trinuclear ZnM^aZn (where M^a = Ca, Sr or Ba) complexes have been reported with *N, N'*-bis(salicylidene) derivatives. These complexes are neutralized by two acetato ligands, which form two acetato bridges in the cases of M^a = Ba or Sr (**45**) or coordinate as monodentate acetato ligands in the case of M^a = Ca (**46**) (Chart 3.1).[98]

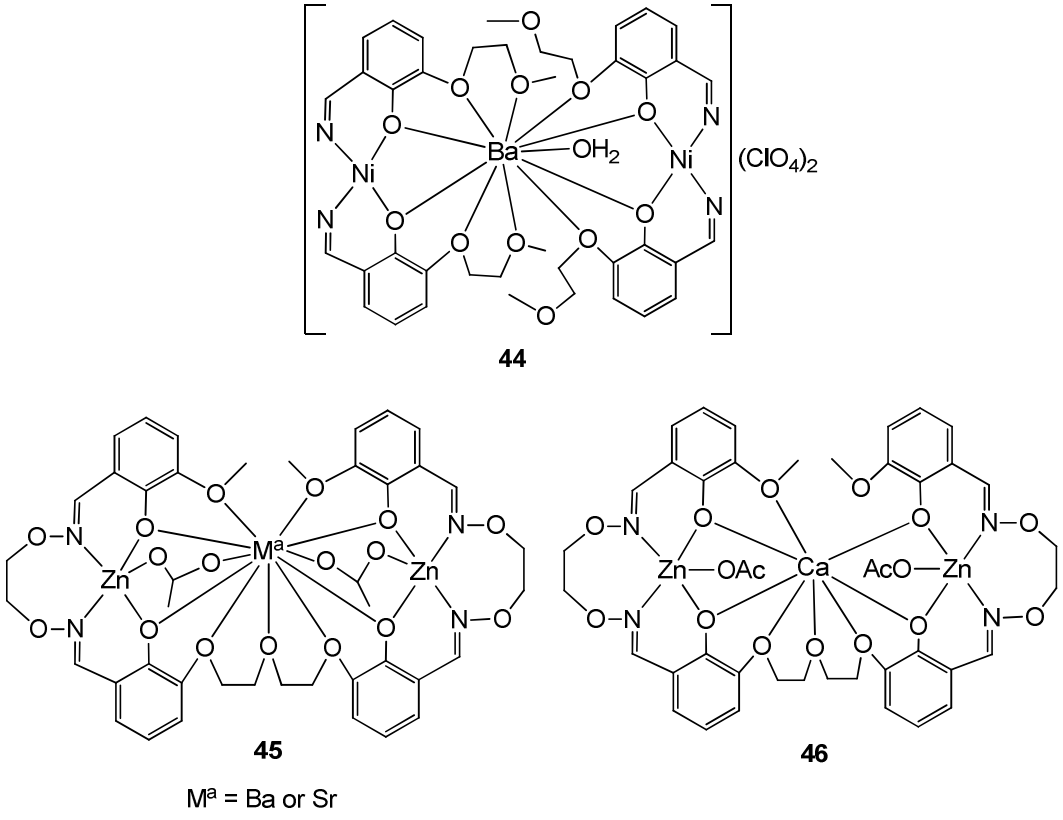

44

45

M^a = Ba or Sr

46

Chart 3.1 Previously reported trinuclear alkaline earth metal and transition metal complexes.[98, 102]

The 2,6-dipicolinoylbis(*N,N*-dialkylthioureas) seem to be well suitable for the preparation of mixed metal complexes with 'soft' and 'hard' metal ions as has been demonstrated in the previous Chapters. Synthesis and structural studies of complexes with alkaline earth and transition metals may lead to further experiments on metal-metal interactions.

In this thesis, a series of trinuclear mixed-metal complexes of transition metals and alkaline earth metals with 2,6-dipycolinoylbis(*N,N*-dialkylthiourea) (H_2L) ligands is described. Two different H_2L ligands were used, which differ in the residuals of the thiourea. H_2L^a contains the diethylamine residue, while H_2L^b has a morpholine residue. Three equivalents of such ligands reacts with two equivalents of $M^b(OAc)_2 \cdot 4\ H_2O$ (where M^b = Mn, Co or Ni) and one equivalent of M^aCl_2 (where M^a = Ba, Sr or Ca) in MeOH at 40 °C in the presence of NEt_3. Precipitates of the composition $[M^aM^b{}_2(L)_3]$ were collected in high yields (≥90%) after a maximum of 20 minutes reaction (Scheme 3.1).

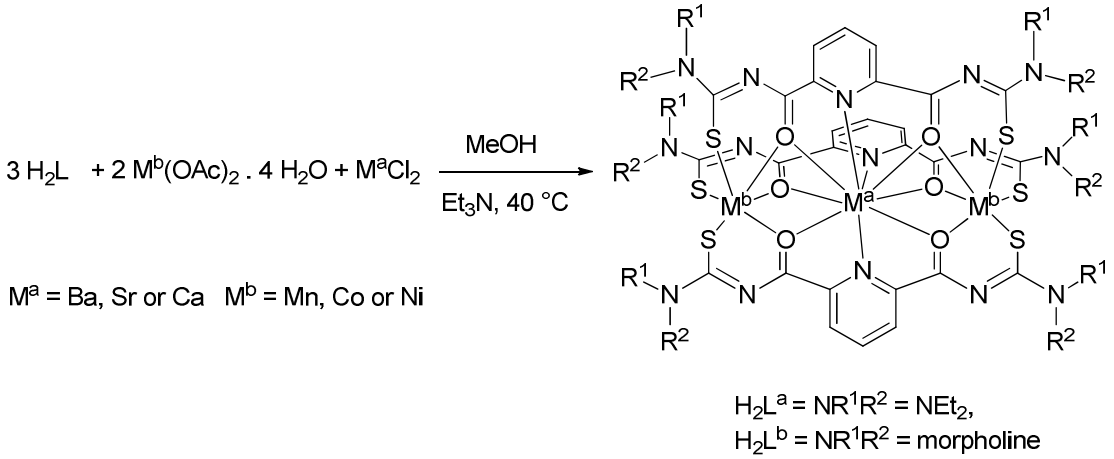

Scheme 3.1 Synthesis of trinuclear complexes of alkaline-earth and transition metal ions.

The colors of the precipitates depend on the transition metals used. Mn complexes are orange-red, Co complexes are dark green and Ni complexes are brown. Most of the precipitates are soluble in CH_2Cl_2 and $CHCl_3$ and can be purified by recrystallization from CH_2Cl_2/MeOH (1:1) mixtures. The analysis of the complexes by IR spectroscopy showed the absence of NH bands at 3273 cm^{-1} for H_2L^a and at 3360 cm^{-1} for H_2L^b which confirms the deprotonation of the chelating ligands. A bathochromic shift of the C=O stretching vibration from 1690 cm^{-1} to around 1590 cm^{-1} confirms the chelate coordination of ligand with electron delocalization. Analysis by ESI mass spectrometry and elemental analysis confirm the formation of neutral trinuclear complexes having a composition of $[M^aM^b{}_2(L)_3]$. Furthermore, ^1H NMR

spectroscopy could not be applied due to the paramagnetic behavior of the transition metal ions applied. Single crystals suitable for X-ray analysis could be obtained in the cases of $[SrMn_2(L^b)_3]$, $[BaMn_2(L^a)_3]$, $[BaMn_2(L^b)_3]$, $[BaCo_2(L^a)_3]$, $[BaCo_2(L^b)_3]$, $[BaNi_2(L^b)_3]$. X-ray crystallographic analyses of these complexes confirm the proposed composition in each case. In addition, coordination of the applied solvent molecules (MeOH or THF) to the alkaline earth metal ions is observed in the cases of $[SrMn_2(L^b)_3]$, $[BaMn_2(L^b)_3]$ and $[BaCo_2(L^a)_3]$. More interestingly, polymerization of the single complex units by the coordination of the morpholine *O* atoms are observed in the cases of $[BaMn_2(L^b)_3]$ and $[BaCo_2(L^b)_3]$.The following Chapters describe the complexes in detail in each transition metal category.

3.1 Complexes of alkaline earth metals and manganese [$Mn^{II}(M^{a})^{II}Mn^{II}$]

Trinuclear mixed metal complexes containing alkaline earth metal ions and Mn^{2+} ions are introduced for the first time in this chapter. The complexes of 2,6-dipycolinoylbis(*N,N*-dialkylthioureas), which contain alkaline earth metal and manganese ions, are orange. Except the Ca complexes, which are almost insoluble, the complexes are perfectly soluble in CH_2Cl_2 or $CHCl_3$. Therefore, the measurements of ESI mass spectra were not possible for the Ca complexes. However all complexes have been characterized by elemental analysis and the formation of trinuclear [$M^{a}Mn_2(L_3)$] complexes (where M^{a} = Ba, Sr or Ca) is confirmed. Additionally single crystals suitable for X-ray analysis were obtained from CH_2Cl_2/MeOH (1:1) mixtures in the cases of [$SrMn_2(L^{b})_3$], [$BaMn_2(L^{a})_3$] and [$BaMn_2(L^{b})_3$].

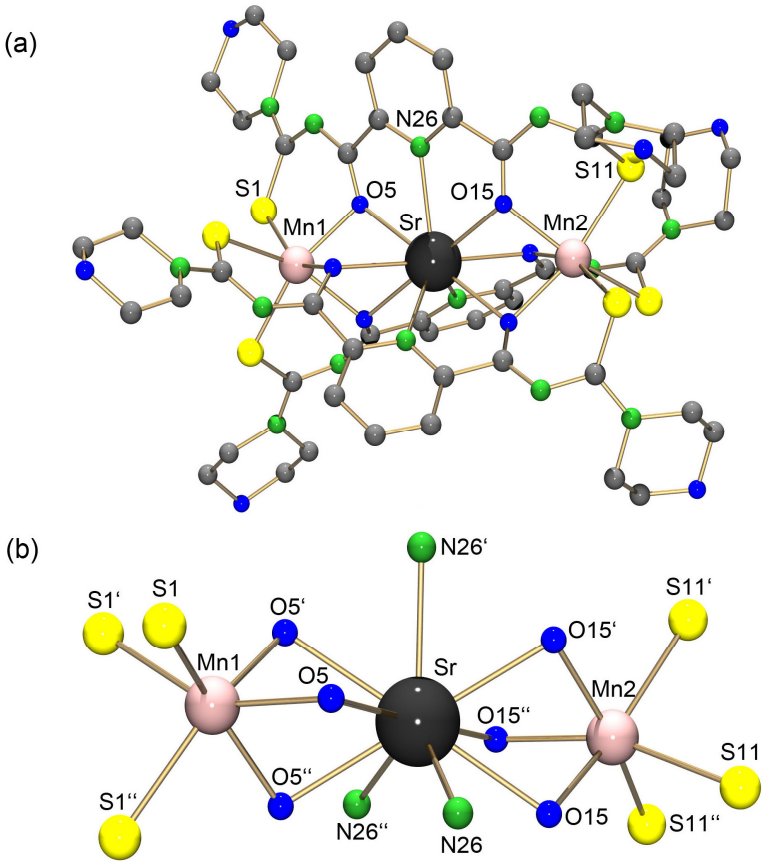

Figure 3.1 (a) Molecular structure of [$SrMn_2(L^{b})_3$]. Hydrogen atoms are omitted for clarity. (b) Coordination patterns of Sr^{2+} and Mn^{2+} ions in [$SrMn_2(L^{b})_3$]. Symmetry related atoms are produced by a C_3 rotation axis.

Table 3.1 Selected bond lengths (Å) in $SrMn_2L^b_3$.

Sr–O5	2.647(6)	Sr–O15	2.629(5)	Sr–N26	2.749(6)
Mn1–S1	2.537(2)	Mn2–S11	2.562(2)	Mn1–O5	2.182(6)
Mn2–O15	2.182(6)				

The complex $[SrMn_2(L^b)_3]$ crystallized from the solvent mixture CH_2Cl_2/THF (1:1) and gave crystals of X-ray quality. Several attempts to get good quality crystals of $[SrMn_2(L^a)_3]$ from different solvent mixtures were not successful. The complex $[SrMn_2(L^b)_3]$ crystallizes in the trigonal crystal system in the primitive space group $P\bar{3}$. One third of the molecule is seen in the asymmetric unit, which means that the three metal atoms are situated on a threefold axis and the whole molecule is generated by a C_3 symmetry operation. The molecular structure of $[SrMn_2(L^b)_3]$ and the coordination patterns of the metal ions are presented in Figure 3.1 and selected bond lengths are summarized in Table 3.1. The Sr–Mn1 and Sr–Mn2 distances are 3.597(3) Å and 3.588(4) Å respectively. Each Mn atom is coordinated to three sulfur and three oxygen donor atoms giving a distorted octahedral coordination sphere. The Mn1–S1 and Mn2–S11 bond lengths are 2.537(2) Å and 2.562(2) Å respectively. Mn1–O5 and Mn2–O15 bond lengths are both 2.182(6) Å. The Sr atom is coordinated to three *N* donor atoms of the pyridine rings and to six *O* donor atoms from carbonyl groups, and consequently shows a coordination number of nine. The Sr–N bond length is 2.749(6) Å and Sr–O5/O15 bond lengths are 2.647(6)/2.629(5) Å. The coordination polyhedron of Sr is a tricapped trigonal prism.

A crystallization attempt of the complex $[SrMn_2(L^b)_3]$ from the solvent mixture dioxane/THF (1:1) gave good quality crystals for X-ray analysis. The molecular structure reveals the coordination of an additional THF molecule to the Sr atom (Fig 3.2), and a half dioxane molecule is co crystallized per asymmetric unit. The molecular structure reveals two $\{L^b\}^{2-}$ ligands in one plane and the third chelating ligand and the THF molecule are perpendicular to that plane. In this case, Sr atom has the coordination number 10, while the Mn atoms remain with a distorted octahedral geometry. The Sr–Mn distances are 3.724(3) and 3.736(4) Å. These values are higher than the distances observed in the complex $[SrMn_2(L^b)_3]$ (Table 3.1). Selected bond lengths are summarized in Table 3.2. The Sr atom is coordinated by three *N* donor atoms of the pyridine rings and the *O* donor atom of the THF, all lying in one plane. Three carbonyl *O* atoms are above to this plane and another three carbonyl *O* atoms are below

to this plane. Therefore the Sr atom exhibits an irregular polyhedron which could be similar to a tetracapped trigonal prism.

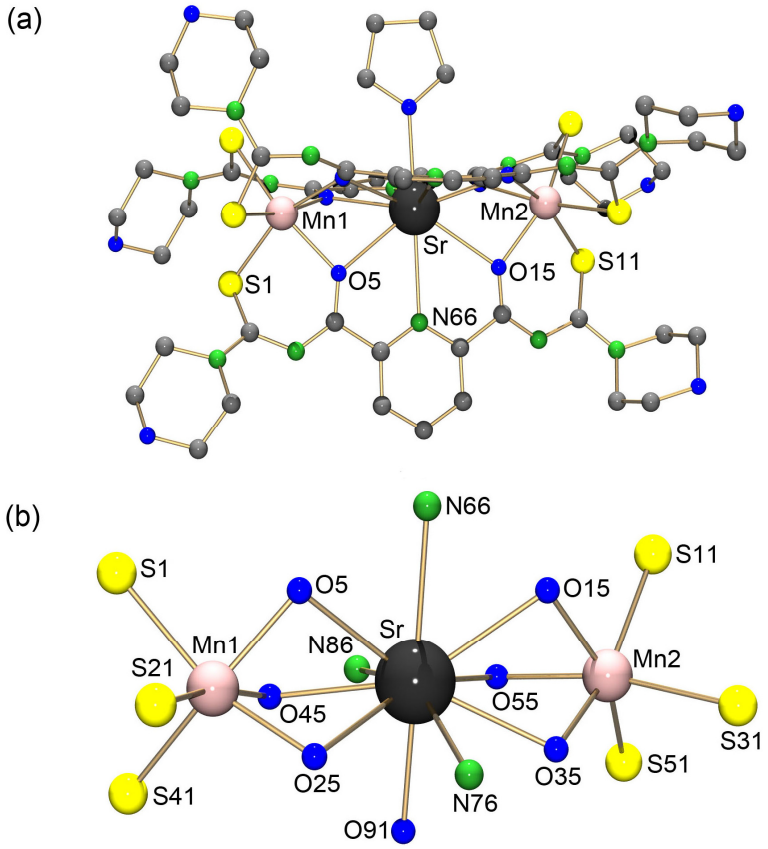

Figure 3.2 (a) Molecular structure of $[SrMn_2(L^b)_3(THF)]$. Hydrogen atoms are omitted for clarity. (b) Coordination patterns of Sr^{2+} and Mn^{2+} ions in $[SrMn_2(L^b)_3(THF)]$.

Table 3.2 Selected bond lengths (Å) in $[SrMn_2(L^b)_3(THF)]$.

Sr–O5	2.716(3)	Sr–O15	2.871(3)	Sr–O25	2.682(3)
Sr–O35	2.659(3)	Sr–O45	2.781(3)	Sr–O55	2.827(3)
Sr–N66	2.851(4)	Sr–N76	2.878(4)	Sr–N86	2.973(3)
Mn1–S1	2.561(2)	Mn1–S21	2.611(2)	Mn1–S41	2.543(1)
Mn2–S11	2.484(2)	Mn2–S31	2.582(2)	Mn2–S51	2.544(1)
Mn1–O5	2.160(3)	Mn1–O25	2.146(3)	Mn1–O45	2.204(3)
Mn2–O15	2.152(3)	Mn2–O35	2.154(3)	Mn2–O55	2.178(3)
Sr–O91	2.647(3)				

The bond lengths between the Sr atom and carbonyl oxygen atoms are in the range between 2.659(3) Å and 2.871(3) Å. The Sr–N bond lengths are in the range between 2.851(4) and 2.973(3) Å. Both Sr–O and Sr–N bond lengths are longer than those observed in $[SrMn_2(L^b)_3]$ (Table 3.1). Mn–S bond lengths are in the range between 2.484(2) Å and 2.611(2) Å and Mn–O bond lengths are in the range between 2.146(3) Å and 2.204(3) Å. Both Mn–S and Mn–O bond lengths are in the range as observed in the trinuclear $Mn^{II}Ln^{III}Mn^{II}$ complexes $[GdMn_2(L^a)_2(\mu\text{-}OAc)_2(OAc)(MeOH)_2]$ and $[CeMn_2(L^a)_2(\mu\text{-}OAc)_2Cl(MeOH)(H_2O)]$ (Chapter 2.3).

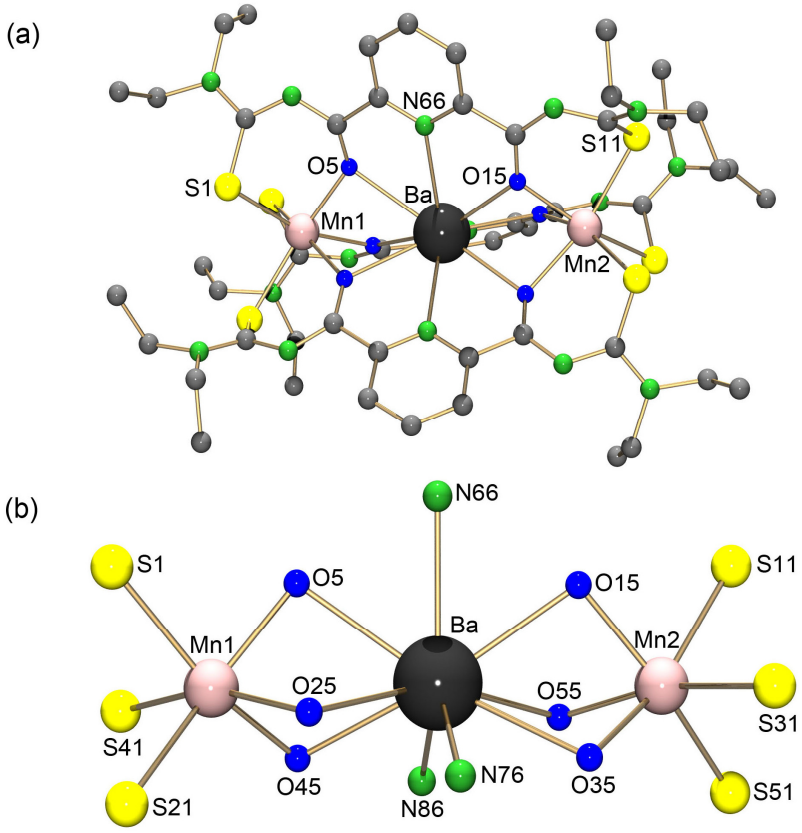

Figure 3.3 (a) Molecular structure of $[BaMn_2(L^a)_3]$. Hydrogen atoms are omitted for clarity. (b) Coordination patterns of Ba^{2+} and Mn^{2+} ions in $[BaMn_2(L^a)_3]$.

The complex $[BaMn_2(L^a)_3]$ crystallizes in the monoclinic system with the space group $P2_1/c$. The molecular structure and the coordination patterns of the metal atoms in $BaMn_2L^a_3$ are presented in Figure 3.3. The coordination situation in $[BaMn_2(L^a)_3]$ is similar to that in the $[SrMn_2(L^b)_3]$ complex. The Mn^{2+} ions show distorted octahedral coordination spheres. The Ba^{2+} ion is coordinated to 6 oxygen and 3 nitrogen donor atoms and has a coordination

number of 9. Three *N* donor atoms of the pyridine rings are in one plane. Three *O* donor atoms of the carbonyl groups are lying above to this plane and three another *O* donor atoms of the carbonyl groups are lying below to this plane. Therefore the coordination polyhedron of Ba atom is a tricapped trigonal prism like the Sr atom in the complex $[SrMn_2(L^b)_3]$. Selected bond lengths of $[BaMn_2(L^a)_3]$ are summarized in Table 3.3. The Ba–O bond lengths are in the range between 2.751(3) and 2.883(3) Å and Ba–N bond lengths are in the range between 2.912(4) and 2.999(4) Å. The Mn–S and Mn–O bond lengths are in the range observed for the trinuclear Mn complexes described before.

Table 3.3 Selected bond lengths (Å) in $[BaMn_2(L^a)_3]$.

Ba–O5	2.806(3)	Ba–O15	2.883(3)	Ba–O25	2.808(3)
Ba–O35	2.782(3)	Ba–O45	2.761(3)	Ba–O55	2.751(3)
Ba–N66	2.999(4)	Ba–N76	2.912(4)	Ba–N86	2.933(4)
Mn1–S1	2.588(2)	Mn1–S21	2.560(1)	Mn1–S41	2.587(2)
Mn2–S11	2.556(2)	Mn2–S31	2.552(2)	Mn2–S51	2.586(2)
Mn1–O5	2.189(3)	Mn1–O25	2.195(3)	Mn1–O45	2.174(3)
Mn2–O15	2.176(3)	Mn2–O35	2.186(3)	Mn2–O55	2.176(3)

The complex $[BaMn_2(L^b)_3]$ crystallizes in the triclinic space group of $P\overline{1}$. The molecular structure and the coordination pattern are presented in Figure 3.4. The coordination of the chelating ligands to the metal atoms is similar to the situation in $[BaMn_2(L^a)_3]$. The bond lengths of Ba and Mn to the donor atoms are within the ranges observed in the $[BaMn_2(L^a)_3]$ complex. The crystal structure reveals coordination of an additional MeOH molecule to the Ba^{2+} ion with a Ba–O91 bond length of 3.12(2) Å. Additionally, polymerization of the complex unit through the coordination of the oxygen atoms of the morpholine rings of the adjacent molecules to the Ba atom is observed. The bond lengths between the Ba and oxygen atoms of the morpholine rings of the neighboring complex units Ba–O20a and Ba–O30a, are 3.081(9) Å and 3.031(9) Å respectively. Two types of coordination environments on Ba atoms are observed in the polymeric chain. The complex unit where the Ba atom coordinates to a MeOH molecule shows the coordination number of 10 for the Ba atom, which shows a similar polyhedron like the Sr atom in the complex $[SrMn_2(L^b)_3(THF)]$. The complex unit where the Ba atom coordinates to a MeOH molecule and additionally to two adjacent morpholine oxygen atoms shows a coordination number of 12 for the Ba atom. This Ba atom coordinates to three *N* donor atoms and three oxygen donor atoms in one hexagonal plane.

Three *O* donors of the carbonyl groups are lying above this hexagonal plane and another three *O* donors of the carbonyl groups are lying below this plane.

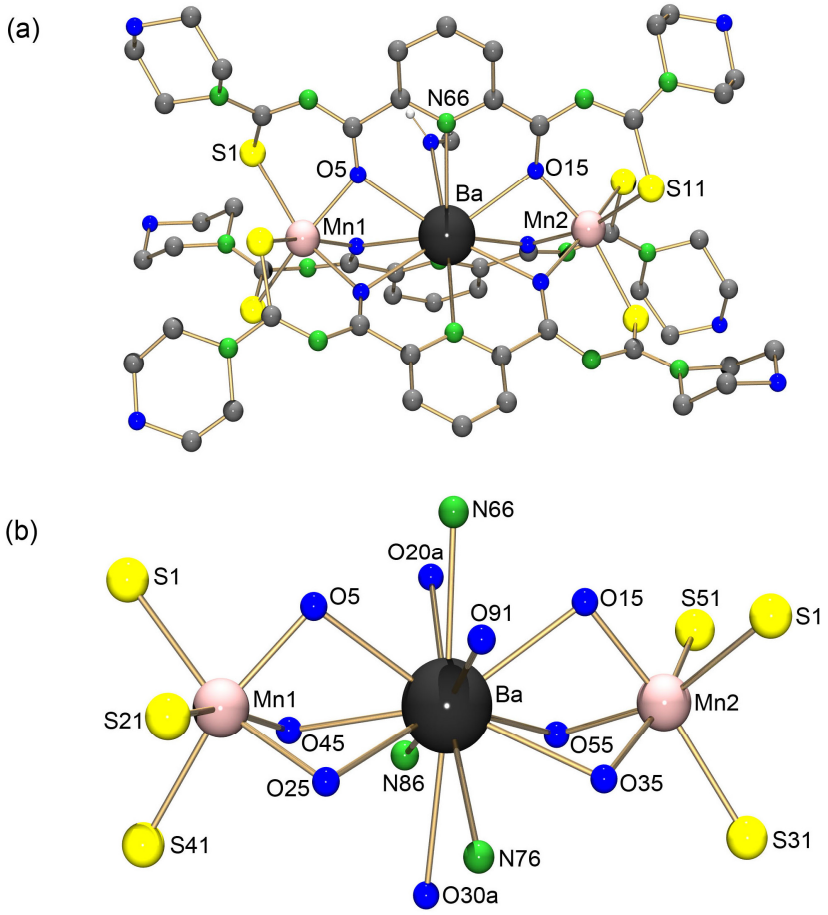

Figure 3.4 (a) Molecular structure of $[BaMn_2(L^a)_3(MeOH)]$. Hydrogen atoms are omitted for clarity. (b) Coordination patterns of Ba^{2+} and Mn^{2+} ions in polymerized $[BaMn_2(L^a)_3(MeOH)]$.

Table 3.4 Selected bond lengths (Å) in $[BaMn_2(L^a)_3(MeOH)]$.

Ba–O5	2.817(8)	Ba–O15	2.803(9)	Ba–O25	2.78(1)
Ba–O35	2.783(4)	Ba–O45	2.807(4)	Ba–O55	2.815(9)
Ba–N66	2.98(1)	Ba–N76	3.01(1)	Ba–N86	2.98(1)
Ba–O91	3.12(2)	Ba–O20a	3.081(9)	Ba–O30a	3.031(9)
Mn1–S1	2.557(4)	Mn1–S21	2.549(4)	Mn1–S41	2.560(5)
Mn2–S11	2.608(5)	Mn2–S31	2.582(4)	Mn2–S51	2.544(4)
Mn1–O5	2.123(9)	Mn1–O25	2.154(8)	Mn1–O45	2.158(9)
Mn2–O15	2.164(8)	Mn2–O35	2.128(8)	Mn2–O55	2.18(1)

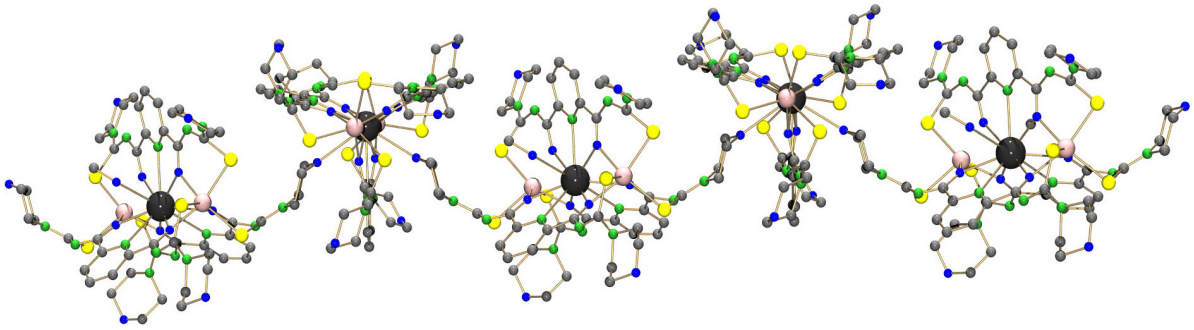

Figure 3.5 Polymerization of $[BaMn_2(L^a)_3(MeOH)]$ by *O* atoms of the morpholine rings of the adjacent units. Hydrogen atoms are omitted for clarity.

In all crystallographically characterized trinuclear $[M^aMn_2(L)_3]$ (M^a = Sr or Ba) complexes, the observed Mn–S and Mn–O bond lengths of aroyl thiourea moieties are in the similar range of Mn–S and Mn–O bond lengths observed in the trinuclear $[Mn^{II}Ln^{III}Mn^{II}]$ complexes (Chapter 2.3).

EPR spectra of the$[BaMn_2(L^a)_3]$ complexes in the solvent mixture of $CHCl_3$/toluene were recorded at 80 K and 5 K (Figure 3.6). Despite the better resolution of the signals at 5 K compared to 80 K, the interpretation of the spectrum is unfortunately not possible.

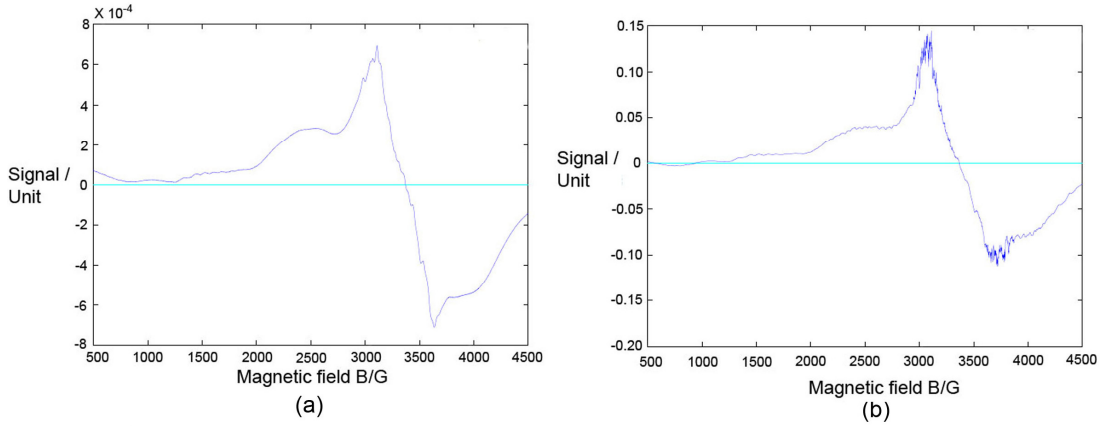

Figure 3.6 W-band EPR Spectra of $[BaMn_2(L^a)_3]$ complex in $CHCl_3$/toluene mixture (a) at 80 K and (b) at 5 K.

3.2 Complexes of alkaline earth metals and cobalt [$Co^{II}(M^a)^{II}Co^{II}$]

This chapter introduces the first trinuclear mixed-metal complexes of alkaline earth metal ions and Co^{2+} ions. The precipitates from one-pot reactions of H_2L^a or H_2L^b with M^aCl_2 (where M^a = Ca, Sr or Ba) and $Co(CH_3COO)_2 \cdot 4\ H_2O$ are dark green (Scheme 3.1). The complexes $[BaCo_2(L^a)_3]$, $[BaCo_2(L^b)_3]$, $[SrCo_2(L^a)_3]$ and $[SrCo_2(L^b)_3]$ are readily soluble in CH_2Cl_2 and $CHCl_3$. They can easily be crystallized from CH_2Cl_2/MeOH (1:1). But only the crystals of $[BaCo_2(L^a)_3]$ and $[BaCo_2(L^b)_3]$ were suitable for X-ray analysis. Several attempts to get X-ray quality crystals of $[SrCo_2(L^a)_3]$ and $[SrCo_2(L^b)_3]$ from different solvent mixtures were not successful.

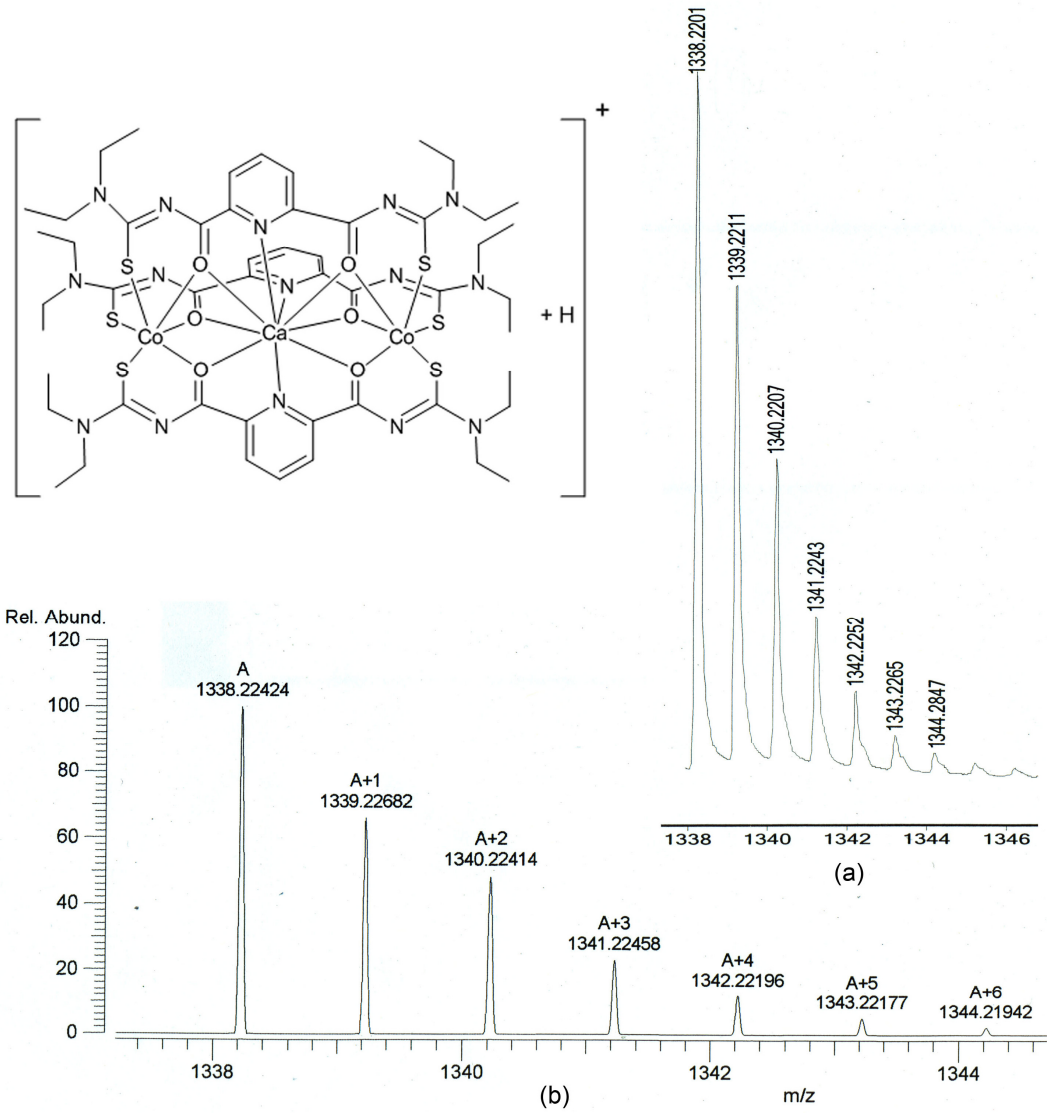

Figure 3.7 a) Observed isotopic pattern corresponding to the molecular ion peak of $[CaCo_2(L^a)_3+H]^+$ in the mass spectrum of $[CaCo_2(L^a)_3]$. b) Calculated isotropic pattern for $[CaCo_2(L^a)_3+H]^+$.

The solubility of the Ca complexes is very low. $[CaCo_2(L^a)_3]$ is only slightly soluble in CH_2Cl_2 or $CHCl_3$, but $[CaCo_2(L^b)_3]$ is completely insoluble in CH_2Cl_2 or $CHCl_3$. Therefore, the recording of a ESI-Mass spectrum was only possible in the case of the first complex (Fig 3. 7) and it shows signals at 1338 m/z and 1360 m/z, which correspond to the ions $[CaCo_2(L^a)_3 + H]^+$ and $[CaCo_2(L^a)_3 + Na]^+$ respectively. Both Ca complexes are soluble in warm DMSO or DMF. Attempts to crystallize them from the solvent mixtures of DMSO/MeOH or DMF/MeOH in different ratios were not successful.

The complex $[BaCo_2(L^a)_3]$ crystallizes in the triclinic space group $P\bar{1}$ from CH_2Cl_2/MeOH (1:1). The molecular structure and the coordination pattern of the metal ions in $[BaCo_2(L^a)_3(MeOH)]$ are presented in Figure 3.8. The molecular structure reveals that the Ba atom is coordinated by three 2,6-dipicolyl moieties, each with three donor atoms *ONO*, and as well as by a MeOH molecule. Consequently, it shows a coordination number of 10 which is similar to the $[SrMn_2(L^b)_3(THF)]$ complex (see Chapter 3.1).

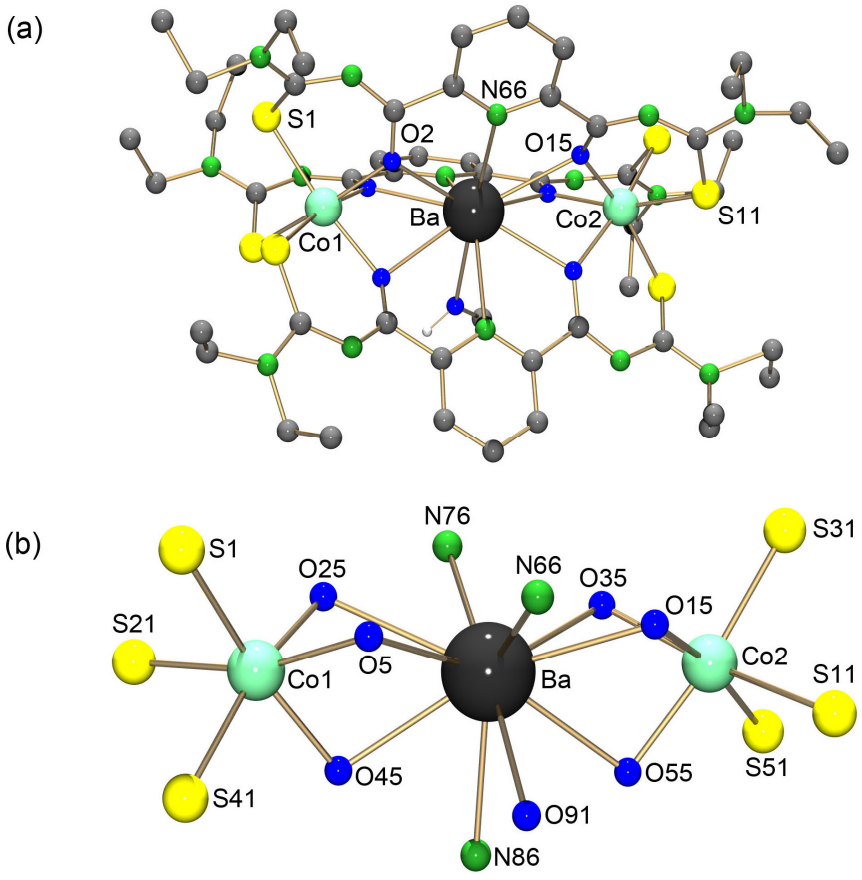

Figure 3.8 (a) Molecular structure of $[BaCo_2(L^a)_3(MeOH)]$. Hydrogen atoms are omitted for clarity. (b) Coordination patterns of Ba^{2+} and Co^{2+} ions in $[BaCo_2(L^a)_3(MeOH)]$.

Table 3.5 Selected bond lengths (Å) in $[BaCo_2(L^a)_3(MeOH)]$.

Ba–O5	2.749(3)	Ba–O15	2.751(3)	Ba–O25	2.876(3)
Ba–O35	2.831(3)	Ba–O45	2.755(3)	Ba–O55	2.859(3)
Ba–N66	2.914(3)	Ba–N76	2.970(3)	Ba–N86	2.882(3)
Ba–O91	2.893(3)				
Co1–S1	2.515(1)	Co1–S21	2.383(1)	Co1–S41	2.432(1)
Co2–S11	2.514(1)	Co2–S31	2.422(1)	Co2–S51	2.416(1)
Co1–O5	2.097(3)	Co1–O25	2.079(3)	Co1–O45	2.111(3)
Co2–O15	2.119(3)	Co2–O35	2.070(3)	Co2–O55	2.096(3)

In the case of $[BaCo_2(L^a)_3(MeOH)]$, the coordination polyhedron of the Ba^{2+} ion is an irregular tetracapped trigonal prism. Selected bond lengths are presented in Table 3.5. The Ba–O bond lengths are in the range between 2.749(3) Å – 2.876(3) Å. The Ba–N bond lengths are in the range between 2.882(3) Å – 2.970(3) Å. The Ba–O and Ba–N bond lengths are almost in the similar range as previously reported for the $[BaMn_2(L)_3]$ complexes, where the Ba–O bond lengths are shorter than the Ba–N bond lengths (Chapter 3.1). The Ba–O91 bond length is 2.893(3) Å. The distances between Ba^{2+} and Co^{2+} ions are 3.697(1) Å and 3.703(1) Å. Both Co atoms are coordinated to three aroylthiourea moieties and show a distorted octahedral geometry. Co–S bond lengths are in the range between 2.383(1) Å and 2.515(1) Å and the Co–O bond lengths are in the range between 2.070(3) Å and 2.119(3) Å. Both Co–S and Co–O bond lengths observed in this complex are longer than those in $[LnCo_2(L^a)_2(OAc)_2X]$ (where X = OAc or Cl).

$[BaCo_2(L^b)_3]$ crystallizes in the tetragonal space group *I4₁/a*. Its molecular structure reveals the expected coordination of three $\{L^b\}^{2-}$ ligands to one Ba^{2+} and two Co^{2+} ions. No solvent molecule is coordinated to the Ba^{2+} ion (Fig 3.9). Selected bond lengths are presented in Table 3.6. The range of Ba–O bond lengths is 2.749(5) Å – 2.909(5) Å and the range of Ba–N bond lengths is 2.893(6) Å – 2.952(6) Å. These are similar to the complexes with Mn^{2+} ions (Chapter 3.1). The distances between the Ba^{2+} and the Co^{2+} ions are 3.659(1) and 3.673(1) Å. Both Co atoms show distorted octahedral environments and are coordinated by three *S* and three *O* donor atoms each. The Co–S bond lengths are in the range of 2.361(2) Å – 2.502(2) Å and the Co–O bond lengths are in the range of 2.075(5) Å – 2.140(5) Å. The observed Co–S and Co–O bond lengths in the complex $[BaCo_2(L^b)_3]$ are in agreement with the corresponding bond lengths observed in the complex $[BaCo_2(L^a)_3(MeOH)]$.

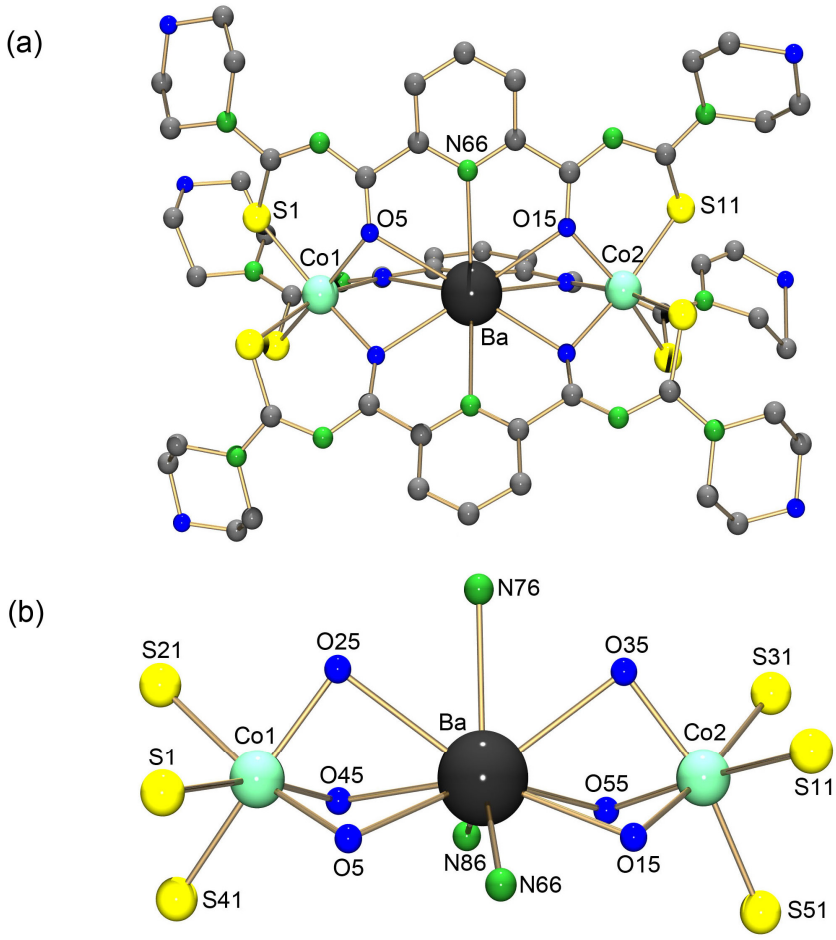

Figure 3.9 (a) Molecular structure of $[BaCo_2(L^b)_3]$. Hydrogen atoms are omitted for clarity. (b) Coordination pattern of Ba^{2+} and Co^{2+} ions in $[BaCo_2(L^b)_3]$.

Table 3.6 Selected bond lengths (Å) in $[BaCo_2(L^b)_3]$.

Ba–O5	2.758(5)	Ba–O15	2.771(5)	Ba–O25	2.909(5)
Ba–O35	2.834(5)	Ba–O45	2.749(4)	Ba–O55	2.749(5)
Ba–N66	2.952(6)	Ba–N76	2.893(6)	Ba–N86	2.940(6)
Co1–S1	2.478(2)	Co1–S21	2.361(2)	Co1–S41	2.502(2)
Co2–S11	2.475(3)	Co2–S31	2.413(3)	Co2–S51	2.429(2)
Co1–O5	2.099(5)	Co1–O25	2.140(5)	Co1–O45	2.092(4)
Co2–O15	2.075(5)	Co2–O35	2.111(5)	Co2–O55	2.083(5)

The complex polymerized through the coordination of the oxygen atom of the morpholine ring to the Ba atom of the adjacent molecule. This phenomenon is also observed in $[BaMn_2(L^b)_3]$ complexes in a different way. The manganese compound forms a polymer chain, while the complex $[BaCo_2(L^b)_3]$ polymerizes in form of a polymer network (Fig 3.10).

Three *N* and eight *O* donor atoms are coordinated to Ba^{2+} ion giving an overall coordination number of 11. In this case, three *N* donor atoms from the pyridine rings and two *O* donor atoms from the morpholine rings of the adjacent units are lying in a pentagonal plane. Three *O* donor atoms from the carbonyl groups form a trigonal plane above this pentagonal plane and another three *O* donors from the carbonyl groups form a trigonal plane below to this pentagonal plane.

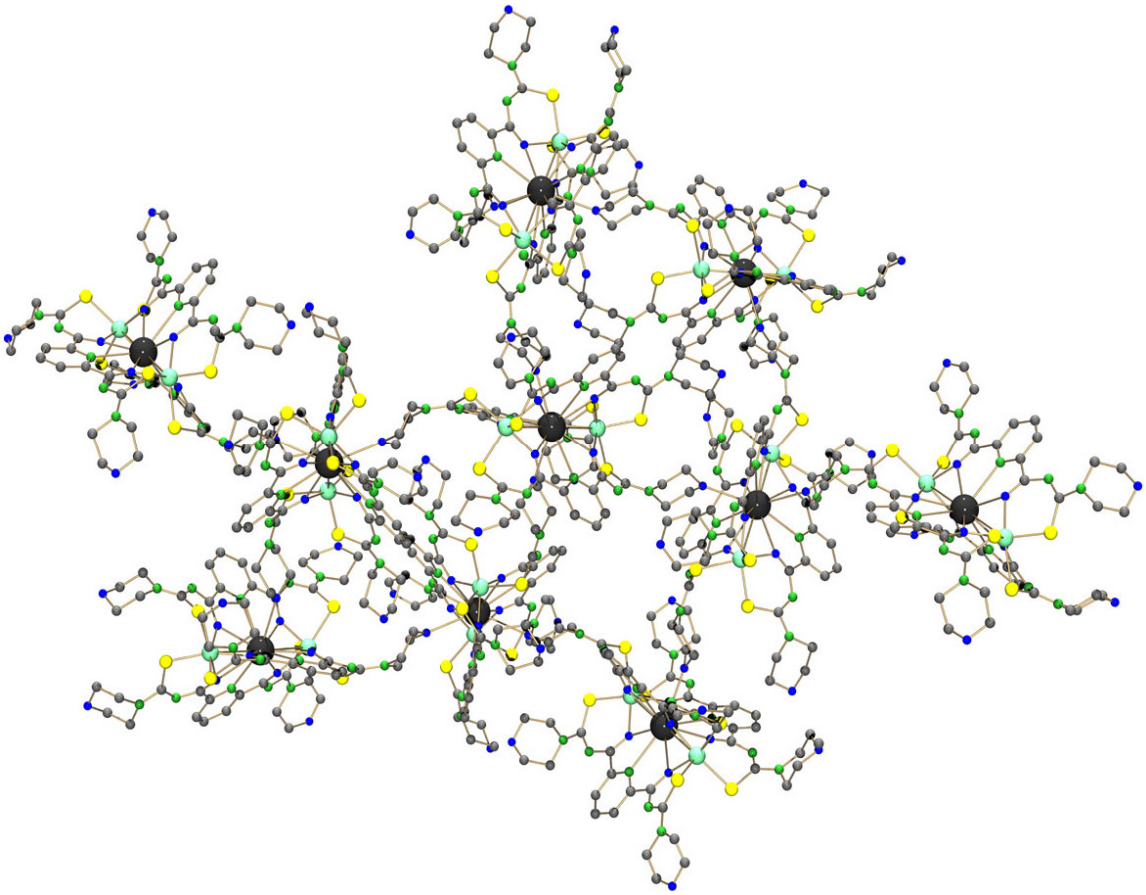

Figure 3.10 Polymerization of $[BaCo_2(L^b)_3]$ by the *O* atoms of the morpholine rings of the adjacent units. Hydrogen atoms were omitted for clarity. For a more simplified sketch see Chart 3.2.

Sketches of the coordination polymers of the complexes $[BaMn_2(L^b)_3]$ and $[BaCo_2(L^b)_3]$ are presented in Chart 3.2. Obviously, there are clear differences between both polymers. The complex $[BaMn_2(L^b)_3]$ forms a linear coordination polymer through the coordination of every second Ba^{2+} ion to the *O* donor atoms of the morpholine rings of the adjacent complex units (Chart 3.2 a). In this case, two different coordination environments of Ba^{2+} are observed.

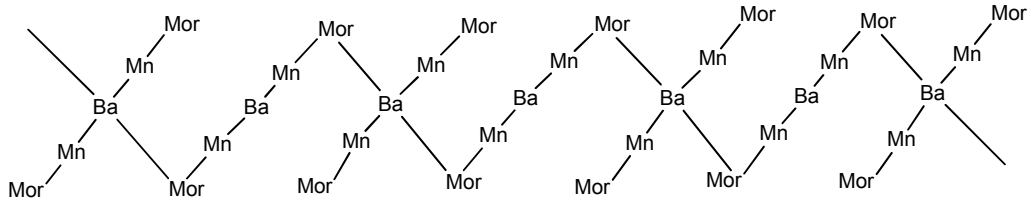

(a)

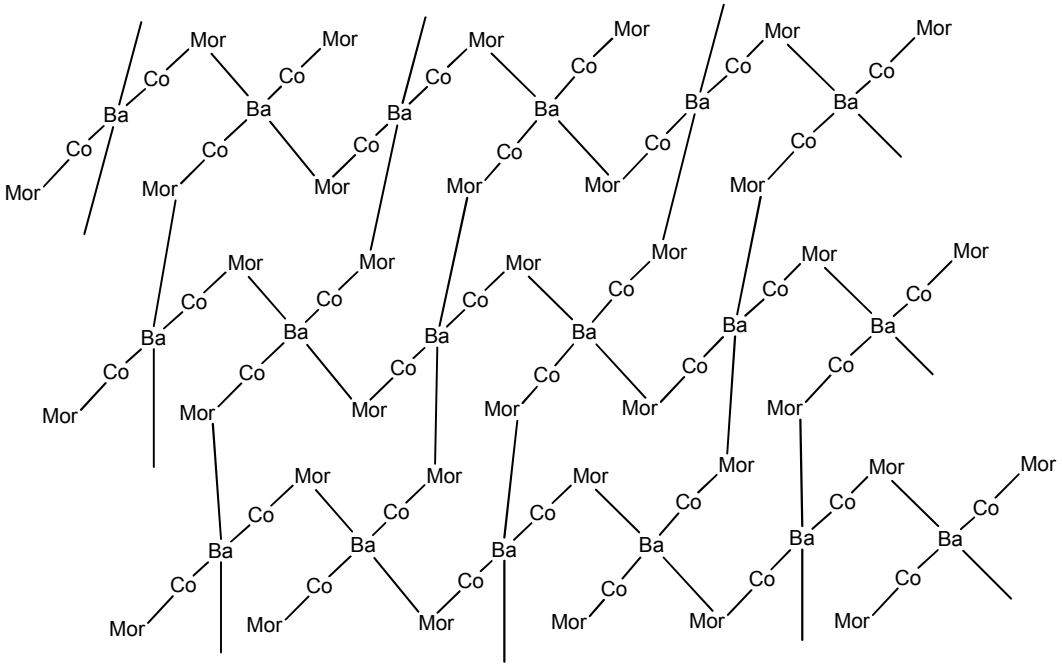

(b)

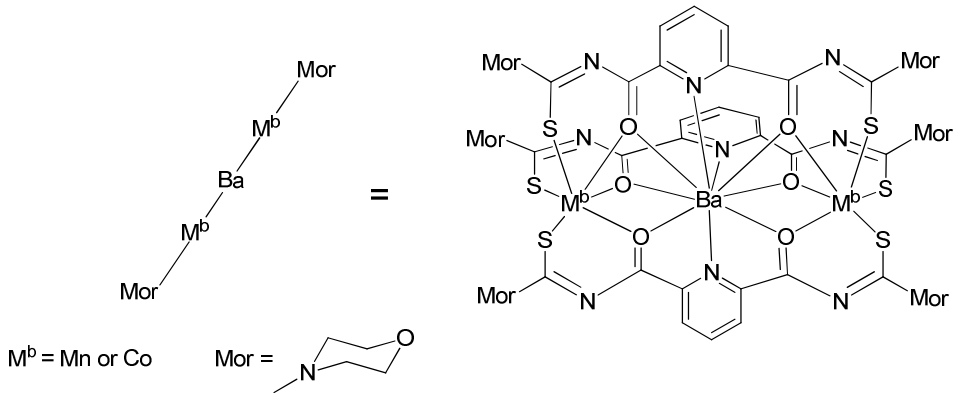

M^b = Mn or Co Mor =

Chart 3.2 Simplified sketches of the coordination polymers of (a) $[BaMn_2(L^b)_3]$ and (b) $[BaCo_2(L^b)_3]$.

The complex $[BaCo_2(L^b)_3]$ forms a polymeric network. In this case, a polymer chain which is similar to the $[BaMn_2(L^b)_3]$ polymer is also present. These polymer chains are further connected each other through the coordination of Ba^{2+} ions of one polymeric chain to the *O*

donor atoms of the uncoordinated morpholine rings of the parallel polymer chains (Chart 3.2 b). This results in a polymer network with uniformly coordinated Ba^{2+} ions. They all are coordinated additionally by two adjacent morpholine rings.

3.3 Complexes of alkaline earth metals and nickel [$Ni^{II}(M^{a})^{II}Ni^{II}$]

The trinuclear complexes of H_2L^a or H_2L^b with Ni^{2+} and alkaline earth metal ions are brown. The complexes with Ba^{2+} and Sr^{2+} ions are well soluble in CH_2Cl_2 or $CHCl_3$, which is also observed in the cases of Mn and Co combinations. Therefore, they are easy to purify and crystallize from the solvent mixture CH_2Cl_2/MeOH (1:1).

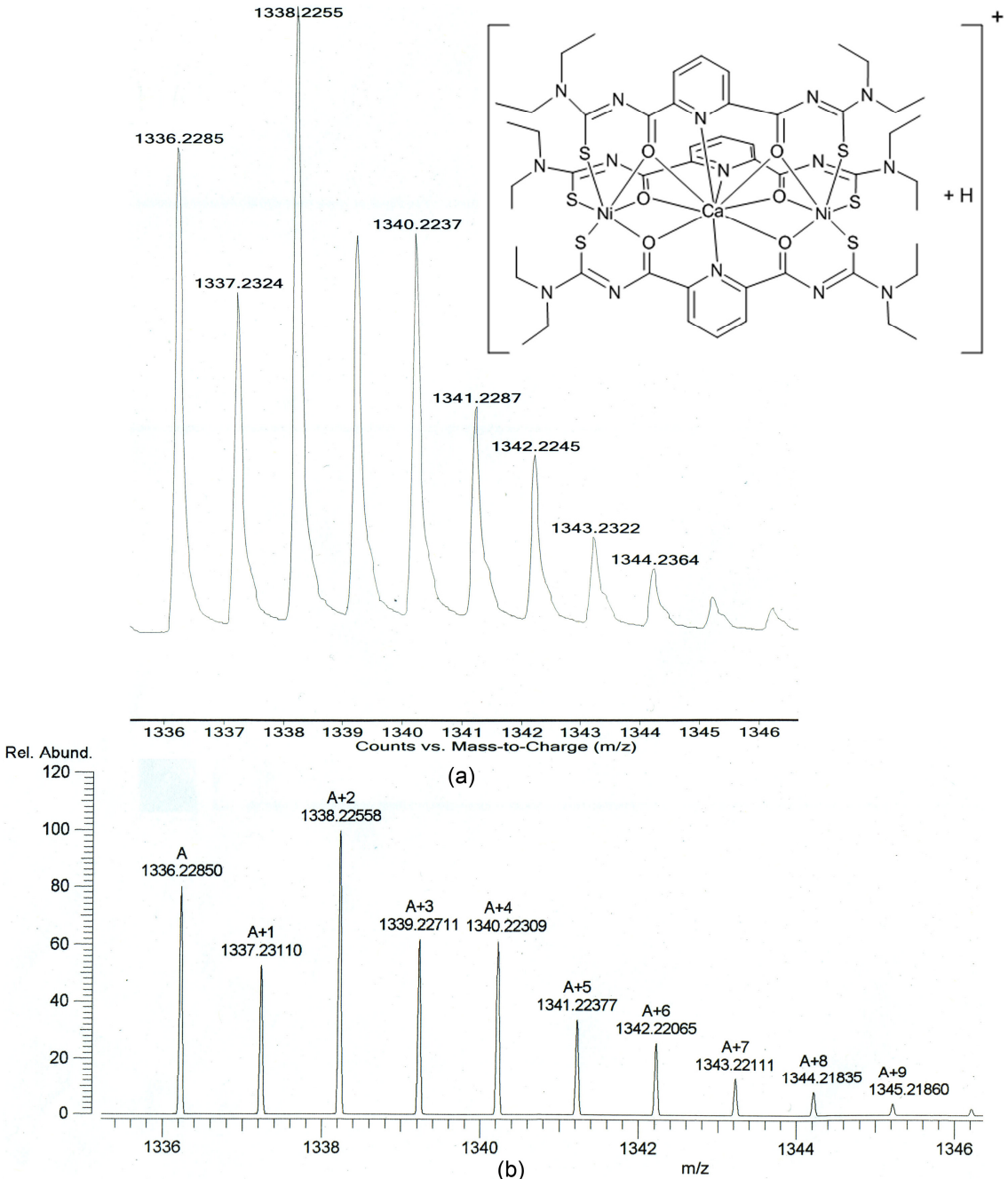

Figure 3.11 a) Observed isotopic pattern corresponding to the molecular ion peak $[CaNi_2(L^a)_3+H]^+$ in the mass spectrum of $[CaNi_2(L^a)_3]$. b) Calculated isotopic pattern for $[CaNi_2(L^a)_3+H]^+$.

The complexes $[CaNi_2(L^a)_3]$ and $[CaNi_2(L^b)_3]$ are better soluble in CH_2Cl_2 or $CHCl_3$ than the analogous cobalt complexes $[CaCo_2(L^a)_3]$ and $[CaCo_2(L^b)_3]$. Moreover, the $[CaNi_2(L^a)_3]$ and $[CaNi_2(L^b)_3]$ complexes are well soluble in DMSO or DMF at room temperature, while the complexes $[CaCo_2(L^a)_3]$ and $[CaCo_2(L^b)_3]$ are only soluble in warm solution of DMSO or DMF, and the complexes $[CaMn_2(L^a)_3]$ and $[CaMn_2(L^b)_3]$ are completely insoluble in all common solvents.

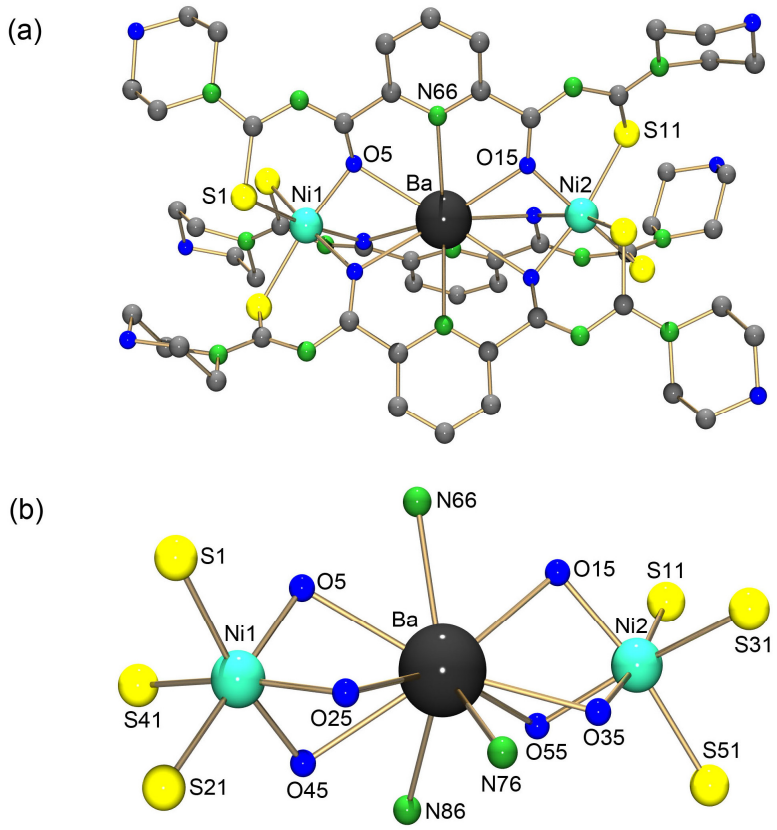

Figure 3.12 (a) Molecular structure of $[BaNi_2(L^b)_3]$. Hydrogen atoms are omitted for clarity. (b) Coordination pattern of Ba^{2+} and Co^{2+} ions in $[BaNi_2(L^b)_3]$.

All Ni complexes have been characterized by IR spectroscopy, ESI mass spectrometry and elemental analysis and the formation of tris complexes in each case is confirmed. The ESI mass spectrum of $[CaNi_2(L^a)_3]$ is given in Figure 3.11. A signal at 1338 m/z corresponds to the molecular ion $[CaNi_2(L^a)_3+H]^+$. Several attempts to get good quality single-crystals of the complexes $[CaNi_2(L^a)_3]$, $[CaNi_2(L^b)_3]$, $[SrNi_2(L^a)_3]$, $[SrNi_2(L^b)_3]$ and $[BaNi_2(L^a)_3]$ are failed. X-ray quality crystals could only be obtained in the case of $[BaNi_2(L^b)_3]$ from a

CH_2Cl_2/MeOH (1:1) mixture. The molecular structure of $[BaNi_2(L^b)_3]$ reveals the typical coordination of three ligands to one Ba^{2+} and two Ni^{2+} ions (Fig 3.12).

Table 3.7 Selected bond lengths (Å) in $[BaNi_2(L^b)_3]$.

Ba–O5	2.745(6)	Ba–O15	2.703(6)	Ba–O25	2.821(5)
Ba–O35	2.762(5)	Ba–O45	2.705(6)	Ba–O55	2.853(6)
Ba–N66	2.877(7)	Ba–N76	2.934(6)	Ba–N86	2.896(8)
Ni1–S1	2.387(3)	Ni1–S21	2.421(3)	Ni1–S41	2.425(2)
Ni2–S11	2.408(2)	Ni2–S31	2.437(3)	Ni2–S51	2.357(3)
Ni1–O5	2.068(6)	Ni1–O25	2.100(5)	Ni1–O45	2.047(6)
Ni2–O15	2.038(6)	Ni2–O35	2.090(5)	Ni2–O55	2.059(6)

There are no solvent molecules coordinated to Ba^{2+} and the coordination number of the Ba^{2+} ion is 9. Three *N* donor atoms of the pyridine rings are lying in a trigonal plane. Three *O* donor atoms of the carbonyl groups form a trigonal plane above the *N* plane. Another three *O* donor atoms of the carbonyl groups form a trigonal plane below the N plane. This results a coordination polyhedron of tricapped trigonal prism to the Ba atom. Both Ni atoms show a distorted octahedral environment being coordinated with three *S* and three *O* donor atoms of the aroylthiourea moieties. The selected bond lengths in $[BaNi_2(L^b)_3]$ are summarized in Table 3.7. The Ba–O bond lengths are in the range between 2.703(6) Å and 2.853(6) Å. The Ba–N bond lengths are in the range between 2.877(7) Å and 2.934(6) Å, that means in the range of those observed in the similar type of complexes reported above for Mn (Chapter 3.1) and Co (Chapter 3.2). The distances between the Ba and Ni atoms are 3.627(1) and 3.616(1) Å. The Ni–S bonds are in the range between 2.357(3) Å and 2.437(3) Å. The Ni–O bond lengths are in the range between 2.038(6) Å and 2.100(5) Å. These bond lengths are in the range of those observed in the trinuclear $Ni^{II}Ln^{III}Ni^{II}$ complexes (Chapter 2.2).

3.4 Coordination polyhedra in $[(M^b)^{II}(M^a)^{II}(M^b)^{II}]$ complexes

There are four different kinds of coordination polyhedra observed for the Ba^{2+} and Sr^{2+} ions in the crystallographically characterized mixed-metal complexes of H_2L^a and H_2L^b with transition metal ions. The shapes of the polyhedra are illustrated in Figure 3.13. The coordination numbers of the alkaline earth metal ions vary from 9 to 12. It depends on the additional coordination of solvent molecules and/or polymerization of the complex units. The alkaline earth metal ions exhibit a coordination number of 9 in the complexes $[SrMn_2(L^b)_3]$ (Fig 3.1), $[BaMn_2(L^a)_3]$ (Fig 3.3) and $[BaNi_2(L^b)_3]$ (Fig 3.12). In these cases no addition coordination of the solvent molecules or polymerization of the complex units are observed. The polyhedron is a tricapped trigonal prism (Fig 3.13 a). A coordination number of 10 is observed for the Sr^{2+} ion in $[SrMn_2(L^b)_3(THF)]$ (Fig 3.2) and for the Ba^{2+} ion in $[BaCo_2(L^a)_3(MeOH)]$ (Fig 3.8). In both cases coordination of an additional solvent molecule to the alkaline earth metal ions is observed. The coordination polyhedron in this case is an irregular tetracapped trigonal prism and is shown in Figure 3.13 b.

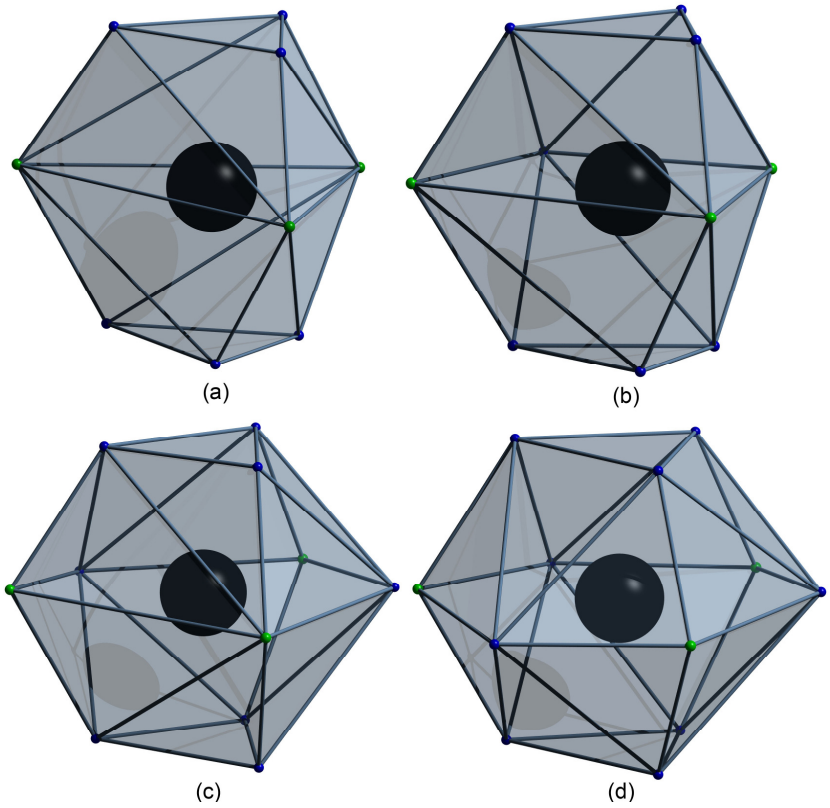

Figure 3.13 The observed coordination polyhedrons of the Sr and Ba atoms in the trinuclear $[(M^b)^{II}(M^a)^{II}(M^b)^{II}]$ complexes.

The higher coordination numbers 11 and 12 are observed in the coordination polymers of the Ba complexes. The polymerized $[BaCo_2(L^b)_3]$ complex exhibits a coordinated Ba^{2+} ion in the polymeric network with the coordination number of 11 (Fig 3.10). The shape of the polyhedron in this case is shown in Figure 3.13c. The polymerized $[BaMn_2(L^b)_3(MeOH)]$ complex exhibits the maximum coordination number of 12 for the every second Ba^{2+} ion in the polymeric chain. The polyhedron of Ba in this case is given in Figure 3.13d.

In all observed polyhedra the trigonal planes are formed by the carbonyl oxygen donor atoms of the organic ligands. They form a trigonal prismatic skeleton in all cases. The shapes of the polyhedra differ only by the middle plane. The middle plane is formed by the pyridine nitrogen donor atoms and the oxygen donor atoms of the solvent molecules and/or morpholine rings. It can be trigonal (3.13a), tetragonal (3.13b), pentagonal (3.13c) or hexagonal (3.13d) planes.

Chapter 4

Bi- and tetranuclear oxidorhenium(V) complexes of 2,6-dipicolinoylbis(*N,N*-diethylthiourea) with guest metal cations

---

Bi- and tetranuclear oxidorhenium(V) complexes of 2,6-dipicolinoylbis(*N,N*-diethylthiourea) with guest metal cations

The coordination chemistry of rhenium and technetium with benzoylthiourea ligand systems has extensively been investigated. The earliest report on this chemistry by *Abram* et al. in 1983 describes a synthetic and spectroscopic study on neutral benzoylthioureato complexes of technetium.[103] However, the first structurally characterized benzoylthiourea complex of rhenium was reported by *Dilworth* et al. in 1993.[104] A detailed investigation of the synthetic and structural chemistry of benzoylthiourea complexes of rhenium and technetium was reported by *Nguyen* and *Abram* in 2007.[21] Benzoylthiourea ligands form stable complexes with oxidorhenium(V) and oxidotechnetium(V) cores and the oxidorhenium(V) complexes can undergo dimerization by the formation of oxygen bridges between two rhenium centers. Recently, planar binuclear oxidorhenium(V) complexes (**47**) with the extended bipodal isophthaloylbis(thiourea) ligand system have been reported.[53]

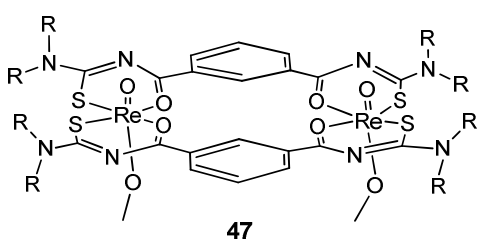

47

R = Et or i-Bu

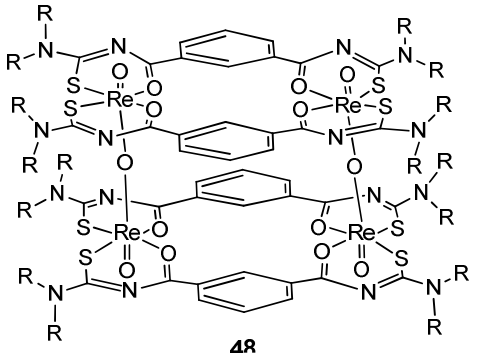

48

Chart 4.1 Previously reported oxidorhenium(V) complexes with bipodal isophthaloylbis(thioureas).[53]

Dimerization of two of such planar binuclear oxidorhenium(V) units to tetranuclear oxidorhenium(V) complexes produces a cage structure (**48**) with a free space having a distance of about 8.5 Å between the two oxidorhenium(V) cores (Chart 4.1). The extension of the structural chemistry of the isophthaloylbis(thioureato) complexes of Re(V) to the 2,6-dipicolinoyl derivative H_2L^a should allow the synthesis of a new type of oligonuclear compounds. It should be possible to " fill " the cavity formed by the coordination of the $\{ReO\}^{3+}$ cores with additional hard metal cations, such as K^+, Rb^+, Cs^+ or Tl^+. The following Chapters describe the synthesis and structural studies on such bi- and tetranuclear oxidorhenium(V) complexes with 2,6-dipicolinoylbis(*N,N*-diethylthiourea) ligands with different guest metal cations.

4.1 Binuclear oxidorhenium(V) complexes with guest metal cations $[M^1\{ReO(OCH_3)\}_2(L^a)_2]X$

Two equivalents of $(NBu_4)[ReOCl_4]$ rapidly react with two equivalents of H_2L^a and one equivalent of M^1Cl (where M^1 = K, Rb, Cs or Tl) in MeOH at 40 °C. Addition of a supporting base such as NEt_3 is needed for the deprotonation of H_2L^a. The initial green color of the reaction mixture turns immediately to red. Addition of one equivalent of $(NBu_4)(PF_6)$ or $(NBu_4)(ReO_4)$ to the reaction mixtures lead to the immediate precipitation of complexes of the compositions $[M^1\{ReO(OCH_3)\}_2(L^a)_2]X$ (**49**) (where X = PF_6 or ReO_4) (Scheme 4.1a). The same synthetic method works with KPF_6 instead of KCl, where the precipitation of $[K\{ReO(OCH_3)\}_2(L^a)_2](PF_6)$ (**50**) starts within 10 min. (Scheme 4.1b). All complexes of the composition $[M^1\{ReO(OCH_3)\}_2(L^a)_2]X$ (**49**) (M^1 = K, Rb, Cs or Tl, X = PF_6 or ReO_4) are red and good soluble in organic solvents such as acetone, $CHCl_3$ or CH_2Cl_2. They can be recrystallized by the slow evaporation of CH_2Cl_2/CH_3OH (1:1) mixtures.

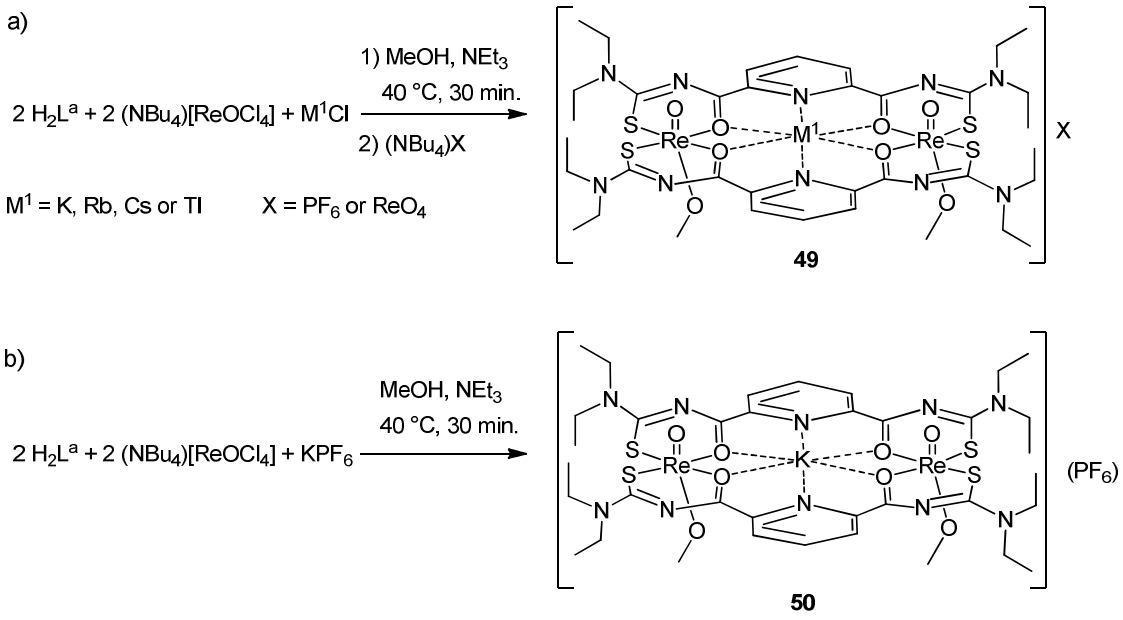

Scheme 4.1 Synthesis of binuclear oxidorhenium(V) complexes with guest metal cations.

Moreover, corresponding Cl^- salts $[M^1\{ReO(OCH_3)\}_2(L^a)_2]Cl$ (**51**) (where M^1 = K or Rb) can be isolated by slow evaporation of the reaction mixture. In this case, the addition of $(NBu_4)(PF_6)$ or $(NBu_4)(ReO_4)$ must be avoided. The analysis of the obtained red crystals confirms the formation of $[M^1\{ReO(OCH_3)\}_2(L^a)_2]Cl$. However the qualities of the obtained single crystals were too low to carry out an X-ray structural analysis.

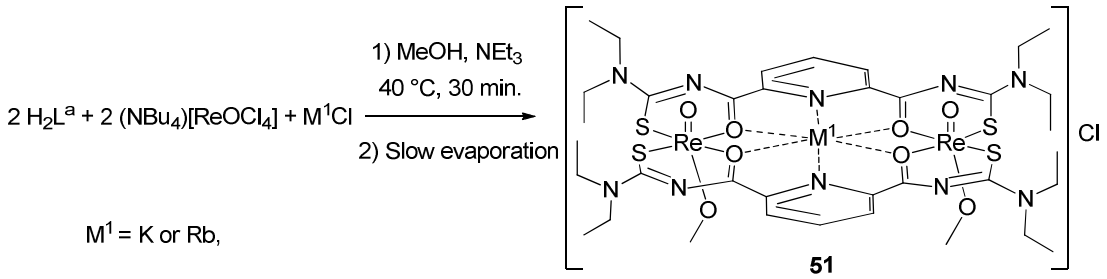

Scheme 4.2 Synthesis of binuclear oxidorhenium(V) complexes $[M^1\{ReO(OCH_3)\}_2(L^a)_2]Cl$ with K^+ or Rb^+ as guest metal cations.

IR spectra of the complexes show the absence of NH vibrations, which confirms the deprotonation of the organic ligand. Strong absorptions in the range between 1508 and 1539 cm^{-1} can be assigned to the coordinated ν C=O stretching vibrations. The ν C=O stretch of the non-coordinated ligand is observed at 1687 cm^{-1}. The bathochromic shift confirms the chelate formation with a large degree of electron delocalization through the aroylthiourea moieties. This phenomenon has already been observed for other metal complexes with aroylthioureas.[7, 9, 11-12] The presence of oxidorhenium(V) species is confirmed by ν Re=O stretching vibrations between 920 and 960 cm^{-1}.[105] ^{1}H-NMR spectra of complexes each show triplet and doublet signals in the range between 8.10 – 8.66 ppm which can be assigned to pyridine protons. Methylene protons of the complexes show a broad multiplet in the range of 3.80 – 4.20 ppm, while two well resolved multiplets in the ranges of 3.57 – 3.72 ppm and 3.95 – 4.08 ppm appear in the spectrum of H_2L^a. Moreover, two separate multiplets are observed for the methylene protons in mononuclear oxidorhenium(V) complexes of *N,N*-diethyl-*N'*-benzoylthioureas.[21] In addition to that, two well resolved triplets at 1.35 ppm and 1.46 ppm can be assigned to methyl protons which give a broad signal at 1.33 ppm in the spectrum of the ligand. Finally, the absence of NH proton signals is an additional proof of the deprotonation of the ligand in the rhenium complexes. ESI-Mass spectroscopy is a useful method to analyze this kind of complexes, since the binuclear oxidorhenium(V) complex ions with the guest metal cations $[M^1\{ReO(OCH_3)\}_2(L^a)_2]^+$ always appear as major peaks. The comparison of the observed and estimated isotopic patterns of the major peak in the ESI-mass spectrum of $[Tl\{ReO(OCH_3)\}_2(L^a)_2](PF_6)$ is presented in Figure 4.1. Additional signals with the compositions of $[Na\{ReO(OCH_3)\}_2(L^a)_2]^+$ and $[K\{ReO(OCH_3)\}_2(L^a)_2]^+$ are commonly observed in the mass spectra of $[M^1\{ReO(OCH_3)\}_2(L^a)_2]^+$ (M^1 = Rb^+, Cs^+ or Tl^+) complexes,

which confirms the exchange of the guest metal cation $(M^1)^+$ by Na^+ and K^+ ions from the matrix.

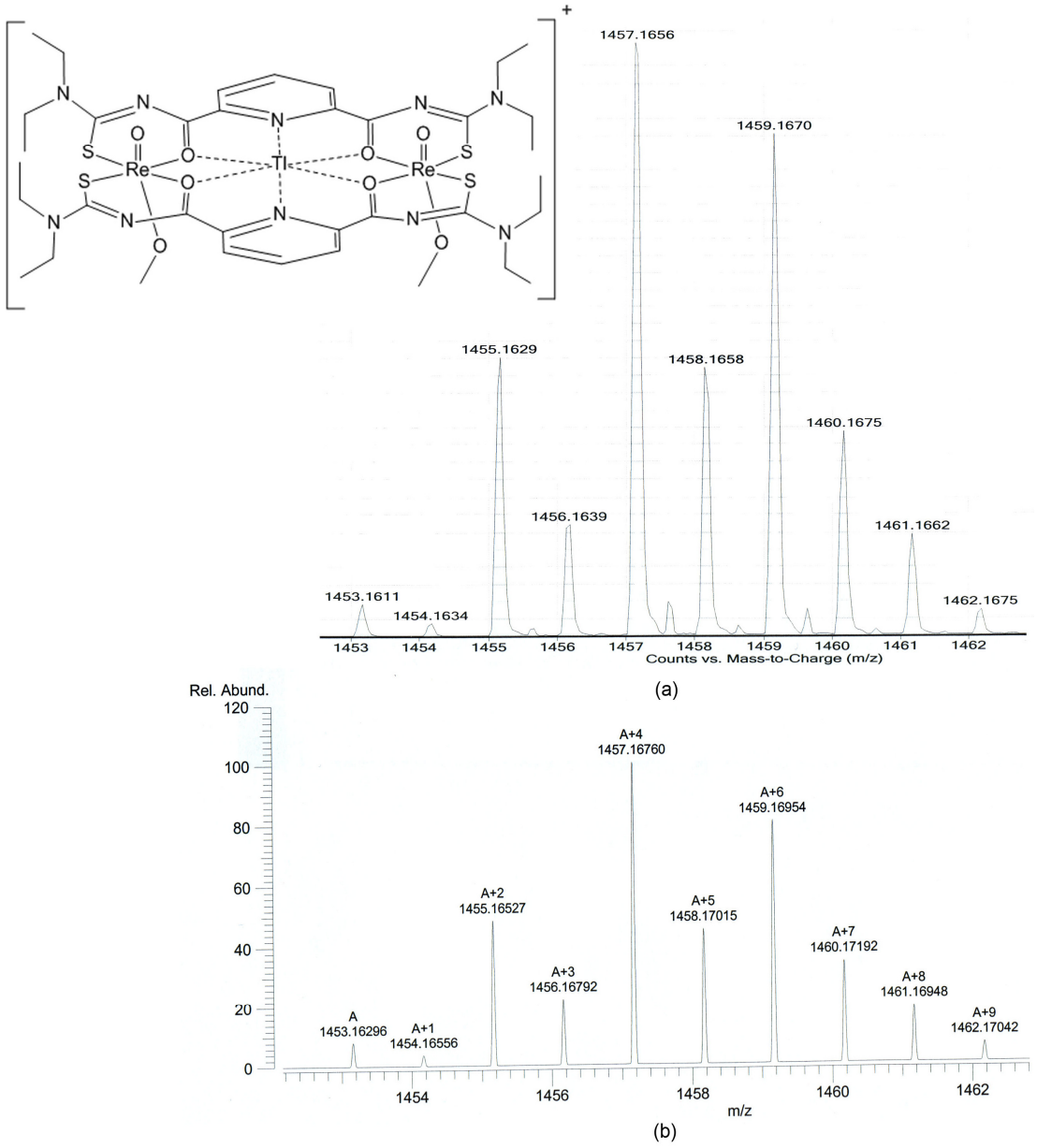

Figure 4.1 a) Observed isotopic pattern of the molecular ion $[Tl\{ReO(OCH_3)\}_2(L^a)_2]^+$ in the mass spectrum of $[Tl\{ReO(OCH_3)\}_2(L^a)_2](PF_6)$ b) Calculated isotopic pattern for $[Tl\{ReO(OCH_3)\}_2(L^a)_2]^+$.

Good quality single-crystals suitable for X-ray structural analysis can be obtained by the slow evaporation of CH_2Cl_2/CH_3OH (1:1) mixtures in the cases of $[M^1\{ReO(OCH_3)\}_2(L^a)_2](PF_6)$ and $[M^1\{ReO(OCH_3)\}_2(L^a)_2](ReO_4)$ (M^1 = K and Cs). The molecular structures of *anti*-

[K{ReO(OCH$_3$)}$_2$(L^a)$_2$](PF$_6$) and *syn*-[K{ReO(OCH$_3$)}$_2$(L^a)$_2$](ReO$_4$) and the coordination patterns of the metal ions are presented in Figure 4.2 and 4.3 respectively.

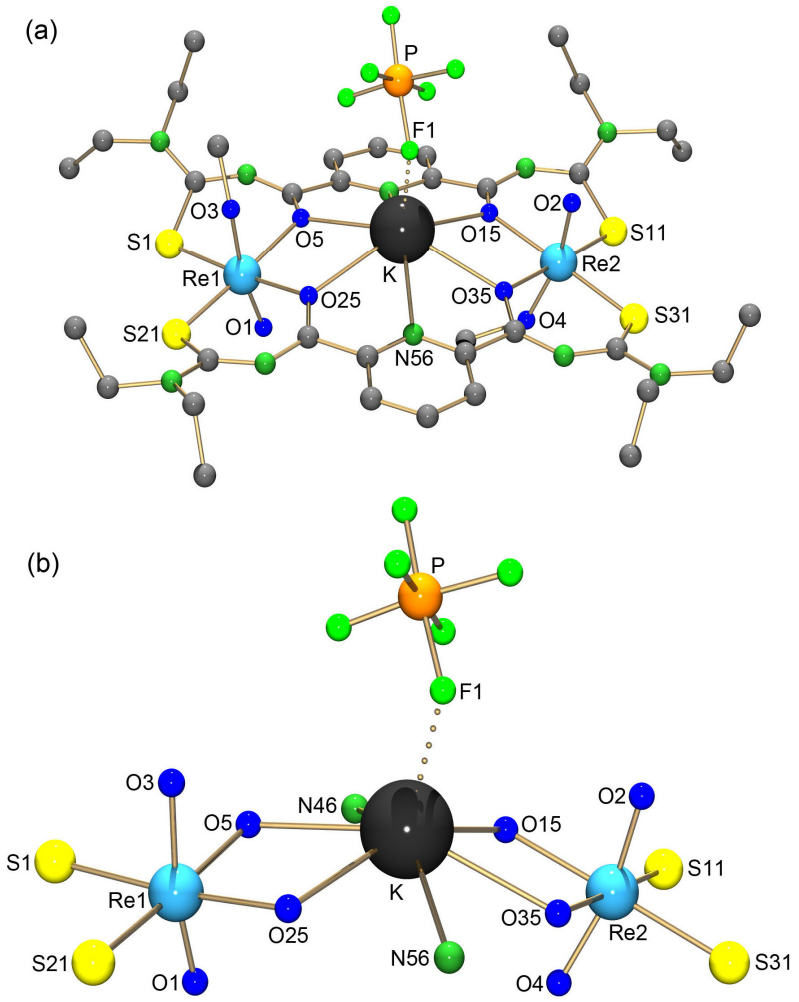

Figure 4.2 (a) Molecular structure of *anti*-[K{ReO(OCH$_3$)}$_2$(L^a)$_2$](PF$_6$). Hydrogen atoms are omitted for clarity. (b) Coordination environments of K and Re atoms in *anti*-[K{ReO(OCH$_3$)}$_2$(L^a)$_2$](PF$_6$).

Table 4.1 Selected bond lengths (Å) in *anti*-[K{ReO(OCH$_3$)}$_2$(L^a)$_2$](PF$_6$).

K–O5	2.750(5)	K–O15	2.793(6)	K–N46	2.887(6)
K–O25	2.855(5)	K–O35	2.821(6)	K–N56	2.934(6)
K···F1	2.75(1)	Re1–S1	2.353(2)	Re1–O5	2.141(5)
Re1–S21	2.318(2)	Re1–O25	2.115(4)	Re1–O1	1.690(5)
Re1–O3	1.856(5)	Re2–S11	2.305(3)	Re2–O15	2.140(5)
Re2–S31	2.330(2)	Re2–O35	2.163(6)	Re2–O2	1.757(7)
Re2–O4	1.780(7)				

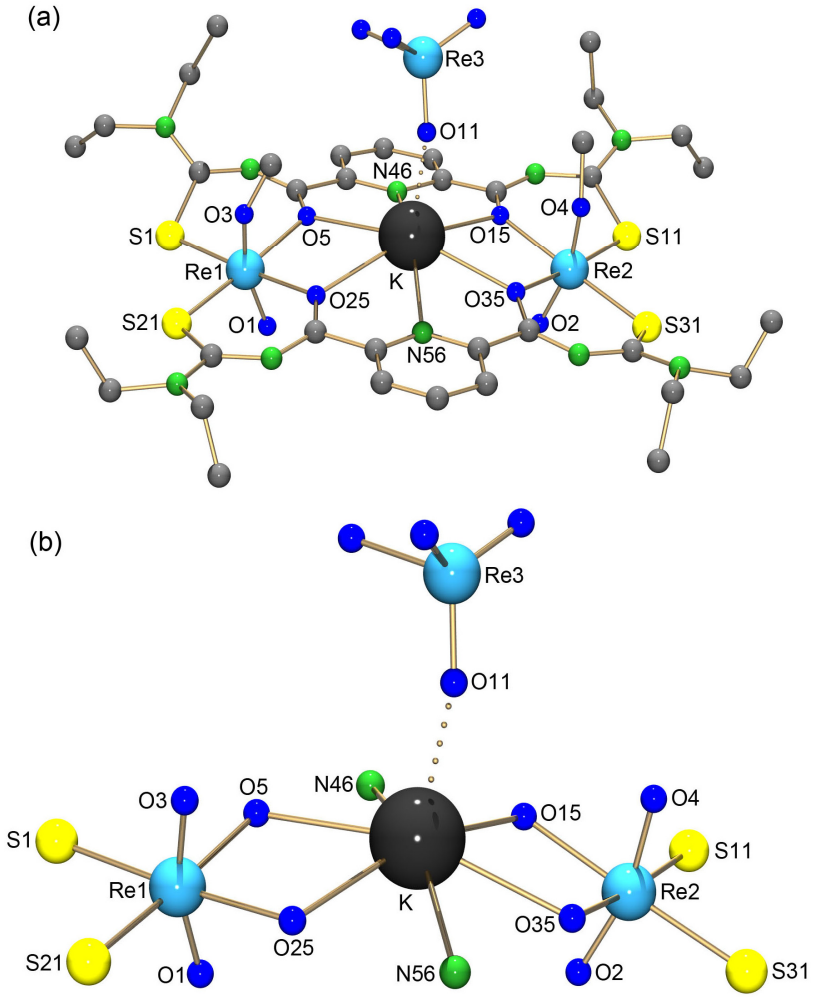

Figure 4.3 (a) Molecular structure of *syn*-[K{ReO(OCH$_3$)}$_2$(L^a)$_2$](ReO$_4$). Hydrogen atoms are omitted for clarity. (b) Coordination environments of K and Re atoms in *syn*-[K{ReO(OCH$_3$)}$_2$(L^a)$_2$](ReO$_4$).

Table 4.2 Selected bond lengths (Å) in *syn*-[K{ReO(OCH$_3$)}$_2$(L^a)$_2$](ReO$_4$).

K–O5	2.77(1)	K–O15	2.82(1)	K–N46	2.89(1)
K–O25	2.76(1)	K–O35	2.75(1)	K–N56	2.86(1)
K···O11	2.72(2)	Re1–S1	2.331(5)	Re1–O5	2.139(9)
Re1–S21	2.333(4)	Re1–O25	2.15(1)	Re1–O1	1.66(1)
Re1–O3	1.66(2)	Re2–S11	2.324(5)	Re2–O15	2.14(1)
Re2–S31	2.349(5)	Re2–O35	2.15(1)	Re2–O2	1.69(1)
Re2–O4	1.55(3)				

Both structures reveal, that two {L^a}$^{2-}$ ligands coordinate to two Re^V and one K$^+$ center. The K$^+$ ion selectively coordinates to the *O, N, O* donors of 2,6-dipicolinoyl moiety of both

ligands and each $\{ReO\}^{3+}$ unit coordinates to two equatorial aroylthiourea moieties via *S* and *O* donors. The distorted octahedral coordination sphere of the rhenium atoms are completed by the axial coordination of an oxido and a methoxido ligand. The arrangement of the axial oxido and methoxido ligands of Re^{V} are different in each complex. They show an *anti* arrangement in $[K\{ReO(OCH_3)\}_2(L^a)_2](PF_6)$ and a *syn* arrangement in $[K\{ReO(OCH_3)\}_2(L^a)_2](ReO_4)$. Both *syn* and *anti* isomers are possible in solution. There is an interchange between the isomers and they are in equilibrium in the presence of water. The similar *syn* and *anti* isomerism of oxido and methoxido ligands of Re^{V} cores have also been observed for the binuclear oxidorhenium(V) complexes of isophthaloylbis(thioureas).[53] A similar mechanism can also be proposed for the *syn* and *anti* isomerism of the binuclear oxidorhenium(V) complexes with guest metal cations (Scheme 4.3)

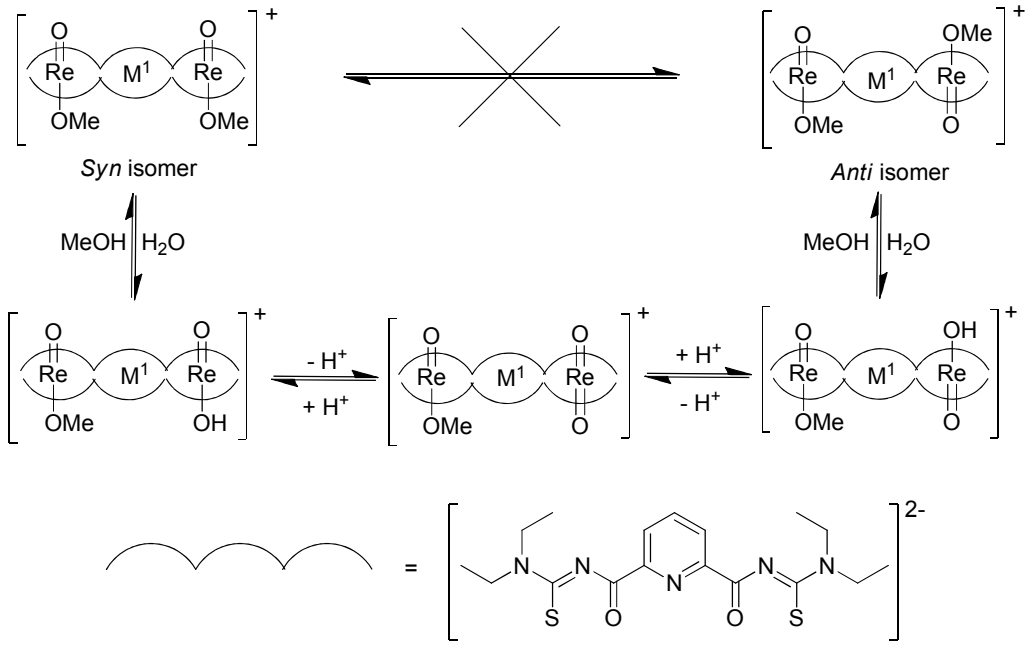

Scheme 4.3 Proposed mechanism for the interchange of *syn* and *anti* isomers of binuclear oxidorhenium(V) complexes with guest metal cations in solution.

Selected bond lengths of the complexes *anti*-$[K\{ReO(OCH_3)\}_2(L^a)_2](PF_6)$ and *syn*-$[K\{ReO(OCH_3)\}_2(L^a)_2](ReO_4)$ are presented in Tables 4.1 and 4.2, respectively. Bond lengths between the K^+ ion and donor atoms of the organic ligands are in the ranges between 2.86(1) and 2.934(6) Å for K–N bonds and 2.75(1) and 2.855(5) Å for K–O bonds. The anionic parts PF_6^- or ReO_4^- show week interactions to K^+ ions.

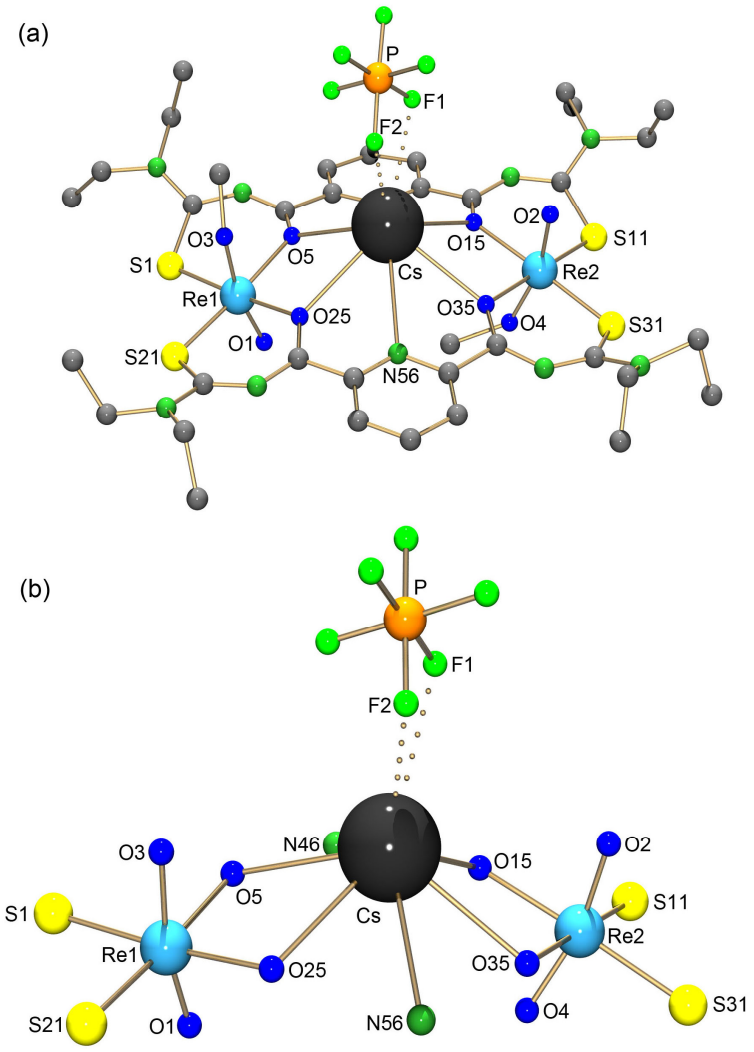

Figure 4.4 (a) Molecular structure of *anti*-[Cs{ReO(OCH$_3$)}$_2$(L^a)$_2$](PF$_6$). Hydrogen atoms are omitted for clarity. (b) Coordination environment of Cs and Re atoms in *anti*-[Cs{ReO(OCH$_3$)}$_2$(L^a)$_2$](PF$_6$).

Table 4.3 Selected bond lengths (Å) in [Cs{ReO(OCH$_3$)}$_2$(L^a)$_2$](PF$_6$).

Cs–O5	3.015(7)	Cs–O15	3.033(4)	Cs–N46	3.209(9)
Cs–O25	3.071(7)	Cs–O35	3.050(9)	Cs–N56	3.218(9)
Cs···F1	3.09(2)	Cs···F2	3.14(2)	Re1–S1	2.341(3)
Re1–O5	2.136(6)	Re1–S21	2.317(2)	Re1–O25	2.129(7)
Re1–O1	1.696(9)	Re1–O3	1.78(1)	Re2–S11	2.299(3)
Re2–O15	2.047(4)	Re2–S31	2.324(4)	Re2–O35	2.164(8)
Re2–O2	1.75(1)	Re2–O4	1.72(1)		

The molecular structures and coordination patterns of the metal centers in the complexes *anti*-[Cs{ReO(OCH$_3$)}$_2$(L^a)$_2$](PF$_6$) and *anti*-[Cs{ReO(OCH$_3$)}$_2$(L^a)$_2$](ReO$_4$) are presented in Figure 4.4 and 4.5 respectively. Two chelating {L^a}$^{2-}$ ligands coordinate to a Cs$^+$ ion and two oxidorhenium(V) units in a similar way observed in *anti*-[K{ReO(OCH$_3$)}$_2$(L^a)$_2$](PF$_6$) or *syn*-[K{ReO(OCH$_3$)}$_2$(L^a)$_2$](ReO$_4$). Axial oxido and methoxido ligands complete the octahedral coordination sphere of rhenium. The both oxidorhenium(V) cores have an *anti* arrangement in the cesium complexes. The anionic parts PF$_6^-$ or ReO$_4^-$ show week interactions to Cs$^+$ ions.

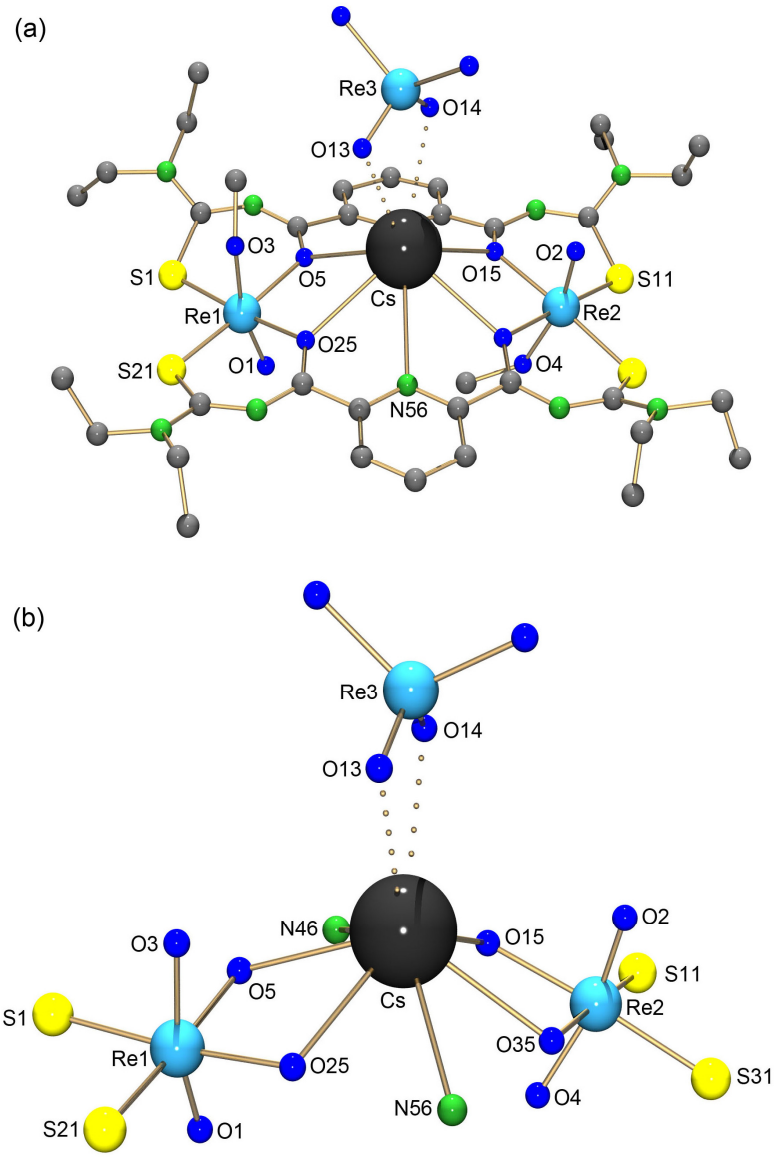

Figure 4.5 (a) Molecular structure of *anti*-[Cs{ReO(OCH$_3$)}$_2$(L^a)$_2$](ReO$_4$). Hydrogen atoms are omitted for clarity. (b) Coordination environment of Cs and Re in *anti*-[Cs{ReO(OCH$_3$)}$_2$(L^a)$_2$](ReO$_4$).

Table 4.4 Selected bond lengths (Å) in *anti*-[Cs{$ReO(OCH_3)$}$_2$(L^a)$_2$](ReO_4).

Cs–O5	3.001(9)	Cs–O15	3.025(7)	Cs–N46	3.196(8)
Cs–O25	3.090(7)	Cs–O35	3.043(8)	Cs–N56	3.219(9)
Cs···O13	3.21(2)	Cs···O14	3.50(2)	Re1–S1	2.343(3)
Re1–O5	2.145(7)	Re1–S21	2.314(2)	Re1–O25	2.123(8)
Re1–O1	1.714(7)	Re1–O3	1.857(9)	Re2–S11	2.325(3)
Re2–O15	2.153(8)	Re2–S31	2.333(3)	Re2–O35	2.157(7)
Re2–O2	1.67(1)	Re2–O4	1.885(9)		

Selected bond lengths of the complexes *anti*-[Cs{$ReO(OCH_3)$}$_2$(L^a)$_2$](PF_6) and *anti*-[Cs{$ReO(OCH_3)$}$_2$(L^a)$_2$](ReO_4) are summarized in Tables 4.3 and 4.4 respectively. Cs–N bond lengths are in the range between 3.196(8) Å and 3.219(9) Å and Cs–O bond lengths are in the range between 3.001(9) Å and 3.090(7) Å. Both bond lengths are expectedly much longer than the K–N or K–O bonds in the potassium complexes. The Cs···F1 and Cs···F2 distances are 3.09(2) Å and 3.14(2) Å respectively in the complex *anti*-[Cs{$ReO(OCH_3)$}$_2$(L^a)$_2$](PF_6) and the Cs···O13 and Cs···O14 distances are 3.21(2) Å and 3.50(2) Å respectively in the complex *anti*-[Cs{$ReO(OCH_3)$}$_2$(L^a)$_2$](ReO_4). The equatorial bond lengths of the Re atoms in all crystalographically characterized binuclear oxidorhenium(V) complexes with K^+ and Cs^+ cations are in the range between 2.305(3) Å and 2.353(2) Å for Re–S bonds and between 2.047(4) Å and 2.164(8) Å for Re–O bonds. Both Re–S and Re–O equatorial bond lengths are in the similar range of Re–S and Re–O bond lengths in the binuclear oxidorhenium(V) complexes with isophthaloylbis(thiourea) ligands.[53]

The K^+ and Cs^+ ions are coordinated by two 2,6-dipicolinoyl moieties of the chelating ligands via *O,N,O* donor atoms. The 4 oxygen and 2 nitrogen donor atoms of two 2,6-dipicolinoyl moieties form a hexagonal plane. The distances between the alkali metal ions and the mean least square plane formed by the donor atoms of these hexagonal planes in each complex are summarized in the Table 4.5. These distances are shorter in the potassium complexes than in the Cs complexes. These observations confirm that the K^+ ion is situated more close to the ligand plane compared to the situation in the cesium complexes (Fig 4.6). This can be explained on the basis of their ionic radii.

Table 4.5 The distances between the alkali metal ions and the hexagonal mean least square planes formed by the donor atoms of the bis(2,6-dipicolinoyl) parts of the ligands in the $[M^1\{ReO(OCH_3)\}_2(L^a)_2]X$ complexes (M^1 = K or Cs).

M^1	$[M^1\{ReO(OCH_3)\}_2(L^a)_2](PF_6)$	$[M^1\{ReO(OCH_3)\}_2(L^a)_2](ReO_4)$
K	0.719(1) Å	0.525(1) Å
Cs	1.385(1) Å	1.393(1) Å

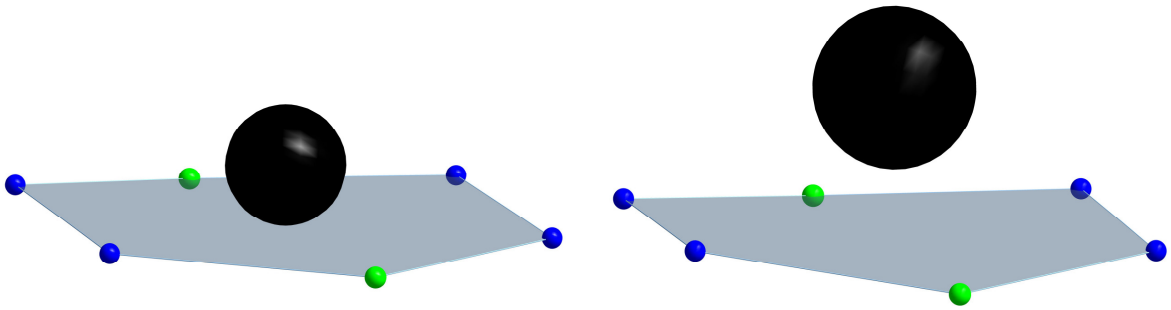

Figure 4.6 The positions of (a) K^+ and (b) Cs^+ ions above the hexagonal mean least square planes formed by the donor atoms of the bis(2,6-dipicolinoyl) parts of the ligands in the $[M^1\{ReO(OCH_3)\}_2(L^a)_2]X$ complexes (M^1 = K or Cs).

The coordination chemistry of metal ions with cyclic polyethers (crown ethers) play an important role in host-guest chemistry since their first invention in 1967 by Pedersen.[106] Crown ethers became popular and extremely useful ligands because of their high coordination affinity towards the majority of metal ions in the periodic table.[107] However, metal ions such as Li^+, Na^+, K^+, Rb^+, Cs^+ and Tl^+ being the major guests to crown ethers and most of the crown ether complexes have been reported with those cations.[108] The coordination of the *O,N,O* donor atoms of two chelating $\{L^a\}^{2-}$ ligands to the $(M^1)^+$ ions in the complexes $[M^1\{ReO(OCH_3)\}_2(L^a)_2](X)$ (**49**) are similar to the coordination of diaza-18-crown-6 (**52**) ethers to metal ions (Chart 4.2).

A number of complexes of diaza-18-crown-6 ether derivatives with Li^+, Na^+, K^+, Rb^+, Cs^+ and Tl^+ has been reported.[109-114] A search for such complexes in the Cambridge Structural Database (CSD) results in 703 hits including the complexes with 2,2,2-cryptand (**53**) because 2,2,2-cryptand itself has a diaza-18-crown-6 moiety. Among them, only the complexes with 2,2,2-cryptand are 649. The reason, obviously, is the 2,2,2-cryptand complexes are more stable because of the compact structure with 2 additional oxygen donor atoms. The remaining

54 are complexes of diaza-18-crown-6 ether and their derivatives. Majority of these complexes are with potassium and sodium ions.

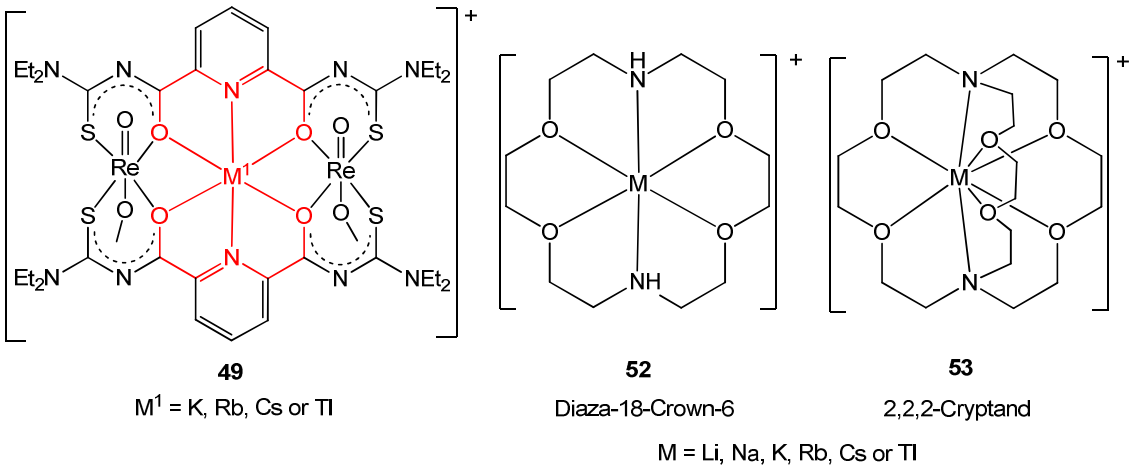

49 **52** **53**

M^1 = K, Rb, Cs or Tl Diaza-18-Crown-6 2,2,2-Cryptand

M = Li, Na, K, Rb, Cs or Tl

Chart 4.2 Comparison of the coordination situation of the metal ions in $[M^1\{ReO(OCH_3)\}_2(L^a)_2]^+$ with the complexes of diaza-18-crown-6 (**52**) and 2,2,2-cryptand (**53**).

The diaza-18-crown-6, similar to 18-crown-6, is flexible to accept metal cations from smaller ionic diameter such as Li^+ (1.56 Å) to bigger ionic diameter such as Cs^+ (3.34 Å). This flexibility comes from the sp^3 hybridization of the carbon, oxygen and nitrogen atomic orbitals. It allows the bending of the diaza-18-crown-6 molecule during the coordination to smaller metal ions, which is observed in the case of lithium complexes.[115] In the case of sodium complexes, the metal ion is situated almost in the plane of the diaza-18-crown-6 molecule.[116-117]

Table 4.6 Ionic diameters of the applied guest metal ions.

M	Ionic diameter of M^+ (Å)
Li	1.56
Na	1.94
K	2.66
Rb	2.96
Cs	3.34
Tl	2.96

The K^+, Rb^+, Cs^+ and Tl^+ ions are bigger to be hosted in the same plane of the diaza-18-crown-6 molecule.[117-121] In those cases, the metal ions are situated above the plane of the diaza-18-crown-6 molecule which is known as 'Sunrise' conformation.[122] The distance of

the metal cation from the plane of the diaza-18-crown-6 molecule increases with the size of the metal cation. It means, the K^+ ion is closer to the plane and the resulting complex is more stable than such with bigger metal cations. The Rb^+, Tl^+ and Cs^+ ions are situated above the planes and are less stable. The ionic diameters of the alkali metal ions and Tl^+ ion are summarized in the Table 4.6.

The diameters of the central cavities between two 2,6-dipicolinoyl moieties in the $[M^1\{ReO(OCH_3)\}_2(L^a)_2]X$ complexes are calculated by the distances between diagonal carbonyl oxygen donor atoms and pyridine nitrogen donor atoms which made the cavity. These distances are in the range between 5.413 Å – 5.566 Å in all crystallographically characterized $[M^1\{ReO(OCH_3)\}_2(L^a)_2]X$ complexes. There is less flexibility possible because of the sp^2 hybridization of the carbon, nitrogen and oxygen atoms of the 2,6-dipicolinoyl moieties. Due to this reason, only the metal ions with the size of K^+ ion and bigger are stable in the binuclear oxidorhenium(V) complexes. The Na^+ ion with the diameter of 1.94 Å might not be stabilized in this less-flexible environment with a diameter of around 5.5 Å. The diameter of Li^+ ion is 1.56 Å and it is expectedly too small to be stabilized inside the rigid space. The K^+ and Cs^+ ions are situated above the plane of the cavity in the $[M^1\{ReO(OCH_3)\}_2(L^a)_2]X$ complexes. The M^1–O and M^1–N bond lengths observed in the $[M^1\{ReO(OCH_3)\}_2(L^a)_2]X$ (**49**) complexes are in the range of those reported in the corresponding crown ether complexes.[122]

4.2 Tetranuclear oxidorhenium(V) complexes with guest metal cations $[M^{I}(Re_2O_3)_2(L^{a})_4]X$

Dimerization of oxidorhenium(V) cores via formation of oxygen-bridges is a known phenomenon and has previously been reported.[53] Similarly, the binuclear oxidorhenium(V) complexes containing a guest-metal cation, $[M^{I}\{ReO(OCH_3)\}_2(L^{a})_2]X$ (**49**), undergo dimerization. In the solvent mixture CH_2Cl_2/CH_3CN(aq) (1:1) they form tetranuclear oxidorhenium(V) complexes containing guest-metal cations, $[M^{I}(Re_2O_3)_2(L^{a})_4]X$ (**54**) (Scheme 4.4). The counter anions of the binuclear complexes, PF_6^- or ReO_4^-, remain and also stabilize the tetranuclear complexes.

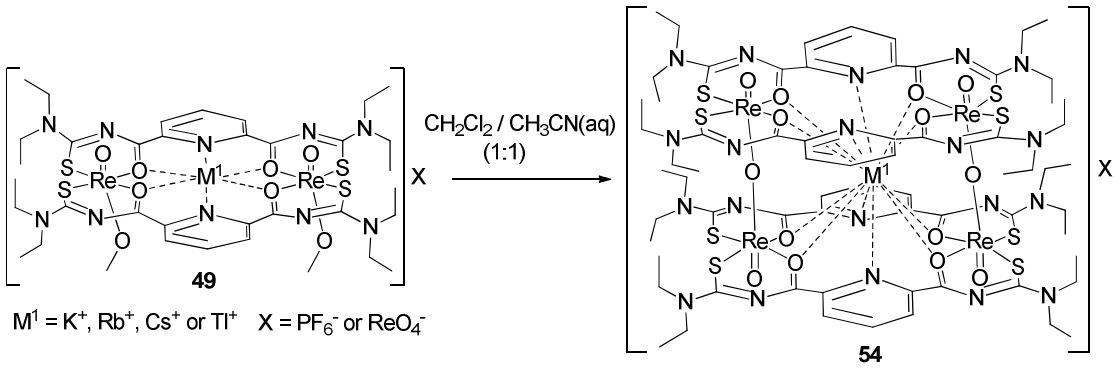

Scheme 4.4 Formation of tetranuclear oxidorhenium(V) complexes with guest metal cations.

A proposed mechanism for the dimerization of $[M^{I}\{ReO(OCH_3)\}_2(L^{a})_2]X$ (**49**) complexes to the $[M^{I}(Re_2O_3)_2(L^{a})_4]X$ (**54**) complexes is illustrated in Scheme 4.5. The mechanism shows, that the presence of water is necessary for the dimerization process. Aqueous CH_3CN solution fulfills this requirement. CH_2Cl_2 solution is applied because of the solubility of the binuclear oxidorhenium(V) complexes in this solvent. Obviously, the dimerization to tetranuclear oxidorhenium(V) complexes is only directly possible from a *syn* isomer of binuclear oxidorhenium(V) complexes because of the alignments of the methoxido ligands in same direction. But also the *anti* isomer forms the described oxygen bridges. Their direct formation would result in coordination polymers and has already been reported for the complexes with isophthaloylbis(thiourea) ligands.[53] However, *syn* and *anti* isomers are in equilibrium in solution and a possible mechanism for this interchange between *syn* and *anti* isomers is discussed in the previous chapter (Chapter 4.1, see also Scheme 4.3). Therefore the formation of well-defined tetranuclear oxidorhenium(V) complexes is independent of the *syn* and *anti* isomerism of the binuclear oxidorhenium(V) complexes.

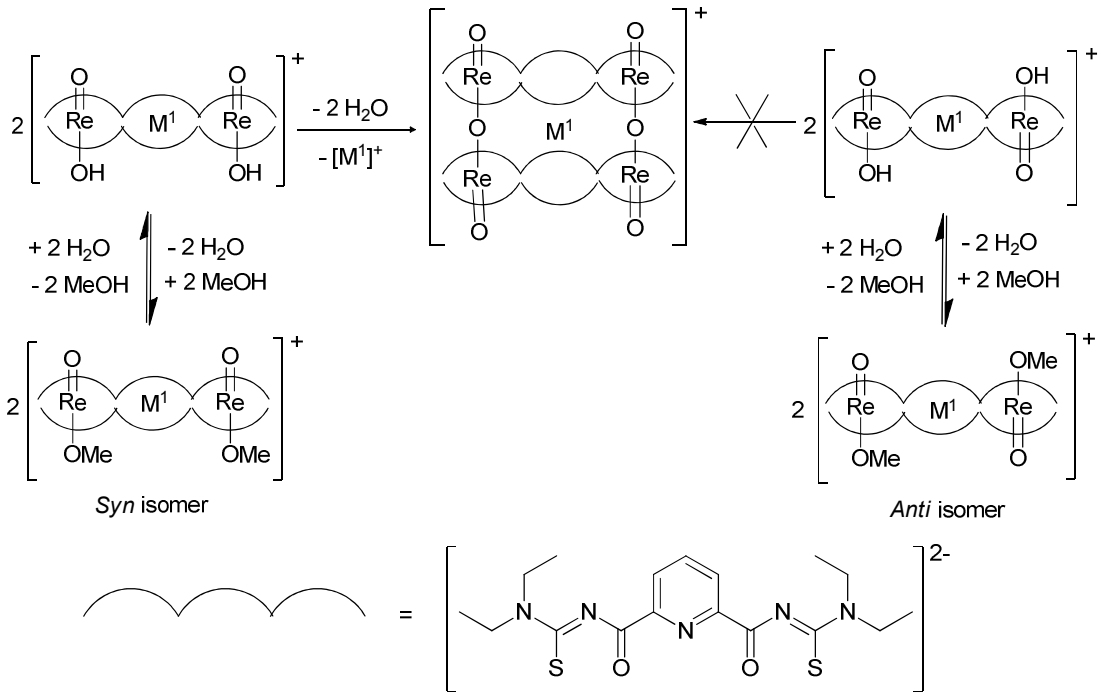

Scheme 4.5 Proposed mechanism for the formation of tetranuclear oxidorhenium(V) complexes from binuclear oxidorhenium(V) complexes with guest metal cations.

IR spectra of the complexes show strong absorptions in the range between 650 and 720 cm^{-1}, which are typical for the Re–O–Re unit of the $\{Re_2O_3\}^{4+}$ core.[105] Additionally, Re=O stretches become weaker due to the formation of the oxygen bridges and the corresponding bands appear around 910 cm^{-1}. There is no particular difference observed in the C=O stretching vibrations of the dimeric and tetrameric complexes. The bands appear in the range between 1508 and 1533 cm^{-1} for both complex types. ESI-mass spectra show as major peaks the molecular ions of the cationic species having the composition $[M^l(Re_2O_3)_2(L^a)_4]^+$. Additionally, a peak corresponding to $[K(Re_2O_3)_2(L^a)_4]^+$ is observed in some cases. ^{1}H-NMR spectra of tetranuclear oxidorhenium(V) complexes confirm the absence of methoxido ligands and show the signals of the pyridine protons in the range between 7.9 – 8.3 ppm. Methylene protons give three or four sets of multiplets and appear in the same range where they appear in the spectra of binuclear oxidorhenium(V) complexes. Methyl protons give two separate triplets with chemical shifts similar to the signals for the binuclear oxidorhenium(v) complexes.

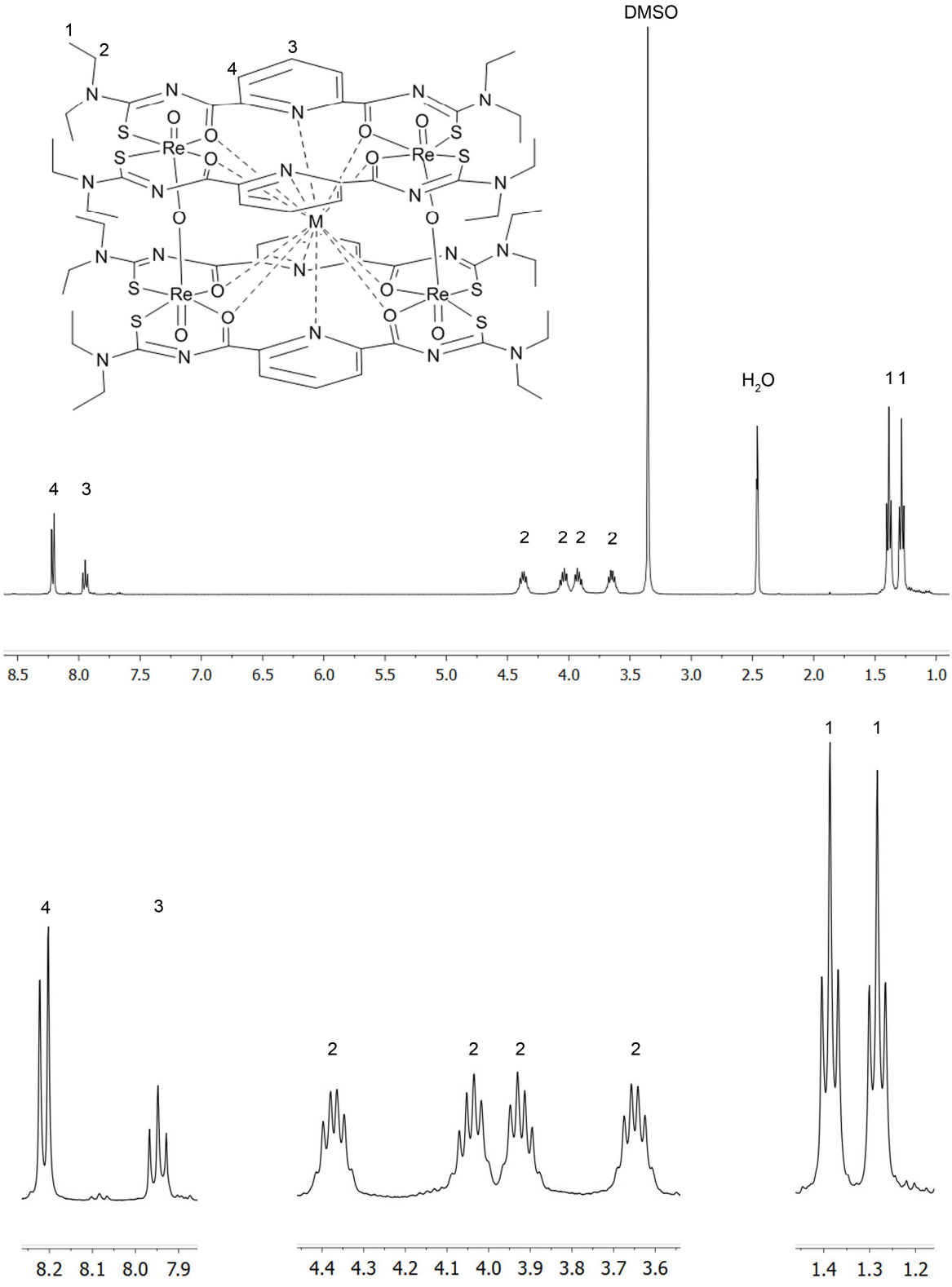

Figure 4.7 ^{1}H-NMR spectrum of $[Rb(Re_2O_3)_2(L^a)_4](PF_6)$ in DMSO-d6.

The ^{1}H-NMR spectrum of $[Rb(Re_2O_3)_2(L^a)_4](PF_6)$ is chosen for the detailed explanation of the typical ^{1}H-NMR pattern of the tetranuclear oxidorhenium(V) cages and is presented in Figure 4.7. The spectrum shows a well resolved doublet at 8.21 ppm, which is assigned to the *meta* protons of the pyridine ring. A triplet at 7.95 ppm is due to the proton at the *para* position of the pyridine ring. These signals confirm the four chelating $\{L^a\}^{2-}$ ligands in the complex being magnetically equivalent. Moreover, two well resolved triplets at 1.28 ppm and 1.39 ppm can be assigned to methyl protons of the ethyl residues, while four sets of multiplets in the range between 3.6 and 4.4 ppm are due to the methylene protons of the ethyl residues. These sets of signals for the methyl and methylene protons of the ethyl residues are due to the hindered rotation around the C–NEt_2 bonds and are also observed in the ^{1}H-NMR spectrum of the H_2L^a ligand (Chapter 1.2).

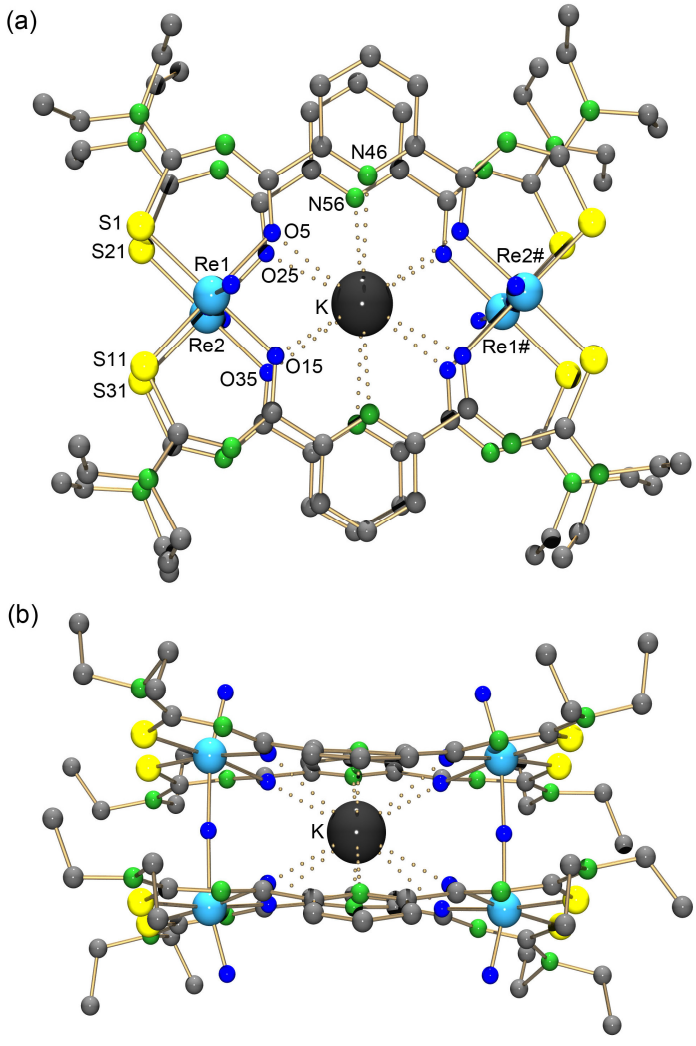

Figure 4.8 Molecular structure of $[K(Re_2O_3)_2(L^a)_4]^+$. Hydrogen atoms are omitted for clarity. (a) View perpendicular to the thioureato ligand planes. (b) View parallel to the thioureato ligand planes.

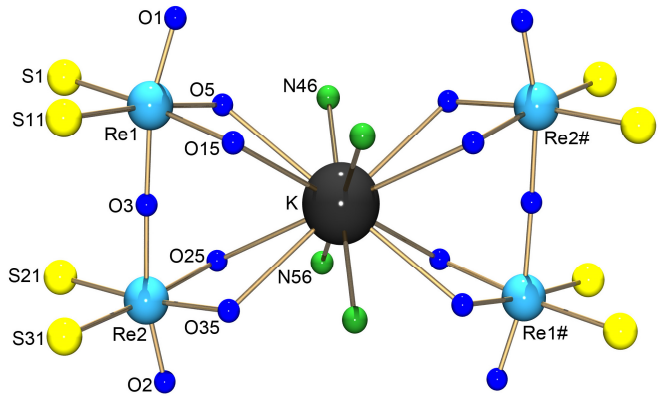

Figure 4.9 Coordination patterns of K and Re atoms in $[K(Re_2O_3)_2(L^a)_4]^+$. Only donor atoms of the ligands are shown.

Table 4.7 Selected bond lengths (Å) in $[K(Re_2O_3)_2(L^a)_4]^+$.

K–O5	3.175(5)	K–O15	3.114(6)	K–N46	3.431(7)
K–O25	3.154(5)	K–O35	3.210(6)	K–N56	3.045(7)
Re1–O1	1.700(7)	Re1–S1	2.320(2)	Re1–O5	2.135(6)
Re1–O3	1.916(6)	Re1–S11	2.311(2)	Re1–O15	2.127(5)
Re2–O2	1.691(7)	Re2–S21	2.320(2)	Re2–O25	2.099(5)
Re2–O3	1.900(6)	Re2–S31	2.327(2)	Re2–O35	2.130(5)

Good quality crystals suitable for X-ray analysis were obtained in the cases of $[K(Re_2O_3)_2(L^a)_4](PF_6)$, $[Rb(Re_2O_3)_2(L^a)_4](PF_6)$, $[Cs(Re_2O_3)_2(L^a)_4](PF_6)$ and $[Tl(Re_2O_3)_2(L^a)_4](PF_6)$ from CH_2Cl_2/CH_3CN (1:1) solutions. Several attempts to crystallize the $[M^1(Re_2O_3)_2(L^a)_4](ReO_4)$ complexes were not successful. Crystallographic analysis of $[M^1(Re_2O_3)_2(L^a)_4](PF_6)$ complexes show that the guest metal cations are captured inside the void between four oxidorhenium(V) centers. This space is ideal to accommodate metal ions such as K^+, Rb^+, Cs^+ or Tl^+. The metal ions are coordinated by the *O,N,O* donor atoms of four 2,6-dipicoloyl moieties from four $\{L^a\}^{2-}$ ligands.

The molecular structure of $[K(Re_2O_3)_2(L^a)_4]^+$ cation is presented in Figure 4.8. The complex $[K(Re_2O_3)_2(L^a)_4](PF_6)$ crystallizes in the monoclinic crystal system in the space group *C2/c* with one half of the molecule in the asymmetric unit. The complete molecule is generated by a C_2 axis, which is perpendicular to the thioureato ligand planes and passes through the K^+ cation in the cage. The coordination patterns of the metal ions are presented in Figure 4.9. Selected bond lengths are presented in Table 4.6. The K–O distances are in the range between 3.114(6) – 3.210(6) Å and the K–N distances are 3.045(7) Å and 3.431 (7) Å. This is in both

cases significantly longer than the K–O and K–N bond lengths in the complex $[K\{ReO(OCH_3)\}_2(L^a)_2](PF_6)$, where we find K–O bonds in the range between range of 2.750(5) and 2.855(5) Å and K–N bonds in the range between 2.887(6) and 2.934(6) Å. Thus, in the tetranuclear oxidorhenium(V) complexes, these contacts are better explained as bonding interactions than as covalent bonds. The equatorial Re–S bond lengths are in the range between 2.311(2) Å and 2.327(2) Å. The equatorial Re–O bond lengths are in the range between 2.099(5) Å and 2.135(6) Å. These are in the similar range of corresponding bonds observed in the $[K\{ReO(OCH_3)\}_2(L^a)_2](PF_6)$ complexes (Chapter 4.1). Re=O bond lengths are 1.691(7) Å and 1.700(7) Å, which are in the typical range of Re=O bonds. The bond lengths between Re and the bridging oxygen atoms are 1.900(6) Å and 1.916(6) Å. Summarizing, it can be stated that the bond lengths between Re atom and the donor atoms in $[K(Re_2O_3)_2(L^a)_4](PF_6)$ are in the same ranges of those observed in the previously reported tetranuclear oxidorhenium(V) cage complexes with isophthaloylbis(thioureas).[53] A space filling model of the cation $[K\{ReO(OCH_3)\}_2(L^a)_2]^+$ is presented in Figure 4.10.

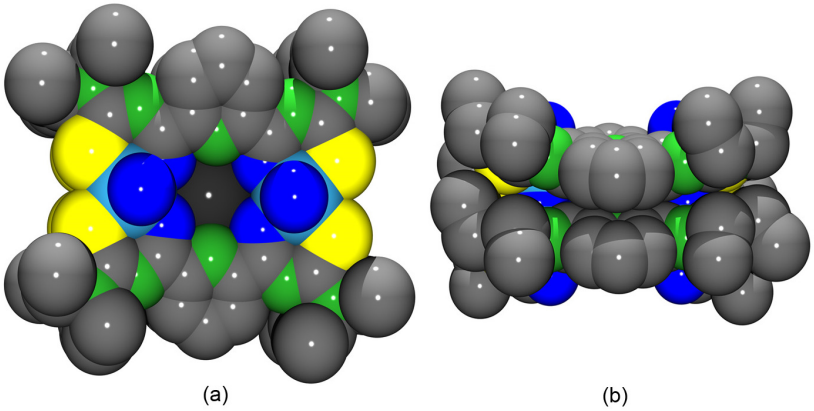

Figure 4.10 Space filling model of the $[K(Re_2O_3)_2(L^a)_4]^+$ cation. (a) View perpendicular to the thioureato ligand planes. (b) View parallel to the thioureato ligand planes.

The complex $[Rb(Re_2O_3)_2(L^a)_4](PF_6)$ crystallizes in the monoclinic space group *C2/c* like the potassium analogue. One half of the molecule is seen in the asymmetric unit and the symmetry related atoms are produced by a C_2 axis, which goes through the Rb atom. The molecular structure of the $[Rb(Re_2O_3)_2(L^a)_4]^+$ cation is presented in Figure 4.11. The coordination patterns of the metal ions are presented in Figure 4.12. Selected bond lengths are summarized in Table 4.7. The Rb–N distances are 3.105(5) Å and 3.435(5) Å respectively. The Rb–O distances are in the range of 3.111(4) Å and 3.218(4) Å.

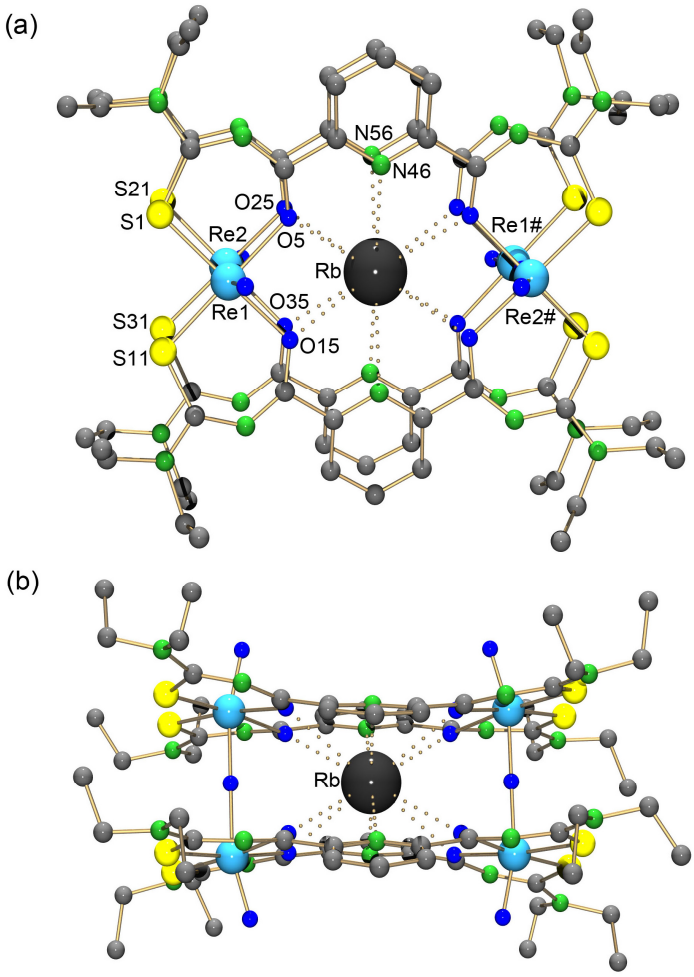

Figure 4.11 Molecular structure of $[Rb(Re_2O_3)_2(L^a)_4]^+$. Hydrogen atoms are omitted for clarity. (a) View perpendicular to the thioureato ligand planes. (b) View parallel to the thioureato ligand planes.

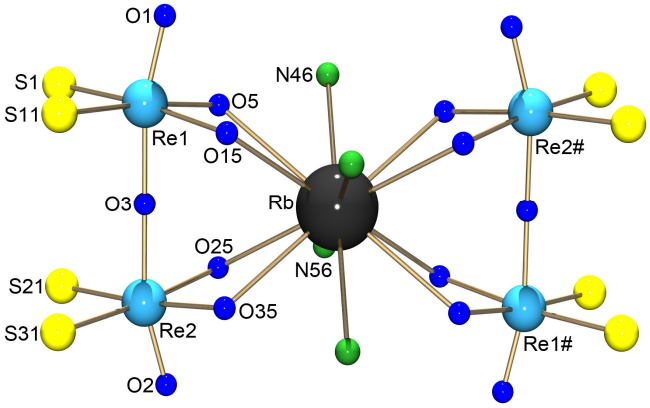

Figure 4.12 Coordination patterns of Rb and Re atoms in $[Rb(Re_2O_3)_2(L^a)_4]^+$. Only donor atoms of the ligands are shown.

Table 4.8 Selected bond lengths (Å) in $[Rb(Re_2O_3)_2(L^a)_4]^+$.

Rb–O5	3.189(4)	Rb–O15	3.218(4)	Rb–N46	3.105(5)
Rb–O25	3.161(4)	Rb–O35	3.111(4)	Rb–N56	3.435(5)
Re1–O1	1.680(5)	Re1–S1	2.325(2)	Re1–O5	2.129(4)
Re1–O3	1.905(4)	Re1–S11	2.331(2)	Re1–O15	2.141(4)
Re2–O2	1.674(5)	Re2–S21	2.322(2)	Re2–O25	2.150(4)
Re2–O3	1.909(4)	Re2–S31	2.316(2)	Re2–O35	2.140(4)

These values are in the range of K–O and K–N bond lengths observed in the potassium complex and the corresponding discussion done for the potassium compound also applies for the rubidium compound. The Re=O bond lengths are 1.680(5) Å and 1.674(5) Å. The Re–O bond lengths between bridging oxygen donor atoms are 1.905(4) Å and 1.909(4) Å. All Re^V bond lengths in the $[Rb(Re_2O_3)_2(L^a)_4](PF_6)$ complex are in the range of those observed in the potassium complex.

The complex $[Cs(Re_2O_3)_2(L^a)_4](PF_6)$ crystallizes in the triclinic space group $P\bar{1}$. The molecular structure of $[Cs(Re_2O_3)_2(L^a)_4]^+$ is presented in Figure 4.13. The coordination pattern of the metal ions is illustrated in Figure 4.14 and it shows a coordination of Cs^+ ion like in the potassium and rubidium analogs. Selected bond lengths are summarized in Table 4.8. Bond distances between Cs and the organic ligands are in the range between 3.139(8) Å – 3.271(9) Å for the Cs–O bonds and 3.199(7) Å – 3.417(8) Å for the Cs–N bonds. There are no specific differences observed in the bond distances between the potassium, rubidium and cesium containing complexes. The oxidorhenium(V) centers show distorted octahedral geometry. The Re=O bond lengths are in the range between 1.674(3) Å – 1.698(2) Å. The Re–O bond lengths between bridging oxygen donor atoms are in the range between 1.891(6) Å – 1.923(6) Å. The bond lengths between Re^V and the organic ligands are in the range between 2.316(3) Å – 2.341(3) Å for Re–S bonds and 2.105(8) Å – 2.147(8) Å for Re–O bonds. These bond lengths are in the range of those observed in the K and Rb complexes.

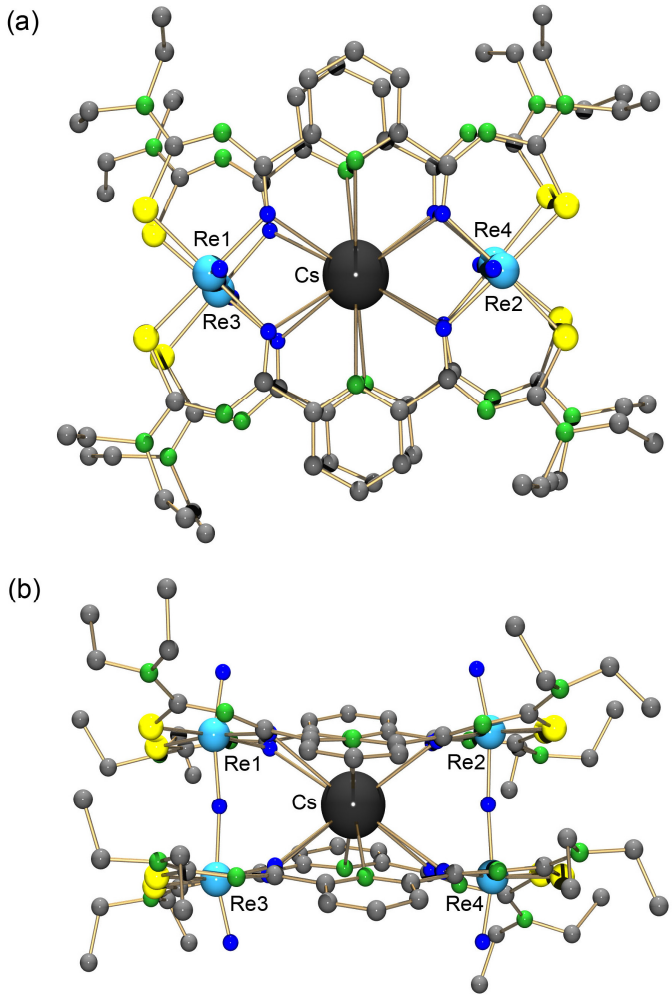

Figure 4.13 Molecular structure of $[Cs(Re_2O_3)_2(L^a)_4]^+$. Hydrogen atoms are omitted for clarity. (a) View perpendicular to the thioureato ligand planes. (b) View parallel to the thioureato ligand planes.

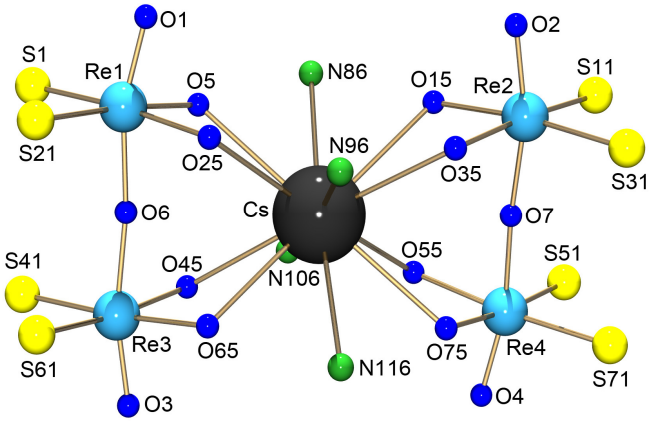

Figure 4.14 Coordination patterns of the Cs and Re atoms in $[Cs(Re_2O_3)_2(L^a)_4]^+$. Only donor atoms of the ligands are shown.

Table 4.9 Selected bond lengths (Å) in $[Cs(Re_2O_3)_2(L^a)_4]^+$.

Cs–O5	3.197(8)	Cs–O15	3.245(8)	Cs–N86	3.201(9)
Cs–O25	3.271(9)	Cs–O35	3.178(8)	Cs–N96	3.415(6)
Cs–O45	3.200(9)	Cs–O55	3.186(8)	Cs–N106	3.417(8)
Cs–O65	3.139(8)	Cs–O75	3.253(8)	Cs–N116	3.199(7)
Re1–O1	1.691(2)	Re1–S1	2.341(3)	Re1–O5	2.117(7)
Re1–O6	1.906(5)	Re1–S21	2.328(3)	Re1–O25	2.116(8)
Re2–O2	1.674(3)	Re2–S11	2.316(3)	Re2–O15	2.116(8)
Re2–O7	1.923(6)	Re2–S31	2.323(3)	Re2–O35	2.128(7)
Re3–O3	1.698(2)	Re3–S41	2.329(3)	Re3–O45	2.118(8)
Re3–O6	1.909(5)	Re3–S61	2.326(3)	Re3–O65	2.144(8)
Re4–O4	1.685(2)	Re4–S51	2.330(4)	Re4–O55	2.147(8)
Re4–O7	1.891(6)	Re4–S71	2.324(3)	Re4–O75	2.105(8)

The complex $[Tl(Re_2O_3)_2(L^a)_4](PF_6)$ crystallizes in the monoclinic space group *C2/c*. The molecular structure of the complex cation is presented in Figure 2.15. The coordination patterns of metal ions are similar to those in the potassium, rubidium and cesium complexes and are presented in Figure 2.16. Selected bond lengths are summarized in Table 4.8. The Tl–N bond lengths are in the range between 3.065(5) Å and 3.445(5) Å. The Tl–O bond lengths are in the range between 3.113(4) Å and 3.212(4) Å. There are no specific differences observed in the bond distances of the guest metal ions in all $[M^1(Re_2O_3)_2(L^a)_4](PF_6)$ complexes, which underlies the fact that the size of the void inside the tetranuclear complexes is determined by the dimeric rhenium chelates. The size of the incorporated M^+ ions, however, is important in the sense that stabilization by bonding interaction with appropriate donor atoms is possible.

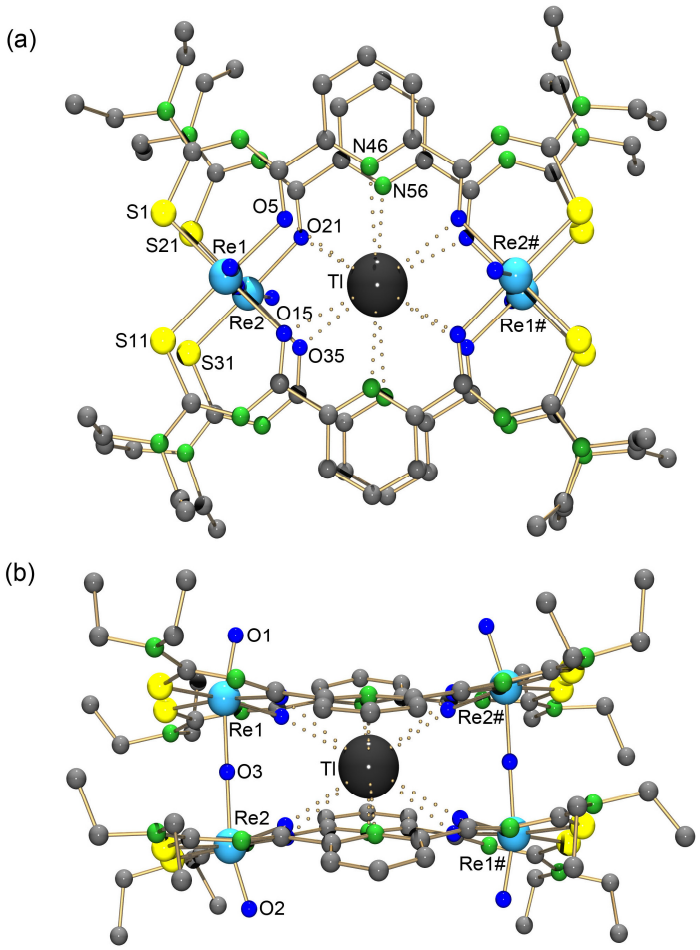

Figure 4.15 Molecular structure of $[Tl(Re_2O_3)_2(L^a)_4]^+$. Hydrogen atoms are omitted for clarity. (a) View perpendicular to the thioureato ligand planes. (b) View parallel to the thioureato ligand planes.

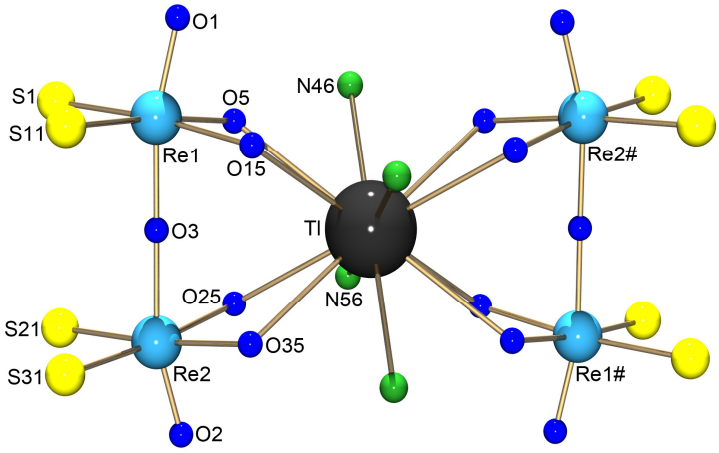

Figure 4.16 Coordination patterns of the Tl and Re atoms in $[Tl(Re_2O_3)_2(L^a)_4](PF_6)$. Only donor atoms of the ligands are shown.

Table 4.8 Selected bond lengths (Å) in $[Tl(Re_2O_3)_2(L^a)_4]^+$.

Tl–O5	3.194(4)	Tl–O15	3.133(4)	Tl–N46	3.065(5)
Tl–O25	3.180(4)	Tl–O35	3.212(4)	Tl–N56	3.445(5)
Re1–O1	1.678(8)	Re1–S1	2.317(2)	Re1–O5	2.131(6)
Re1–O3	1.926(7)	Re1–S11	2.311(2)	Re1–O15	2.132(6)
Re2–O2	1.694(9)	Re2–S21	2.318(2)	Re2–O25	2.114(6)
Re2–O3	1.896(7)	Re2–S31	2.326(2)	Re2–O35	2.140(6)

With regard to the previous discussion, it is not surprising that the coordination polyhedra of the central metal ions $(M^1)^+$ in all crystallographically characterized $[M^1(Re_2O_3)_2(L^a)_4](PF_6)$ complexes are practically identical. The polyhedron is presented in Figure 4.17 and can be explained as a hexagonal prism. The metal ions are coordinated by four nitrogen and eight oxygen donor atoms and have the coordination number of 12. The two parallel hexagonal planes are each formed by 4 oxygen and 2 nitrogen donor atoms of two 2,6-dipicolinoyl moieties.

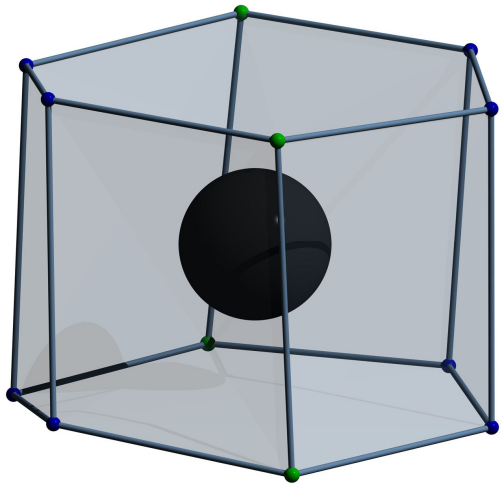

Figure 4.17 General coordination polyhedron of the guest metal ion M^1 in $[M^1(Re_2O_3)_2(L^a)_4]X$ complexes.

The diameter of the central void can be given by the space diagonal distances of the hexagonal prism. The four diagonal distances between the opposite oxygen donor atoms of the carbonyl groups are in the range between 6.229 Å and 6.450 Å. The two diagonal distances between opposite nitrogen donor atoms of the pyridine rings are in the range between 6.090 Å and 6.862 Å. Obviously, smaller alkaline metal ions such as Na^+ and Li^+ with the diameters of 1.94 Å and 1.56 Å, respectively (Table 4.6), are too small to be

stabilized inside the void. Therefore, tetranuclear oxidorhenium(V) complexes with smaller Na^+ or Li^+ ions should have different structure. The corresponding sodium compound could be prepared by two methods: (I) cation exchange starting from the potassium compound and (II) a one-pot reaction starting from $(NBu_4)[ReOCl_4]$, H_2L^a and NaCl.

4.3 Guest metal cation exchange in tetranuclear oxidorhenium(V) complexes

The guest metal cations of the cage can be exchanged, but all attempts to remove them completely in order to obtain a tetranuclear oxidorhenium(V) complex with an unoccupied void, $[(Re_2O_3)_2(L^a)_4]$, were not successful. The binding of the metal ions inside the cage is obviously controlled by their ionic radii. The least stable bonds inside the cage are formed with K^+ ions.

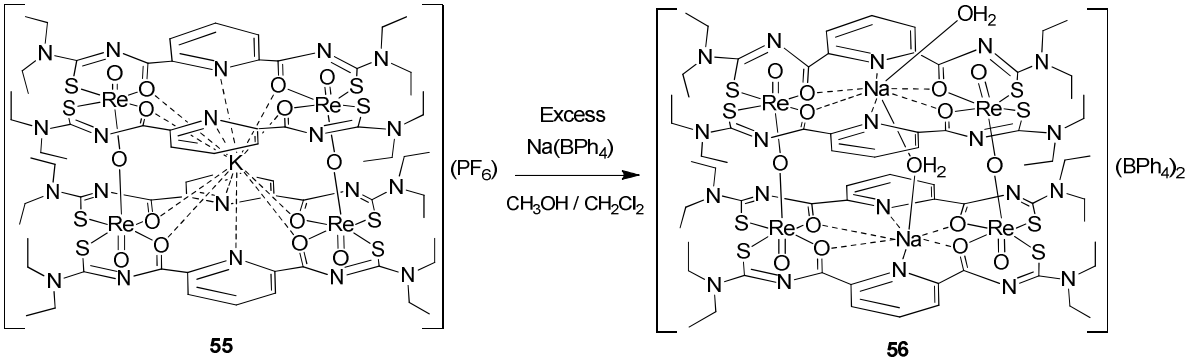

Scheme 4.6 Reaction of $[K(Re_2O_3)_2(L^a)_4](PF_6)$ with excess of Kalignost.

The potassium ions can be removed from $[K(Re_2O_3)_2(L^a)_4](PF_6)$ (**55**) as $K(BPh_4)$ by the addition of an excess $Na(BPh_4)$ in MeOH. $K(BPh_4)$ is less soluble and immediately precipitates from the reaction mixture. It should be noted that at least a three-fold excess of $Na(BPh_4)$ was required to complete the reaction. The reason for this unexpected fact was finally found in the composition and structure of the rhenium complex formed (Scheme 4.6). Finally, the potassium ions could be removed as colorless $K(BPh_4)$ precipitate. After the complete removal of $K(BPh_4)$ from the reaction mixture by filtration, dark-red cube-like single crystals were isolated by slow evaporation of the resulting mixture. Surprisingly, the crystallographic analysis reveals that the tetranuclear oxidorhenium(V) complex contains two Na^+ ions inside the void. Obviously, the diameter of Na^+ (1.94 Å) is too small to allow the stabilization of one Na^+ in the center of the void with the diameter of 6.229 Å – 6.862 Å. Therefore the coordination of one Na^+ ion to the oxygen and nitrogen atoms of both $\{(ReO)_2(L^a)_2\}^{2-}$ subunits is not possible. That's why two Na^+ ions are coordinated each near to one of these two layers.

The complex $[Na_2(Re_2O_3)_2(L^a)_4(H_2O)_2](BPh_4)_2$ (**56**) crystallizes in the triclinic space group $P\bar{1}$ and the molecular structure is presented in Figure 4.18. A half of the molecule is seen in the asymmetric unit with one Na^+ and one water molecule inside the void. The sodium ions are disordered with the oxygen atoms of the water molecules.

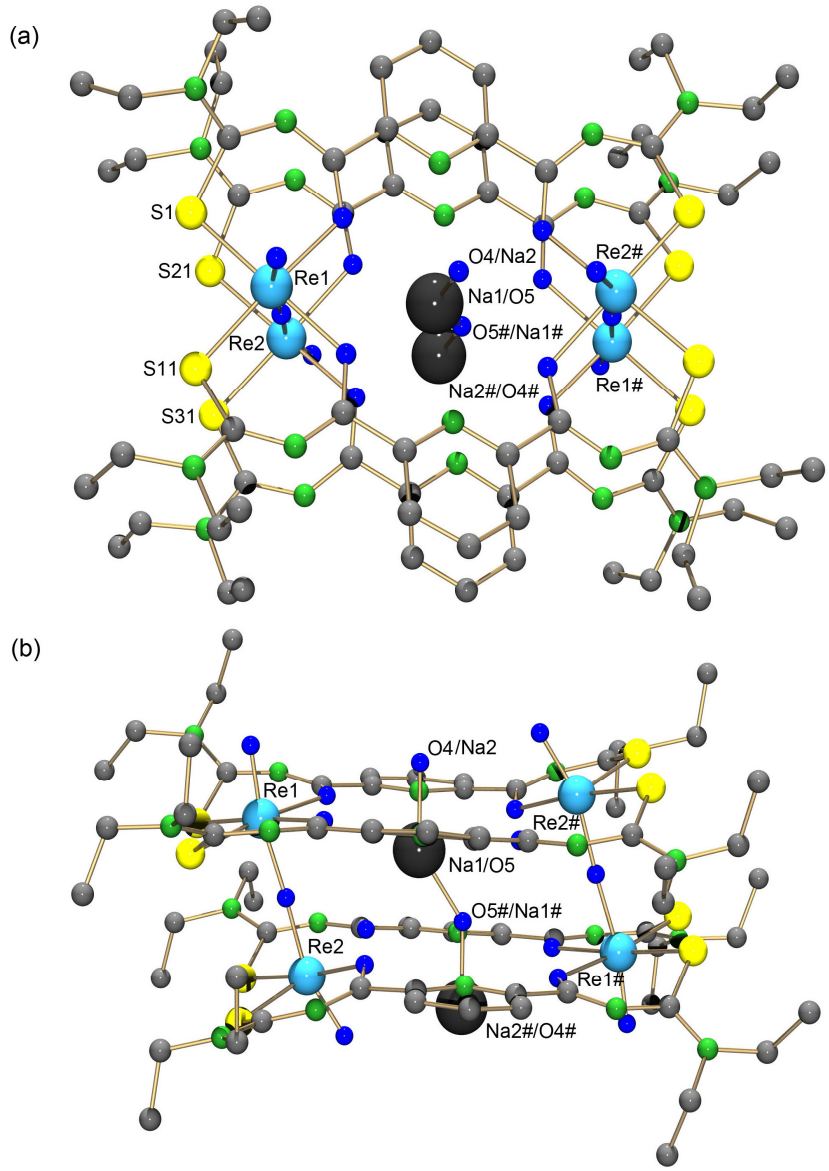

Figure 4.18 Molecular structure of $[Na_2(Re_2O_3)_2(L^a)_4(H_2O)_2]^{2+}$ in $[Na_2(Re_2O_3)_2(L^a)_4(H_2O)_2](BPh_4)_2$. Hydrogen atoms are omitted for clarity. (a) View perpendicular to the thioureato ligand plane. (b) View parallel to the thioureato ligand plane.

Both positions of disordered sodium and oxygen atoms are shown in Figure 4.18, but only one of both atoms is shown in each case in the molecular structure. The symmetry related sodium and oxygen atoms inside the void are produced by inversion. Selected bond lengths are summarized in Table 4.9. The distances between Na^+ and the oxygen atom of the water molecules, Na1–O5# and Na1–O4, are 2.01(1) Å and 1.973(6) Å respectively. Bond lengths between Na^+ and the organic ligands are in the range between 2.802(4) Å and 2.848(5) Å for Na–O bonds. Na1–N46 and Na1–N56 bond lengths are 2.958(5) and 2.909(5) Å, respectively.

Table 4.9 Selected bond lengths (Å) in $[Na_2(Re_2O_3)_2(L^a)_4(H_2O)_2](BPh_4)_2$.

Na1–O5	2.844(5)	Na1–O15	2.802(4)	Na1–N46	2.958(5)
Na1–O25	2.848(5)	Na1–O35	2.811(4)	Na1–N56	2.909(5)
Re1–O1	1.701(5)	Re1–S1	2.309(1)	Re1–O5	2.130(4)
Re1–O3	1.907(3)	Re1–S11	2.314(1)	Re1–O15	2.157(4)
Re2–O2	1.696(5)	Re2–S21	2.326(2)	Re2–O25	2.107(4)
Re2–O3	1.910(3)	Re2–S31	2.353(1)	Re2–O35	2.120(4)
Na1–O5#	2.01(1)	Na1–O4	1.973(6)		

These Na–O and Na–N bond lengths in $[Na_2(Re_2O_3)_2(L^a)_4(H_2O)_2](BPh_4)_2$ are longer than those observed in the sodium complexes of diaza-18-crown-6 derivatives, where the typical Na–O bond lengths are in the range of 2.33 – 2.64 Å and Na–N bond lengths are in the range of 2.45 – 2.67 Å.[115-117] In the sodium complexes of diaza-18-crown-6 derivatives, the Na^+ ions are situated more close to or almost in the crown ether plane. But in the complex $[Na_2(Re_2O_3)_2(L^a)_4(H_2O)_2](BPh_4)_2$, the Na^+ ions are away from the thioureato ligand plane by 0.805(1) and 1.200(1) Å. Bond lengths inside the rhenium chelates are unexceptional.

Starting from $(NBu_4)[ReOCl_4]$, NaCl and H_2L^a, the isolation of the binuclear oxidorhenium(V) complex with Na^+ was successful, after the addition of $(NBu_4)[BPh_4]$ in CH_3CN followed by a slow evaporation. X-ray structural analysis of the crystals reveals a similar product to that obtained from the kalignost reaction. The only difference between the two solid state structures is the co-crystallized solvent. Thus, no detailed discussion of the solvent-free structure from the latter synthesis shall be included here.

Interestingly, the exchange of guest metal cations $(M^1)^+$ from the complex cations $[M^1(Re_2O_3)_2(L^a)_4]^+$ is possible in the presence of an additional metal cation $(M^2)^+$. All of the exchange reactions were carried out in CH_2Cl_2/MeOH mixtures. The complexes $[M^1(Re_2O_3)_2(L^a)_4]^+$ were dissolved in CH_2Cl_2 and the introducing metal salts (M^2Cl) were dissolved in MeOH. Slow evaporation of the reaction mixtures gave good quality single crystals and crystallographic analyses confirmed the exchange of the metal ion. Additionally, the metal ion exchange can readily be confirmed by the major peaks in the ESI-mass spectra, which correspond to the molecular ions $[M^2(Re_2O_3)_2(L^a)_4]^+$. The experimental results show that the K^+ ions can be exchanged by Rb^+, Tl^+ or Cs^+ ions, where Rb^+ and Tl^+ ions can only be exchanged by Cs^+ ions, and not by K^+ ions (Scheme 4.7).

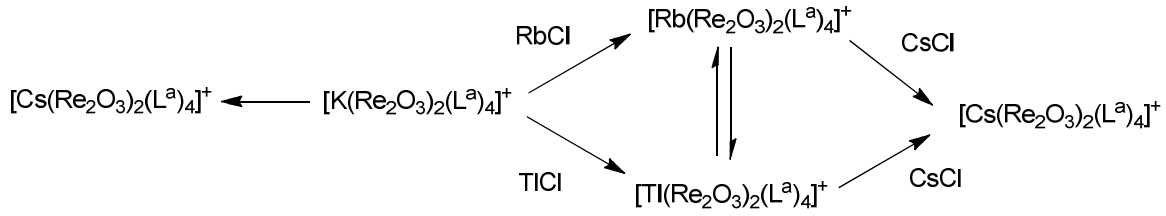

Scheme 4.7 Possible exchanges of the guest metal cations $(M^1)^+$ of the $[M^1(Re_2O_3)_2(L^a)_4]^+$ complexes.

No exchange of Cs^+ ions by K^+, Rb^+ and Tl^+ ions is possible. The stabilization of Rb^+ and Tl^+ ions inside the void might be similar due to the similar ionic radii. Therefore, the metal cations inside the cage can be exchanged in the order $K^+ < Rb^+ = Tl^+ < Cs^+$. These exchange processes are in equilibrium in the solution and the formation of stable complexes seems to depend on the size of the cations. The equilibrium, in each case, favors the stabilization of the bigger metal cation inside the void. The least stable cation inside the void is K^+ ion, whereas the most stable one is Cs^+ ion. A comparison of typical M^1–O and M^1–N bond distances derived from the crown ether complexes with those observed in the $[M^1(Re_2O_3)_2(L^a)_4]^+$ complexes give an additional prove for the stabilization of the metal cations in the detected order. The typical M^1–O and M^1–N bond length ranges of the metal ions $M^1 = K^+$, Rb^+, Cs^+ and Tl^+ in crown ether complexes are summarized in Table 4.10 and are compared with the observed M^1–O and M^1–N bond lengths in $[M^1(Re_2O_3)_2(L^a)_4]^+$ complexes.

Table 4.10 The comparison of the typical and the observed M^1–O and M^1–N bond distances.

M^1	Typical bond length ranges in crown ether complexes (Å)		Observed bond length ranges in $[M^1(Re_2O_3)_2(L^a)_4]X$ (Å)	
	M^1–O	M^1–N	M^1–O	M^1–N
K[108, 122]	2.74. – 2.85	2.79 – 2.92	3.114(6) – 3.210(6)	3.045(7) – 3.431(7)
Rb[118, 122]	2.83. – 2.97	2.96 – 3.14	3.111(4) – 3.218(4)	3.105(5) – 3.435(5)
Tl[119-120]	2.81. – 2.91	2.97 – 3.02	3.133(4) – 3.212(4)	3.065(5) – 3.445(5)
Cs[122]	3.04. – 3.21	3.18 – 3.31	3.139(8) – 3.271(9)	3.199(7) – 3.417(8)

The ranges of M^1–O and M^1–N bond distances between the metal ions and the donor atoms of the void are similar in all complexes (Table 4.11). The M^1–O bond distances are in the range of 3.111(2) Å – 3.271(3) Å and the M^1–N bond distances are in the range of 3.045(3) Å – 3.445(4) Å. Only the observed Cs–O and Cs–N bond distances in the $[Cs(Re_2O_3)_2(L^a)_4]^+$ complexes are in the range of those observed for typical Cs–O and Cs–N bond lengths.[109-110, 121] That's why the Cs^+ ion is most stable inside the void than the others. In other words, the

size of the void is perfect for the size of the Cs^+ ion. Moreover, the observed M^1–O and M^1–N bond distances for $M^1 = K^+$, Rb^+ and Tl^+ in the $[M^1(Re_2O_3)_2(L^a)_4]^+$ complexes are higher compared to the typical M–O and M–N bond distances. These distances could rather be explained as interactions than bonds in such cases. That's why; K^+, Rb^+ and Tl^+ are not stable enough inside the void and could easily be exchanged by the Cs^+ ions presence in the solution. However, these observations are only the qualitative proof of the exchanges of guest metal cations.

There are two possible mechanisms for the exchange process. One possibility is, that the tetranuclear oxidorhenium(V) complex undergoes partial hydrolyzation in solution and forms the binuclear oxidorhenium(V) complex with $\{O=Re\text{-}OH\}^{2+}$ cores. After the metal ion exchange, the binuclear complex again undergoes dimerization to form the tetranuclear complex. Since the detected exchange strongly depends on the sizes of the metal ions present in the solution, this hydrolyzation mechanism is not probable.

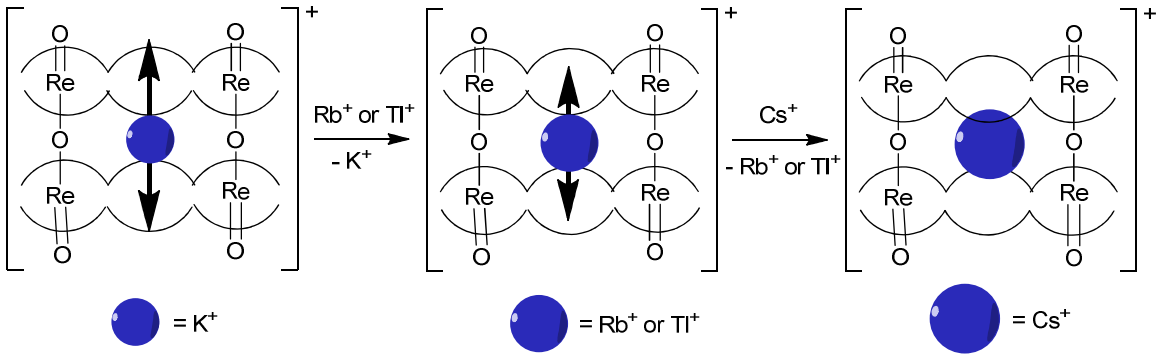

Scheme 4.8 Propossed mechanism for the exchanges of the guest metal cations $(M^1)^+$ inside the $[M^1(Re_2O_3)_2(L^a)_4]^+$ complexes.

The other possibility is, that the tetranuclear oxidorhenium(V) skeleton remains unchanged and the metal ion with smaller ionic radius is eliminated by the metal ion with bigger ionic radius presence in the solution. In this case the elimination of the non-stable metal cation from the void might be induced by possible micro vibrational mechanism of the interactive bonds between the metal ion and the donor atoms of the void. The smaller cations with weaker interactions vibrate stronger and leave the void faster than the bigger ones. The size of both pores of the void is big enough for the movements of the cations. The diameters of the pores are in a range between 5.435 Å and 5.560 Å. The ionic diameter of K^+ is 2.66 Å, and this ion can pass through the pore easily. The Rb^+ and Tl^+ ions are similar in size and have a diameter

of 2.96 Å. The ionic diameter of Cs^+ is 3.34 Å. Therefore, this mechanism is more appropriate and agrees with the observations.

Chapter 5

Experimental section

Experimental section

5.1 Starting materials

All chemicals and reagents were purchased from commercial sources (Acros Organics, Fluka, Sigma-Aldrich, Alfa Aesar, Merck).

All solvent were used as received (pure for synthesis) unless otherwise stated. THF and diethyl lether were dried intensively by heating over sodium metal.

The synthesis of $(NBu_4)[ReOCl_4]$ was performed by the procedure of *Alberto* et al.[123]

5.2 Analytical methods

All IR spectra were measured from KBr pellets on a Shimadzu-FTIR 8300 spectrometer.

The ^{1}H, ^{13}C NMR spectra were recorded on a JEOL-400MHz nuclear magnetic resonance spectrometer (Lambda- software).

Carbon, hydrogen, nitrogen and sulfur contents were measured by a Heraeus (Vario EL) elemental analyzer.

The ESI-TOF mass spectra were measured on an Agilent 6210 ESI-TOF, Agilent Technologies, Santa Clara, CA, USA. Solvent flow rate was adjusted to 4 μL/min. spray voltage was set to 4 kV. Drying gas flow rate was set to 15 psi (1 bar). All other parameters were adjusted for a maximum abundance of the relative $[M+H]^+$ peaks.

The W-band (94 GHz) EPR measurements were performed on a Bruker E680 Elexsys spectrometer equipped with a DICEENDOR accessory and an RF amplifier (Amplifier Research 250A250A). The ENDOR resonator (Bruker Teraflex EN600-1021 H) was immersed in a helium-gas flow cryostat (Oxford) regulated by a temperature controller (Oxford ITC-503).

The magnetic susceptibility measurements were carried out on powdered samples with a QUANTUM DESIGN MPMS 7XL SQUID-magnetometer in the temperature range of 2-300 K and under an external magnetic field of 1T. The obtained data were analyzed with the simulation software DAVE.[124]

5.3 Syntheses

5.3.1 Ligands

5.3.1.1 *N,N*-Dialkylthioureas

The synthesis of (R_2tu) was performed by the procedure of *Hartmann* et al.[54]

a) *N,N*-Diethylthiourea (Et_2TU)

Yield: 14.5 g (55%)

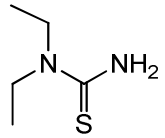

Elemental analysis:

Calcd. for $C_5H_{12}N_2S$: C, 45.42; H, 9.15; N, 21.19; S, 24.25%.

Found: C, 45.41; H, 9.16; N, 20.92; S, 22.10%.

IR (KBr, cm^{-1}): 3375 (m), 3298 (m), 3190 (m), 2974 (w), 2934 (w), 2922 (w), 1628 (vs), 1518 (vs), 1360 (vs), 1074 (m), 1059 (m), 841 (m), 519 (m).

^{1}H NMR (400 MHz, $CDCl_3$, ppm): 1.19 (t, 6H, J = 8.0 Hz, CH_3), 3.65 (bs, 4H, CH_2), 5.85 (bs, 2H, NH_2).

^{13}C NMR (400 MHz, $CDCl_3$, ppm): 12.6 (CH_3), 45.9 (CH_2), 180.5 (C=S)

b) *N*-Morpholinethiourea (MoTU)

Yield: 16.9 g (58%)

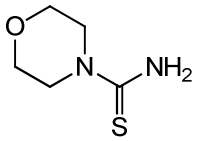

Elemental analysis:

Calcd. for $C_5H_{10}N_2OS$: C, 41.07; H, 6.89; N, 19.16; S, 21.93%.

Found: C, 41.10; H, 6.86; N, 18.91; S, 21.08%.

IR (KBr, cm^{-1}): 3426 (m), 3327 (m), 3215 (m), 2970 (w), 2911 (w), 2872 (w), 1626 (vs), 1508 (vs), 1350 (vs), 1107 (vs), 1001 (vs), 833 (m), 590 (m).

^{1}H NMR (400 MHz, $CDCl_3$, ppm): 3.74 (m, 8H, CH_2), 5.78 (bs, 2H, NH_2).

^{13}C NMR (400 MHz, $CDCl_3$, ppm): 47.9 (CH_2-N), 66.1 (CH_2-O), 179.3 (C=S)

5.3.1.2 Pyridine-2,6-dicarbonyl dichloride

Dry pyridine-2,6-dicarboxylic acid (5.01 g, 30.0 mmol) was added to a 10 mL freshly distilled $SOCl_2$. After stirring under reflux for 8h, the mixture was evaporated to dryness under vacuum. The product was used for the next step without further purification.

Yield: 6.0 g (98%)

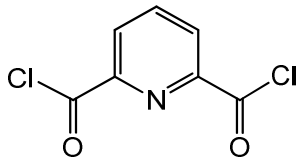

IR (KBr, cm^{-1}): 3084 (m), 1755 (vs), 1258 (vs), 1244 (vs), 871 (vs),
829 (vs), 735 (vs), 640 (vs), 625 (vs).

^1H NMR (400 MHz, $CDCl_3$, ppm): 8.15 (t, 1H, *J* = 8.0 Hz, Py-H),
8.35 (d, 2H, *J* = 8.0 Hz, Py-H)

^{13}C NMR (400 MHz, $CDCl_3$, ppm): 129.1 (Py), 139.5 (Py), 149.3 (Py), 169.5 (C=O)

5.3.1.3 2,6- Dipicolinoylbis(*N,N*-dialkylthioureas)

A solution of pyridine-2,6-dicarbonyl dichloride (0.76 g, 3.72 mmol) in 10 mL of THF was added dropwise to a mixture of *N,N*-dialkylthiourea (7.56 mmol) and triethylamine (0.76 g, 7.51 mmol) in 10 mL THF at 40 °C. After stirring for 1 h, mixture was allowed cool to RT and filtered. The filtrate was evaporated to dryness and was crystallized from CH_2Cl_2/EtOH (2:1) mixture.

a) 2,6- Dipicolinoylbis(*N,N*-diethylthiourea) (H_2L^a)

Yield: 1.38 g (94%)

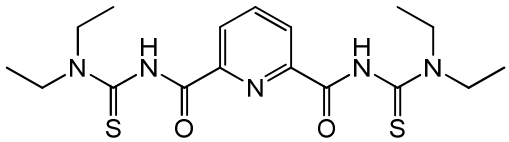

Elemental analysis:

Calcd. for $C_{17}H_{25}N_5O_2S_2$: C, 51.62; H, 6.37; N, 17.71; S, 16.21%.

Found: C, 51.64; H, 6.05; N, 17.76; S, 16.34%.

IR (KBr, cm^{-1}): 32673 (m), 2974 (w), 2935 (w), 2874 (w), 1687 (vs), 1524 (vs), 1423 (vs), 1277 (m), 1223 (vs), 1134 (m), 752 (m).

^1H NMR (400 MHz, $CDCl_3$, ppm): 1.25 – 1.40 (m, 12H, CH_3), 3.57 – 3.72 (m, 4H, CH_2), 3.95 – 4.08 (m, 4H, CH_2), 8.07 (t, 1H, *J* = 8.0 Hz, Py), 8.37 (d, 2H, *J* = 8.0 Hz, Py), 9.91 (s, 2H, NH).

^{13}C NMR (400 MHz, $CDCl_3$, ppm): 11.5 (CH_3), 13.6 (CH_3), 47.8 (CH_2), 126.8 (Py), 139.7 (Py), 148.0 (Py), 159.4 (C=O), 178.3 (C=S)

ESI^+ MS : m/z = 418 $(M+Na)^+$, 434 $(M+K)^+$, 813 $(2M+Na)^+$.

b) 2,6- Dipicolinoylbis(*N,N*-morpholinethiourea) (H_2L^b)

Yield: 1.43 g (91%)

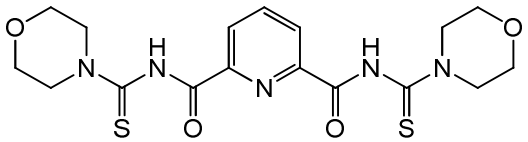

Elemental analysis:

Calcd. for $C_{17}H_{21}N_5O_4S_2$: C, 48.21; H, 5.00; N, 16.54; S, 15.14%.

Found: C, 47.61; H, 4.48; N, 16.20; S, 15.20%.

IR (KBr, cm^{-1}): 3360 (m), 2978 (w), 2907 (w), 2851 (w), 1711 (vs), 1533 (vs), 1464 (vs) 1435 (vs), 1250 (vs), 1223 (vs), 1111 (m), 847 (m), 746 (m).

^{1}H NMR (400 MHz, $CDCl_3$, ppm): 3.60 – 4.40 (m, 16H, CH_2), 8.12 (t, 1H, *J* = 8.0 Hz, Py), 8.40 (d, 2H, *J* = 8.0 Hz, Py), 10.10 (s, 2H, NH).

^{13}C NMR (400 MHz, $CDCl_3$, ppm): 51.5 (CH_2-N), 52.8 (CH_2-N), 66.4 (CH_2-O), 127.2 (Py), 139.9 (Py), 147.7 (Py), 158.7 (C=O), 178.4 (C=S).

ESI^+ MS : m/z = 446 $(M+Na)^+$, 869 $(2M+Na)^+$.

5.3.2 Trinuclear mixed-metal complexes of lanthanides and transition metals

5.3.2.1 Complexes of lanthanides and cobalt ($Co^{II}Ln^{III}Co^{II}$)

A solution of $Co(CH_3COO)_2 \cdot 4H_2O$ (50 mg, 0.2 mmol) in MeOH (3 mL) was added to a solution of $LnCl_3$ (0.1 mmol) (Ln = Ce, Nd, Sm, Gd, Dy, Er or Yb) and H_2L^a (79.1 mg, 0.2 mmol) in MeOH (3 mL). Two drops of triethylamine were added to the mixture, which was stirred for 30 min. at 40 °C. In the cases of Ln = Ce, Nd, Sm, and Gd, the formed precipitates were filtered off, washed with MeOH, dried under vacuum and recrystallized from CH_2Cl_2/MeOH (1:1) mixtures. In the cases of Ln = Dy, Er and Yb, no precipitates were obtained after 30 min., and the reaction mixtures were allowed to stand overnight. The formed crystals were collected, washed twice with MeOH and dried under vacuum.

Two types of complexes were obtained.

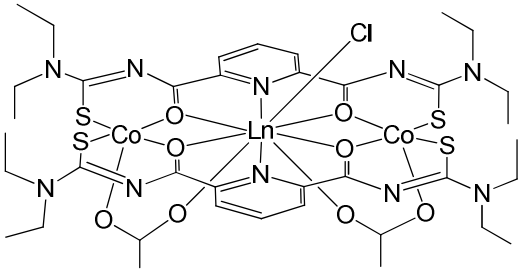

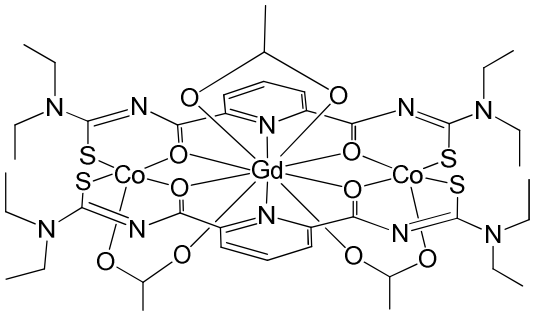

1. $[CeCo_2(L^a)_2(\mu\text{-}OAc)_2Cl]$

Yield: 110.4 mg (92%),

Elemental analysis:

Calcd. for $C_{38}H_{52}CeClCo_2N_{10}O_8S_4$: C, 38.08; H, 4.37; N, 11.69; S, 10.70%.

Found: C, 37.64; H, 4.15; N, 11.76; S, 10.34%.

IR (KBr, cm^{-1}): 2974 (w), 2935 (w), 1589 (vs), 1566 (vs), 1531 (vs), 1500 (vs), 1427 (vs), 1404 (vs), 1373 (m), 1307 (m), 1284 (m), 1250 (m), 1146 (w), 1076 (w), 760 (m), 663 (w).

ESI^+ MS : m/z = 1162 $(M\text{-}Cl)^+$.

2. [$NdCo_2(L^a)_2(\mu\text{-}OAc)_2Cl$]

Yield: 115.6 mg (96%)

Elemental analysis:

Calcd. for $C_{38}H_{52}ClCo_2N_{10}NdO_8S_4$: C, 37.95; H, 4.36; N, 11.65; S, 10.66%.

Found: C, 36.64; H, 4.05; N, 11.72; S, 10.44%.

IR (KBr, cm^{-1}): 2970 (w), 2935 (w), 1589 (vs), 1566 (vs), 1527 (vs), 1500 (vs), 1427 (vs), 1404 (vs), 1373 (m), 1307 (m), 1284 (m), 1250 (m), 1146 (w), 1076 (w), 760 (m), 663 (w).

ESI^+ MS : m/z = 1166 $(M\text{-}Cl)^+$.

3. [$SmCo_2(L^a)_2(\mu\text{-}OAc)_2Cl$]

Yield: 110.2 mg (91%)

Elemental analysis:

Calcd. for $C_{38}H_{52}ClCo_2N_{10}O_8S_4Sm$: C, 37.76; H, 4.34; N, 11.59; S, 10.61%.

Found: C, 36.24; H, 4.55; N, 11.76; S, 10.84%.

IR (KBr, cm^{-1}): 2970 (w), 2935 (w), 1589 (vs), 1566 (vs), 1531 (vs), 1500 (vs), 1427 (vs), 1404 (vs), 1373 (m), 1307 (m), 1284 (m), 1250 (m), 1146 (w), 1076 (w), 760 (m), 663 (w).

ESI^+ MS : m/z = 1176 $(M\text{-}Cl)^+$.

4. [$GdCo_2(L^a)_2(\mu\text{-}OAc)_2(OAc)$]

Yield: 121.7 mg (98%)

Elemental analysis:

Calcd. for $C_{40}H_{55}Co_2GdN_{10}O_{10}S_4$: C, 38.77; H, 4.47; N, 11.30; S, 10.35%.

Found: C, 38.82; H, 4.15; N, 11.24; S, 10.55%.

IR (KBr, cm^{-1}): 2974 (w), 2935 (w), 1585 (vs), 1562 (vs), 1512 (vs), 1427 (vs), 1400 (vs), 1358 (m), 1311 (m), 1288 (m), 1254 (m), 1150 (w), 1076 (w), 760 (m), 656 (w).

ESI^+ MS : m/z = 1180 $(M\text{-}OAc)^+$.

5. [$DyCo_2(L^a)_2(\mu\text{-}OAc)_2Cl$]

Yield: 103.9 mg (85%)

Elemental analysis:

Calcd. for $C_{38}H_{52}ClCo_2DyN_{10}O_8S_4$: C, 37.38; H, 4.29; N, 11.47; S, 10.50%.

Found: C, 36.94; H, 4.33; N, 11.25; S, 10.56%.

IR (KBr, cm^{-1}): 2978 (w), 2935 (w), 1593 (vs), 1562 (vs), 1516 (vs), 1431 (vs), 1396 (vs), 1373 (m), 1308 (m), 1284 (m), 1254 (m), 1150 (w), 1076 (w), 760 (m), 656 (w).

ESI^+ MS : m/z = 1186 $(M\text{-}Cl)^+$.

6. [$ErCo_2(L^a)_2(\mu\text{-}OAc)_2Cl$]

Yield: 115.4 mg (94%)

Elemental analysis:

Calcd. for $C_{38}H_{52}ClCo_2ErN_{10}O_8S_4$: C, 37.24; H, 4.28; N, 11.43; S, 10.46%.

Found: C, 36.14; H, 4.25; N, 11.46; S, 10.44%.

IR (KBr, cm^{-1}): 2974 (w), 2935 (w), 1589 (vs), 1566 (vs), 1542 (vs), 1504 (vs), 1431 (vs), 1404 (vs), 1381 (m), 1373 (m), 1288 (m), 1254 (m), 1146 (w), 1076 (w), 760 (m), 660 (w).

ESI^+ MS : m/z = 1192 $(M\text{-}Cl)^+$.

7. [$YbCo_2(L^a)_2(\mu\text{-}OAc)_2Cl$]

Yield: 119.7 mg (97%)

Elemental analysis:

Calcd. for $C_{38}H_{52}ClCo_2N_{10}O_8S_4Yb$: C, 37.06; H, 4.26; N, 11.37; S, 10.41%.

Found: C, 37.64; H, 4.05; N, 11.76; S, 10.44%.

IR (KBr, cm^{-1}): 2974 (w), 2935 (w), 1593 (vs), 1566 (vs), 1520 (vs), 1431 (vs), 1392 (vs), 1373 (m), 1308 (m), 1288 (m), 1254 (m), 1150 (w), 1076 (w), 764 (m), 656 (w).

ESI^+ MS : m/z = 1196 $(M\text{-}Cl)^+$.

5.3.2.2 Complexes of lanthanides and nickel ($Ni^{II}Ln^{III}Ni^{II}$)

A solution of $Ni(CH_3COO)_2 \cdot 4H_2O$ (49.7 mg, 0.2 mmol) in MeOH (3 mL) was added to a solution of $LnCl_3$ (0.1 mmol) (Ln = Ce, Nd, Sm, Gd, Dy, Er or Yb) and H_2L^a (79.1 mg, 0.2 mmol) in MeOH (3 mL). Two drops of triethylamine were added to the mixture, which was stirred for 1 hour at 40 °C. In the cases of Ln = Ce, Nd, and Gd the formed precipitates were filtered off, washed with MeOH, dried under vacuum and recrystallized from CH_2Cl_2/MeOH (1:1) mixtures. In the cases of Ln = Sm, Dy, Er and Yb, no precipitates were observed after 30 min. and the reaction mixtures were overlayered with diethyl ether (1:6). The obtained crystals were filtered off, washed with diethyl ether and dried under vacuum.

Two types of complexes were obtained

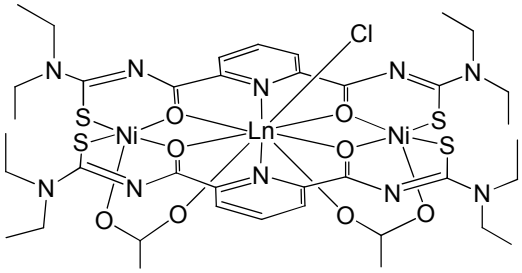

Ln = Sm, Gd, Dy, Er or Yb

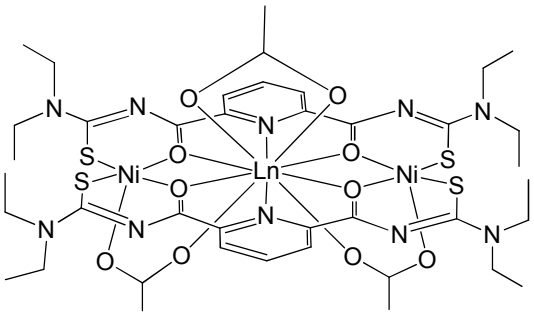

Ln = Ce or Nd

1. $[CeNi_2(L^a)_2(\mu\text{-}OAc)_2(OAc)]$

Yield: 120.0 mg (98%)

Elemental analysis:

Calcd. For $C_{40}H_{55}CeN_{10}Ni_2O_{10}S_4$: C, 39.32; H, 4.54; N, 11.47; S, 10.50%.

Found: C, 38.71; H, 4.88; N, 11.24; S, 10.29%.

IR (KBr, cm^{-1}): 2972 (w), 2935 (w), 1587 (vs), 1564 (vs), 1515 (vs), 1428 (vs), 1400 (vs), 1360 (m), 1311 (m), 1286 (m), 1254 (m), 1150 (w), 1077 (w), 760 (m), 654 (w).

ESI^+ MS : m/z = 551 $(M\text{-}2Oac)^{2+}$, 1162 $(M\text{-}Oac)^+$, 1192 $(M\text{-}Oac+CH_3OH)^+$.

2. [$NdNi_2(L^a)_2(\mu\text{-}OAc)_2(OAc)$]

Yield: 111.8 mg (91%)

Elemental analysis:

Calcd. For $C_{40}H_{55}N_{10}NdNi_2O_{10}S_4$: C, 39.19; H, 4.52; N, 11.43; S, 10.46%.

Found: C, 39.13; H, 4.75; N, 11.34; S, 10.59%.

IR (KBr, cm^{-1}): 2973 (w), 2935 (w), 1585 (vs), 1563 (vs), 1515 (vs), 1428 (vs), 1400 (vs), 1359 (m), 1311 (m), 1286 (m), 1255 (m), 1150 (w), 1078 (w), 762 (m), 654 (w).

ESI^+ MS : m/z = 1166 $(M\text{-}Oac)^+$, 1196 $(M\text{-}Oac+CH_3OH)^+$.

3. [$SmNi_2(L^a)_2(\mu\text{-}OAc)_2Cl$]

Yield: 99.2 mg (82%)

Elemental analysis:

Calcd. For $C_{38}H_{52}ClN_{10}Ni_2O_8S_4Sm$: C, 37.76; H, 4.34; N, 11.59; S, 10.61%.

Found: C, 36.54; H, 4.25; N, 11.66; S, 10.24%.

IR (KBr, cm^{-1}): 2970 (w), 2935 (w), 1589 (vs), 1566 (vs), 1531 (vs), 1500 (vs), 1427 (vs), 1404 (vs), 1373 (m), 1307 (m), 1284 (m), 1250 (m), 1146 (w), 1076 (w), 760 (m), 663 (w).

ESI^+ MS : m/z = 1174 $(M\text{-}Cl)^+$.

4. [$GdNi_2(L^a)_2(\mu\text{-}OAc)_2Cl$]

Yield: 113.2 mg (93%)

Elemental analysis:

Calcd. For $C_{38}H_{52}ClGdN_{10}Ni_2O_{10}S_4$: C, 37.56; H, 4.31; N, 11.53; S, 10.55%.

Found: C, 37.98; H, 4.71; N, 10.27; S, 9.72%.

IR (KBr, cm^{-1}): 2972 (w), 2934 (w), 1587 (vs), 1565 (vs), 1532 (vs), 1500 (vs), 1428 (vs), 1405 (vs), 1374 (m), 1282 (m), 1146 (w), 1078 (w), 755 (m), 660 (w).

ESI^+ MS : m/z = 1180 $(M\text{-}Cl)^+$

5. $[DyNi_2(L^a)_2(\mu\text{-}OAc)_2Cl]$

Yield: 100.3 mg (82%)

Elemental analysis:

Calcd. For $C_{38}H_{52}ClDyN_{10}Ni_2O_8S_4$: C, 37.40; H, 4.29; N, 11.48; S, 10.51%.

Found: C, 37.28; H, 4.54; N, 11.27; S, 10.32%.

IR (KBr, cm^{-1}): 2976 (w), 2935 (w), 1592 (vs), 1562 (vs), 1516 (vs), 1433 (vs), 1398 (vs), 1373 (m), 1308 (m), 1286 (m), 1254 (m), 1150 (w), 1076 (w), 760 (m), 656 (w).

ESI^+ MS : m/z = 1184 $(M\text{-}Cl)^+$.

6. $[ErNi_2(L^a)_2(\mu\text{-}OAc)_2Cl]$

Yield: 106.7 mg (87%)

Elemental analysis:

Calcd. For $C_{38}H_{52}ClErN_{10}Ni_2O_8S_4$: C, 37.25; H, 4.28; N, 11.43; S, 10.47%.

Found: C, 37.24; H, 4.64; N, 10.75; S, 10.06%.

IR (KBr, cm^{-1}): 2974 (w), 2935 (w), 1585 (vs), 1564 (vs), 1543 (vs), 1504 (vs), 1431 (vs), 1404 (vs), 1381 (m), 1373 (m), 1288 (m), 1254 (m), 1146 (w), 1076 (w), 760 (m), 660 (w).

ESI^+ MS : m/z = 1190 $(M\text{-}Cl)^+$.

7. $[YbNi_2(L^a)_2(\mu\text{-}OAc)_2Cl]$

Yield: 102.3 mg (83%)

Elemental analysis:

Calcd. For $C_{38}H_{52}ClN_{10}Ni_2O_8S_4Yb$: C, 37.08; H, 4.26; N, 11.38; S, 10.42%.

Found: C, 36.46; H, 4.04; N, 10.62; S, 10.09%.

IR (KBr, cm^{-1}): 2974 (w), 2935 (w), 1593 (vs), 1564 (vs), 1520 (vs), 1433 (vs), 1392 (vs), 1373 (m), 1308 (m), 1285 (m), 1254 (m), 1150 (w), 1073 (w), 764 (m), 658 (w).

ESI^+ MS : m/z = 1196 $(M\text{-}Cl)^+$.

5.3.2.3 Complexes of lanthanides and manganese ($Mn^{II}Ln^{III}Mn^{II}$)

A solution of $Mn(CH_3COO)_2 \cdot 4H_2O$ (49 mg, 0.2 mmol) in MeOH (3 mL) was added to a solution of $LnCl_3$ (0.1 mmol) (Ln = Ce, Nd, Sm, Gd, Dy, Er or Yb) and H_2L^a (79.1 mg, 0.2 mmol) in MeOH (3 mL). Two drops of triethylamine were added to the mixture, which was stirred for 15 min. at room temperature. In all cases, the obtained orange precipitates were filtered off, washed with MeOH and dried under vacuum. The precipitates are readily soluble in CH_2Cl_2 and were recrystallized from CH_2Cl_2/MeOH (1:1) mixtures. The filtrates from the reaction mixtures were allowed to stand overnight. Very low amounts of single crystals were obtained in the cases of Ln = Gd and Ce. The crystals were collected manually and analyzed only by the X-ray crystallography.

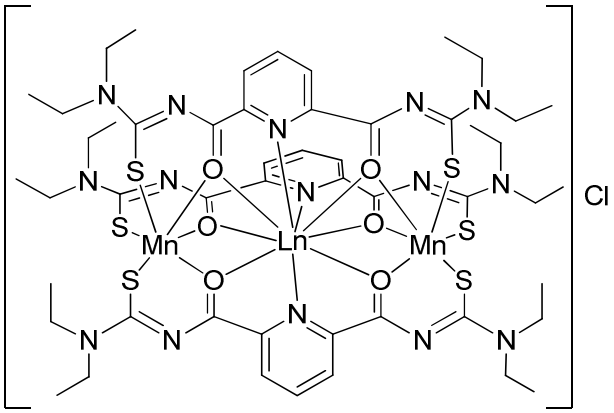

$[LnMn_2(L^a)_3]Cl$

Ln = Ce, Nd, Sm, Gd, Dy, Er or Yb

1. $[CeMn_2(L^a)_3]Cl$

Yield: 80.6 mg (55%)

Elemental analysis:

Calcd. For $C_{51}H_{69}CeClMn_2N_{15}O_6S_6$: C, 41.78; H, 4.74; N, 14.33; S, 13.12%.

Found: C, 41.64; H, 4.25; N, 14.06; S, 12.94%.

IR (KBr, cm^{-1}): 2972 (w), 2935 (w), 1590 (vs), 1564 (vs), 1524 (vs), 1433 (vs), 1392 (vs), 1308 (m), 1285 (m), 1254 (m), 1155 (w), 1073 (w), 765 (m), 662 (w).

ESI^+ MS : m/z = 1429 $(M\text{-}Cl)^+$.

2. $[NdMn_2(L^a)_3]Cl$

Yield: 86.7 mg (59%)

Elemental analysis:

Calcd. For $C_{51}H_{69}ClMn_2N_{15}NdO_6S_6$: C, 41.67; H, 4.73; N, 14.29; S, 13.09%.

Found: C, 40.64; H, 3.44; N, 13.26; S, 12.34%.

IR (KBr, cm^{-1}): 2974 (w), 2935 (w), 1587 (vs), 1562 (vs), 1524 (vs), 1431 (vs), 1392 (vs), 1311 (m), 1285 (m), 1250 (m), 1158 (w), 1073 (w), 766 (m), 666 (w).

ESI^+ MS : m/z = 1433 $(M\text{-}Cl)^+$.

3. $[SmMn_2(L^a)_3]Cl$

Yield: 90.0 mg (61%)

Elemental analysis:

Calcd. For $C_{51}H_{69}ClMn_2N_{15}O_6S_6Sm$: C, 41.49; H, 4.71; N, 14.23; S, 13.03%.

Found: C, 40.03; H, 5.10; N, 13.56; S, 12.66%.

IR (KBr, cm^{-1}): 2978 (w), 2934 (w), 1589 (vs), 1562 (vs), 1529 (vs), 1431 (vs), 1398 (vs), 1309 (m), 1283 (m), 1250 (m), 1158 (w), 1075 (w), 766 (m), 667 (w).

ESI^+ MS : m/z = 1443 $(M\text{-}Cl)^+$.

4. $[GdMn_2(L^a)_3]Cl$

Yield: 86.0 mg (58%)

Elemental analysis:

Calcd. For $C_{51}H_{69}ClGdMn_2N_{15}O_6S_6$: C, 41.30; H, 4.69; N, 14.17; S, 12.97%.

Found: C, 39.62; H, 5.12; N, 13.32; S, 12.47%.

IR (KBr, cm^{-1}): 2974 (w), 2935 (w), 1591 (vs), 1563 (vs), 1529 (vs), 1431 (vs), 1395 (vs), 1309 (m), 1281 (m), 1245 (m), 1158 (w), 1075 (w), 762 (m), 657 (w).

ESI^+ MS : m/z = 1447 $(M\text{-}Cl)^+$.

5. $[DyMn_2(L^a)_3]Cl$

Yield: 75.9 mg (51%)

Elemental analysis:

Calcd. For $C_{51}H_{69}ClDyMn_2N_{15}O_6S_6$: C, 41.15; H, 4.67; N, 14.12; S, 12.93%.

Found: C, 39.54; H, 4.81; N, 13.30; S, 12.82%.

IR (KBr, cm^{-1}): 2972 (w), 2935 (w), 1586 (vs), 1560 (vs), 1529 (vs), 1433 (vs), 1392 (vs), 1309 (m), 1284 (m), 1241 (m), 1158 (w), 1076 (w), 765 (m), 659 (w).

ESI^+ MS : m/z = 1453 $(M\text{-}Cl)^+$.

6. $[ErMn_2(L^a)_3]Cl$

Yield: 89.6 mg (60%)

Elemental analysis:

Calcd. For $C_{51}H_{69}ClErMn_2N_{15}O_6S_6$: C, 41.02; H, 4.66; N, 14.07; S, 12.88%.

Found: C, 39.83; H, 5.05; N, 13.37; S, 12.65%.

IR (KBr, cm^{-1}): 2974 (w), 2935 (w), 1588 (vs), 1568 (vs), 1527 (vs), 1433 (vs), 1394 (vs), 1309 (m), 1282 (m), 1240 (m), 1156 (w), 1075 (w), 763 (m), 656 (w).

ESI^+ MS : m/z = 1457 $(M\text{-}Cl)^+$.

7. $[YbMn_2(L^a)_3]Cl$

Yield: 85.4 mg (57%)

Elemental analysis:

Calcd. For $C_{51}H_{69}ClMn_2N_{15}O_6S_6Yb$: C, 40.86; H, 4.64; N, 14.02; S, 12.83%.

Found: C, 39.57; H, 5.03; N, 13.43; S, 12.75%.

IR (KBr, cm^{-1}): 2975 (w), 2934 (w), 1588 (vs), 1565 (vs), 1529 (vs), 1433 (vs), 1390 (vs), 1309 (m), 1285 (m), 1238 (m), 1156 (w), 1073 (w), 763 (m), 655 (w).

ESI^+ MS : m/z = 1463 $(M\text{-}Cl)^+$.

5.3.2.4 Complexes of lanthanides and copper ($Cu^{II}Ln^{III}Cu^{II}$)

A solution of $Cu(CH_3COO)_2 \cdot H_2O$ (40 mg, 0.2 mmol) in MeOH (3 mL) was added to a solution of $LnCl_3$ (0.1 mmol) (Ln = Ce, Nd, Sm, Gd, Dy, Er or Yb) and H_2L^a (79.1 mg, 0.2 mmol) in MeOH (3 mL). Two drops of triethylamine were added to the mixture, which was stirred for 2 hours at 50 °C. In the cases of Ln = Ce, Nd, Sm, Gd, Er and Yb the formed precipitates were filtered off, washed with MeOH, dried under vacuum and recrystallized from CH_2Cl_2/MeOH (1:1) mixtures. The filtrates from the reaction mixtures were allowed to stand overnight. Very low amounts of single crystals were obtained in the cases of Ln = Ce. The crystals were collected manually and analyzed only by X-ray crystallography. In the case of Dy, no precipitate was observed after 2 hours of reaction and the reaction mixture was allowed to stand overnight. The formed brown precipitate was filtered off and recrystallized from a CH_2Cl_2/MeOH (1:1) mixture.

Two types of complexes were obtained

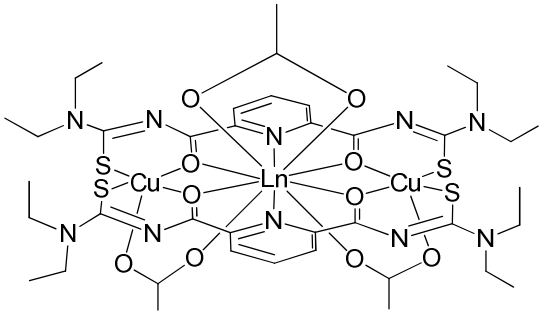

Ln = Ce, Nd, Sm, Gd or Dy

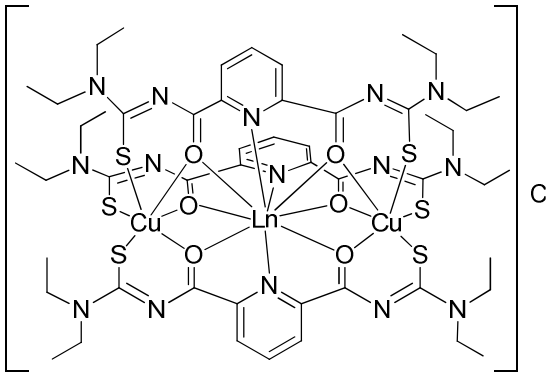

Ln = Er or Yb

1. $[CeCu_2(L^a)_2(\mu\text{-}OAc)_2(OAc)]$

Yield: 107.4 mg (87%)

Elemental analysis:

Calcd. For $C_{40}H_{58}CeCu_2N_{10}O_8S_4$: C, 38.92; H, 4.74; N, 11.35; S, 10.39%.

Found: C, 37.64; H, 4.25; N, 11.76; S, 10.34%.

IR (KBr, cm^{-1}): 2974 (w), 2935 (w), 1589 (vs), 1566 (vs), 1531 (vs), 1500 (vs), 1427 (vs), 1404 (vs), 1373 (m), 1307 (m), 1284 (m), 1250 (m), 1146 (w), 1076 (w), 760 (m), 663 (w).

ESI^+ MS : m/z = 1174 $(M\text{-}OAc)^+$.

2. [$NdCu_2(L^a)_2(\mu\text{-}OAc)_2(OAc)$]

Yield: 100.4 mg (81%)

Elemental analysis:

Calcd. For $C_{40}H_{58}Cu_2N_{10}NdO_{10}S_4$: C, 38.79; H, 4.72; N, 11.31; S, 10.36%.

Found: C, 37.84; H, 4.35; N, 11.06; S, 10.14%.

IR (KBr, cm^{-1}): 2974 (w), 2938 (w), 1586 (vs), 1565 (vs), 1528 (vs), 1433 (vs), 1385 (vs), 1310 (m), 1285 (m), 1241 (m), 1155 (w), 1072 (w), 764 (m), 665 (w).

ESI^+ MS : m/z = 1176 $(M\text{-}OAc)^+$.

3. [$SmCu_2(L^a)_2(\mu\text{-}OAc)_2(OAc)$]

Yield: 113.3 mg (91%)

Elemental analysis:

Calcd. For $C_{40}H_{58}Cu_2N_{10}O_{10}S_4Sm$: C, 38.60; H, 4.70; N, 11.25; S, 10.30%.

Found: C, 38.64; H, 4.00; N, 10.76; S, 9.74%.

IR (KBr, cm^{-1}): 2978 (w), 2934 (w), 1589 (vs), 1562 (vs), 1529 (vs), 1431 (vs), 1398 (vs), 1309 (m), 1283 (m), 1250 (m), 1158 (w), 1075 (w), 766 (m), 667 (w).

ESI^+ MS : m/z = 1186 $(M\text{-}OAc)^+$.

4. [$GdCu_2(L^a)_2(\mu\text{-}OAc)_2(OAc)$]

Yield: 105.2 mg (84%)

Elemental analysis:

Calcd. For $C_{40}H_{58}Cu_2GdN_{10}O_{10}S_4$: C, 38.39; H, 4.67; N, 11.19; S, 10.25%.

Found: C, 37.24; H, 4.55; N, 11.01; S, 9.54%.

IR (KBr, cm^{-1}): 2973 (w), 2934 (w), 1585 (vs), 1564 (vs), 1529 (vs), 1433 (vs), 1395 (vs), 1307 (m), 1282 (m), 1250 (m), 1160 (w), 1070 (w), 766 (m), 667 (w).

ESI^+ MS : m/z = 1190 $(M\text{-}OAc)^+$.

5. $[DyCu_2(L^a)_2(\mu\text{-}OAc)_2(OAc)]$

Yield: 103.1 g (82%)

Elemental analysis:

Calcd. For $C_{40}H_{58}Cu_2DyN_{10}O_{10}S_4$: C, 38.23; H, 4.65; N, 11.14; S, 10.21%.

Found: C, 37.14; H, 4.75; N, 11.16; S, 10.34%.

IR (KBr, cm^{-1}): 2976 (w), 2935 (w), 1586 (vs), 1565 (vs), 1529 (vs), 1431 (vs), 1394 (vs), 1308 (m), 1283 (m), 1252 (m), 1162 (w), 1070 (w), 765 (m), 667 (w).

ESI^+ MS : m/z = 1196 $(M\text{-}OAc)^+$.

6. $[ErCu_2(L^a)_3]Cl$

Yield: 78.6 mg (52%)

Elemental analysis:

Calcd. For $C_{51}H_{69}ClCu_2ErN_{15}O_6S_6$: C, 40.56; H, 4.60; N, 13.91; S, 12.74%.

Found: C, 40.49; H, 4.77; N, 13.85; S, 12.78%.

IR (KBr, cm^{-1}): 2973 (w), 2934 (w), 1590 (vs), 1566 (vs), 1529 (vs), 1431 (vs), 1389 (vs), 1309 (m), 1283 (m), 1237 (m), 1155 (w), 1071 (w), 765 (m), 660 (w).

ESI^+ MS : m/z = 1475 $(M\text{-}Cl)^+$.

7. $[YbCu_2(L^a)_3]Cl$

Yield: 87.9 g (58%)

Elemental analysis:

Calcd. For $C_{51}H_{69}ClCu_2N_{15}O_6S_6Yb$: C, 40.40; H, 4.59; N, 13.86; S, 12.69%.

Found: C, 40.17; H, 4.74; N, 13.72; S, 13.17%.

IR (KBr, cm^{-1}): 2977 (w), 2934 (w), 1587 (vs), 1565 (vs), 1527 (vs), 1431 (vs), 1387 (vs), 1311 (m), 1285 (m), 1239 (m), 1158 (w), 1071 (w), 755 (m), 668 (w).

ESI^+ MS : m/z = 1481 $(M\text{-}Cl)^+$.

5.3.2.5 Complexes of lanthanides and zinc ($Zn^{II}Ln^{III}Zn^{II}$)

A solution of $Zn(CH_3COO)_2 \cdot 2H_2O$ (44 mg, 0.2 mmol) in MeOH (3 mL) was added to a solution of $LnCl_3$ (0.1 mmol) (Ln = Ce, Nd, Sm, Gd, Dy, Er and Yb) or H_2L^a (79.1 mg, 0.2 mmol) in MeOH (3 mL). Two drops of tryethylamine were added to the mixture, which was stirred for 15 min. at 40 °C. In the cases of Ln = Ce, Nd, Sm, Gd and Dy, the formed precipitates were filtered off, washed with MeOH, dried under vacuum. The precipitates are readily soluble in CH_2Cl_2 and were recrystallized from CH_2Cl_2/MeOH (1:1) mixtures. In the cases of Ln = Er and Yb, no precipitates were observed. The reaction mixtures were allowed to stand overnight. The formed precipitates were collected and recrystallized from CH_2Cl_2/MeOH (1:1) mixtures.

Two types of complexes were obtained

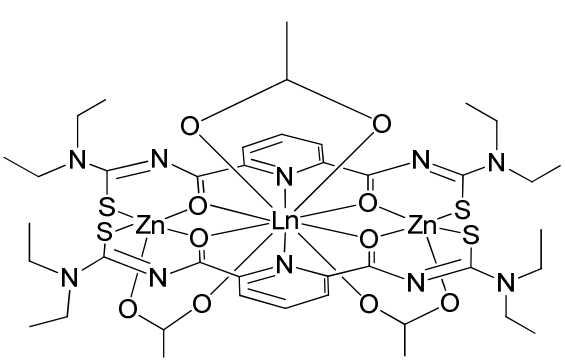

Ln = Ce, Nd, Sm, Gd or Dy

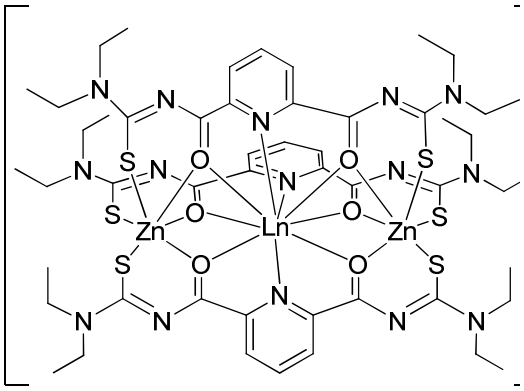

Ln = Er or Yb

1. $[CeZn_2(L^a)_2(\mu\text{-}OAc)_2(OAc)]$

Yield: 107.7 mg (87%)

Elemental analysis:

Calcd. For $C_{40}H_{58}CeN_{10}O_{10}S_4Zn_2$: C, 38.80; H, 4.72; N, 11.31; S, 10.36%.

Found: C, 37.04; H, 3.95; N, 10.96; S, 10.34%.

IR (KBr, cm^{-1}): 2975 (w), 2937 (w), 1588 (vs), 1564 (vs), 1528 (vs), 1431 (vs), 1385 (vs), 1312 (m), 1286 (m), 1243 (m), 1157 (w), 1073 (w), 766 (m), 667 (w).

ESI^+ MS : m/z = 1178 $(M\text{-}OAc)^+$.

2. $[NdZn_2(L^a)_2(\mu\text{-}OAc)_2(OAc)]$

Yield: 110.5 mg (89%)

Elemental analysis:

Calcd. For $C_{40}H_{58}N_{10}NdO_{10}S_4Zn_2$: C, 38.68; H, 4.71; N, 11.28; S, 10.33%.

Found: C, 37.64; H, 4.05; N, 10.76; S, 9.34%.

IR (KBr, cm^{-1}): 2974 (w), 2938 (w), 1586 (vs), 1565 (vs), 1528 (vs), 1433 (vs), 1385 (vs), 1310 (m), 1285 (m), 1241 (m), 1155 (w), 1072 (w), 764 (m), 665 (w).

ESI^+ MS : m/z = 1180 $(M\text{-}OAc)^+$.

3. $[SmZn_2(L^a)_2(\mu\text{-}OAc)_2(OAc)]$

Yield: 113.6 mg (91%)

Elemental analysis:

Calcd. For $C_{40}H_{58}N_{10}O_{10}S_4SmZn_2$: C, 38.49; H, 4.68; N, 11.22; S, 10.27%.

Found: C, 37.64; H, 4.05; N, 11.76; S, 9.84%.

IR (KBr, cm^{-1}): 2975 (w), 2935 (w), 1587 (vs), 1566 (vs), 1527 (vs), 1431 (vs), 1386 (vs), 1309 (m), 1285 (m), 1239 (m), 1155 (w), 1073 (w), 766 (m), 663 (w).

ESI^+ MS : m/z = 1188 $(M\text{-}OAc)^+$.

4. $[GdZn_2(L^a)_2(\mu\text{-}OAc)_2(OAc)]$

Yield: 119.2 mg (95%)

Elemental analysis:

Calcd. For $C_{40}H_{55}GdN_{10}O_{10}S_4Zn_2$: C, 38.37; H, 4.43; N, 11.19; S, 10.24%.

Found: C, 38.18; H, 4.41; N, 11.08; S, 10.40%.

IR (KBr, cm^{-1}): 2973 (w), 2934 (w), 1590 (vs), 1566 (vs), 1529 (vs), 1431 (vs), 1389 (vs), 1309 (m), 1283 (m), 1237 (m), 1155 (w), 1071 (w), 765 (m), 660 (w).

ESI^+ MS : m/z = 1196 $(M\text{-}OAc)^+$.

5. $[DyZn_2(L^a)_2(\mu\text{-}OAc)_2(OAc)]$

Yield: 104.6 mg (83%)

Elemental analysis:

Calcd. For $C_{40}H_{58}DyN_{10}O_{10}S_4Zn_2$: C, 38.12; H, 4.64; N, 11.11; S, 10.18%.

Found: C, 38.18; H, 4.41; N, 11.08; S, 10.40%.

IR (KBr, cm^{-1}): 2975 (w), 2934 (w), 1587 (vs), 1566 (vs), 1526 (vs), 1435 (vs), 1389 (vs), 1309 (m), 1286 (m), 1234 (m), 1156 (w), 1071 (w), 769 (m), 664 (w).

ESI^+ MS : m/z = 1202 $(M\text{-}OAc)^+$.

6. $[ErZn_2(L^a)_3]Cl$

Yield: 87.6 mg (58%)

Elemental analysis:

Calcd. For $C_{51}H_{69}ClErN_{15}O_6S_6Zn_2$: C, 40.46; H, 4.59; N, 13.88; S, 12.71%.

Found: C, 38.94; H, 4.59; N, 13.33; S, 12.34%.

IR (KBr, cm^{-1}): 2973 (w), 2934 (w), 1590 (vs), 1566 (vs), 1529 (vs), 1431 (vs), 1389 (vs), 1309 (m), 1283 (m), 1237 (m), 1155 (w), 1071 (w), 765 (m), 660 (w).

ESI^+ MS : m/z = 1477 $(M\text{-}Cl)^+$.

7. $[YbZn_2(L^a)_3]Cl$

Yield: 94.2 g (62%)

Elemental analysis:

Calcd. For $C_{51}H_{69}ClN_{15}O_6S_6YbZn_2$: C, 40.30; H, 4.58; N, 13.82; S, 12.66%.

Found: C, 39.49; H, 4.82; N, 13.56; S, 12.56%.

IR (KBr, cm^{-1}): 2975 (w), 2935 (w), 1589 (vs), 1564 (vs), 1529 (vs), 1432 (vs), 1386 (vs), 1309 (m), 1282 (m), 1237 (m), 1152 (w), 1075 (w), 763 (m), 658 (w).

ESI^+ MS : m/z = 1483 $(M\text{-}Cl)^+$.

5.3.3 Trinuclear mixed-metal complexes of alkaline earth and transition metals

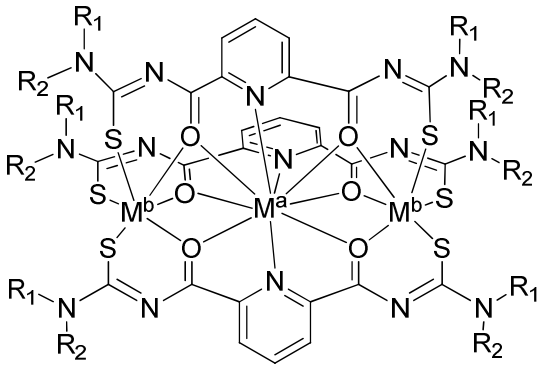

Where $H_2L^a = NR_1R_2 = NEt_2$,
$H_2L^b = NR_1R_2$ = morpholine

M^a = Ba, Sr or Ca M^b = Mn, Co or Ni

5.3.3.1 Complexes of alkaline-earth metals and manganese ($Mn^{II}M^{II}Mn^{II}$)

a) Complexes with ligand H_2L^a

A solution of $Mn(CH_3COO)_2 \cdot 4H_2O$ (49 mg, 0.2 mmol) in MeOH (3 mL) was added to a solution of MCl_2 (0.1 mmol) (M = Ba, Sr or Ca) and H_2L^a (118.5 mg, 0.3 mmol) in MeOH (3 mL). Two drops of triethylamine were added to the mixture, which was stirred for 30 min. at 40 °C. The formed orange precipitates were filtered off, washed with MeOH and dried under vacuum. The precipitates with Ba and Sr are readily soluble in CH_2Cl_2 and were recrystallized from CH_2Cl_2/MeOH (1:1). The formed crystals were collected, washed with MeOH and dried under vacuum. The precipitate with Ca is insoluble in all common solvents.

1. $[BaMn_2(L^a)_3] \cdot CH_3OH$

Yield: 134.3 mg (92%)

Elemental analysis:

Calcd. For $C_{52}H_{73}BaMn_2N_{15}O_7S_6$: C, 42.78; H, 5.04; N, 14.39; S, 13.18%.

Found: C, 42.19; H, 5.51; N, 14.07; S, 13.14%.

IR (KBr, cm^{-1}): 2974 (m), 2932 (m), 2870 (w), 1587 (vs), 1560 (vs), 1548 (vs), 1493 (vs), 1429 (vs), 1406 (vs), 1356 (vs), 1267 (m), 1254 (m), 1146 (m), 1076 (m), 750 (m).

ESI^+ MS : m/z = 1428 $(M\text{-}CH_3OH+H)^+$, 1450 $(M\text{-}CH_3OH+Na)^+$, 2878 $(2M\text{-}2CH_3OH+Na)^+$.

2. $[SrMn_2(L^a)_3]\cdot CH_3OH$

Yield: 133.9 mg (95%)

Elemental analysis:

Calcd. For $C_{52}H_{73}Mn_2N_{15}O_7S_6Sr$: C, 44.29; H, 5.22; N, 14.90; S, 13.64%.

Found: C, 44.30; H, 5.32; N, 14.90; S, 13.58%.

IR (KBr, cm^{-1}): 2974 (m), 2932 (m), 2870 (w), 1585 (vs), 1557 (vs), 1541 (vs), 1495 (vs), 1454 (m), 1427 (vs), 1398 (vs), 1356 (vs), 1273 (m), 1252 (m), 1146 (m), 1076 (m), 754 (m).

ESI^+ MS : m/z = 1378 $(M\text{-}CH_3OH+H)^+$, 1400 $(M\text{-}CH_3OH+Na)^+$, 1416 $(M\text{-}CH_3OH+K)^+$.

3. $[CaMn_2(L^a)_3]\cdot CH_3OH$

Yield: 119.9 mg (88%)

Elemental analysis:

Calcd. For $C_{52}H_{73}CaMn_2N_{15}O_7S_6$: C, 45.84; H, 5.40; N, 15.42; S, 14.12%.

Found: C, 44.81; H, 5.39; N, 14.93; S, 13.77%.

IR (KBr, cm^{-1}): 2974 (m), 2934 (m), 2870 (w), 1585 (vs), 1557 (vs), 1541 (vs), 1497 (vs), 1456 (m), 1429 (vs), 1396 (vs), 1356 (vs), 1277 (m), 1254 (m), 1146 (m), 1076 (m), 756 (m).

b) Complexes with ligand H_2L^b

A solution of $Mn(CH_3COO)_2\cdot 4H_2O$ (50 mg, 0.2 mmol) in MeOH (3 mL) was added to a solution of MCl_2 (0.1 mmol)(M = Ba, Sr or Ca) and H_2L^b (127 mg, 0.3 mmol) in MeOH (3 mL). Two drops of triethylamine were added to the mixture, which was stirred for 1 hour at 50 °C. The formed orange precipitates were filtered off, washed with MeOH and dried under vacuum. The precipitates with Ba and Sr are readily soluble in CH_2Cl_2 and were crystallized from CH_2Cl_2/MeOH (1:1). The formed crystals were collected, washed with MeOH and dried under vacuum. The precipitate with Ca is insoluble in all common solvents.

1. $[BaMn_2(L^b)_3]\cdot CH_3OH$

Yield: 143.6 mg (93%)

Elemental analysis:

Calcd. For $C_{52}H_{61}BaMn_2N_{15}O_{13}S_6$: C, 40.46; H, 3.98; N, 13.61; S, 12.46%.

Found: C, 39.78; H, 3.62; N, 13.48; S, 12.21%.

IR (KBr, cm^{-1}): 2955 (w), 2903 (w), 2852 (w), 1585 (m), 1558 (vs), 1539 (vs), 1475 (vs), 1435 (vs), 1410 (vs), 1284 (m), 1226 (vs), 1211 (m), 1111 (m), 1028 (m), 959 (m), 748 (m).

ESI^+ MS : m/z = 1511 $(M\text{-}CH_3OH)^+$, 1534 $(M\text{-}CH_3OH+Na)^+$.

2. $[SrMn_2(L^b)_3]\cdot CH_3OH$

Yield: 133.0 mg (89%)

Elemental analysis:

Calcd. For $C_{52}H_{61}Mn_2N_{15}O_{13}S_6Sr$: C, 41.80; H, 4.12; N, 14.06; S, 12.88%.

Found: C, 40.45; H, 4.30; N, 13.69; S, 12.82%.

IR (KBr, cm^{-1}): 2955 (w), 2903 (w), 2855 (w), 1587 (m), 1560 (vs), 1541 (vs), 1477 (vs), 1435 (vs), 1412 (vs), 1284 (m), 1226 (vs), 1213 (m), 1111 (m), 1028 (m), 960 (m), 750 (m).

ESI^+ MS : m/z = 1462 $(M\text{-}CH_3OH+H)^+$, 1484 $(M\text{-}CH_3OH+Na)^+$, 1500 $(M\text{-}CH_3OH+K)^+$.

3. $[CaMn_2(L^b)_3]\cdot CH_3OH$

Yield: 118.6 g (82%)

Elemental analysis:

Calcd. For $C_{52}H_{61}CaMn_2N_{15}O_{13}S_6$: C, 43.18; H, 4.25; N, 14.52; S, 13.30%.

Found: C, 42.08; H, 4.25; N, 14.37; S, 13.13%.

IR (KBr, cm^{-1}): 2965 (w), 2922 (w), 2855 (w), 1578 (m), 1555 (vs), 1533 (vs), 1479 (m), 1460 (m), 1427 (vs), 1396 (m), 1282 (vs), 1224 (m), 1111 (m), 1030 (m), 964 (m), 754 (m).

5.3.3.2 Complexes of alkaline-earth metals and cobalt ($Co^{II}M^{II}Co^{II}$)

a) Complexes with ligand H_2L^a

A solution of $Co(CH_3COO)_2 \cdot 4H_2O$ (50 mg, 0.2 mmol) in MeOH (3 mL) was added to a solution of MCl_2 (0.1 mmol) (M = Ba, Sr or Ca) and H_2L^a (118.5 mg, 0.3 mmol) in MeOH (3 mL). Two drops of triethylamine were added to the mixture, which was stirred for 45 min. at 40 °C. The obtained green precipitates were filtered off, washed with MeOH and dried under vacuum. The precipitates with Ba and Sr are readily soluble in CH_2Cl_2 and were recrystallized from CH_2Cl_2/MeOH (1:1). The formed crystals were collected, washed with MeOH and dried under vacuum. The precipitate with Ca is partially soluble in DMSO.

1. $[BaCo_2(L^a)_3]$

Yield: 135.0 mg (94%)

Elemental analysis:

Calcd. For $C_{51}H_{69}BaCo_2N_{15}O_6S_6$: C, 42.66; H, 4.84; N, 14.63; S, 13.40%.

Found: C, 42.60; H, 4.53; N, 14.49; S, 13.41%.

IR (KBr, cm^{-1}): 2974 (m), 2930 (m), 2868 (w), 1584 (vs), 1557 (vs), 1493 (vs), 1425 (vs), 1406 (vs), 1375 (m), 1356 (vs), 1285 (m), 1269 (m), 1254 (m), 1146 (m), 1076 (m), 752 (m).

ESI^+ MS : m/z = 1435 $(M+H)^+$, 1458 $(M+Na)^+$.

2. $[SrCo_2(L^a)_3] \cdot CH_3OH$

Yield: 129.0 mg (91%)

Elemental analysis:

Calcd. For $C_{52}H_{73}Co_2N_{15}O_7S_6Sr$: C, 44.04; H, 5.19; N, 14.82; S, 13.57%.

Found: C, 42.45; H, 5.08; N, 14.15; S, 12.70%.

IR (KBr, cm^{-1}): 2974 (m), 2932 (m), 2870 (w), 1587 (vs), 1558 (vs), 1493 (vs), 1408 (vs), 1375 (m), 1356 (vs), 1314 (m), 1273 (m), 1256 (m), 1146 (m), 1076 (m), 754 (m).

ESI^+ MS : m/z = 1385 $(M-CH_3OH+H)^+$, 1408 $(M-CH_3OH+Na)^+$, 1424 $(M-CH_3OH+K)^+$.

3. $[CaCo_2(L^a)_3]\cdot CH_3OH$

Yield: 120.6 mg (88%)

Elemental analysis:

Calcd. For $C_{52}H_{73}CaCo_2N_{15}O_7S_6$: C, 45.57; H, 5.37; N, 15.33; S, 14.04%.

Found: C, 44.47; H, 5.28; N, 14.72; S, 13.55%.

IR (KBr, cm^{-1}): 2974 (m), 2932 (m), 2870 (w), 1584 (vs), 1557 (vs), 1497 (vs), 1454 (vs), 1429 (vs), 1398 (vs), 1356 (vs), 1314 (m), 1279 (m), 1256 (m), 1146 (m), 1076 (m), 754 (m).

ESI^+ MS : m/z = 1338 $(M\text{-}CH_3OH+H)^+$, 1360 $(M\text{-}CH_3OH+Na)^+$.

b) Complexes with ligand H_2L^b

A solution of $Co(CH_3COO)_2\cdot 4H_2O$ (50 mg, 0.2 mmol) in MeOH (3 mL) was added to a solution of MCl_2 (0.1 mmol) (M = Ba, Sr or Ca) and H_2L^b (127 mg, 0.3 mmol) in MeOH (3 mL). Two drops of triethylamine were added to the mixture, which was stirred for 1 hour at 40 °C. The formed green precipitates were filtered off, washed with MeOH and dried under vacuum. The precipitates with Ba and Sr are readily soluble in CH_2Cl_2 and were recrystallized from CH_2Cl_2/MeOH (1:1). The formed crystals were collected, washed with MeOH and dried under vacuum. The precipitate with Ca is partially soluble in DMSO.

1. $[BaCo_2(L^b)_3]\cdot CH_3OH$

Yield: 139.7.3 mg (90%)

Elemental analysis:

Calcd. For $C_{52}H_{62}BaCo_2N_{15}O_{13}S_6$: C, 40.25; H, 3.96; N, 13.54; S, 12.40%.

Found: C, 38.92; H, 3.59; N, 13.18; S, 12.05%.

IR (KBr, cm^{-1}): 2959 (w), 2903 (w), 2853 (w), 1581 (m), 1556 (vs), 1541 (vs), 1477 (vs), 1435 (vs), 1409 (vs), 1285 (m), 1227 (vs), 1211 (m), 1111 (m), 1028 (m), 961 (m), 750 (m).

ESI^+ MS : m/z = 1519 $(M\text{-}CH_3OH)^+$, 1558 $(M\text{-}CH_3OH+K)^+$.

2. $[SrCo_2(L^b)_3]\cdot CH_3OH$

Yield: 130.7 g (87%)

Elemental analysis:

Calcd. For $C_{52}H_{61}Co_2N_{15}O_{13}S_6Sr$: C, 41.58; H, 4.09; N, 13.99; S, 12.81%.

Found: C, 38.85; H, 4.32; N, 13.35; S, 12.22%.

IR (KBr, cm^{-1}): 2965 (w), 2906 (w), 2857 (w), 1584 (m), 1545 (vs), 1489 (vs), 1462 (vs), 1435 (vs), 1412 (vs), 1352 (m), 1285 (m), 1229 (vs), 1111 (m), 1028 (m), 961 (m), 750 (m).

ESI^+ MS : m/z = 1469 $(M\text{-}CH_3OH)^+$, 1492 $(M\text{-}CH_3OH+Na)^+$.

3. $[CaCo_2(L^b)_3]$

Yield: 119.2 mg (82%)

Elemental analysis:

Calcd. For $C_{51}H_{57}CaCo_2N_{15}O_{12}S_6$: C, 43.06; H, 4.04; N, 14.77; S, 13.53%.

Found: C, 42.64; H, 3.05; N, 13.16; S, 12.34%.

IR (KBr, cm^{-1}): 2967 (w), 2920 (w), 2857 (w), 1557 (m), 1485 (vs), 1429 (vs), 1395 (vs), 1354 (m), 1285 (vs), 1231 (vs), 1109 (m), 1028 (m), 959 (m), 756 (m).

5.3.3.3 Complexes of alkaline-earth metals and nickel ($Ni^{II}M^{II}Ni^{II}$)

a) Complexes with ligand H_2L^a

A solution of $Ni(CH_3COO)_2\cdot 4H_2O$ (49.7 mg, 0.2 mmol) in MeOH (3 mL) was added to a solution of MCl_2 (0.1 mmol) (M = Ba, Sr or Ca) and H_2L^a (118.5 mg, 0.3 mmol) in MeOH (3 mL). Two drops of triethylamine were added to the mixture, which was stirred for 30 min. at 40 °C. The obtained brown precipitates were filtered off, washed with MeOH and dried under vacuum. The precipitates with Ba and Sr are readily soluble in CH_2Cl_2 and were recrystallized from CH_2Cl_2/MeOH (1:1). The formed crystals were collected, washed with MeOH and dried under vacuum. The precipitate with Ca is soluble in hot DMSO and was crystallized from a DMSO/MeOH (1:6) mixture. A brown powder was obtained.

1. **$[BaNi_2(L^a)_3]$**

Yield: 123.4 mg (86%)

Elemental analysis:

Calcd. For $C_{51}H_{69}BaN_{15}Ni_2O_6S_6$: C, 42.68; H, 4.85; N, 14.64; S, 13.40%.

Found: C, 42.69; H, 3.97; N, 14.54; S, 13.40%.

IR (KBr, cm^{-1}): 2972 (m), 2930 (m), 2868 (w), 1586 (vs), 1559 (vs), 1544 (vs), 1491 (vs), 1445 (vs), 1411 (vs), 1354 (vs), 1272 (m), 1256 (m), 1148 (m), 1076 (m), 752 (m).

ESI^+ MS : m/z = 1436 $(M+H)^+$, 1458 $(M+Na)^+$, 1474.10 $(M+K)^+$.

2. **$[SrNi_2(L^a)_3]\cdot CH_3OH$**

Yield: 117.7 g (83%)

Elemental analysis:

Calcd. For $C_{52}H_{73}N_{15}Ni_2O_7S_6Sr$: C, 44.06; H, 5.19; N, 14.82; S, 13.57%.

Found: C, 44.43; H, 5.11; N, 14.82; S, 13.49%.

IR (KBr, cm^{-1}): 2974 (m), 2930 (m), 2868 (w), 1589 (vs), 1559 (vs), 1548 (vs), 1491 (vs), 1443 (vs), 1411 (vs), 1355 (vs), 1275 (m), 1256 (m), 1146 (m), 1076 (m), 754 (m).

ESI^+ MS : m/z = 1386 $(M-CH_3OH+H)^+$, 1408 $(M-CH_3OH+Na)^+$, 1424 $(M-CH_3OH+K)^+$.

3. **$[CaNi_2(L^a)_3]\cdot CH_3OH$**

Yield: 109.6 mg (80%)

Elemental analysis:

Calcd. For $C_{52}H_{73}CaN_{15}Ni_2O_7S_6$: C, 45.59; H, 5.37; N, 15.33; S, 14.04%.

Found: C, 43.43; H, 5.10; N, 14.45; S, 13.27%.

IR (KBr, cm^{-1}): 2976 (m), 2932 (m), 2870 (w), 1584 (vs), 1557 (vs), 1545 (vs), 1493 (vs), 1456 (m), 1435 (vs), 1402 (vs), 1356 (vs), 1279 (m), 1254 (m), 1146 (m), 1076 (m), 760 (m).

ESI^+ MS : m/z = 1338 $(M-CH_3OH+H)^+$.

b) Complexes with ligand H_2L^b

A solution of $Ni(CH_3COO)_2 \cdot 4H_2O$ (49.7 mg, 0.2 mmol) in MeOH (3 mL) was added to a solution of MCl_2 (0.1 mmol) (M = Ba, Sr or Ca) and H_2L^b (127 mg, 0.3 mmol) in MeOH (3 mL). Two drops of triethylamine were added to the mixture which was stirred for 45 min. at 50 °C. The obtained brown precipitates were filtered off, washed with MeOH and dried under vacuum. The precipitates with Ba and Sr are readily soluble in CH_2Cl_2 and were recrystallized from a CH_2Cl_2/MeOH (1:1) mixture. The formed crystals were collected, washed with MeOH and dried under vacuum. The precipitate with Ca is soluble in hot DMSO and was crystallized from DMSO/MeOH (1:6) mixture. A brown powder was obtained.

1. $[BaNi_2(L^b)_3]$

Yield: 132.2 mg (87%)

Elemental analysis:

Calcd. For $C_{51}H_{57}BaN_{15}Ni_2O_{12}S_6$: C, 40.32; H, 3.78; N, 13.83; S, 12.66%.

Found: C, 40.15; H, 3.70; N, 13.47; S, 12.61%.

IR (KBr, cm^{-1}): 2961 (w), 2905 (w), 2855 (w), 1582 (vs), 1557 (vs), 1539 (vs), 1479 (vs), 1456 (vs), 1435 (vs), 1410 (vs), 1285 (vs), 1226 (m), 1111 (m), 1028 (m), 962 (m), 752 (m).

ESI^+ MS : m/z = 1520 $(M+H)^+$, 1542 $(M+Na)^+$, 1558 $(M+K)^+$.

2. $[SrNi_2(L^b)_3] \cdot CH_3OH$

Yield: 117.1 mg (78%)

Elemental analysis:

Calcd. For $C_{52}H_{61}N_{15}Ni_2O_{13}S_6Sr$: C, 41.59; H, 4.09; N, 13.99; S, 12.81%.

Found: C, 39.71; H, 4.17; N, 13.64; S, 12.42%.

IR (KBr, cm^{-1}): 2961 (w), 2905 (w), 2855 (w), 1585 (s), 1560 (vs), 1541 (vs), 1479 (vs), 1458 (vs), 1416 (vs), 1287 (m), 1226 (s), 1213 (m), 1111 (m), 1028 (m), 964 (m), 752 (m).

ESI^+ MS : m/z = 983 $(Ni_2L^b{}_2+Na)^+$, 1492 $(M-CH_3OH+Na)^+$.

3. $[CaNi_2(L^b)_3]$

Yield: 115.2 g (81%)

Elemental analysis:

Calcd. For $C_{51}H_{57}CaN_{15}Ni_2O_{12}S_6$: C, 43.08; H, 4.04; N, 14.78; S, 13.53%.

Found: C, 42.64; H, 3.85; N, 13.76; S, 12.34%.

IR (KBr, cm^{-1}): 2968 (w), 2922 (w), 2862 (w), 1585 (s), 1562 (vs), 1557 (vs), 1481 (vs), 1431 (vs), 1395 (vs), 1373 (vs), 1300 (s), 1283 (vs), 1109 (m), 1030 (m), 957 (m), 758 (m).

5.3.4 Bi- and tetranuclear oxidorhenium(V) complexes of 2,6-dipicolinoylbis(*N*,*N*-diethylthioureas) with guest metal cations

5.3.4.1 Binuclear oxidorhenium(V) complexes with guest metal cations $[M^1\{ReO(OCH_3)\}_2(L^a)_2](PF_6)$

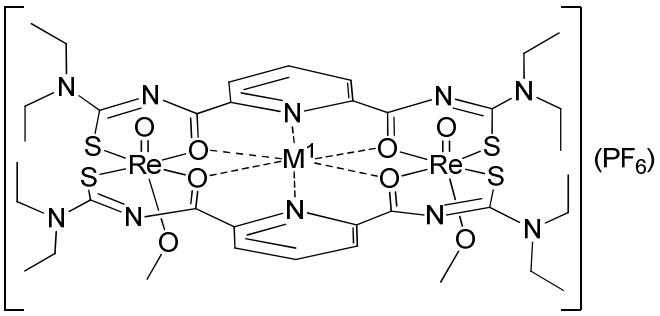

a) $[K\{ReO(OCH_3)\}_2(L^a)_2](PF_6)$

A solution of $(NBu_4)[ReOCl_4]$ (117.7 mg, 0.2 mmol) in MeOH (3 mL) was added to a solution of KPF_6 (18.4 mg, 0.1 mmol) and H_2L^a (79.1 mg, 0.2 mmol) in MeOH (3 mL). Two drops of triethylamine were added to the mixture, which was stirred for 30 min. at 40 °C. The formed wine-red precipitate was filtered off, washed with MeOH and recrystallized from CH_2Cl_2/MeOH (1:1). The formed crystals were collected, washed twice with MeOH and dried under vacuum.

Yield: 138.0 mg (96%)

Elemental analysis:

Calcd. For $C_{36}H_{52}F_6KN_{10}O_8PRe_2S_4$: C, 30.08; H, 3.65; N, 9.74; S, 8.92%.

Found: C, 30.24; H, 3.52; N, 9.89; S, 9.11%.

IR (KBr, cm^{-1}): 2974 (w), 2932 (w), 1533 (s), 1508 (s), 1429 (s), 1408 (s), 1354 (m), 1269 (w), 1254 (w), 1096 (w), 1080 (w), 945 (m), 843 (m), 743 (m).

^1H NMR (400 MHz, $CDCl_3$, ppm): 1.37 (t, 12H, *J* = 8.0 Hz, CH_3), 1.46 (t, 12H, *J* = 8.0 Hz, CH_3), 3.31 (s, 3H, OCH_3), 3.46 (s, 3H, OCH_3), 3.90-4.16 (m, 16H, CH_2), 8.12 (t, 2H, *J* = 8.0 Hz, Py), 8.60 (d, 4H, *J* = 8.0 Hz, Py).

ESI^+ MS : m/z = 1277 $(M\text{-}K\text{-}PF_6+Na)^+$, 1291 $(M\text{-}PF_6)^+$.

b) $[M^1\{ReO(OCH_3)\}_2(L^a)_2](PF_6)$ (M^1 = Rb, Cs or Tl)

A solution of $(NBu_4)[ReOCl_4]$ (117.7 mg, 0.2 mmol) in MeOH (3 mL) was added to a solution of M^1Cl (0.1 mmol) (M^1 = Rb, Cs or Tl), $(NBu_4)(PF_6)$ (38.7 mg, 0.1 mmol) and H_2L^a (79.1 mg, 0.2 mmol) in MeOH (3 mL). Two drops of triethylamine were added to the mixture, which was stirred for 30 min. at 40 °C. The formed wine-red precipitates were filtered off, washed with MeOH and recrystallized from CH_2Cl_2/MeOH (1:1). The formed crystals were collected, washed twice with MeOH and dried under vacuum.

1. $[Rb\{ReO(OCH_3)\}_2(L^a)_2](PF_6)$

Yield: 135.0 mg (91%)

Elemental analysis:

Calcd. For $C_{36}H_{52}F_6N_{10}O_8PRbRe_2S_4$: C, 29.14; H, 3.53; N, 9.44; S, 8.64%.

Found: C, 28.64; H, 3.25; N, 8.76; S, 8.34%.

IR (KBr, cm^{-1}): 2976 (w), 2934 (w), 1531 (s), 1510 (s), 1429 (s), 1406 (s), 1354 (m), 1269 (w), 1252 (w), 1096 (w), 1080 (w), 943 (m), 841 (m), 742 (m).

^1H NMR (400 MHz, $CDCl_3$, ppm): 1.35 (t, 12H, *J* = 8.0 Hz, CH_3), 1.44 (t, 12H, *J* = 8.0 Hz, CH_3), 3.30 (s, 3H, OCH_3), 3.45 (s, 3H, OCH_3), 3.95-4.26 (m, 16H, CH_2), 8.14 (t, 2H, *J* = 8.0 Hz, Py), 8.62 (d, 4H, *J* = 8.0 Hz, Py).

ESI^+ MS : m/z = 1277 $(M\text{-}Rb\text{-}PF_6+Na)^+$, 1291 $(M\text{-}Rb\text{-}PF_6+K)^+$, 1337 $(M\text{-}PF_6)^+$

2. $[Cs\{ReO(OCH_3)\}_2(L^a)_2](PF_6)$

Yield: 134.7 mg (88%)

Elemental analysis:

Calcd. For $C_{36}H_{52}CsF_6N_{10}O_8PRe_2S_4$: C, 28.23; H, 3.42; N, 9.15; S, 8.38%.

Found: C, 27.90; H, 3.18; N, 9.01; S, 8.41%.

IR (KBr, cm^{-1}): 2978 (w), 2936 (w), 1537 (s), 1510 (s), 1429 (s), 1408 (s), 1356 (m), 1269 (w), 1252 (w), 1107 (w), 1078 (w), 945 (m), 841 (m), 743 (m).

^1H NMR (400 MHz, $CDCl_3$, ppm): 1.25 (t, 12H, *J* = 8.0 Hz, CH_3), 1.33 (t, 12H, *J* = 8.0 Hz, CH_3), 3.12 (s, 3H, OCH_3), 3.18 (s, 3H, OCH_3), 3.90-4.11 (m, 16H, CH_2), 8.25 (t, 2H, *J* = 8.0 Hz, Py), 8.63 (d, 4H, *J* = 8.0 Hz, Py).

ESI^+ MS : m/z = 1277 $(M\text{-}Cs\text{-}PF_6+Na)^+$, 1291 $(M\text{-}Cs\text{-}PF_6+K)^+$, 1387 $(M\text{-}PF_6)^+$

3. $[Tl\{ReO(OCH_3)\}_2(L^a)_2](PF_6)$

Yield: 145.9 mg (91%)

Elemental analysis:

Calcd. For $C_{36}H_{52}F_6N_{10}O_8PRe_2S_4Tl$: C, 26.98; H, 3.27; N, 8.74; S, 8.00%.

Found: C, 25.63; H, 2.75; N, 8.46; S, 7.98%.

IR (KBr, cm^{-1}): 2976 (w), 2934 (w), 1533 (s), 1512 (s), 1429 (s), 1404 (s), 1354 (m), 1267 (w), 1252 (w), 1094 (w), 1082 (w), 943 (m), 844 (m), 743 (m).

^1H NMR (400 MHz, $CDCl_3$, ppm): 1.38 (t, 12H, *J* = 8.0 Hz, CH_3), 1.47 (t, 12H, *J* = 8.0 Hz, CH_3), 3.32 (s, 3H, OCH_3), 3.38 (s, 3H, OCH_3), 3.95-4.15 (m, 16H, CH_2), 8.19 (t, 2H, *J* = 8.0 Hz, Py), 8.66 (d, 4H, *J* = 8.0 Hz, Py).

ESI^+ MS : m/z = 1277 $(M\text{-}Tl\text{-}PF_6+Na)^+$, 1291 $(M\text{-}Tl\text{-}PF_6+K)^+$, 1457 $(M\text{-}PF_6)^+$

5.3.4.2 Binuclear oxidorhenium(V) complexes with guest metal cations $[M^1\{ReO(OCH_3)\}_2(L^a)_2](ReO_4)$ (M = K, Rb, Cs and Tl)

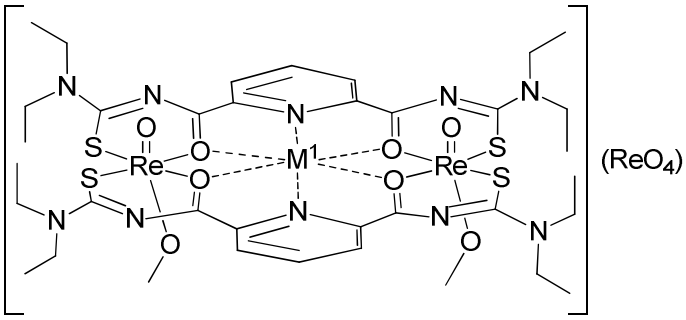

A solution of $(NBu_4)[ReOCl_4]$ (117.7 mg, 0.2 mmol) in MeOH (3 mL) was added to a solution of M^1Cl (0.1 mmol) (M^1 = K, Rb, Cs or Tl), $(NBu_4)(ReO_4)$ (49.3 mg, 0.1 mmol) and H_2L^a (79.1 mg, 0.2 mmol) in MeOH (3 mL). Two drops of triethylamine were added to the mixture, which was stirred for 30 min. at 40 °C. The formed wine-red precipitates were filtered off, washed with MeOH and recrystallized from CH_2Cl_2/MeOH (1:1). The formed crystals were collected, washed twice with MeOH and dried under vacuum.

1. $[K\{ReO(OCH_3)\}_2(L^a)_2](ReO_4)$

Yield: 140.4 mg (91%)

Elemental analysis:

Calcd. For $C_{36}H_{52}KN_{10}O_{12}Re_3S_4$: C, 28.03; H, 3.40; N, 9.08; S, 8.31%.

Found: C, 28.10; H, 3.01; N, 8.97; S, 8.57%.

IR (KBr, cm^{-1}): 2974 (w), 2934 (w), 1530 (s), 1511 (s), 1429 (s), 1409 (s), 1354 (m), 1268 (w), 1252 (w), 1096 (w), 1080 (w), 942 (m), 911 (m), 743 (m).

^1H NMR (400 MHz, $CDCl_3$, ppm): 1.33 (t, 12H, *J* = 8.0 Hz, CH_3), 1.43 (t, 12H, *J* = 8.0 Hz, CH_3), 3.31 (s, 3H, OCH_3), 3.46 (s, 3H, OCH_3), 3.80-4.06 (m, 16H, CH_2), 8.10 (t, 2H, *J* = 8.0 Hz, Py), 8.50 (d, 4H, *J* = 8.0 Hz, Py).

ESI^+ MS : m/z = 1277 $(M\text{-}K\text{-}ReO_4\text{+}Na)^+$, 1291 $(M\text{-}ReO_4)^+$.

2. $[Rb\{ReO(OCH_3)\}_2(L^a)_2](ReO_4)$

Yield: 141.4 mg (89%)

Elemental analysis:

Calcd. For $C_{36}H_{52}N_{10}O_{12}RbRe_3S_4$: C, 27.21; H, 3.37; N, 8.81; S, 8.07%.

Found: C, 26.85; H, 2.25; N, 8.27; S, 8.29%.

IR (KBr, cm^{-1}): 2976 (w), 2934 (w), 1531 (s), 1510 (s), 1429 (s), 1406 (s), 1354 (m), 1269 (w), 1252 (w), 1096 (w), 1080 (w), 943 (m), 912 (m), 742 (m).

^1H NMR (400 MHz, $CDCl_3$, ppm): 1.35 (t, 12H, *J* = 8.0 Hz, CH_3), 1.44 (t, 12H, *J* = 8.0 Hz, CH_3), 3.30 (s, 3H, OCH_3), 3.45 (s, 3H, OCH_3), 3.95-4.26 (m, 16H, CH_2), 8.14 (t, 2H, *J* = 8.0 Hz, Py), 8.62 (d, 4H, *J* = 8.0 Hz, Py).

ESI^+ MS : m/z = 1277 $(M\text{-}Rb\text{-}ReO_4\text{+}Na)^+$, 1291 $(M\text{-}Rb\text{-}ReO_4\text{+}K)^+$, 1337 $(M\text{-}ReO_4)^+$.

3. $[Cs\{ReO(OCH_3)\}_2(L^a)_2](ReO_4)$

Yield: 135.9 mg (83%)

Elemental analysis:

Calcd. For $C_{36}H_{52}CsN_{10}O_{12}Re_3S_4$: C, 26.42; H, 3.20; N, 8.56; S, 7.84%.

Found: C, 25.64; H, 3.76; N, 8.12; S, 7.28%.

IR (KBr, cm^{-1}): 2976 (w), 2934 (w), 1531 (s), 1512 (s), 1431 (s), 1408 (s), 1356 (m), 1267 (w), 1252 (w), 1094 (w), 1080 (w), 941 (m), 912 (m), 743 (m).

^{1}H NMR (400 MHz, $CDCl_3$, ppm): 1.24 (t, 12H, *J* = 8.0 Hz, CH_3), 1.31 (t, 12H, *J* = 8.0 Hz, CH_3), 3.12 (s, 3H, OCH_3), 3.18 (s, 3H, OCH_3), 3.90-4.18 (m, 16H, CH_2), 8.29 (t, 2H, *J* = 8.0 Hz, Py), 8.68 (d, 4H, *J* = 8.0 Hz, Py).

ESI^+ MS : m/z = 1277 $(M\text{-}Cs\text{-}ReO_4+Na)^+$, 1291 $(M\text{-}Cs\text{-}ReO_4+K)^+$, 1387 $(M\text{-}ReO_4)^+$.

4. $[Tl\{ReO(OCH_3)\}_2(L^a)_2](ReO_4)$

Yield: 146.9 mg (86%)

Elemental analysis:

Calcd. For $C_{36}H_{52}N_{10}O_{12}Re_3S_4Tl$: C, 25.31; H, 3.07; N, 8.20; S, 7.51%.

Found: C, 25.45; H, 2.91; N, 8.09; S, 7.90%.

IR (KBr, cm^{-1}): 2976 (w), 2934 (w), 1533 (s), 1512 (s), 1429 (s), 1404 (s), 1354 (m), 1267 (w), 1252 (w), 1094 (w), 1082 (w), 943 (m), 912 (m), 743 (m).

^{1}H NMR (400 MHz, $CDCl_3$, ppm): 1.35 (t, 12H, *J* = 8.0 Hz, CH_3), 1.45 (t, 12H, *J* = 8.0 Hz, CH_3), 3.31 (s, 3H, OCH_3), 3.39 (s, 3H, OCH_3), 3.90-4.10 (m, 16H, CH_2), 8.21 (t, 2H, *J* = 8.0 Hz, Py), 8.69 (d, 4H, *J* = 8.0 Hz, Py).

ESI^+ MS : m/z = 1277 $(M\text{-}Tl\text{-}ReO_4+Na)^+$, 1291 $(M\text{-}Tl\text{-}ReO_4+K)^+$, 1457 $(M\text{-}ReO_4)^+$.

5.3.4.3 Binuclear oxidorhenium(V) complexes with guest metal cations $[M^1\{ReO(OCH_3)\}_2(L^a)_2]Cl$ (M = K or Rb)

A solution of $(NBu_4)[ReOCl_4]$ (117.7 mg, 0.2 mmol) in MeOH (3 mL) was added to a solution of M^1Cl (0.1 mmol) (M^1 = K, Rb, Cs or Tl) and H_2L^a (79.1 mg, 0.2 mmol) in MeOH (3 mL). Two drops of triethylamine were added to the mixture, which was stirred for 30 min. at 40 °C. No precipitates were obtained. The reaction mixture was allowed to stand overnight. Red crystals were obtained in the cases of M^1 = K and Rb. The formed crystals were collected, washed twice with MeOH and dried under vacuum. Only black, oily products were obtained in the cases of M^1 = Cs and Tl.

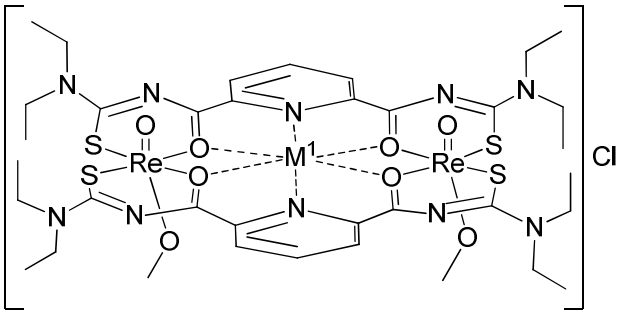

M^1 = K or Rb

1. $[K\{Re_2O_3\}_2(L^a)_4]Cl$

Yield: 95.6 mg (72%)

Elemental analysis:

Calcd. for $C_{36}H_{52}ClKN_{10}O_8Re_2S_4$: C, 32.56; H, 3.95; N, 10.55; S, 9.66%.

Found: C, 31.64; H, 4.05; N, 11.06; S, 10.34%.

IR (KBr, cm^{-1}): 2974 (w), 2934 (w), 1535 (s), 1508 (s), 1430 (s), 1406 (s), 1354 (m), 1268 (w), 1252 (w), 1097 (w), 1080 (w), 944 (m), 741 (m).

^1H NMR (400 MHz, $CDCl_3$, ppm): 1.33 (t, 12H, *J* = 8.0 Hz, CH_3), 1.48 (t, 12H, *J* = 8.0 Hz, CH_3), 3.31 (s, 3H, OCH_3), 3.46 (s, 3H, OCH_3), 3.95-4.19 (m, 16H, CH_2), 8.18 (t, 2H, *J* = 8.0 Hz, Py), 8.64 (d, 4H, *J* = 8.0 Hz, Py).

ESI^+ MS : m/z = 1277 $(M-K-Cl+Na)^+$, 1291 $(M-Cl)^+$.

2. $[Rb\{Re_2O_3\}_2(L^a)_4]Cl$

Yield: 92.1 mg (67%)

Elemental analysis:

Calcd. for $C_{36}H_{52}ClN_{10}O_8RbRe_2S_4$: C, 31.46; H, 3.81; N, 10.19; S, 9.33%.

Found: C, 31.24; H, 2.85; N, 9.72; S, 9.34%.

IR (KBr, cm^{-1}): 2976 (w), 2934 (w), 1531 (s), 1510 (s), 1429 (s), 1406 (s), 1354 (m), 1269 (w), 1252 (w), 1096 (w), 1080 (w), 943 (m), 742 (m).

^1H NMR (400 MHz, $CDCl_3$, ppm): 1.37 (t, 12H, *J* = 8.0 Hz, CH_3), 1.46 (t, 12H, *J* = 8.0 Hz, CH_3), 3.31 (s, 3H, OCH_3), 3.46 (s, 3H, OCH_3), 3.90-4.16 (m, 16H, CH_2), 8.12 (t, 2H, *J* = 8.0 Hz, Py), 8.59 (d, 4H, *J* = 8.0 Hz, Py).

ESI^+ MS : m/z = 1277 $(M-Rb-Cl+Na)^+$, 1291 $(M-Rb-Cl+K)^+$, 1337 $(M-Cl)^+$.

5.3.4.4 Tetranuclear oxidorhenium(V) complexes with guest metal ions $[M^1\{Re_2O_3\}_2(L^a)_4](PF_6)$ and $[M^1\{Re_2O_3\}_2(L^a)_4](ReO_4)$

The complexes $[M^1\{ReO(OCH_3)\}_2(L^a)_2](X)$ (0.05 mmol) (M^1 = K^+, Rb^+, Cs^+ or Tl^+, X = PF_6^- and ReO_4^-) were dissolved in a mixture of CH_2Cl_2/MeCN (1:1) and allowed to evaporate slowly overnight. The obtained crystals were collected, washed twice with MeOH and dried under vacuum. The elemental analyses were done with the powdered, dried crystals.

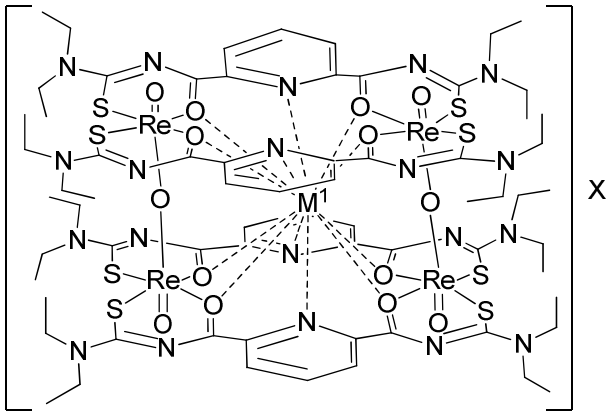

M^1 = K, Rb, Cs or Tl X = PF_6 or ReO_4

1. **$[K\{Re_2O_3\}_2(L^a)_4](PF_6)$**

Yield: 114.4 mg (88%)

Elemental analysis:

Calcd. for $C_{68}H_{92}F_6KN_{20}O_{14}PRe_4S_8$: C, 31.42; H, 3.57; N, 10.78; S, 9.87%.

Found: C, 31.64; H, 3.27; N, 10.76; S, 10.14%.

IR (KBr, cm^{-1}): 2978 (w), 2936 (w), 1537 (s), 1510 (s), 1433 (s), 1414 (s), 1356 (m), 845 (m), 742 (m), 723 (m), 700 (m), 681 (m), 650 (m).

^{1}H NMR (400 MHz, DMSO-d_6, ppm): 1.27 (t, 24H, J = 8.0 Hz, CH_3), 1.38 (t, 24H, J = 8.0 Hz, CH_3), 3.59 – 3.68 (m, 8H, CH_2), 3.92 – 4.03 (m, 16H, CH_2), 4.33 – 4.42 (m, 8H, CH_2), 7.99 (t, 4H, J = 8.0 Hz, Py), 8.24 (d, 8H, J = 8.0 Hz, Py).

ESI^+ MS : m/z = 2437 $(M\text{-}K\text{-}PF_6+Na)^+$, 2453 $(M\text{-}PF_6)^+$.

2. [K{Re_2O_3}$_2$(L^a)$_4$](ReO_4)

Yield: 109.5 mg (81%)

Elemental analysis:

Calcd. for $C_{68}H_{92}KN_{20}O_{18}Re_5S_8$: C, 30.20; H, 3.43; N, 10.36; S, 9.49%.

Found: C, 29.64; H, 2.98; N, 9.93; S, 9.03%.

IR (KBr, cm^{-1}): 2978 (w), 2936 (w), 1537 (s), 1510 (s), 1433 (s), 1414 (s), 1356 (m), 910 (m), 742 (m), 723 (m), 700 (m), 681 (m), 650 (m).

^{1}H NMR (400 MHz, DMSO-d_6, ppm): 1.27 (t, 24H, J = 8.0 Hz, CH_3), 1.38 (t, 24H, J = 8.0 Hz, CH_3), 3.59 – 3.68 (m, 8H, CH_2), 3.92 – 4.03 (m, 16H, CH_2), 4.33 – 4.42 (m, 8H, CH_2), 7.99 (t, 4H, J = 8.0 Hz, Py), 8.24 (d, 8H, J = 8.0 Hz, Py).

ESI^+ MS : m/z = 2437 $(M\text{-}K\text{-}ReO_4+Na)^+$, 2453 $(M\text{-}ReO_4)^+$.

3. [Rb{Re_2O_3}$_2$(L^a)$_4$](PF_6)

Yield: 111.1 g (84%),

Elemental analysis:

Calcd. for $C_{68}H_{92}F_6N_{20}O_{14}PRbRe_4S_8$: C, 30.87; H, 3.51; N, 10.59; S, 9.70%.

Found: C, 29.94; H, 4.05; N, 10.28; S, 9.36%.

IR (KBr, cm^{-1}): 2978 (w), 2934 (w), 1537 (s), 1510 (s), 1433 (s), 1414 (s), 1356 (m), 845 (m), 742 (m), 723 (m), 700 (m), 681 (m), 650 (m).

^{1}H NMR (400 MHz, DMSO-d_6, ppm): 1.28 (t, 24H, J = 8.0 Hz, CH_3), 1.39 (t, 24H, J = 8.0 Hz, CH_3), 3.61 – 3.69 (m, 8H, CH_2), 3.88 – 3.95 (m, 8H, CH_2), 4.02 – 4.09 (m, 8H, CH_2), 4.33 – 4.42 (m, 8H, CH_2), 7.95 (t, 4H, J = 8.0 Hz, Py), 8.21 (d, 8H, J = 8.0 Hz, Py).

ESI^+ MS : m/z = 2437 $(M\text{-}Rb\text{-}PF_6+Na)^+$, 2453 $(M\text{-}Rb\text{-}PF_6+K)^+$, 2500 $(M\text{-}PF_6)^+$.

4. [Rb{Re_2O_3}$_2$(L^a)$_4$](ReO_4)

Yield: 104.5 mg (76%)

Elemental analysis:

Calcd. for $C_{68}H_{92}N_{20}O_{18}RbRe_5S_8$: C, 29.69; H, 3.37; N, 10.18; S, 9.33%.

Found: C, 29.24; H, 3.05; N, 9.96; S, 8.89%.

IR (KBr, cm^{-1}): 2978 (w), 2934 (w), 1537 (s), 1510 (s), 1433 (s), 1414 (s), 1356 (m), 908 (m), 743 (m), 723 (m), 700 (m), 681 (m), 650 (m).

^{1}H NMR (400 MHz, DMSO-d_6, ppm): 1.28 (t, 24H, J = 8.0 Hz, CH_3), 1.39 (t, 24H, J = 8.0 Hz, CH_3), 3.61 – 3.69 (m, 8H, CH_2), 3.88 – 3.95 (m, 8H, CH_2), 4.02 – 4.09 (m, 8H, CH_2), 4.33 – 4.42 (m, 8H, CH_2), 7.95 (t, 4H, J = 8.0 Hz, Py), 8.21 (d, 8H, J = 8.0 Hz, Py).

ESI^+ MS : m/z = 2437 $(M\text{-}Rb\text{-}ReO_4+Na)^+$, 2453 $(M\text{-}Rb\text{-}ReO_4+K)^+$, 2500 $(M\text{-}ReO_4)^+$.

5. $[Cs\{Re_2O_3\}_2(L^a)_4](PF_6)$

Yield: 105.0 mg (78%)

Elemental analysis:

Calcd. for $C_{68}H_{92}CsF_6N_{20}O_{14}PRe_4S_8$: C, 30.33; H, 3.44; N, 10.40; S, 9.53%.

Found: C, 30.16; H, 2.95; N, 10.76; S, 10.04%.

IR (KBr, cm^{-1}): 2977 (w), 2933 (w), 1532 (s), 1508 (s), 1431 (s), 1410 (s), 1354 (m), 844 (s), 744 (m), 723 (m), 700 (m), 681 (m), 650 (m).

^{1}H NMR (400 MHz, DMSO-d_6, ppm): 1.25 (t, 24H, J = 8.0 Hz, CH_3), 1.36 (t, 24H, J = 8.0 Hz, CH_3), 3.63 – 3.72 (m, 8H, CH_2), 3.88 – 3.95 (m, 8H, CH_2), 4.03 – 4.11 (m, 8H, CH_2), 4.33 – 4.42 (m, 8H, CH_2), 7.93 (t, 4H, J = 8.0 Hz, Py), 8.19 (d, 8H, J = 8.0 Hz, Py).

ESI^+ MS : m/z = 2437 $(M\text{-}Cs\text{-}PF_6+Na)^+$, 2453 $(M\text{-}Cs\text{-}PF_6+K)^+$, 2547 $(M\text{-}PF_6)^+$.

6. $[Cs\{Re_2O_3\}_2(L^a)_4](ReO_4)$

Yield: 109.1 mg (78%)

Elemental analysis:

Calcd. for $C_{68}H_{92}CsN_{20}O_{18}Re_5S_8$: C, 29.19; H, 3.31; N, 10.01; S, 9.17%.

Found: C, 28.93; H, 3.83; N, 9.86; S, 8.96%.

IR (KBr, cm^{-1}): 2975 (w), 2933 (w), 1531 (s), 1510 (s), 1435 (s), 1410 (s), 1356 (m), 913 (m), 745 (m), 725 (m), 700 (m), 681 (m), 652 (m).

^{1}H NMR (400 MHz, DMSO-d_6, ppm): 1.25 (t, 24H, J = 8.0 Hz, CH_3), 1.36 (t, 24H, J = 8.0 Hz, CH_3), 3.63 – 3.72 (m, 8H, CH_2), 3.88 – 3.95 (m, 8H, CH_2), 4.03 – 4.11 (m, 8H, CH_2), 4.33 – 4.42 (m, 8H, CH_2), 7.93 (t, 4H, J = 8.0 Hz, Py), 8.19 (d, 8H, J = 8.0 Hz, Py).

ESI^+ MS : m/z = 2437 $(M\text{-}Cs\text{-}ReO_4+Na)^+$, 2453 $(M\text{-}Cs\text{-}ReO_4+K)^+$, 2547 $(M\text{-}ReO_4)^+$.

7. $[Tl\{Re_2O_3\}_2(L^a)_4](PF_6)$

Yield: 103.6 mg (75%)

Elemental analysis:

Calcd. for $C_{68}H_{92}F_6N_{20}O_{14}PRe_4S_8Tl$: C, 29.55; H, 3.35; N, 10.13; S, 9.28%.

Found: C, 29.34; H, 3.06; N, 10.06; S, 9.34%.

IR (KBr, cm^{-1}): 2978 (w), 2933 (w), 1533 (s), 1510 (s), 1431 (s), 1410 (s), 1356 (m), 845 (s), 743 (m), 723 (m), 700 (m), 681 (m), 650 (m).

^1H NMR (400 MHz, DMSO-d_6, ppm): 1.29 (t, 24H, J = 8.0 Hz, CH_3), 1.39 (t, 24H, J = 8.0 Hz, CH_3), 3.61 – 3.69 (m, 8H, CH_2), 3.88 – 3.94 (m, 8H, CH_2), 4.02 – 4.10 (m, 8H, CH_2), 4.35 – 4.43 (m, 8H, CH_2), 7.96 (t, 4H, J = 8.0 Hz, Py), 8.22 (d, 8H, J = 8.0 Hz, Py).

ESI^+ MS : m/z = 2437 $(M\text{-}Tl\text{-}PF_6+Na)^+$, 2453 $(M\text{-}Tl\text{-}PF_6+K)^+$, 2617 $(M\text{-}PF_6)^+$.

8. $[Tl\{Re_2O_3\}_2(L^a)_4](ReO_4)$

Yield: 101.9 mg (71%)

Elemental analysis:

Calcd. for $C_{68}H_{92}N_{20}O_{18}Re_5S_8Tl$: C, 28.46; H, 3.23; N, 9.76; S, 8.94%.

Found: C, 28.06; H, 2.97; N, 10.17; S, 9.24%.

IR (KBr, cm^{-1}): 2978 (w), 2933 (w), 1533 (s), 1510 (s), 1431 (s), 1410 (s), 1356 (m), 912 (m), 743 (m), 723 (m), 700 (m), 681 (m), 650 (m).

^1H NMR (400 MHz, DMSO-d_6, ppm): 1.29 (t, 24H, J = 8.0 Hz, CH_3), 1.39 (t, 24H, J = 8.0 Hz, CH_3), 3.61 – 3.69 (m, 8H, CH_2), 3.88 – 3.94 (m, 8H, CH_2), 4.02 – 4.10 (m, 8H, CH_2), 4.35 – 4.43 (m, 8H, CH_2), 7.96 (t, 4H, J = 8.0 Hz, Py), 8.22 (d, 8H, J = 8.0 Hz, Py).

ESI^+ MS : m/z = 2437 $(M\text{-}Tl\text{-}ReO_4+Na)^+$, 2453 $(M\text{-}Tl\text{-}ReO_4+K)^+$, 2617 $(M\text{-}ReO_4)^+$.

5.3.4.5 Guest metal cation exchange processes in tetranuclear oxidorhenium(V) complexes

a) Removal of the central K^+ cation by $Na(BPh_4)$

A solution of $Na(BPh_4)$ (68.4 mg, 0.2 mmol) in MeOH (3 mL) was added to a solution of $[K\{Re_2O_3\}_2(L^a)_4](PF_6)$ (130.0 mg, 0.05 mmol) in CH_2Cl_2 (3 mL). The mixture was stirred for 2 hours at 50 °C. The resulting solution was cooled down to room temperature and filtered. The filtrate was allowed to stand overnight for a slow evaporation. The obtained red crystals were collected, washed twice with MeOH and dried under vacuum. The elemental analysis was done with the powdered dry crystalline samples.

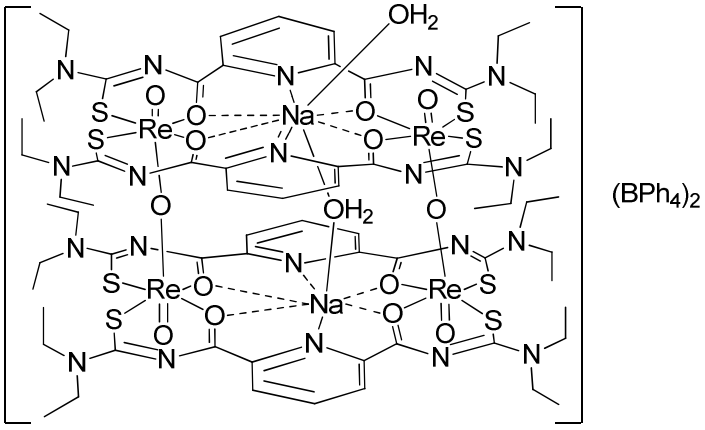

$[Na_2(Re_2O_3)_2(L^a)_4(H_2O)_2](BPh_4)_2$

Yield: 123.8 mg (79%)

Elemental analysis:

Calcd. for $C_{116}H_{136}B_2N_{20}Na_2O_{16}Re_4S_8$: C, 44.44; H, 4.37; N, 8.93; S, 8.18%.

Found: C, 43.64; H, 3.95; N, 8.76; S, 7.98%.

IR (KBr, cm^{-1}): 3053 (w), 2978 (w), 2932 (w), 1535 (s), 1508 (s), 1433 (s), 1414 (s), 1356 (m), 743 (m), 725 (m), 702 (m), 681 (m), 652 (m).

^1H NMR (400 MHz, DMSO-d_6, ppm): 1.29 (t, 24H, J = 8.0 Hz, CH_3), 1.39 (t, 24H, J = 8.0 Hz, CH_3), 3.61 – 3.69 (m, 8H, CH_2), 3.88 – 3.94 (m, 8H, CH_2), 4.02 – 4.10 (m, 8H, CH_2), 4.35 – 4.43 (m, 8H, CH_2), 7.34 – 7.58 (m, 40H, Ph), 7.96 (t, 4H, J = 8.0 Hz, Py), 8.22 (d, 8H, J = 8.0 Hz, Py).

ESI^+ MS : m/z = 2437 $(M\text{-}Na\text{-}2(BPh_4)\text{-}2(H_2O))^+$, 2453 $(M\text{-}2Na\text{-}2(BPh_4)\text{-}2(H_2O)+K)^+$.

b) Synthesis of $[Na_2(Re_2O_3)_2(L^a)_4(H_2O)_2](BPh_4)_2$

A solution of $(NBu_4)[ReOCl_4]$ (117.7 mg, 0.2 mmol) in MeOH (3 mL) was added to a solution of NaCl (0.1 mmol), $(NBu_4)(X)$ (0.1 mmol) (X = PF_6^- or ReO_4^-) and H_2L^a (79.1 mg, 0.2 mmol) in MeOH (3 mL). Two drops of triethylamine were added to the mixtures, which were stirred for 1 hour at 40 °C. The reaction mixtures were cooled down to room temperature. A solution of $Na(BPh_4)$ (68.4 mg, 0.2 mmol) in MeOH/CH_3CN (1:1) was added to the reaction mixture. The mixture was evaporated slowly overnight. The formed red crystals were collected, washed twice with MeOH and dried under vacuum. All analyses were done with powdered dry crystalline samples.

Yield: 252.2 mg (81%)

Elemental analysis:

Calcd. for $C_{116}H_{136}B_2N_{20}Na_2O_{16}Re_4S_8$: C, 44.44; H, 4.37; N, 8.93; S, 8.18%.

Found: C, 43.98; H, 4.95; N, 9.46; S, 7.95%.

The IR, NMR and ESI^+ MS data are identical to the previous one (5.3.4.5 a)

c) Exchange of the central K^+ cation

A solution of M^1Cl (0.05 mmol) (M^1 = Rb, Cs or Tl) in MeOH (3 mL) was added to a solution of $[K\{Re_2O_3\}_2(L^a)_4](PF_6)$ (130 mg, 0.05 mmol) in CH_2Cl_2 (3mL). The mixture was stirred for 1 hour at 50 °C. The resulting solution was allowed to stand overnight for a slow evaporation at room temperature. The obtained red crystals were collected, washed twice with MeOH and dried under vacuum.

The IR, NMR and ESI^+ MS data of the obtained crystals shows the presence of $[Rb\{Re_2O_3\}_2(L^a)_4](PF_6)$, $[Cs\{Re_2O_3\}_2(L^a)_4](PF_6)$ and $[Tl\{Re_2O_3\}_2(L^a)_4](PF_6)$ and are identical to the analytical data obtained in chapter 5.3.4.4.

Elemental analysis:

1)$[Rb\{Re_2O_3\}_2(L^a)_4](PF_6)$

Calcd. for $C_{68}H_{92}F_6N_{20}O_{14}PRbRe_4S_8$: C, 30.87; H, 3.51; N, 10.59; S, 9.70%.

Found: C, 30.34; H, 4.15; N, 10.08; S, 9.32%.

1)$[Cs\{Re_2O_3\}_2(L^a)_4](PF_6)$

Calcd. for $C_{68}H_{92}CsF_6N_{20}O_{14}PRe_4S_8$: C, 30.33; H, 3.44; N, 10.40; S, 9.53%.

Found: C, 30.20; H, 3.65; N, 10.26; S, 9.23%.

1)[Tl{Re_2O_3}$_2$(L^a)$_4$](PF_6)

Calcd. for $C_{68}H_{92}F_6N_{20}O_{14}PRe_4S_8Tl$: C, 29.55; H, 3.35; N, 10.13; S, 9.28%.

Found: C, 29.34; H, 3.25; N, 10.16; S, 9.34%.

d) Exchange of the central Rb^+ and Tl^+ cations

A solution of CsCl (0.05 mmol) in MeOH (3 mL) was added to solutions of [M^1{Re_2O_3}$_2$(L^a)$_4$](PF_6) (0.05 mmol) (M^1 = Rb^+ or Tl^+) in CH_2Cl_2 (3mL). The mixtures were stirred for 1 hour at 50 °C. The resulting solutions were allowed to stand overnight for a slow evaporation at room temperature. The obtained red crystals were collected, washed twice with MeOH and dried under vacuum.

The IR, NMR and ESI^+ MS data of the obtained crystals shows the presence of [Cs{Re_2O_3}$_2$(L^a)$_4$](PF_6) and are identical to the values obtained in chapter 5.3.4.4.

Elemental analysis:

Calcd. for $C_{68}H_{92}CsF_6N_{20}O_{14}PRe_4S_8$: C, 30.33; H, 3.44; N, 10.40; S, 9.53%.

Found: C, 30.10; H, 3.55; N, 10.23; S, 9.89%.

5.4 Crystal structure determination

The intensities for the X-ray determinations were collected on *STOE* IPDS 2T or *Brucker*-Smart-CCD-100-M instruments with Mo/Kα radiation. The space groups were determined using *CHECKHKL*.[125] Empirical or numerical absorption corrections were carried out by the *SADABS* [126]or *X-RED*32[127] programs. Structure solution and refinement were performed with the *SIR 97*,[128] *SHELXS 97* [129-130] or *SHELXS 86* [129-130] and *SHELXL 97* [131] programs. Hydrogen atom positions were calculated for idealized positions and treated with the 'riding model' option of *SHELXL* 97. Tables containing more information about crystal data, refinement, positional parameters and ellipsoid drawings are given as Appendix of this thesis. Full crystallographic material including full crystallographic Table, hkl, res and cif files together with the corresponding validation files are given as Supplementary material on the enclosed CD-ROM.

Summary

This thesis contains synthesis and structural characterization of novel multinuclear mixed metal complexes with bipodal 2,6-dipicolinoylbis(*N,N*-dialkylthioureas) (H_2L). The multidentate chelating ligands were synthesized by coupling reactions of 2,6-dipicolinoylchloride with *N,N*-dialkylthioureas.

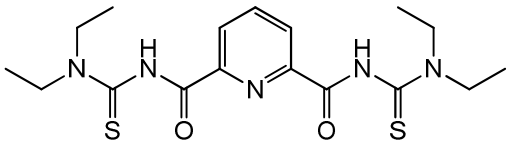

H_2L^a

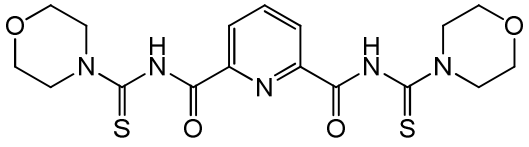

H_2L^b

The presence of the 'hard' donor atoms *N* and *O* and the 'soft' donor atom *S* leads to the coordination of 'hard' and 'soft' metal atoms to the ligand simultaneously. Preferably, lanthanides, alkaline and alkaline earth metals coordinate to the central 2,6-dipicolinoyl moiety of the ligand via *O,N,O* donors. Transition metal ions including oxidorhenium(V) units prefer the coordination with both aroylthiourea moieties via *O,S* donors.

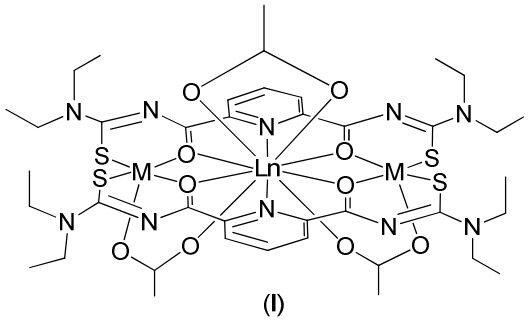

(I)

Ln = Ce, Nd, Sm, Gd, Dy, Er or Yb
M = Co, Ni, Cu or Zn

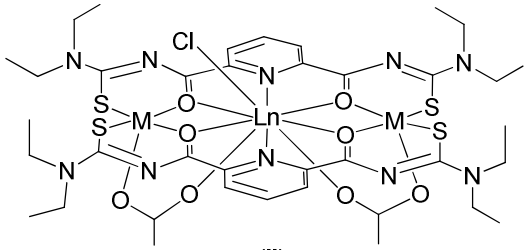

(II)

Ln = Ce, Nd, Sm, Gd, Dy, Er or Yb
M = Co, Ni, Cu or Zn

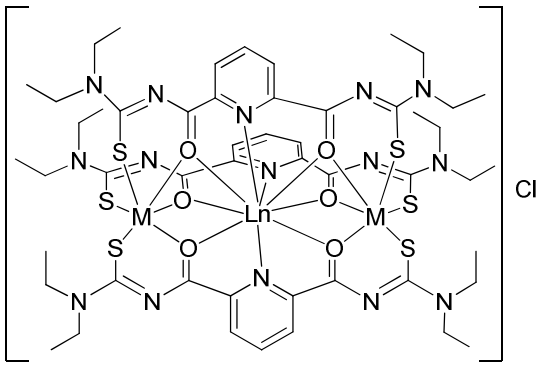

(III)

Ln = Ce, Nd, Sm, Gd, Dy, Er or Yb
M = Mn, Cu or Zn

Three groups of mixed metal complexes are reported in this thesis with respect to the metal combinations. The first group of complexes contains a trinuclear $M^{II}Ln^{III}M^{II}$ core (where Ln = Ce, Nd, Sm, Gd, Dy, Er or Yb and M = Mn, Co, Ni, Cu or Zn) coordinated to 2,6-dipicolinoylbis(*N,N*-diethylthioureas) (H_2L^a). Regarding to the numbers of coordinated organic ligands and the types of co-ligands, such as acetato or chlorido, the complexes can be further divided into three sub-groups: $[LnM_2(L^a)_2(\mu\text{-}OAc)_2(OAc)]$ (**I**), $[LnM_2(L^a)_2(\mu\text{-}OAc)_2Cl]$ (**II**) and $[LnM_2(L^a)_3]Cl$ (**III**).

The second group of complexes has a trinuclear $M^bM^aM^b$ core (where M^a = Ba, Sr or Ca and M^b = Mn, Co or Ni). This group is further divided into two sub-groups where complexes of 2,6-dipicolinoylbis(*N,N*-diethylthiourea) (H_2L^a) belongs to one group and complexes of 2,6-dipicolinoylbis(*N,N*-morpholinethioureas) (H_2L^b) belongs to the other. All complexes of this group show the coordination of three deprotonated organic ligands to the trinuclear core and have the composition $[M^aM^b{}_2(L)_3]$ (**IV**).

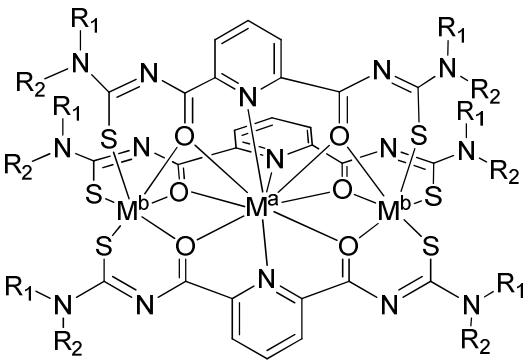

(IV)

M^a = Ba, Sr or Ca
M^b = Mn, Co or Ni

$H_2L^a = NR_1R_2 = NEt_2$,
$H_2L^b = NR_1R_2$ = morpholine

The third group of complexes is exclusively with $(Re{=}O)^{3+}$ cores. Binuclear oxidorhenium(V) complexes of the organic ligand 2,6-dipicolinoylbis(*N,N*-diethylthiourea) (H_2L^a) with additional guest metal cations such as K^+, Rb^+, Cs^+ or Tl^+ could be synthesized. They have the composition of $[M^I\{ReO(OCH_3)\}_2(L^a)_2]X$ (**V**) (M^1 = K, Rb, Cs or Tl) and the positive charge of the complexes can be neutralized by $(PF_6)^-$ or $(ReO_4)^-$. In addition to that, tetranuclear oxidorhenium(V) complexes of the composition $[M^I(Re_2O_3)_2(L^a)_4]X$ (**VI**) with the same guest metal cations can be obtained by slow evaporation in the solvent mixture of CH_2Cl_2/CH_3CN(aq) (1:1).

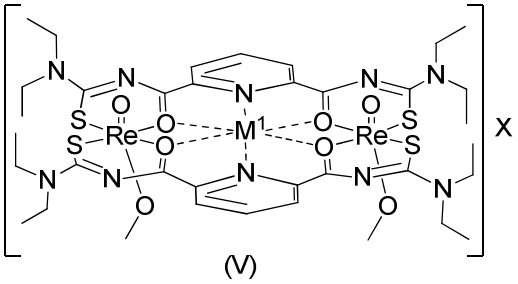

(V)

M^1 = K, Rb, Cs or Tl

X = PF_6 or ReO_4

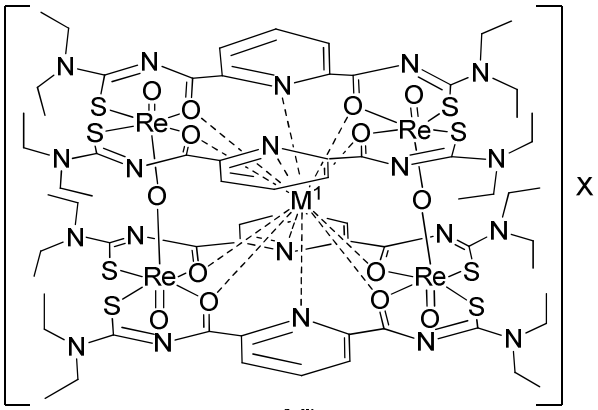

(VI)

The smaller K^+ ion inside the cage of complex (VI) can be exchanged by bigger cations such as Rb^+, Tl^+ and Cs^+. The Rb^+ and Tl^+ ions can be exchanged only by Cs^+ ion, but not by K^+ ion. Therefore the metal ion exchange strongly depends on the size of the metal ion.

Zusammenfassung

In der vorliegenden Arbeit werden Synthese und strukturelle Charakterisierung neuartiger mehrkerniger Metallkomplexe mit bipodalen 2,6-Dipicolinoylbis(*N,N*-dialkylthioharnstoffen) (H_2L) vorgestellt. Die mehrzähnigen Liganden wurden durch Kupplung von 2,6-Dipicolinoylchlorid mit *N,N*-Dialkylthioharnstoffen synthetisiert.

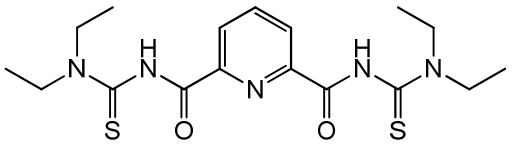

H_2L^a

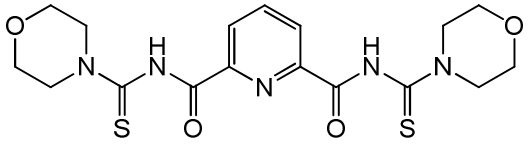

H_2L^b

Die Anwesenheit von „harten“ (*N* und *O*) und „weichen“ Donoratomen (*S*) ermöglicht die gleichzeitige Koordination von „harten“ und „weichen“ Metallionen an die Liganden. Während Lanthanoide, Alkali- und Erdalkali- Metallionen vorzugsweise über die Donoratome *O,N,O* an die zentrale 2,6-Dipicolinoyl-Einheit des Liganden koordinieren, bevorzugen Übergangsmetallionen die Koordination an den beiden Aroylthioharnstoff-Resten über die *O,S*-Donoratome.

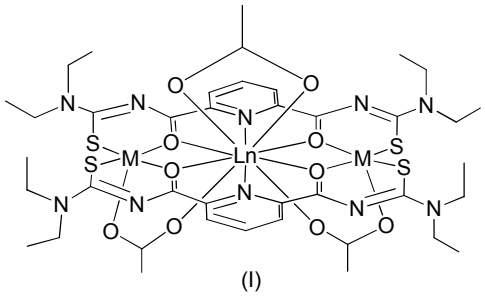

(I)

Ln = Ce, Nd, Sm, Gd, Dy, Er oder Yb
M = Co, Ni, Cu oder Zn

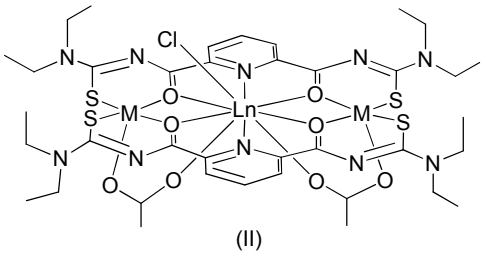

(II)

Ln = Ce, Nd, Sm, Gd, Dy, Er oder Yb
M = Co, Ni, Cu oder Zn

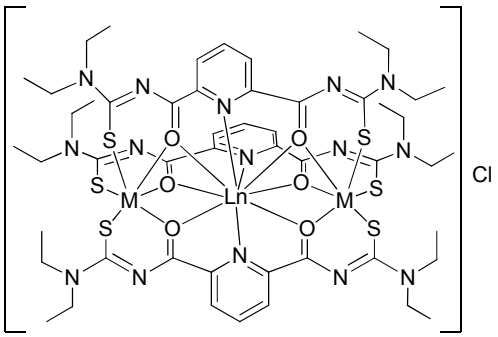

(III)

Ln = Ce, Nd, Sm, Gd, Dy, Er oder Yb
M = Mn, Cu oder Zn

Es werden drei Kategorien von gemischten Metallkomplexen beschrieben. Die erste Kategorie enthält eine dreikernige $M^{II}Ln^{III}M^{II}$–Einheit (Ln = Ce, Nd, Sm, Gd, Dy, Er oder Yb, M = Mn, Co, Ni, Cu oder Zn), die mit 2,6-Dipicolinoylbis(*N,N*-diethyl–thioharnstoff) (H_2L^a) koordiniert. Mit Blick auf die Zahl der koordinierten organischen Liganden und die Art der Co-Liganden (Acetato oder Chlorido) können die Komplexen in weitere drei Unterkategorien eingeteilt werden: $[LnM_2(L^a)_2(\mu\text{-}OAc)_2(OAc)]$ (**I**), $[LnM_2(L^a)_2(\mu\text{-}OAc)_2Cl]$ (**II**) und $[LnM_2(L^a)_3]Cl$ (**III**).

Die zweite Kategorie von Komplexen enthält eine dreikernige Einheit $M^bM^aM^b$ (M^a = Ba, Sr oder Cs, M^b = Mn, Co oder Ni). Diese Kategorie ist in weitere zwei Unterkategorien geteilt, wobei Komplexe mit 2,6-Dipicolinoylbis(*N,N*-diethylthioharnstoff) (H_2L^a) zu einer Unterkategorie gehören und Komplexe mit 2,6-Dipicolinoylbis(*N,N*-morpholinthioharnstoff) (H_2L^b) zu einer zweiten Unterkategorie gehören. Alle Komplexen dieser zweiten Kategorie zeigen die Koordination von drei deprotonierten organischen Liganden mit den drei Metallionen und besitzen die allgemeine Formel $[M^aM^b{}_2(L)_3]$ (**IV**).

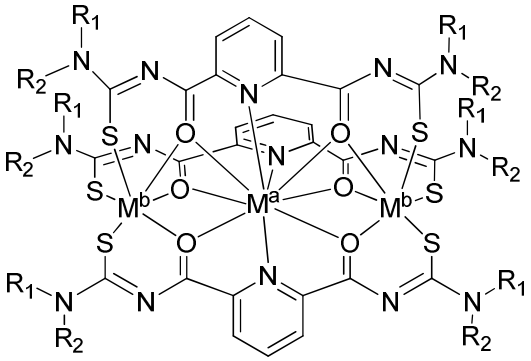

M^a = Ba, Sr oder Ca
M^b = Mn, Co oder Ni

$H_2L^a = NR_1R_2 = NEt_2$,
$H_2L^b = NR_1R_2$ = morpholine

(IV)

Die dritte Kategorie von Komplexen enthält $(Re{=}O)^{3+}$-Einheiten. Es konnten zweikernige, kationische Oxidorhenium(V)-Komplexe mit 2,6-Dipicolinoylbis(*N,N*-diethylthioharnstoff) (H_2L^a) und einem zusätzlichen Gast-Metallkation, wie K^+, Rb^+, Cs^+ oder Tl^+, synthetisiert werden. Diese Komplexe besitzen die allgemeine Formel $[M^I\{ReO(OCH_3)\}_2(L^a)_2]X$ (**V**) (M^I = K, Rb, Cs oder Tl). Die positive Ladung der Komplexe wird durch PF_6^-- oder ReO_4^--Ionen kompensiert. Zusätzlich konnten vierkernige Oxidorhenium(V)-Komplexe der Zusammensetzung $[M^I(Re_2O_3)_2(L^a)_4]X$ (**VI**) mit den gleichen Gast-Metallkationen erhalten werden. In diesen Verbindungen werden die einwertigen Metallionen in einer Käfigstruktur im Inneren der vierkernigen Rheniumkomplexe stabilisiert.

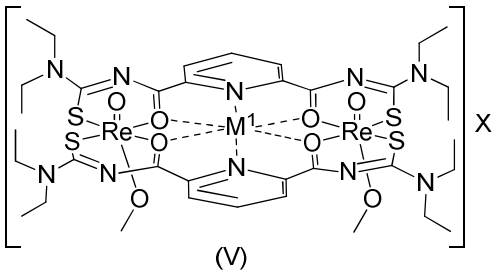

(V)

M^1 = K, Rb, Cs oder Tl

X = PF_6 oder ReO_4

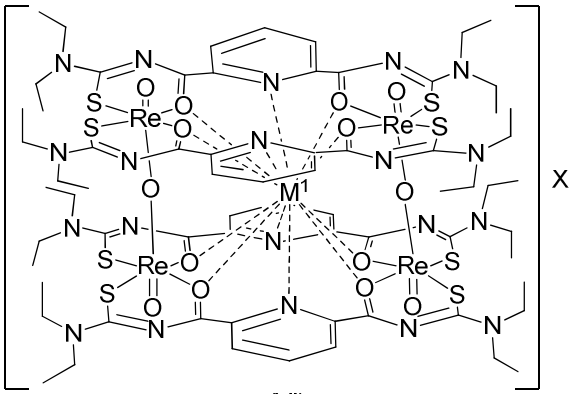

(VI)

Die relativ kleinen K^+-Kationen im Käfig des Komplexes (VI) können durch größere Kationen wie Rb^+, Tl^+ und Cs^+ ausgetauscht werden. Die Kationen Rb^+ und Tl^+ können durch Cs^+, aber nicht durch K^+ ausgetauscht werden. Dementsprechend hängt der Austausch der Metallionen stark von deren Größe ab.

References

[1] Beyer, L.; Hoyer, E.; Hennig, H.; Kirmse, R.; Hartmann, H.; Liebscher, J. *J. Prakt. Chem.* **1975**, *317*, 829.

[2] Salyn, J. V.; Zumadilov, E. K.; Nefedov, V. I.; Scheibe, R.; Leonhardt, G.; Beyer, L.; Hoyer, E. *Z. Anorg. Allg. Chem.* **1977**, *432*, 275.

[3] Beyer, L.; Hoyer, E.; Liebscher, J.; Hartmann, H. *Z. Chem.* **1981**, *21*, 81.

[4] Schmidt, S.; Dietze, F.; Hoyer, E. *Z. Anorg. Allg. Chem.* **1991**, *603*, 33.

[5] Mohamadou, A.; Dechampsolivier, I.; Barbier, J. P. *Polyhedron* **1994**, *13*, 1363.

[6] Koch, K. R. *Coord. Chem. Rev.* **2001**, *216*, 473.

[7] del Campo, R.; Criado, J. J.; Gheorghe, R.; Gonzalez, F. J.; Hermosa, M. R.; Sanz, F.; Manzano, J. L.; Monte, E.; Rodriguez-Fernandez, E. *J. Inorg. Biochem.* **2004**, *98*, 1307.

[8] Mühl, P.; Gloe, K.; Dietze, F.; Hoyer, E.; Beyer, L. *Z. Chem.* **1986**, *26*, 81.

[9] Egan, T. J.; Koch, K. R.; Swan, P. L.; Clarkson, C.; Van Schalkwyk, D. A.; Smith, P. J. *J. Med. Chem.* **2004**, *47*, 2926.

[10] Kampf, M.; Richter, R.; Gerber, S.; Kirmse, R. *Z. Anorg. Allg. Chem.* **2004**, *630*, 1437.

[11] Westra, A. N.; Bourne, S. A.; Esterhuysen, C.; Koch, K. R. *Dalton Trans.* **2005**, 2162.

[12] Zhou, W. Q.; Wen, Y.; Qiu, L. H.; Zhang, Y.; Yu, Z. F. *J. Mol. Struct.* **2005**, *749*, 89.

[13] Fitzl, G.; Beyer, L.; Sieler, J.; Richter, R.; Kaiser, J.; Hoyer, E. *Z. Anorg. Allg. Chem.* **1977**, *433*, 237.

[14] Richter, R.; Beyer, L.; Kaiser, J. *Z. Anorg. Allg. Chem.* **1980**, *461*, 67.

[15] Irving, A.; Koch, K. R.; Matoetoe, M. *Inorg. Chim. Acta* **1993**, *206*, 193.

[16] del Campo, R.; Criado, J. J.; Garcia, E.; Hermosa, M. R.; Jimenez-Sanchez, A.; Manzano, J. L.; Monte, E.; Rodriguez-Fernandez, E.; Sanz, F. *J. Inorg. Biochem.* **2002**, *89*, 74.

[17] Arslan, H.; Kulcu, N.; Florke, U. *Transition Met. Chem.* **2003**, *28*, 816.

[18] Sieler, J.; Richter, R.; Hoyer, E.; Beyer, L.; Lindqvist, O.; Andersen, L. *Z. Anorg. Allg. Chem.* **1990**, *580*, 167.

[19] Bensch, W.; Schuster, M. *Z. Anorg. Allg. Chem.* **1992**, *615*, 93.

[20] Bensch, W.; Schuster, M. *Zeitschrift Fur Kristallographie* **1995**, *210*, 68.

[21] Huy, N. H.; Abram, U. *Inorg. Chem.* **2007**, *46*, 5310.

[22] Braun, U.; Richter, R.; Sieler, J.; Yanovsky, A. I.; Struchkov, Y. T. *Z. Anorg. Allg. Chem.* **1985**, *529*, 201.

[23] Bensch, W.; Schuster, M. *Z. Anorg. Allg. Chem.* **1992**, *611*, 99.

[24] Koch, K. R.; Bourne, S. *J. Mol. Struct.* **1998**, *441*, 11.

[25] Koch, K. R.; Bourne, S. A.; Coetzee, A.; Miller, J. *J. Chem. Soc., Dalton Trans.* **1999**, 3157.

[26] Koch, K. R.; Hallale, O.; Bourne, S. A.; Miller, J.; Bacsa, J. *J. Mol. Struct.* **2001**, *561*, 185.

[27] Hallale, O.; Bourne, S. A.; Koch, K. R. *CrystEngComm* **2005**, *7*, 161.

[28] Hallale, O.; Bourne, S. A.; Koch, K. R. *New J. Chem.* **2005**, *29*, 1416.

[29] Westra, A. N.; Bourne, S. A.; Koch, K. R. *Dalton Trans.* **2005**, 2916.

[30] Rodenstein, A.; Richter, R.; Kirmse, R. *Z. Anorg. Allg. Chem.* **2007**, *633*, 1713.

[31] Rodenstein, A.; Griebel, J.; Richter, R.; Kirmse, R. *Z. Anorg. Allg. Chem.* **2008**, *634*, 867.

[32] Schwade, V. D.; Kirsten, L.; Hagenbach, A.; Schulz Lang, E.; Abram, U. *Polyhedron* **2013**, *55*, 155.

[33] Richter, R.; Sieler, J.; Kohler, R.; Hoyer, E.; Beyer, L.; Hansen, L. K. *Z. Anorg. Allg. Chem.* **1989**, *578*, 191.

[34] Schubiger, P. A.; Alberto, R.; Smith, A. *Bioconjugate Chem.* **1996**, *7*, 165.

[35] Jurisson, S. S.; Lydon, J. D. *Chem. Rev.* **1999**, *99*, 2205.

[36] Volkert, W. A.; Hoffman, T. J. *Chem. Rev.* **1999**, *99*, 2269.

[37] Lis, T. *Acta Crystallogr., Sect. B: Struct. Sci.* **1976**, *32*, 2707.

[38] Gambino, D.; Benitez, J.; Otero, L.; Kremer, E.; Baran, E. J.; Piro, O. E. *Polyhedron* **1999**, *18*, 2099.

[39] Wang, Y.; Liu, X. Q.; Liu, Y. F.; Wang, X. Y. *Radiochim. Acta* **2003**, *91*, 273.

[40] Nguyen, H. H.; Abram, U. *Z. Anorg. Allg. Chem.* **2008**, *634*, 1560.

[41] Nguyen, H. H.; Deflon, V. M.; Abram, U. *Eur. J. Inorg. Chem.* **2009**, 3179.

[42] Schröder, U.; Beyer, L.; Sieler, J. *Inorg. Chem. Commun.* **2000**, *3*, 630.

[43] Andruh, M.; Ramade, I.; Codjovi, E.; Guillou, O.; Kahn, O.; Trombe, J. C. *J. Am. Chem. Soc.* **1993**, *115*, 1822.

[44] Costes, J. P.; Dahan, F.; Dupuis, A.; Laurent, J. P. *Inorg. Chem.* **1997**, *36*, 4284.

[45] Shiga, T.; Ito, N.; Hidaka, A.; Ohkawa, H.; Kitagawa, S.; Ohba, M. *Inorg. Chem.* **2007**, *46*, 3492.

[46] Shiga, T.; Ohba, M.; Okawa, H. *Inorg. Chem.* **2004**, *43*, 4435.

[47] Ding, E.; Sturgeon, M. R.; Rath, A.; Chen, X.; Keane, M. A.; Shore, S. G. *Inorg. Chem.* **2009**, *48*, 325.

[48] Yachandra, V. K.; Derose, V. J.; Latimer, M. J.; Mukerji, I.; Sauer, K.; Klein, M. P. *Science* **1993**, *260*, 675.

[49] Yano, J.; Kern, J.; Sauer, K.; Latimer, M. J.; Pushkar, Y.; Biesiadka, J.; Loll, B.; Saenger, W.; Messinger, J.; Zouni, A.; Yachandra, V. K. *Science* **2006**, *314*, 821.

[50] Mishra, A.; Yano, J.; Pushkar, Y.; Yachandra, V. K.; Abboud, K. A.; Christou, G. *Chem. Commun.* **2007**, 1538.

[51] Yano, J.; Yachandra, V. K. *Inorg. Chem.* **2008**, *47*, 1711.

[52] Moulton, B.; Zaworotko, M. J. *Chem. Rev.* **2001**, *101*, 1629.

[53] Hung, H. N.; Pham, C. T.; Rodenstein, A.; Kirmse, R.; Abram, U. *Inorg. Chem.* **2011**, *50*, 590.

[54] Hartmann, H.; Reuther, I. *J. Prakt. Chem.* **1973**, *315*, 144.

[55] Kleinpeter, E.; Beyer, L. *J. Prakt. Chem.* **1975**, *317*, 938.

[56] Beyer, L.; Behrendt, S.; Kleinpeter, E.; Borsdorf, R.; Hoyer, E. *Z. Anorg. Allg. Chem.* **1977**, *437*, 282.

[57] Hartmann, H.; Beyer, L.; Hoyer, E. *J. Prakt. Chem.* **1978**, *320*, 647.

[58] Behrendt, S.; Beyer, L.; Dietze, F.; Kleinpeter, E.; Hoyer, E. *Inorg. Chim. Acta* **1980**, *43*, 141.

[59] Nguyen, H. H. *PhD Thesis*, *Freie Universität Berlin*, **2009**.

[60] da Silva, M. A. V. R.; Santos, L. M. N. B. F.; Schröder, B.; Beyer, L.; Dietze, F. *J. Chem. Thermodyn.* **2007**, *39*, 279.

[61] Okawa, H.; Furutachi, H.; Fenton, D. E. *Coord. Chem. Rev.* **1998**, *174*, 51.

[62] Winpenny, R. E. P. *Chem. Soc. Rev.* **1998**, *27*, 447.

[63] Sakamoto, M.; Manseki, K.; Okawa, H. *Coord. Chem. Rev.* **2001**, *219*, 379.

[64] Benelli, C.; Gatteschi, D. *Chem. Rev.* **2002**, *102*, 2369.

[65] Costes, J. P.; Dahan, F.; Dupuis, A.; Laurent, J. P. *Inorg. Chem.* **1997**, *36*, 3429.

[66] Kahn, M. L.; Mathoniere, C.; Kahn, O. *Inorg. Chem.* **1999**, *38*, 3692.

[67] Figuerola, A.; Diaz, C.; Ribas, J.; Tangoulis, V.; Sangregorio, C.; Gatteschi, D.; Maestro, M.; Mahia, J. *Inorg. Chem.* **2003**, *42*, 5274.

[68] Manna, S. C.; Zangrando, E.; Bencini, A.; Benelli, C.; Chaudhuri, N. R. *Inorg. Chem.* **2006**, *45*, 9114.

[69] Yamaguchi, T.; Costes, J. P.; Kishima, Y.; Kojima, M.; Sunatsuki, Y.; Brefuel, N.; Tuchagues, J. P.; Vendier, L.; Wernsdorfer, W. *Inorg. Chem.* **2010**, *49*, 9125.

[70] Bencini, A.; Benelli, C.; Caneschi, A.; Carlin, R. L.; Dei, A.; Gatteschi, D. *J. Am. Chem. Soc.* **1985**, *107*, 8128.

[71] Costes, J. P.; Dahan, F.; Dupuis, A. *Inorg. Chem.* **2000**, *39*, 5994.

[72] Shiga, T.; Ohba, M.; Okawa, H. *Inorg. Chem. Commun.* **2003**, *6*, 15.

[73] Costes, J. P.; Clemente-Juan, J. M.; Dahan, F.; Milon, J. *Inorg. Chem.* **2004**, *43*, 8200.

[74] Novitchi, G.; Shova, S.; Caneschi, A.; Costes, J. P.; Gdaniec, M.; Stanica, N. *Dalton Trans.* **2004**, 1194.

[75] He, F.; Tong, M. L.; Chen, X. M. *Inorg. Chem.* **2005**, *44*, 8285.

[76] Barta, C. A.; Bayly, S. R.; Read, P. W.; Patrick, B. O.; Thompson, R. C.; Orvig, C. *Inorg. Chem.* **2008**, *47*, 2294.

[77] Fellah, F. Z. C.; Costes, J. P.; Dahan, F.; Duhayon, C.; Novitchi, G.; Tuchagues, J. P.; Vendier, L. *Inorg. Chem.* **2008**, *47*, 6444.

[78] Shimada, T.; Okazawa, A.; Kojima, N.; Yoshii, S.; Nojiri, H.; Ishida, T. *Inorg. Chem.* **2011**, *50*, 10555.

[79] Xu, Z. Q.; Read, P. W.; Hibbs, D. E.; Hursthouse, M. B.; Malik, K. M. A.; Patrick, B. O.; Rettig, S. J.; Seid, M.; Summers, D. A.; Pink, M.; Thompson, R. C.; Orvig, C. *Inorg. Chem.* **2000**, *39*, 508.

[80] Binnemans, K.; Lodewyckx, K. *Supramol. Chem.* **2003**, *15*, 485.

[81] Yamaguchi, T.; Sunatsuki, Y.; Kojima, M.; Akashi, H.; Tsuchimoto, M.; Re, N.; Osa, S.; Matsumoto, N. *Chem. Commun.* **2004**, 1048.

[82] Barta, C. A.; Bayly, S. R.; Read, P. W.; Patrick, B. O.; Thompson, R. C.; Orvig, C. *Inorg. Chem.* **2008**, *47*, 2280.

[83] Yamaguchi, T.; Sunatsuki, Y.; Ishida, H.; Kojima, M.; Akashi, H.; Re, N.; Matsmuoto, N.; Pochaba, A.; Mrozinski, J. *Bull. Chem. Soc. Jpn.* **2008**, *81*, 598.

[84] Costes, J. P.; Yamaguchi, T.; Kojima, M.; Vendier, L. *Inorg. Chem.* **2009**, *48*, 5555.

[85] Singh, S. K.; Tibrewal, N. K.; Rajaraman, G. *Dalton Trans.* **2011**, *40*, 10897.

[86] Bayly, S. R.; Xu, Z. Q.; Patrick, B. O.; Rettig, S. J.; Pink, M.; Thompson, R. C.; Orvig, C. *Inorg. Chem.* **2003**, *42*, 1576.

[87] Chandrasekhar, V.; Pandian, B. M.; Boomishankar, R.; Steiner, A.; Viftal, J. J.; Houri, A.; Clerac, R. *Inorg. Chem.* **2008**, *47*, 4918.

[88] Ma, B. Q.; Gao, S.; Bai, O.; Sun, H. L.; Xu, G. X. *J. Chem. Soc., Dalton Trans.* **2000**, 1003.

[89] Shiga, T.; Okawa, H.; Kitagawa, S.; Ohba, M. *J. Am. Chem. Soc.* **2006**, *128*, 16426.

[90] Chandrasekhar, V.; Pandian, B. M.; Azhakar, R.; Vittal, J. J.; Clerac, R. *Inorg. Chem.* **2007**, *46*, 5140.

[91] Sopasis, G. J.; Orfanoudaki, M.; Zarmpas, P.; Philippidis, A.; Siczek, M.; Lis, T.; O'Brien, J. R.; Milios, C. J. *Inorg. Chem.* **2012**, *51*, 1170.

[92] Stetson, N. T.; Yvon, K. *J. Alloys Compd.* **1995**, *223*, L4.

[93] Parker, S. F.; Refson, K.; Williams, K. P. J.; Braden, D. A.; Hudson, B. S.; Yvon, K. *Inorg. Chem.* **2006**, *45*, 10951.

[94] King, R. B.; Silaghi-Dumitrescu, I.; Uta, A. M. *J. Phys. Chem. A* **2009**, *113*, 527.

[95] Rios, D.; Sevov, S. C. *Inorg. Chem.* **2010**, *49*, 6396.

[96] Chandrasekhar, V.; Pandian, B. M.; Boomishankar, R.; Steiner, A.; Clerac, R. *Dalton Trans.* **2008**, 5143.

[97] Costes, J. P.; Garcia-Tojal, J.; Tuchagues, J. P.; Vendier, L. *Eur. J. Inorg. Chem.* **2009**, 3801.

[98] Akine, S.; Morita, Y.; Utsuno, F.; Nabeshima, T. *Inorg. Chem.* **2009**, *48*, 10670.

[99] Wang, H. L.; Zhang, D. P.; Ni, Z. H.; Li, X. Y.; Tian, L. J.; Jiang, J. Z. *Inorg. Chem.* **2009**, *48*, 5946.

[100] Liao, A.; Yang, X. P.; Stanley, J. M.; Jones, R. A.; Holliday, B. J. *J. Chem. Crystallogr.* **2010**, *40*, 1060.

[101] Hui, Y. N.; Feng, W. X.; Wei, T.; Lu, X. Q.; Song, J. R.; Zhao, S. S.; Wong, W. K.; Jones, R. A. *Inorg. Chem. Commun.* **2011**, *14*, 200.

[102] Costes, J. P.; Laurent, J. P.; Chabert, P.; Commenges, G.; Dahan, F. *Inorg. Chem.* **1997**, *36*, 656.

[103] Abram, U.; Abram, S. *Z. Chem.* **1983**, *23*, 228.

[104] Dilworth, J. R.; Lewis, J. S.; Miller, J. R.; Zheng, Y. F. *Polyhedron* **1993**, *12*, 221.

[105] Abram, U. *Rhenium, in Comprehensive Coordination Chemistry II*; McCleverty, J. A., Meyer, T. J.: Elsevier, **2004**; Vol. 5;271

[106] Pedersen, C. J. *J. Am. Chem. Soc.* **1967**, *89*, 7017.

[107] Christen, J.; Eatough, D. J.; Izatt, R. M. *Chem. Rev.* **1974**, *74*, 351.

[108] Izatt, R. M.; Pawlak, K.; Bradshaw, J. S.; Brüning, R. L. *Chem. Rev.* **1991**, *91*, 1721.

[109] Dietrich, B.; Lehn, J. M.; Sauvage, J. P. *Tetrahedron* **1973**, *29*, 1647.

[110] Goff, C. M.; Matchette, M. A.; Shabestry, N.; Khazaeli, S. *Polyhedron* **1996**, *15*, 3897.

[111] Solov'ev, V. P.; Strakhova, N. N.; Kazachenko, V. P.; Solotnov, A. F.; Baulin, V. E.; Rävsky, O. A.; Rüdiger, V.; Eblinger, F.; Schneider, H. J. *Eur. J. Org. Chem.* **1998**, 1379.

[112] Takamatsu, N.; Akutagawa, T.; Hasegawa, T.; Nakamura, T.; Inabe, T.; Fujita, W.; Awaga, K. *Inorg. Chem.* **2000**, *39*, 870.

[113] Wong, A.; Wu, G. *J. Phys. Chem. A* **2000**, *104*, 11844.

[114] Downie, C.; Mao, J. G.; Parmar, H.; Guloy, A. M. *Inorg. Chem.* **2004**, *43*, 1992.

[115] Alfheim, T.; Dale, J.; Groth, P.; Krautwurst, K. D. *J. Chem. Soc., Chem. Commun.* **1984**, 1502.

[116] Meadows, E. S.; De Wall, S. L.; Barbour, L. J.; Fronczek, F. R.; Kim, M. S.; Gokel, G. W. *J. Am. Chem. Soc.* **2000**, *122*, 3325.

[117] Meadows, E. S.; De Wall, S. L.; Barbour, L. J.; Gokel, G. W. *J. Am. Chem. Soc.* **2001**, *123*, 3092.

[118] Weber, G.; Sänger, W.; Müller, K.; Wehner, W.; Vögtle, F. *Inorg. Chim. Acta. L.* **1983**, *77*, L199.

[119] Balch, A. L.; Neve, F.; Olmstead, M. M. *J. Am. Chem. Soc.* **1991**, *113*, 2995.

[120] Balch, A. L.; Davis, B. J.; Fung, E. Y.; Olmstead, M. M. *Inorg. Chim. Acta* **1993**, *212*, 149.

[121] Alexander, J. S.; Allis, D. G.; Teng, W.; Ruhlandt-Senge, K. *Chem.-Eur. J.* **2007**, *13*, 9899.

[122] Steed, J. W. *Coord. Chem. Rev.* **2001**, *215*, 171.

[123] Alberto, R.; Schibli, R.; Egli, A.; Schubiger, P. A.; Hermann, W. A.; Artus, G.; Abram, U.; Kaden, T. A. *J. Organomet. Chem.* **1995**, *493*, 119.

[124] Azuah, R. T.; Kneller, L. R.; Qiu, Y.; Tregenna-Piggott, P. L. W.; Brown, C. M.; Copley, J. R. D.; Dimeo, R. M. *J. Res. Nat. Inst. Stand. Technol.* **2009**, *114*, 341.

[125] *CHECK-HKL.* Kretschmar, M. Universität Tübingen, **1998**,

[126] *SADABS.* Sheldrick, G. M. Universität Göttingen, Blessing B. *Acta Cryst.*, **1995**, *A51*, 33.

[127] *X-RED32.* STOE&Cie GmbH, Darmstadt, Germany,

[128] *SIR 92*. Altomare, A.; Cascarano, G.; Giacovazzo, C.; Guagliardi, A., *J. Appl. Crystallogr.*, **1993**, *23*, 343.

[129] *SHELXS 86, 97.* Sheldrick, G. M. Universität Göttingen, **1986, 1997**,

[130] Sheldrick, G. M. *Acta Cryst.* **1990**, *A46*, 467.

[131] *SHELXL 97.* Sheldrick, G. M. Universität Göttingen, **1997**,

Appendix

Crystallographic Data

---

1) H_2L^a

Table A1 Crystal data and structure refinement for H_2L^a.

Empirical formula	$C_{17}H_{25}N_5O_2S_2$	
Formula weight	395.54	
Temperature	200(2) K	
Wavelength	0.71073 Å	
Crystal system	Monoclinic	
Space group	Cc	
Unit cell dimensions	a = 12.583(1) Å	α = 90°
	b = 16.624(1) Å	β = 106.59(1)°
	c = 20.547(2) Å	γ = 90°
Volume	4119.1(6) $Å^3$	
Z	8	
Density (calculated)	1.276 g/cm^3	
Absorption coefficient	0.279 mm^{-1}	
F(000)	1680	
Crystal description	Plate	
Crystal color	Colourless	
Crystal size	0.420 x 0.267 x 0.050 mm^3	
Theta range for data collection	3.26 to 29.31	
Index ranges	-17<=h<=17, -22<=k<=22, -26<=l<=28	
Reflections collected	15125	
Independent reflections	9486 [R(int) = 0.1048]	
Completeness to theta = 29.31°	98.2 %	
Absorption correction	None	
Refinement method	Full-matrix least-squares on F^2	
Data / restraints / parameters	9486 / 2 / 473	
Goodness-of-fit on F^2	0.935	
Final R indices [I>2sigma(I)]	R1 = 0.0689, wR2 = 0.1619	
R indices (all data)	R1 = 0.1054, wR2 = 0.1802	
Largest diff. peak and hole	0.817 and -0.335 $e.Å^{-3}$	

Table A2 Atomic coordinates (x 10^4) and equivalent isotropic displacement parameters ($Å^2$x 10^3) for H_2L^a. U(eq) is defined as one third of the trace of the orthogonalized U^{ij} tensor.

	x	y	z	U(eq)
S(1)	2715(1)	8499(1)	-345(1)	56(1)
C(2)	1931(3)	8552(2)	186(2)	39(1)
N(3)	1022(3)	9102(2)	23(2)	40(1)
C(4)	1089(3)	9835(2)	302(2)	41(1)
O(5)	1791(3)	10028(2)	825(2)	54(1)
N(6)	2036(3)	8115(2)	737(2)	46(1)
C(7)	2898(4)	7487(3)	923(3)	60(1)
C(8)	3953(6)	7803(6)	1386(5)	107(3)
C(9)	1277(4)	8179(3)	1164(3)	56(1)
C(10)	240(5)	7696(4)	892(4)	71(2)
S(11)	-2539(1)	8607(1)	-2591(1)	64(1)
C(12)	-3113(3)	9090(3)	-2068(2)	46(1)
N(13)	-2387(3)	9494(2)	-1505(2)	43(1)
C(14)	-2391(3)	10309(2)	-1444(2)	39(1)
O(15)	-3109(2)	10746(2)	-1777(2)	47(1)
N(16)	-4178(3)	9121(3)	-2116(3)	63(1)
C(17)	-4998(5)	8825(7)	-2740(6)	121(4)
C(18)	-5561(14)	9406(10)	-3169(8)	207(8)
C(19)	-4631(5)	9402(4)	-1575(4)	77(2)
C(20)	-5248(14)	8800(9)	-1339(9)	202(8)
C(21)	-1410(3)	10647(2)	-897(2)	37(1)
C(22)	-1374(4)	11467(2)	-744(3)	46(1)
C(23)	-496(3)	11753(2)	-250(2)	45(1)
C(24)	338(3)	11232(2)	108(2)	42(1)
C(25)	218(3)	10426(2)	-74(2)	37(1)
N(26)	-636(3)	10132(2)	-570(2)	37(1)
S(31)	-3947(1)	8953(1)	4726(1)	62(1)
C(32)	-4979(4)	8532(3)	4130(3)	53(1)
N(33)	-4706(3)	8048(2)	3632(2)	44(1)
C(34)	-4825(4)	7240(2)	3595(2)	42(1)
O(35)	-5338(3)	6857(2)	3920(2)	51(1)
N(36)	-6035(4)	8624(4)	4071(3)	82(2)

C(37)	-6397(7)	9109(9)	4582(7)	169(7)
C(38)	-6850(14)	8717(15)	4996(8)	256(1)
C(39)	-6931(5)	8349(5)	3465(5)	101(3)
C(40B)	-7349(18)	8944(13)	3058(13)	205(1)
C(40A)	-7910(30)	7850(20)	3680(20)	205(1)
S(41)	-623(1)	8884(1)	2562(1)	70(1)
C(42)	-1801(4)	8726(2)	1975(3)	48(1)
N(43)	-2612(3)	8241(2)	2148(2)	43(1)
C(44)	-2766(3)	7463(2)	1934(2)	42(1)
O(45)	-2450(3)	7201(2)	1467(2)	62(1)
N(46)	-2081(3)	9010(2)	1336(2)	54(1)
C(47)	-1271(5)	9480(3)	1085(3)	64(1)
C(48)	-1454(5)	10361(3)	1133(4)	70(2)
C(49)	-3210(5)	8935(4)	864(4)	82(2)
C(50)	-3193(18)	8544(15)	184(9)	265(1)
C(51)	-4329(3)	6836(2)	3097(2)	38(1)
C(52)	-4486(4)	6023(2)	2974(3)	47(1)
C(53)	-4057(4)	5670(2)	2501(3)	49(1)
C(54)	-3485(3)	6130(2)	2156(2)	45(1)
C(55)	-3368(3)	6951(2)	2309(2)	38(1)
N(56)	-3770(3)	7302(2)	2779(2)	36(1)

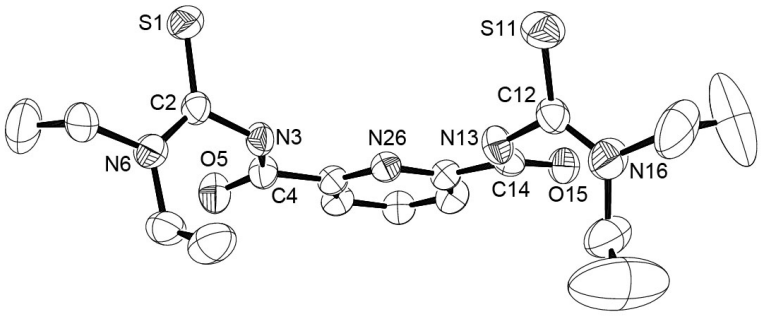

Fig A1 Ellipsoid plot (50% probability) of H_2L^a

2) $[CeCo_2(L^a)_2(\mu\text{-}OAc)_2Cl]$

Table A3 Crystal data and structure refinement for $[CeCo_2(L^a)_2(\mu\text{-}OAc)_2Cl]$.

Empirical formula	$C_{38}H_{52}CeClCo_2N_{10}O_8S_4$	
Formula weight	1198.57	
Temperature	200(2) K	
Wavelength	0.71073 Å	
Crystal system	Monoclinic	
Space group	C2/c	
Unit cell dimensions	a = 26.478(1) Å	α = 90°
	b = 12.029(1) Å	β = 91.07(1)°
	c = 15.302(1) Å	γ = 90°
Volume	4872.9(5) $Å^3$	
Z	4	
Density (calculated)	1.634 g/cm^3	
Absorption coefficient	1.876 mm^{-1}	
F(000)	2428	
Crystal description	Block	
Crystal color	Red	
Crystal size	0.46 x 0.38 x 0.34 mm^3	
Theta range for data collection	1.86 to 29.24	
Index ranges	-36<=h<=29, -14<=k<=16, -20<=l<=20	
Reflections collected	14276	
Independent reflections	6524 [R(int) = 0.1095]	
Completeness to theta = 29.24°	98.5 %	
Absorption correction	Integration	
Max. and min. transmission	0.8701 and 0.7879	
Refinement method	Full-matrix least-squares on F^2	
Data / restraints / parameters	6524 / 0 / 290	
Goodness-of-fit on F^2	0.748	
Final R indices [I>2sigma(I)]	R1 = 0.0429, wR2 = 0.0769	
R indices (all data)	R1 = 0.1215, wR2 = 0.1170	
Largest diff. peak and hole	0.746 and -2.326 e.$Å^{-3}$	

Table A4 Atomic coordinates (x 10^4) and equivalent isotropic displacement parameters ($Å^2$x 10^3) for $[CeCo_2(L^a)_2(\mu\text{-}OAc)_2Cl]$. U(eq) is defined as one third of the trace of the orthogonalized U^{ij} tensor.

	x	y	z	U(eq)
Ce	0	7361(1)	2500	19(1)
Co(1)	1323(1)	7724(1)	3216(1)	25(1)
Cl	0	5066(2)	2500	36(1)
S(1)	2059(1)	8235(2)	2413(1)	36(1)
C(2)	1720(3)	8960(6)	1619(4)	30(2)
N(3)	1416(2)	8408(4)	1030(3)	27(1)
C(4)	1044(2)	7799(5)	1280(3)	22(1)
O(5)	895(1)	7657(4)	2084(2)	25(1)
N(6)	1761(2)	10044(5)	1515(3)	35(1)
C(7)	2092(3)	10737(7)	2069(5)	48(2)
C(8)	1831(3)	11186(7)	2860(5)	52(2)
C(9)	1463(3)	10619(6)	827(5)	44(2)
C(10)	930(4)	10906(7)	1116(6)	64(3)
S(11)	-1819(1)	6706(2)	836(1)	57(1)
C(12)	-1450(3)	6114(6)	46(4)	30(2)
N(13)	-942(2)	6236(5)	-57(3)	28(1)
C(14)	-618(2)	6560(5)	551(3)	24(1)
O(15)	-696(2)	6830(4)	1346(2)	26(1)
N(16)	-1678(2)	5513(4)	-571(3)	29(1)
C(17)	-2228(3)	5278(7)	-576(4)	41(2)
C(18)	-2343(3)	4209(7)	-95(5)	55(2)
C(19)	-1406(3)	5035(6)	-1314(4)	32(2)
C(20)	-1410(3)	5801(7)	-2093(4)	49(2)
C(41)	-83(2)	6628(5)	260(3)	23(1)
C(42)	65(3)	6296(5)	-571(3)	30(1)
C(43)	561(3)	6442(6)	-797(4)	34(2)
C(44)	901(3)	6930(5)	-212(3)	28(1)
C(45)	725(2)	7234(5)	604(3)	23(1)
N(46)	249(2)	7050(4)	847(3)	22(1)
O(61)	1073(2)	9146(4)	3700(3)	41(1)
C(62)	617(3)	9497(6)	3661(4)	36(2)
O(63)	241(2)	9014(4)	3351(3)	36(1)

C(64)	529(4)	10646(8)	4029(7)	73(3)

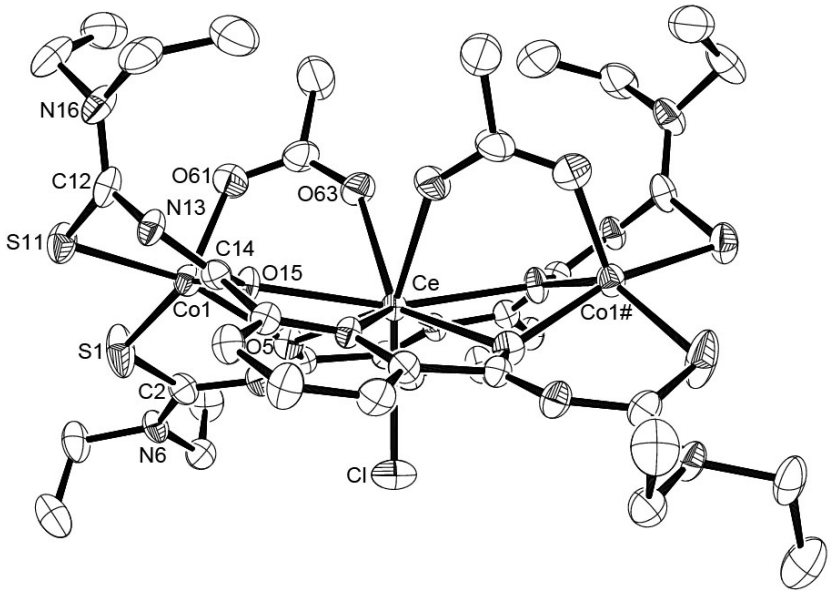

Fig A2 Ellipsoid plot (50% probability) of $[CeCo_2(L^a)_2(\mu\text{-}OAc)_2Cl]$

3) [$NdCo_2(L^a)_2(\mu\text{-}OAc)_2Cl$]

Table A5 Crystal data and structure refinement for [$NdCo_2(L^a)_2(\mu\text{-}OAc)_2Cl$].

Empirical formula	$C_{38}H_{52}ClCo_2N_{10}NdO_8S_4$	
Formula weight	1202.69	
Temperature	200(2) K	
Wavelength	0.71073 Å	
Crystal system	Monoclinic	
Space group	C2/c	
Unit cell dimensions	a = 26.446(1) Å	α = 90°
	b = 12.034(1) Å	β = 91.02(1)°
	c = 15.207(1) Å	γ = 90°
Volume	4838.9(5) $Å^3$	
Z	4	
Density (calculated)	1.651 g/cm^3	
Absorption coefficient	2.021 mm^{-1}	
F(000)	2436	
Crystal description	Block	
Crystal color	Red	
Crystal size	0.38 x 0.33 x 0.30 mm^3	
Theta range for data collection	1.86 to 29.26	
Index ranges	-36<=h<=34, -16<=k<=16, -20<=l<=20	
Reflections collected	25773	
Independent reflections	6530 [R(int) = 0.1204]	
Completeness to theta = 29.26°	99.1 %	
Absorption correction	Integration	
Max. and min. transmission	0.8899 and 0.4684	
Refinement method	Full-matrix least-squares on F^2	
Data / restraints / parameters	6530 / 0 / 291	
Goodness-of-fit on F^2	0.937	
Final R indices [I>2sigma(I)]	R1 = 0.0475, wR2 = 0.1046	
R indices (all data)	R1 = 0.0662, wR2 = 0.1114	
Largest diff. peak and hole	1.556 and -1.706 e.$Å^{-3}$	

Table A6 Atomic coordinates (x 10^4) and equivalent isotropic displacement parameters ($Å^2$x 10^3) for $[NdCo_2(L^a)_2(\mu\text{-}OAc)_2Cl]$. U(eq) is defined as one third of the trace of the orthogonalized U^{ij} tensor.

	x	y	z	U(eq)
Nd	0	7371(1)	2500	22(1)
Co(1)	1320(1)	7731(1)	3221(1)	28(1)
Cl	0	5106(1)	2500	38(1)
S(1)	2053(1)	8250(1)	2413(1)	40(1)
C(2)	1715(1)	8972(3)	1623(3)	33(1)
N(3)	1407(1)	8409(3)	1024(2)	32(1)
C(4)	1038(1)	7815(3)	1288(3)	26(1)
O(5)	882(1)	7699(2)	2087(2)	30(1)
N(6)	1758(1)	10052(3)	1511(3)	39(1)
C(7)	2090(2)	10747(4)	2071(4)	48(1)
C(8)	1832(2)	11196(4)	2874(4)	56(1)
C(9)	1453(2)	10627(4)	825(4)	52(1)
C(10)	923(2)	10905(5)	1119(5)	68(2)
S(11)	-1822(1)	6720(1)	829(1)	58(1)
C(12)	-1447(2)	6097(3)	44(3)	34(1)
N(13)	-942(1)	6210(3)	-50(2)	31(1)
C(14)	-621(1)	6548(3)	560(2)	25(1)
O(15)	-696(1)	6823(2)	1364(2)	28(1)
N(16)	-1678(1)	5486(3)	-569(2)	34(1)
C(17)	-2226(2)	5247(4)	-568(3)	43(1)
C(18)	-2337(2)	4177(5)	-92(4)	56(1)
C(19)	-1405(2)	5001(3)	-1312(3)	36(1)
C(20)	-1415(2)	5758(5)	-2108(4)	54(1)
C(41)	723(1)	7238(3)	606(3)	26(1)
C(42)	895(2)	6940(3)	-214(3)	32(1)
C(43)	560(2)	6437(4)	-797(3)	37(1)
C(44)	63(2)	6300(3)	-568(3)	35(1)
C(45)	-85(1)	6618(3)	268(3)	27(1)
N(46)	244(1)	7047(2)	852(2)	25(1)
O(61)	1055(1)	9147(3)	3703(2)	43(1)
C(62)	604(2)	9497(3)	3659(3)	37(1)

O(63)	232(1)	8995(2)	3356(2)	39(1)
C(64)	516(2)	10636(5)	4035(6)	78(2)

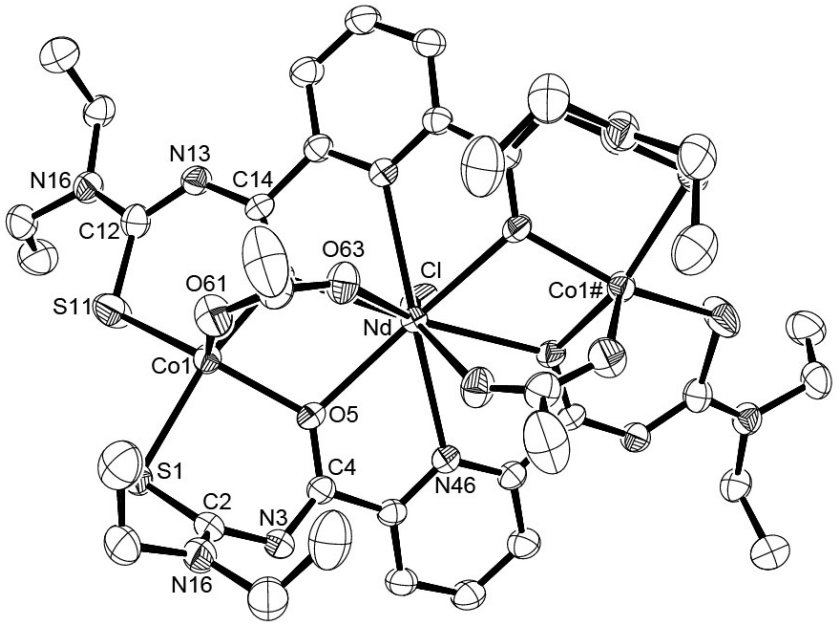

Fig A3 Ellipsoid plot (50% probability) of $[NdCo_2(L^a)_2(\mu\text{-}OAc)_2Cl]$

4) [$SmCo_2(L^a)_2(\mu\text{-}OAc)_2Cl$]

Table A7 Crystal data and structure refinement for [$SmCo_2(L^a)_2(\mu\text{-}OAc)_2Cl$].

Empirical formula	$C_{38}H_{52}ClCo_2N_{10}O_8S_4Sm$	
Formula weight	1208.80	
Temperature	200(2) K	
Wavelength	0.71073 Å	
Crystal system	Monoclinic	
Space group	C2/c	
Unit cell dimensions	a = 26.523(2) Å	α = 90°
	b = 12.049(1) Å	β = 90.98(1)°
	c = 15.145(1) Å	γ = 90°
Volume	4839.3(6) $Å^3$	
Z	4	
Density (calculated)	1.659 g/cm^3	
Absorption coefficient	2.162 mm^{-1}	
F(000)	2444	
Crystal description	Block	
Crystal color	Red	
Crystal size	0.48 x 0.42 x 0.38 mm^3	
Theta range for data collection	1.86 to 29.24	
Index ranges	-36<=h<=36, -15<=k<=16, -20<=l<=18	
Reflections collected	24936	
Independent reflections	6545 [R(int) = 0.1595]	
Completeness to theta = 29.24°	99.5 %	
Absorption correction	Integration	
Max. and min. transmission	0.8833 and 0.3984	
Refinement method	Full-matrix least-squares on F^2	
Data / restraints / parameters	6545 / 0 / 291	
Goodness-of-fit on F^2	0.936	
Final R indices [I>2sigma(I)]	R1 = 0.0616, wR2 = 0.1391	
R indices (all data)	R1 = 0.0779, wR2 = 0.1468	
Largest diff. peak and hole	3.273 and -2.434 $e.Å^{-3}$	

Table A8 Atomic coordinates (x 10^4) and equivalent isotropic displacement parameters ($Å^2$x 10^3) for $[SmCo_2(L^a)_2(\mu\text{-}OAc)_2Cl]$. U(eq) is defined as one third of the trace of the orthogonalized U^{ij} tensor.

	x	y	z	U(eq)
Sm	0	7382(1)	2500	25(1)
Co(1)	1315(1)	7736(1)	3223(1)	33(1)
Cl	0	5139(1)	2500	42(1)
S(1)	2047(1)	8247(1)	2415(1)	47(1)
C(2)	1712(2)	8976(5)	1622(4)	39(1)
N(3)	1403(2)	8425(4)	1025(3)	39(1)
C(4)	1029(2)	7839(4)	1289(3)	30(1)
O(5)	873(1)	7738(3)	2092(2)	34(1)
N(6)	1759(2)	10055(4)	1511(4)	47(1)
C(7)	2095(2)	10736(6)	2078(5)	59(2)
C(8)	1836(3)	11208(6)	2878(6)	69(2)
C(9)	1456(3)	10631(6)	822(5)	62(2)
C(10)	934(3)	10926(7)	1123(7)	80(2)
S(11)	-1815(1)	6717(2)	833(1)	69(1)
C(12)	-1442(2)	6081(4)	57(4)	38(1)
N(13)	-935(2)	6192(3)	-36(3)	36(1)
C(14)	-617(2)	6542(4)	569(3)	30(1)
O(15)	-692(1)	6828(3)	1373(2)	34(1)
N(16)	-1672(2)	5466(4)	-564(3)	39(1)
C(17)	-2215(2)	5224(5)	-557(5)	51(1)
C(18)	-2331(3)	4161(7)	-76(5)	66(2)
C(19)	-1399(2)	4987(4)	-1307(4)	41(1)
C(20)	-1409(3)	5743(6)	-2101(5)	61(2)
C(41)	716(2)	7260(4)	611(3)	30(1)
C(42)	887(2)	6957(5)	-225(4)	41(1)
C(43)	554(2)	6452(5)	-800(4)	44(1)
C(44)	63(2)	6300(5)	-567(4)	41(1)
C(45)	-86(2)	6620(4)	276(3)	31(1)
N(46)	244(2)	7055(3)	854(3)	30(1)
O(61)	1051(2)	9157(3)	3713(3)	54(1)
C(62)	594(2)	9488(5)	3669(4)	47(1)

O(63)	219(1)	8991(3)	3349(3)	43(1)
C(64)	498(3)	10628(7)	4022(9)	96(4)

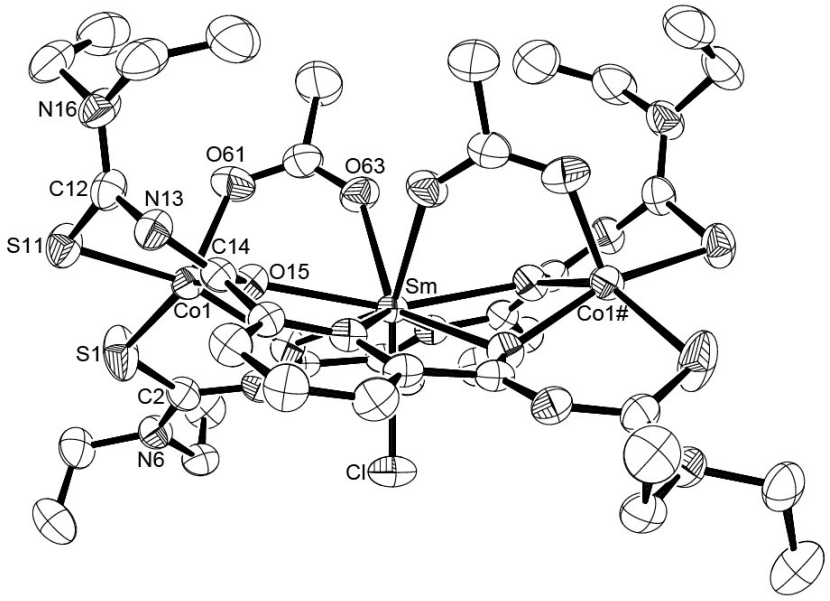

Fig A4 Ellipsoid plot (50% probability) of $[SmCo_2(L^a)_2(\mu\text{-}OAc)_2Cl]$

5) $[GdCo_2(L^a)_2(\mu\text{-}OAc)_2(OAc)]\cdot 2CH_3OH$

Table A9 Crystal data and structure refinement for $[GdCo_2(L^a)_2(\mu\text{-}OAc)_2(OAc)]\cdot 2CH_3OH$.

Empirical formula	$C_{42}H_{63}Co_2GdN_{10}O_{12}S_4$	
Formula weight	1303.37	
Temperature	200(2) K	
Wavelength	0.71073 Å	
Crystal system	Monoclinic	
Space group	C2/c	
Unit cell dimensions	a = 21.909(1) Å	α = 90°
	b = 11.893(1) Å	β = 101.56(1)°
	c = 23.120(1) Å	γ = 90°
Volume	5902.0(6) $Å^3$	
Z	4	
Density (calculated)	1.467 g/cm^3	
Absorption coefficient	1.868 mm^{-1}	
F(000)	2652	
Crystal description	Block	
Crystal color	Red	
Crystal size	0.400 x 0.293 x 0.180 mm^3	
Theta range for data collection	1.80 to 29.21	
Index ranges	-30<=h<=24, -16<=k<=16, -31<=l<=31	
Reflections collected	31963	
Independent reflections	7949 [R(int) = 0.0666]	
Completeness to theta = 29.21°	99.2 %	
Absorption correction	Integration	
Max. and min. transmission	0.7655 and 0.5999	
Refinement method	Full-matrix least-squares on F^2	
Data / restraints / parameters	7949 / 0 / 344	
Goodness-of-fit on F^2	1.060	
Final R indices [I>2sigma(I)]	R1 = 0.0411, wR2 = 0.1071	
R indices (all data)	R1 = 0.0525, wR2 = 0.1194	
Largest diff. peak and hole	1.755 and -1.262 $e.Å^{-3}$	

Table A10 Atomic coordinates (x 10^4) and equivalent isotropic displacement parameters ($Å^2$x 10^3) for $[GdCo_2(L^a)_2(\mu\text{-}OAc)_2(OAc)]\cdot 2CH_3OH$. U(eq) is defined as one third of the trace of the orthogonalized U^{ij} tensor.

	x	y	z	U(eq)
Gd	0	-724(1)	7500	24(1)
Co(1)	-1466(1)	-1171(1)	6481(1)	30(1)
S(1)	-2482(1)	-448(1)	6383(1)	44(1)
C(2)	-2364(2)	660(3)	6873(2)	34(1)
N(3)	-2036(1)	551(3)	7436(2)	33(1)
C(4)	-1480(2)	114(3)	7564(2)	29(1)
O(5)	-1125(1)	-158(2)	7202(1)	28(1)
N(6)	-2645(2)	1640(3)	6735(2)	39(1)
C(7)	-3009(2)	1888(4)	6141(2)	55(1)
C(8)	-3690(2)	1593(5)	6079(3)	63(1)
C(9)	-2573(2)	2561(3)	7166(2)	44(1)
C(10)	-2011(3)	3267(5)	7149(3)	71(2)
S(11)	1673(1)	-1528(1)	9541(1)	38(1)
C(12)	1023(2)	-2367(4)	9527(2)	35(1)
N(13)	438(2)	-1918(3)	9411(1)	37(1)
C(14)	237(2)	-1330(3)	8937(2)	29(1)
O(15)	501(1)	-1195(2)	8495(1)	30(1)
N(16)	1066(2)	-3433(3)	9658(2)	41(1)
C(17)	1668(2)	-4014(4)	9862(2)	49(1)
C(18)	1886(3)	-4633(6)	9376(3)	74(2)
C(19)	494(2)	-4134(4)	9594(3)	56(1)
C(20)	246(3)	-4465(5)	8957(3)	67(2)
C(41)	-396(2)	-816(3)	8872(2)	30(1)
C(42)	-696(2)	-649(4)	9343(2)	38(1)
C(43)	-1284(2)	-160(4)	9222(2)	42(1)
C(44)	-1554(2)	119(3)	8646(2)	35(1)
C(45)	-1224(2)	-91(3)	8205(2)	28(1)
N(46)	-652(1)	-535(2)	8319(1)	27(1)
O(61)	-1421(1)	-2677(2)	6852(1)	39(1)
C(62)	-1008(2)	-2997(3)	7284(2)	33(1)
O(63)	-604(1)	-2392(2)	7587(1)	34(1)

C(64)	-1031(3)	-4227(4)	7443(2)	56(1)
O(81)	-4(2)	1223(2)	7971(2)	47(1)
C(82)	0	1751(4)	7500	42(1)
C(84)	0	3010(6)	7500	71(2)
C(91)	-861(5)	2832(8)	8832(5)	58(3)
O(92)	-287(4)	2333(7)	8924(3)	66(2)
C(93)	-3709(7)	2979(11)	4309(6)	76(4)
O(94)	-4089(5)	2186(7)	4533(4)	78(2)

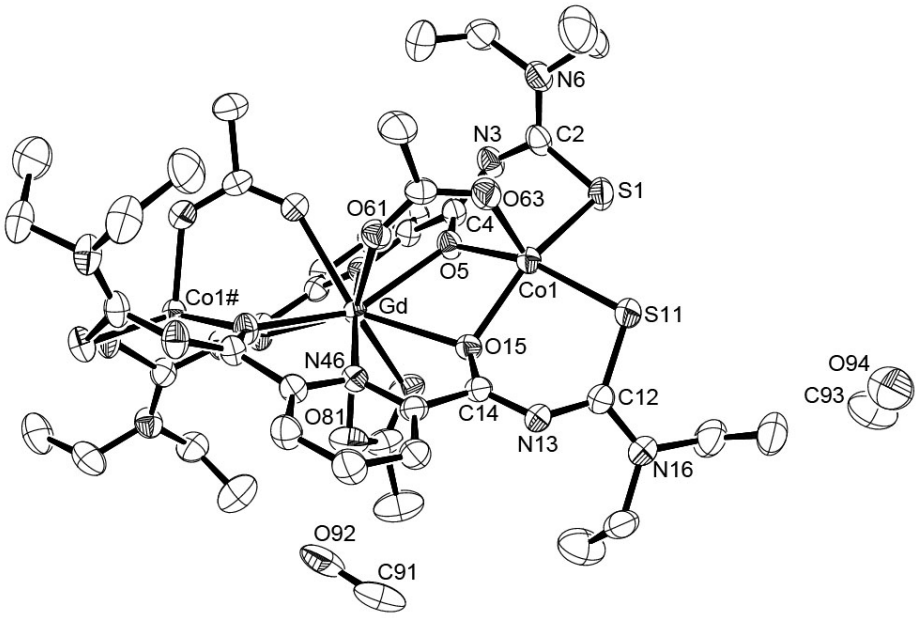

Fig A5 Ellipsoid plot (50% probability) of $[GdCo_2(L^a)_2(\mu\text{-}OAc)_2(OAc)]\cdot 2CH_3OH$

6) [$DyCo_2(L^a)_2(\mu\text{-}OAc)_2Cl$]

Table A11 Crystal data and structure refinement for [$DyCo_2(L^a)_2(\mu\text{-}OAc)_2Cl$].

Empirical formula	$C_{38}H_{52}ClCo_2DyN_{10}O_8S_4$	
Formula weight	1220.95	
Temperature	200(2) K	
Wavelength	0.71073 Å	
Crystal system	Monoclinic	
Space group	C2/c	
Unit cell dimensions	a = 26.534(2) Å	$\gamma = 90°$
	b = 12.028(1) Å	$\beta = 90.93(1)°$
	c = 14.999(2) Å	$\gamma = 90°$
Volume	4786.3(8) $Å^3$	
Z	4	
Density (calculated)	1.694 g/cm^3	
Absorption coefficient	2.520 mm^{-1}	
F(000)	2460	
Crystal description	Prism	
Crystal color	Red	
Crystal size	0.15 x 0.15 x 0.13 mm^3	
Theta range for data collection	1.86 to 29.30	
Index ranges	-36<=h<=30, -16<=k<=16, -20<=l<=20	
Reflections collected	19687	
Independent reflections	6457 [R(int) = 0.0969]	
Completeness to theta = 29.30°	98.5 %	
Absorption correction	Integration	
Max. and min. transmission	0.7498 and 0.6337	
Measurement method	Rotation method	
Refinement method	Full-matrix least-squares on F^2	
Data / restraints / parameters	6457 / 0 / 291	
Goodness-of-fit on F^2	0.852	
Final R indices [I>2sigma(I)]	R1 = 0.0480, wR2 = 0.0930	
R indices (all data)	R1 = 0.1017, wR2 = 0.1108	
Largest diff. peak and hole	0.717 and -2.205 $e.Å^{-3}$	

Table A12 Atomic coordinates (x 10^4) and equivalent isotropic displacement parameters ($Å^2$x 10^3) for $[DyCo_2(L^a)_2(\mu\text{-}OAc)_2Cl]$. U(eq) is defined as one third of the trace of the orthogonalized U^{ij} tensor.

	x	y	z	U(eq)
Dy	0	7404(1)	2500	32(1)
Co(1)	-1312(1)	7745(1)	1772(1)	39(1)
Cl	0	5204(2)	2500	47(1)
S(1)	-1815(1)	6713(2)	832(1)	75(1)
C(2)	-1448(2)	6075(5)	66(4)	45(1)
N(3)	-935(2)	6170(4)	-31(3)	42(1)
C(4)	-620(2)	6531(4)	580(3)	33(1)
O(5)	-691(2)	6837(3)	1387(2)	40(1)
N(6)	-1674(2)	5442(4)	-558(3)	46(1)
C(7)	-2216(2)	5208(6)	-561(5)	57(2)
C(8)	-2325(3)	4147(7)	-64(5)	74(2)
C(9)	-1398(3)	4958(5)	-1308(4)	49(2)
C(10)	-1403(3)	5692(7)	-2115(5)	69(2)
S(11)	2039(1)	8265(2)	2416(1)	54(1)
C(12)	1705(2)	9001(5)	1627(4)	44(1)
N(13)	1397(2)	8447(4)	1025(3)	42(1)
C(14)	1016(2)	7870(4)	1287(3)	35(1)
O(15)	855(1)	7782(3)	2100(2)	38(1)
N(16)	1752(2)	10067(4)	1506(4)	52(1)
C(17)	2091(3)	10766(6)	2086(5)	64(2)
C(18)	1829(3)	11241(6)	2880(5)	77(2)
C(19)	1458(3)	10649(6)	809(5)	68(2)
C(20)	935(3)	10956(7)	1118(6)	89(3)
C(41)	704(2)	7278(4)	614(3)	39(1)
C(42)	881(2)	6989(5)	-226(4)	47(1)
C(43)	555(2)	6466(5)	-815(4)	50(2)
C(44)	61(2)	6289(5)	-566(4)	48(1)
C(45)	-84(2)	6600(4)	278(4)	36(1)
N(46)	238(2)	7055(3)	876(3)	34(1)
O(61)	-1046(2)	9161(4)	1272(3)	63(1)
C(62)	-573(3)	9476(5)	1331(5)	56(2)

O(63)	-209(2)	8967(3)	1645(3)	45(1)
C(64)	-476(3)	10631(7)	1001(8)	101(3)

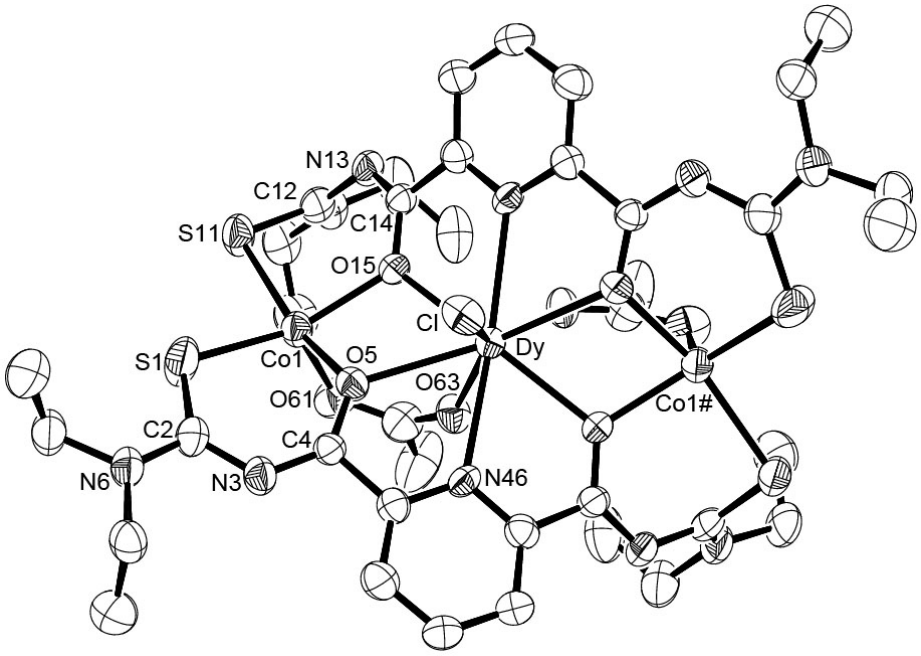

Fig A6 Ellipsoid plot (50% probability) of $[DyCo_2(L^a)_2(\mu\text{-}OAc)_2Cl]$

7) [$ErCo_2(L^a)_2(\mu\text{-}OAc)_2Cl$]

Table A13 Crystal data and structure refinement for [$ErCo_2(L^a)_2(\mu\text{-}OAc)_2Cl$].

Empirical formula	$C_{38}H_{52}ClCo_2ErN_{10}O_8S_4$	
Formula weight	1225.71	
Temperature	200(2) K	
Wavelength	0.71073 Å	
Crystal system	Monoclinic	
Space group	C2/c	
Unit cell dimensions	a = 26.473(2) Å	α = 90°
	b = 12.075(1) Å	β = 90.98(1)°
	c = 14.929(1) Å	γ = 90°
Volume	4771.5(6) $Å^3$	
Z	4	
Density (calculated)	1.706 g/cm^3	
Absorption coefficient	2.720 mm^{-1}	
F(000)	2468	
Crystal description	Block	
Crystal color	Green	
Crystal size	0.36 x 0.31 x 0.28 mm^3	
Theta range for data collection	1.85 to 29.29	
Index ranges	-36<=h<=35, -16<=k<=16, -19<=l<=20	
Reflections collected	26690	
Independent reflections	6438 [R(int) = 0.0746]	
Completeness to theta = 29.29°	98.7 %	
Absorption correction	Integration	
Max. and min. transmission	0.9032 and 0.7506	
Refinement method	Full-matrix least-squares on F^2	
Data / restraints / parameters	6438 / 0 / 291	
Goodness-of-fit on F^2	0.937	
Final R indices [I>2sigma(I)]	R1 = 0.0362, wR2 = 0.0812	
R indices (all data)	R1 = 0.0494, wR2 = 0.0847	
Largest diff. peak and hole	0.850 and -1.521 $e.Å^{-3}$	

Table A14 Atomic coordinates (x 10^4) and equivalent isotropic displacement parameters ($Å^2$x 10^3) for $[ErCo_2(L^a)_2(\mu\text{-}OAc)_2Cl]$. U(eq) is defined as one third of the trace of the orthogonalized U^{ij} tensor.

	x	y	z	U(eq)
Er	0	7410(1)	2500	24(1)
Co(1)	1310(1)	7752(1)	3231(1)	30(1)
Cl	0	5237(1)	2500	38(1)
S(1)	1821(1)	6749(1)	4186(1)	59(1)
C(2)	1448(1)	6075(3)	4947(3)	36(1)
N(3)	941(1)	6170(2)	5038(2)	33(1)
C(4)	623(1)	6527(3)	4421(2)	29(1)
O(5)	695(1)	6827(2)	3613(2)	32(1)
N(6)	1679(1)	5439(3)	5564(2)	37(1)
C(7)	2222(2)	5207(4)	5561(3)	46(1)
C(8)	2333(2)	4146(5)	5055(4)	62(1)
C(9)	1403(2)	4940(3)	6309(3)	39(1)
C(10)	1406(2)	5675(4)	7130(3)	56(1)
S(11)	-2035(1)	8271(1)	2586(1)	43(1)
C(12)	-1698(1)	9005(3)	3380(3)	36(1)
N(13)	-1388(1)	8448(3)	3981(2)	35(1)
C(14)	-1009(1)	7874(3)	3707(2)	29(1)
O(15)	-848(1)	7794(2)	2900(2)	30(1)
N(16)	-1747(1)	10077(3)	3498(2)	41(1)
C(17)	-2087(2)	10763(4)	2933(3)	54(1)
C(18)	-1829(2)	11237(4)	2121(4)	63(1)
C(19)	-1445(2)	10655(4)	4197(3)	54(1)
C(20)	-923(2)	10943(5)	3889(4)	69(2)
C(41)	91(1)	6601(3)	4722(2)	29(1)
C(42)	-54(2)	6283(3)	5572(3)	38(1)
C(43)	-551(2)	6448(3)	5823(3)	41(1)
C(44)	-877(1)	6976(3)	5234(3)	37(1)
C(45)	-704(1)	7271(3)	4396(2)	28(1)
N(46)	-233(1)	7052(2)	4130(2)	27(1)
O(61)	1032(1)	9160(2)	3713(2)	47(1)
C(62)	574(2)	9476(3)	3653(3)	41(1)
O(63)	206(1)	8948(2)	3353(2)	36(1)

C(64)	476(2)	10627(4)	3987(5)	85(2)

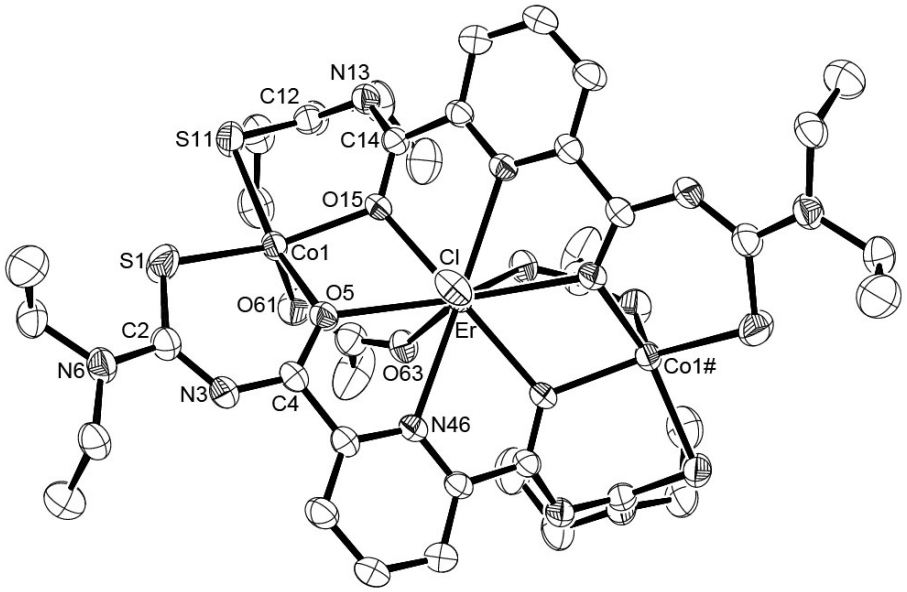

Fig A7 Ellipsoid plot (50% probability) of $[ErCo_2(L^a)_2(\mu\text{-}OAc)_2Cl]$

8) [$YbCo_2(L^a)_2(\mu\text{-}OAc)_2Cl$]

Table A15 Crystal data and structure refinement for [$YbCo_2(L^a)_2(\mu\text{-}OAc)_2Cl$].

Empirical formula	$C_{38}H_{52}ClCo_2N_{10}O_8S_4Yb$	
Formula weight	1231.49	
Temperature	200(2) K	
Wavelength	0.71073 Å	
Crystal system	Monoclinic	
Space group	C2/c	
Unit cell dimensions	a = 26.506(1) Å	α = 90°
	b = 12.086(1) Å	β = 90.94(1)°
	c = 14.849(1) Å	γ = 90°
Volume	4756.3(5) $Å^3$	
Z	4	
Density (calculated)	1.720 g/cm^3	
Absorption coefficient	2.931 mm^{-1}	
F(000)	2476	
Crystal description	Prism	
Crystal color	Blue	
Crystal size	0.160 x 0.120 x 0.080 mm^3	
Theta range for data collection	3.30 to 29.29	
Index ranges	-36<=h<=30, -16<=k<=16, -20<=l<=20	
Reflections collected	28242	
Independent reflections	6421 [R(int) = 0.0750]	
Completeness to theta = 29.29°	98.8 %	
Absorption correction	Integration	
Max. and min. transmission	0.8079 and 0.5808	
Refinement method	Full-matrix least-squares on F^2	
Data / restraints / parameters	6421 / 0 / 291	
Goodness-of-fit on F^2	0.979	
Final R indices [I>2sigma(I)]	R1 = 0.0469, wR2 = 0.1054	
R indices (all data)	R1 = 0.0701, wR2 = 0.1151	
Largest diff. peak and hole	1.435 and -1.977 $e.Å^{-3}$	

Table A16 Atomic coordinates (x 10^4) and equivalent isotropic displacement parameters ($Å^2$x 10^3) for $[YbCo_2(L^a)_2(\mu\text{-}OAc)_2Cl]$. U(eq) is defined as one third of the trace of the orthogonalized U^{ij} tensor.

	x	y	z	U(eq)
Yb	0	7420(1)	2500	27(1)
Cl	0	5268(2)	2500	40(1)
Co(1)	1311(1)	7757(1)	3235(1)	32(1)
S(1)	2033(1)	8273(1)	2408(1)	43(1)
C(2)	1697(2)	8999(5)	1602(3)	37(1)
N(3)	1384(2)	8445(4)	1003(3)	35(1)
C(4)	1003(2)	7871(4)	1282(3)	32(1)
O(5)	840(1)	7800(3)	2098(2)	32(1)
N(6)	1742(2)	10074(4)	1485(3)	41(1)
C(7)	2080(2)	10759(6)	2051(4)	52(2)
C(8)	1821(3)	11244(6)	2867(5)	61(2)
C(9)	1442(2)	10653(5)	788(4)	51(2)
C(10)	918(3)	10948(7)	1091(6)	68(2)
S(11)	-1829(1)	6778(2)	795(1)	55(1)
C(12)	-1457(2)	6084(4)	44(4)	38(1)
N(13)	-950(2)	6164(4)	-43(3)	37(1)
C(14)	-629(2)	6522(4)	578(3)	31(1)
O(15)	-705(1)	6826(3)	1394(2)	30(1)
N(16)	-1686(2)	5432(4)	-576(3)	40(1)
C(17)	-2228(2)	5204(5)	-570(4)	47(1)
C(18)	-2340(3)	4148(7)	-66(5)	63(2)
C(19)	-1410(2)	4927(5)	-1320(4)	41(1)
C(20)	-1407(3)	5638(6)	-2148(4)	59(2)
C(41)	698(2)	7267(4)	593(3)	31(1)
C(42)	871(2)	6975(5)	-245(3)	36(1)
C(43)	542(2)	6433(5)	-831(3)	41(1)
C(44)	48(2)	6270(4)	-583(3)	39(1)
C(45)	-97(2)	6594(4)	274(3)	32(1)
N(46)	226(2)	7044(3)	863(3)	30(1)
O(61)	1023(1)	9166(3)	3687(3)	45(1)
C(62)	573(2)	9481(5)	3637(4)	41(1)

O(63)	202(1)	8930(3)	3350(2)	36(1)
C(64)	468(3)	10650(6)	3945(7)	76(3)

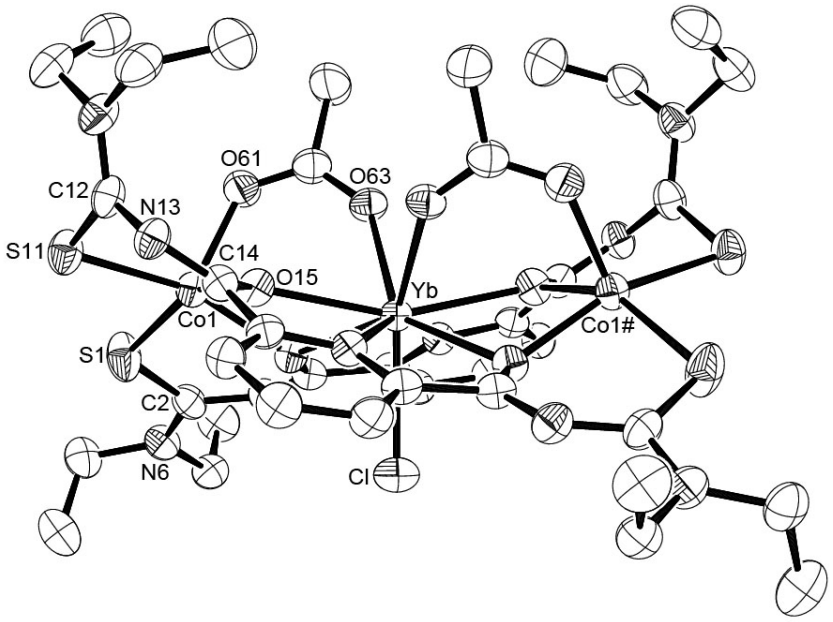

Fig A8 Ellipsoid plot (50% probability) of $[YbCo_2(L^a)_2(\mu\text{-}OAc)_2Cl]$

(9) $[CeNi_2(L^a)_2(\mu\text{-}OAc)_2(OAc)(CH_3OH)_2]\cdot 2CH_3OH$

Table A17 Crystal data and structure refinement for $[CeNi_2(L^a)_2(\mu\text{-}OAc)_2(OAc)(CH_3OH)_2]\cdot 2CH_3OH$.

Empirical formula	$C_{44}H_{71}CeN_{10}Ni_2O_{14}S_4$	
Formula weight	1349.89	
Temperature	200(2) K	
Wavelength	0.71073 Å	
Crystal system	Monoclinic	
Space group	C2/c	
Unit cell dimensions	a = 28.598(3) Å	α = 90°
	b = 13.162(1) Å	β = 126.79(1)°
	c = 19.367(2) Å	γ = 90°
Volume	5838.0(10) $Å^3$	
Z	4	
Density (calculated)	1.536 g/cm^3	
Absorption coefficient	1.615 mm^{-1}	
F(000)	2780	
Crystal description	Block	
Crystal color	Green	
Crystal size	0.190 x 0.157 x 0.130 mm^3	
Theta range for data collection	2.11 to 29.24	
Index ranges	-35<=h<=39, -18<=k<=18, -26<=l<=26	
Reflections collected	34219	
Independent reflections	7895 [R(int) = 0.1219]	
Completeness to theta = 29.24°	99.2 %	
Absorption correction	Integration	
Max. and min. transmission	0.8297 and 0.6885	
Refinement method	Full-matrix least-squares on F^2	
Data / restraints / parameters	7895 / 0 / 342	
Goodness-of-fit on F^2	0.725	
Final R indices [I>2sigma(I)]	R1 = 0.0404, wR2 = 0.0490	
R indices (all data)	R1 = 0.0949, wR2 = 0.0560	
Largest diff. peak and hole	0.729 and -0.777 $e.Å^{-3}$	

Table A18 Atomic coordinates (x 10^4) and equivalent isotropic displacement parameters ($Å^2$x 10^3) for $[CeNi_2(L^a)_2(\mu\text{-}OAc)_2(OAc)(CH_3OH)_2]\cdot 2CH_3OH$. U(eq) is defined as one third of the trace of the orthogonalized U^{ij} tensor.

	x	y	z	U(eq)
Ce	0	1961(1)	2500	19(1)
Ni(1)	906(1)	2075(1)	1747(1)	25(1)
S(1)	1856(1)	1516(1)	2255(1)	38(1)
C(2)	2042(2)	742(3)	3088(2)	40(1)
N(3)	1945(1)	971(2)	3683(2)	35(1)
C(4)	1452(2)	1300(2)	3488(2)	27(1)
O(5)	953(1)	1356(2)	2747(1)	24(1)
N(6)	2361(2)	-92(3)	3268(2)	63(1)
C(7)	2486(3)	-492(4)	2663(4)	77(2)
C(8)	3026(3)	-3(5)	2904(4)	99(2)
C(9)	2630(3)	-674(4)	4078(3)	82(2)
C(10)	2286(4)	-1497(5)	3927(5)	152(4)
S(11)	-787(1)	3023(1)	4372(1)	40(1)
C(12)	-58(2)	3097(3)	5178(2)	33(1)
N(13)	397(1)	2724(2)	5200(2)	30(1)
C(14)	379(2)	2414(2)	4542(2)	25(1)
O(15)	-51(1)	2329(2)	3745(1)	25(1)
N(16)	120(2)	3594(2)	5903(2)	40(1)
C(17)	-290(2)	4057(3)	6038(3)	48(1)
C(18)	-429(2)	5130(3)	5714(3)	58(1)
C(19)	742(2)	3836(3)	6564(3)	54(1)
C(20)	1046(2)	3065(4)	7273(3)	83(2)
C(41)	1479(2)	1628(2)	4259(2)	28(1)
C(42)	2002(2)	1712(3)	5069(2)	37(1)
C(43)	2005(2)	2034(3)	5752(2)	43(1)
C(44)	1477(2)	2256(3)	5596(2)	39(1)
C(45)	970(2)	2158(2)	4769(2)	26(1)
N(46)	970(1)	1864(2)	4105(2)	24(1)
O(63)	612(1)	3474(2)	2867(2)	29(1)
C(62)	1071(2)	3702(2)	2954(2)	28(1)
O(61)	1248(1)	3322(2)	2556(2)	35(1)

C(64)	1442(2)	4536(3)	3594(3)	40(1)
O(81)	-218(1)	163(2)	1804(2)	34(1)
C(82)	0	-301(4)	2500	32(1)
C(84)	0	-1446(4)	2500	98(3)
O(91)	571(1)	757(2)	939(2)	35(1)
C(92)	694(2)	-251(3)	1278(3)	43(1)
O(95)	4136(2)	5531(3)	5152(2)	81(1)
C(96)	3646(3)	5940(4)	5036(3)	71(2)

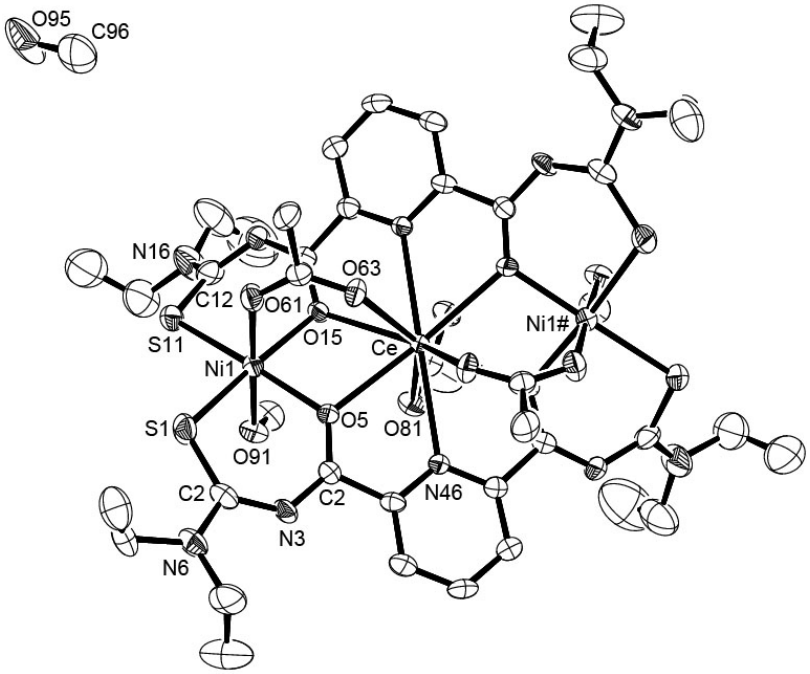

Fig A9 Ellipsoid plot (50% probability) of $[CeNi_2(L^a)_2(\mu\text{-}OAc)_2(OAc)(CH_3OH)_2]\cdot 2CH_3OH$

10) $[NdNi_2(L^a)_2(\mu\text{-}OAc)_2(OAc)(CH_3OH)_2]\cdot 2CH_3OH$

Table A19 Crystal data and structure refinement for $[NdNi_2(L^a)_2(\mu\text{-}OAc)_2(OAc)(CH_3OH)_2]\cdot 2CH_3OH$.

Empirical formula	$C_{44}H_{71}N_{10}NdNi_2O_{14}S_4$	
Formula weight	1357.03	
Temperature	200(2) K	
Wavelength	0.71073 Å	
Crystal system	Monoclinic	
Space group	C2/c	
Unit cell dimensions	a = 28.522(2) Å	α= 90°
	b = 13.150(1) Å	β= 126.89(1)°
	c = 19.393(1) Å	γ = 90°
Volume	5817.4(7) $Å^3$	
Z	4	
Density (calculated)	1.549 g/cm^3	
Absorption coefficient	1.731 mm^{-1}	
F(000)	2800	
Crystal description	Prism	
Crystal color	Green	
Crystal size	0.46 x 0.32 x 0.24 mm^3	
Theta range for data collection	1.79 to 29.34	
Index ranges	-37<=h<=39, -18<=k<=18, -26<=l<=26	
Reflections collected	32131	
Independent reflections	7863 [R(int) = 0.0813]	
Completeness to theta = 29.34°	98.2 %	
Absorption correction	Integration	
Max. and min. transmission	0.8262 and 0.6268	
Refinement method	Full-matrix least-squares on F^2	
Data / restraints / parameters	7863 / 0 / 348	
Goodness-of-fit on F^2	0.989	
Final R indices [I>2sigma(I)]	R1 = 0.0457, wR2 = 0.1043	
R indices (all data)	R1 = 0.0673, wR2 = 0.1220	
Largest diff. peak and hole	1.771 and -1.286 $e.Å^{-3}$	

Table A20 Atomic coordinates (x 10^4) and equivalent isotropic displacement parameters ($Å^2$x 10^3) for $[NdNi_2(L^a)_2(\mu\text{-}OAc)_2(OAc)(CH_3OH)_2]\cdot 2CH_3OH$. U(eq) is defined as one third of the trace of the orthogonalized U^{ij} tensor.

	x	y	z	U(eq)
Nd	5000	3051(1)	2500	28(1)
Ni(1)	4095(1)	2935(1)	3251(1)	34(1)
S(1)	3143(1)	3496(1)	2747(1)	49(1)
C(2)	2959(2)	4275(4)	1914(3)	52(1)
N(3)	3063(2)	4058(3)	1337(2)	47(1)
C(4)	3555(2)	3714(3)	1520(2)	37(1)
O(5)	4058(1)	3659(2)	2265(2)	33(1)
N(6)	2639(3)	5106(4)	1741(3)	84(2)
C(7)	2512(3)	5504(6)	2344(5)	90(2)
C(8)	1976(3)	5039(7)	2107(6)	104(2)
C(9)	2359(4)	5662(7)	917(5)	103(3)
C(10)	2717(5)	6476(9)	1065(7)	143(4)
S(11)	5788(1)	1974(1)	640(1)	49(1)
C(12)	5058(2)	1898(3)	-164(3)	42(1)
N(13)	4599(2)	2273(3)	-188(2)	41(1)
C(14)	4619(2)	2586(3)	471(2)	35(1)
O(15)	5052(1)	2673(2)	1268(2)	34(1)
N(16)	4873(2)	1408(3)	-898(2)	51(1)
C(17)	5281(3)	953(4)	-1038(3)	59(1)
C(18)	5424(3)	-136(4)	-718(4)	71(2)
C(19)	4250(2)	1173(4)	-1560(3)	62(1)
C(20)	3946(3)	1940(5)	-2266(4)	92(2)
C(41)	4033(2)	2834(3)	249(2)	37(1)
C(42)	3513(2)	2740(4)	-587(3)	49(1)
C(43)	2992(2)	2962(4)	-731(3)	55(1)
C(44)	2992(2)	3296(4)	-61(3)	48(1)
C(45)	3523(2)	3380(3)	755(2)	38(1)
N(46)	4032(1)	3138(2)	907(2)	34(1)
O(61)	6247(1)	1695(2)	2563(2)	43(1)
C(62)	6060(2)	1302(3)	2951(2)	36(1)
O(63)	5606(1)	1558(2)	2871(2)	38(1)

C(64)	6427(2)	464(3)	3590(3)	50(1)
O(81)	4788(1)	4820(2)	1807(2)	43(1)
C(82)	5000	5283(4)	2500	46(1)
C(84)	5000	6418(6)	2500	110(4)
O(91)	4437(1)	4248(2)	4068(2)	43(1)
C(92)	4310(2)	5263(3)	3737(3)	51(1)
O(95)	860(2)	554(4)	4836(3)	91(2)
C(96)	1356(3)	955(5)	4959(4)	80(2)

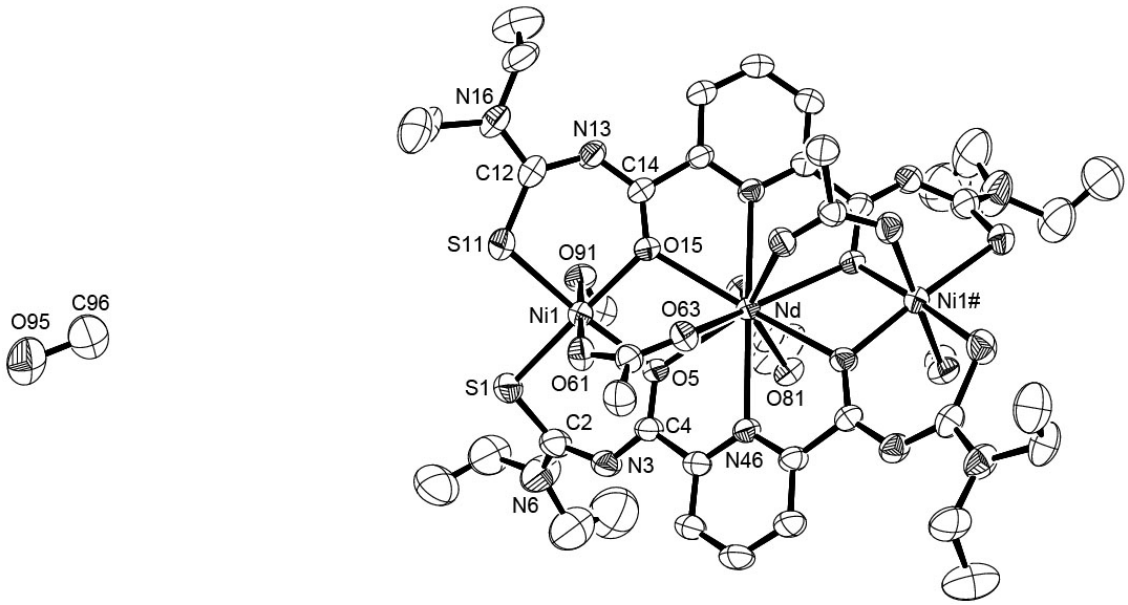

Fig A10 Ellipsoid plot (50% probability) of $[NdNi_2(L^a)_2(\mu\text{-}OAc)_2(OAc)(CH_3OH)_2]\cdot 2CH_3OH$

11) [$GdNi_2(L^a)_2(\mu\text{-}OAc)_2Cl$]

Table A21 Crystal data and structure refinement for [$GdNi_2(L^a)_2(\mu\text{-}OAc)_2Cl$]

Empirical formula	$C_{38}H_{52}ClGdN_{10}Ni_2O_8S_4$	
Formula weight	1215.26	
Temperature	200(2) K	
Wavelength	0.71073 Å	
Crystal system	Monoclinic	
Space group	C2/c	
Unit cell dimensions	a = 26.353(3) Å	α = 90°
	b = 11.955(1) Å	β = 90.82(1)°
	c = 15.149(2) Å	γ = 90°
Volume	4772.2(9) $Å^3$	
Z	4	
Density (calculated)	1.691 g/cm^3	
Absorption coefficient	2.445 mm^{-1}	
F(000)	2460	
Crystal description	Block	
Crystal color	Orange	
Crystal size	0.4 x 0.4 x o.2 mm^3	
Theta range for data collection	2.69 to 29.34	
Index ranges	-34<=h<=36, -16<=k<=16, -20<=l<=20	
Reflections collected	17829	
Independent reflections	6443 [R(int) = 0.1230]	
Completeness to theta = 29.34°	98.4 %	
Absorption correction	Integration	
Max. and min. transmission	0.7366 and 0.6513	
Refinement method	Full-matrix least-squares on F^2	
Data / restraints / parameters	6443 / 0 / 290	
Goodness-of-fit on F^2	0.846	
Final R indices [I>2sigma(I)]	R1 = 0.0563, wR2 = 0.0750	
R indices (all data)	R1 = 0.1497, wR2 = 0.0947	
Largest diff. peak and hole	0.981 and -2.087 $e.Å^{-3}$	

Table A22 Atomic coordinates (x 10^4) and equivalent isotropic displacement parameters ($Å^2$x 10^3) for [$GdNi_2(L^a)_2(\mu\text{-}OAc)_2Cl$]. U(eq) is defined as one third of the trace of the orthogonalized U^{ij} tensor.

	x	y	z	U(eq)
Gd	0	7355(1)	7500	26(1)
Ni(1)	1307(1)	7652(1)	8193(1)	31(1)
Cl	0	5140(2)	7500	48(1)
S(1)	1834(1)	6837(2)	9210(1)	44(1)
C(2)	1462(2)	6144(5)	9956(4)	32(2)
N(3)	957(2)	6231(4)	10053(3)	31(1)
C(4)	627(2)	6534(5)	9420(4)	28(1)
O(5)	702(2)	6770(4)	8620(3)	30(1)
N(6)	1694(2)	5501(4)	10572(4)	34(1)
C(7)	2243(2)	5262(6)	10561(5)	40(2)
C(8)	2351(3)	4202(6)	10055(6)	57(2)
C(9)	1421(3)	4986(6)	11301(4)	39(2)
C(10)	1432(3)	5718(7)	12121(5)	58(2)
S(11)	-2037(1)	8260(2)	7579(1)	40(1)
C(12)	-1702(2)	8988(6)	8365(4)	33(2)
N(13)	-1396(2)	8435(4)	8969(3)	31(1)
C(14)	-1026(2)	7831(5)	8708(4)	29(1)
O(15)	-865(1)	7711(4)	7909(2)	32(1)
N(16)	-1745(2)	10082(5)	8476(4)	37(1)
C(17)	-2088(3)	10776(6)	7916(5)	51(2)
C(18)	-1822(3)	11220(7)	7113(5)	55(2)
C(19)	-1446(3)	10675(6)	9163(6)	52(2)
C(20)	-911(3)	10924(7)	8878(6)	68(3)
C(41)	90(2)	6606(5)	9731(4)	29(2)
C(42)	-59(3)	6288(6)	10570(4)	39(2)
C(43)	-559(3)	6454(6)	10803(5)	42(2)
C(44)	-884(3)	6964(5)	10211(4)	34(2)
C(45)	-711(2)	7243(5)	9398(4)	26(1)
N(46)	-236(2)	7034(4)	9135(3)	26(1)
O(61)	1068(2)	9081(4)	8676(3)	38(1)
C(62)	618(3)	9438(6)	8643(5)	39(2)
O(63)	240(2)	8927(4)	8328(3)	36(1)

C(64)	523(3)	10601(6)	9002(6)	62(3)

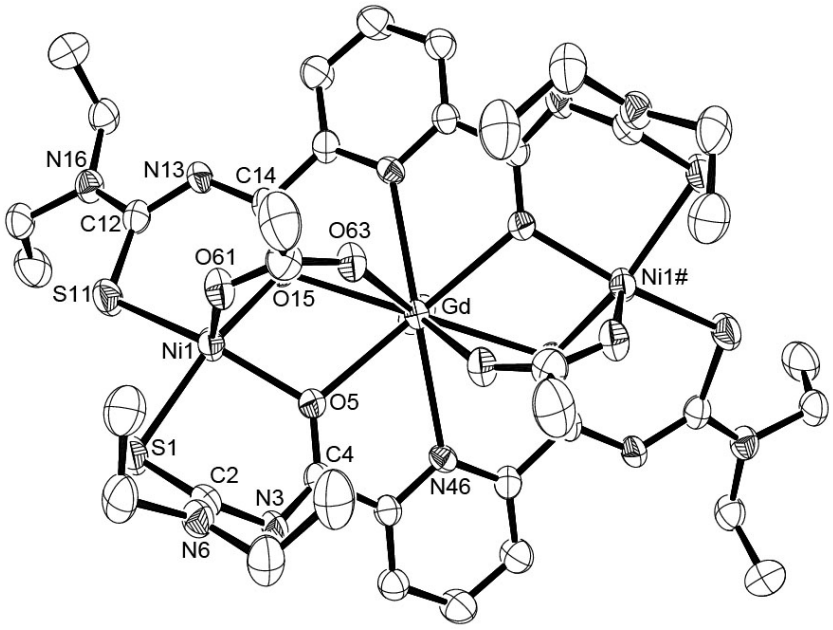

Fig A11 Ellipsoid plot (50% probability) of $[GdNi_2(L^a)_2(\mu\text{-}OAc)_2Cl]$

12) $[SmNi_2(L^a)_2(\mu\text{-}OAc)(OAc)_2(CH_3OH)_2]\cdot H_2O$

Table A23 Crystal data and structure refinement for $[SmNi_2(L^a)_2(\mu\text{-}OAc)(OAc)_2(CH_3OH)_2]\cdot H_2O$.

Empirical formula	$C_{42}H_{63}N_{10}Ni_2O_{13}S_4Sm$	
Formula weight	1312.03	
Temperature	200(2) K	
Wavelength	0.71073 Å	
Crystal system	Monoclinic	
Space group	$P2_1/c$	
Unit cell dimensions	a = 18.020(2) Å	α = 90°
	b = 13.008(1) Å	β = 99.93(1)°
	c = 24.396(3) Å	γ = 90°
Volume	5632.9(10) $Å^3$	
Z	4	
Density (calculated)	1.547 g/cm^3	
Absorption coefficient	1.904 mm^{-1}	
F(000)	2684	
Crystal description	Prism	
Crystal color	Brown	
Crystal size	0.180 x 0.120 x 0.083 mm^3	
Theta range for data collection	1.69 to 29.34	
Index ranges	-24<=h<=24, -17<=k<=16, -33<=l<=33	
Reflections collected	57550	
Independent reflections	15254 [R(int) = 0.3069]	
Completeness to theta = 29.34°	98.6 %	
Absorption correction	Intergration	
Max. and min. transmission	0.9185 and 0.7642	
Refinement method	Full-matrix least-squares on F^2	
Data / restraints / parameters	15254 / 0 / 658	
Goodness-of-fit on F^2	0.811	
Final R indices [I>2sigma(I)]	R1 = 0.0740, wR2 = 0.1442	
R indices (all data)	R1 = 0.2825, wR2 = 0.2507	
Largest diff. peak and hole	1.083 and -1.979 $e.Å^{-3}$	

Table A24 Atomic coordinates (x 10^4) and equivalent isotropic displacement parameters ($Å^2$x 10^3) for $[SmNi_2(L^a)_2(\mu\text{-}OAc)(OAc)_2(CH_3OH)_2]\cdot H_2O$. U(eq) is defined as one third of the trace of the orthogonalized U^{ij} tensor.

	x	y	z	U(eq)
Sm	7282(1)	6524(1)	3192(1)	38(1)
Ni(1)	6094(1)	7948(2)	3954(1)	41(1)
Ni(2)	8606(1)	5208(2)	2410(1)	47(1)
S(1)	4992(2)	7604(4)	4268(2)	63(1)
C(2)	4739(7)	6344(12)	4119(6)	47(4)
N(3)	4970(6)	5731(10)	3736(4)	44(3)
C(4)	5541(7)	5883(13)	3485(5)	43(4)
O(5)	6065(4)	6588(8)	3554(4)	41(2)
N(6)	4229(8)	5941(12)	4381(5)	67(4)
C(7)	3905(11)	6512(17)	4805(8)	90(7)
C(8)	3218(10)	7110(20)	4583(11)	127(1)
C(9)	3799(13)	5000(20)	4187(9)	96(7)
C(10)	4141(15)	4280(20)	4531(11)	132(1)
S(11)	8461(2)	4303(4)	1555(2)	65(1)
C(12)	7527(7)	4574(13)	1309(6)	48(4)
N(13)	6973(5)	4441(10)	1614(5)	41(3)
C(14)	6976(7)	4857(11)	2086(6)	45(4)
O(15)	7473(4)	5455(8)	2378(4)	43(2)
N(16)	7298(6)	4845(11)	783(5)	54(3)
C(17)	7825(10)	5080(18)	397(8)	83(6)
C(18)	7989(13)	4170(20)	79(9)	113(9)
C(19)	6497(8)	4958(16)	572(7)	72(6)
C(20)	6219(10)	6057(17)	659(8)	88(7)
S(21)	5812(2)	9675(3)	4043(2)	50(1)
C(22)	6342(7)	10279(11)	3618(6)	42(3)
N(23)	7064(6)	10026(9)	3591(5)	42(3)
C(24)	7263(6)	9093(13)	3535(6)	41(4)
O(25)	6853(4)	8258(7)	3429(4)	41(2)
N(26)	6100(5)	11137(9)	3360(5)	43(3)
C(27)	5345(7)	11588(14)	3372(6)	54(4)
C(28)	5355(8)	12333(13)	3859(8)	66(5)

C(29)	6570(8)	11734(13)	3028(7)	59(4)
C(30)	6433(9)	11436(16)	2428(8)	77(5)
S(31)	9908(2)	4982(4)	2543(2)	68(1)
C(32)	10264(7)	5692(13)	3106(6)	46(4)
N(33)	9925(6)	6525(12)	3289(5)	55(3)
C(34)	9198(8)	6704(12)	3262(6)	46(4)
O(35)	8631(5)	6110(8)	3111(4)	48(3)
N(36)	10948(6)	5527(11)	3392(5)	56(4)
C(37)	11456(9)	4721(15)	3226(7)	68(5)
C(38)	11937(10)	5152(16)	2847(9)	87(6)
C(39)	11317(9)	6214(18)	3815(8)	83(7)
C(40)	11100(11)	6000(20)	4343(10)	113(8)
C(41)	6279(6)	4660(11)	2341(5)	32(3)
C(42)	5736(7)	3961(12)	2122(6)	42(3)
C(43)	5114(7)	3864(12)	2385(6)	46(4)
C(44)	5031(7)	4432(12)	2839(5)	42(4)
C(45)	5595(7)	5130(12)	3031(5)	41(3)
N(46)	6221(6)	5249(10)	2786(5)	44(3)
C(51)	9033(7)	7764(11)	3449(6)	42(4)
C(52)	9575(7)	8506(15)	3591(7)	59(4)
C(53)	9373(8)	9486(15)	3729(7)	62(5)
C(54)	8612(8)	9700(13)	3704(6)	52(4)
C(55)	8089(6)	8926(13)	3557(6)	41(4)
N(56)	8299(5)	7979(10)	3433(4)	39(3)
O(63)	7634(4)	6656(8)	4174(4)	46(2)
C(62)	7445(9)	7054(15)	4593(6)	59(4)
O(61)	6883(5)	7623(8)	4596(4)	50(3)
C(64)	7898(13)	6820(20)	5162(8)	125(1)
O(81)	7469(5)	7679(8)	2361(4)	51(3)
C(82)	6790(7)	7745(10)	2129(6)	31(3)
O(83)	6325(5)	7242(8)	2354(4)	49(3)
C(84)	6621(6)	8227(11)	1715(5)	40(4)
O(71)	7603(5)	4722(9)	3574(4)	57(3)
C(72)	7335(8)	4237(13)	3944(7)	51(4)
O(73)	6770(7)	4586(11)	4094(5)	81(4)
C(74)	7613(9)	3466(16)	4115(9)	88(7)
O(91)	8622(6)	6636(10)	1992(5)	77(4)

C(92)	9087(12)	6989(18)	1637(10)	103(7)
O(93)	8460(6)	3902(9)	2884(5)	68(3)
C(94)	8598(16)	2856(19)	2811(12)	136(1)
O(95)	716(19)	8790(60)	762(12)	270(4)
O(96)	6(19)	6600(30)	370(30)	220(3)

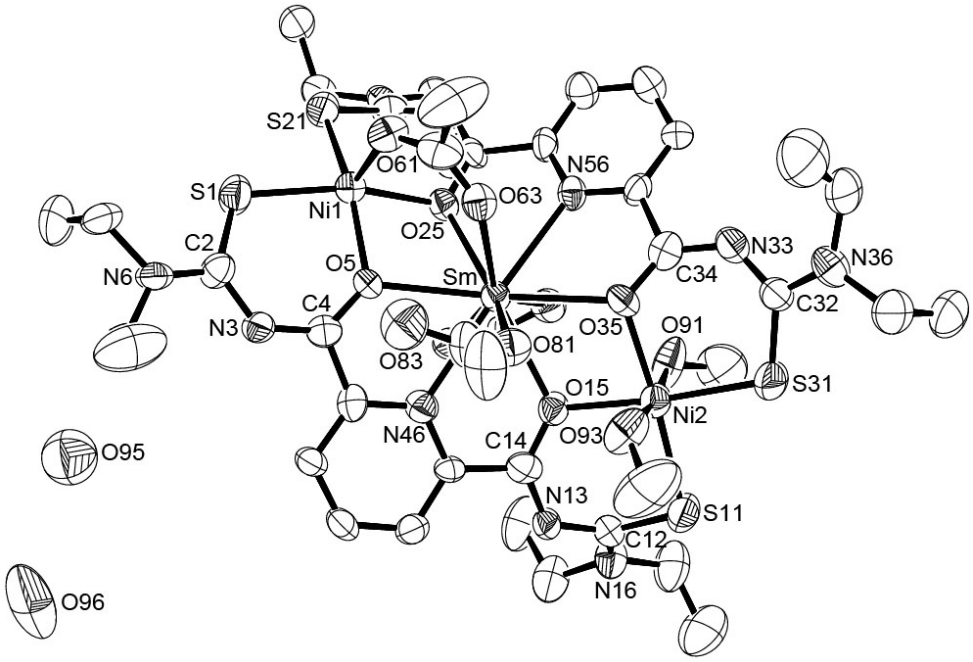

Fig A12 Ellipsoid plot (50% probability) of $[SmNi_2(L^a)_2(\mu\text{-}OAc)(OAc)_2(CH_3OH)_2]\cdot H_2O$

13) [$GdMn_2(L^a)_2(\mu\text{-}OAc)_2(OAc)(CH_3OH)_2$]

Table A25 Crystal data and structure refinement for [$GdMn_2(L^a)_2(\mu\text{-}OAc)_2(OAc)(CH_3OH)_2$].

Empirical formula	$C_{42}H_{63}GdMn_2N_{10}O_{12}S_4$	
Formula weight	1263.35	
Temperature	200(2) K	
Wavelength	0.71073 Å	
Crystal system	Orthorhombic	
Space group	Pbcn	
Unit cell dimensions	a = 26.681(1) Å	α = 90°
	b = 12.078(1) Å	β = 90°
	c = 17.326(1) Å	γ = 90°
Volume	5583.4(6) $Å^3$	
Z	4	
Density (calculated)	1.503 g/cm^3	
Absorption coefficient	1.829 mm^{-1}	
F(000)	2564	
Crystal description	Block	
Crystal color	Yellow	
Crystal size	0.30 x 0.26 x 0.20 mm^3	
Theta range for data collection	2.56 to 29.32	
Index ranges	-36<=h<=36, -16<=k<=16, -21<=l<=23	
Reflections collected	57013	
Independent reflections	7565 [R(int) = 0.0749]	
Completeness to theta = 29.32°	98.9 %	
Absorption correction	Integration	
Max. and min. transmission	0.7815 and 0.6183	
Refinement method	Full-matrix least-squares on F^2	
Data / restraints / parameters	7565 / 0 / 348	
Goodness-of-fit on F^2	0.925	
Final R indices [I>2sigma(I)]	R1 = 0.0449, wR2 = 0.1066	
R indices (all data)	R1 = 0.0917, wR2 = 0.1206	
Largest diff. peak and hole	1.253 and -0.629 $e.Å^{-3}$	

Table A26 Atomic coordinates (x 10^4) and equivalent isotropic displacement parameters ($Å^2$x 10^3) for $[GdMn_2(L^a)_2(\mu\text{-}OAc)_2(OAc)(CH_3OH)_2]$. U(eq) is defined as one third of the trace of the orthogonalized U^{ij} tensor.

	x	y	z	U(eq)
Gd	0	-7836(1)	-2500	34(1)
Mn(1)	1362(1)	-8231(1)	-2473(1)	50(1)
S(1)	1968(1)	-7702(1)	-1447(1)	54(1)
C(2)	1725(2)	-6411(4)	-1252(3)	44(1)
N(3)	1255(1)	-6274(3)	-959(2)	45(1)
C(4)	858(2)	-6736(3)	-1248(3)	38(1)
O(5)	816(1)	-7209(2)	-1910(2)	40(1)
N(6)	2010(1)	-5511(3)	-1288(2)	48(1)
C(7)	2536(2)	-5561(4)	-1557(3)	60(1)
C(8)	2886(2)	-5753(6)	-908(4)	75(2)
C(9)	1823(2)	-4426(4)	-1067(4)	72(2)
C(10)	1611(3)	-3795(6)	-1712(6)	120(3)
S(11)	-1952(1)	-8786(1)	-1462(1)	66(1)
C(12)	-1486(2)	-9254(4)	-869(3)	47(1)
N(13)	-1131(1)	-8548(3)	-569(2)	44(1)
C(14)	-795(2)	-8103(3)	-1011(3)	38(1)
O(15)	-734(1)	-8274(2)	-1745(2)	41(1)
N(16)	-1460(2)	-10290(3)	-617(2)	53(1)
C(17)	-1844(2)	-11126(5)	-815(4)	74(2)
C(18)	-1677(3)	-11882(8)	-1447(5)	123(3)
C(19)	-1053(2)	-10641(5)	-102(3)	64(1)
C(20)	-573(2)	-10900(5)	-536(4)	77(2)
C(41)	395(2)	-6729(3)	-759(3)	39(1)
C(42)	374(2)	-6240(4)	-31(3)	47(1)
C(43)	-64(2)	-6327(4)	382(3)	52(1)
C(44)	-458(2)	-6929(4)	82(3)	45(1)
C(45)	-410(2)	-7392(3)	-637(2)	37(1)
N(46)	5(1)	-7266(2)	-1067(2)	38(1)
O(61)	1141(1)	-9784(3)	-2080(2)	58(1)
C(62)	697(2)	-10051(4)	-1907(3)	44(1)

O(63)	339(1)	-9386(2)	-1861(2)	46(1)
C(64)	593(2)	-11248(4)	-1746(4)	82(2)
O(81)	0	-5869(4)	-2500	63(1)
C(82)	301(7)	-5105(7)	-2802(8)	96(6)
O(83)	682(5)	-5206(8)	-3296(7)	108(4)
C(84)	172(6)	-3955(8)	-2528(16)	84(6)
O(91)	1439(2)	-6398(6)	-3051(4)	54(2)
C(92)	1727(5)	-5889(12)	-3603(8)	82(4)

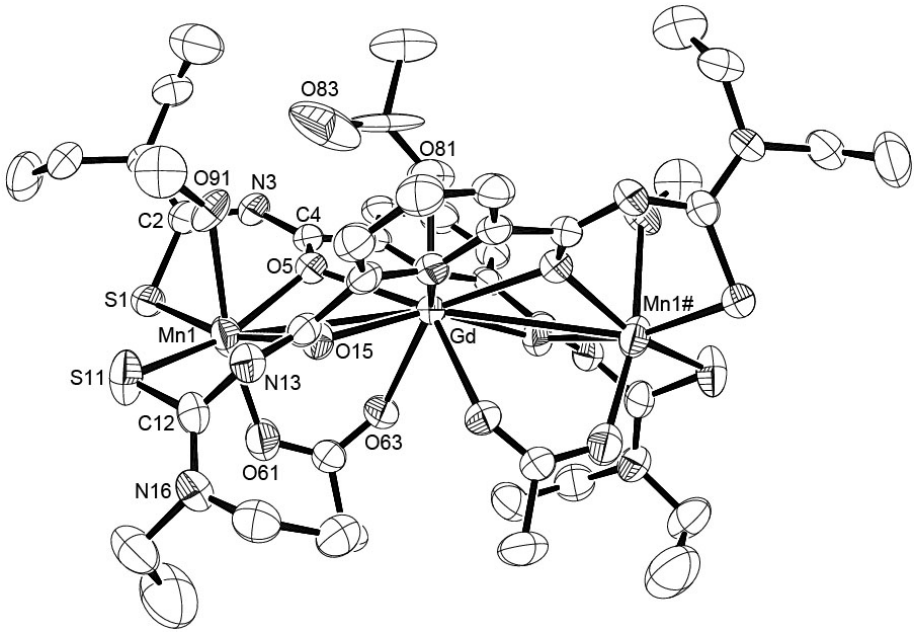

Fig A13 Ellipsoid plot (50% probability) of $[GdMn_2(L^a)_2(\mu\text{-}OAc)_2(OAc)(CH_3OH)_2]$

14) $[CeMn_2(L^a)_2(\mu\text{-}OAc)_2Cl(CH_3OH)]\cdot H_2O$

Table A27 Crystal data and structure refinement for $[CeMn_2(L^a)_2(\mu\text{-}OAc)_2Cl(CH_3OH)]\cdot H_2O$.

Empirical formula	$C_{39}H_{56}CeClMn_2N_{10}O_{10}S_4$	
Formula weight	1238.63	
Temperature	200(2) K	
Wavelength	0.71073 Å	
Crystal system	Orthorhombic	
Space group	$Pc2_1n$	
Unit cell dimensions	a = 11.840(1) Å	α = 90°
	b = 27.002(1) Å	β = 90°
	c = 16.708(1) Å	γ = 90°
Volume	5341.6(6) $Å^3$	
Z	4	
Density (calculated)	1.540 g/cm^3	
Absorption coefficient	1.569 mm^{-1}	
F(000)	2516	
Crystal description	Block	
Crystal color	Orange	
Crystal size	0.45 x 0.35 x 0.28 mm^3	
Theta range for data collection	1.88 to 29.27	
Index ranges	-16<=h<=16, -37<=k<=37, -16<=l<=22	
Reflections collected	39066	
Independent reflections	14372 [R(int) = 0.0650]	
Completeness to theta = 29.27°	99.0 %	
Absorption correction	Integration	
Max. and min. transmission	0.6595 and 0.5582	
Refinement method	Full-matrix least-squares on F^2	
Data / restraints / parameters	14372 / 1 / 613	
Goodness-of-fit on F^2	0.945	
Final R indices [I>2sigma(I)]	R1 = 0.0503, wR2 = 0.1184	
R indices (all data)	R1 = 0.0702, wR2 = 0.1329	
Largest diff. peak and hole	1.124 and -1.630 $e.Å^{-3}$	

Table A28 Atomic coordinates (x 10^4) and equivalent isotropic displacement parameters ($Å^2$x 10^3) for $[CeMn_2(L^a)_2(\mu\text{-}OAc)_2Cl(CH_3OH)]\cdot H_2O$. U(eq) is defined as one third of the trace of the orthogonalized U^{ij} tensor.

	x	y	z	U(eq)
Ce(1)	5162(1)	2502(1)	2782(1)	32(1)
Cl(1A)	2755(3)	2301(1)	2849(2)	52(1)
Cl(1B)	2776(5)	2734(2)	2689(3)	52(1)
Mn(1)	5458(1)	1131(1)	2768(1)	42(1)
Mn(2)	5607(1)	3858(1)	2833(1)	46(1)
S(1)	5935(2)	544(1)	3913(1)	56(1)
C(2)	6492(6)	1003(2)	4475(4)	45(1)
N(3)	5825(5)	1372(2)	4818(3)	42(1)
C(4)	5369(5)	1705(2)	4373(3)	35(1)
O(5)	5478(4)	1751(1)	3610(2)	39(1)
N(6)	7589(5)	1030(2)	4678(3)	51(1)
C(7)	8431(8)	662(3)	4422(5)	69(2)
C(8)	9275(10)	862(4)	3837(7)	94(3)
C(9)	8016(8)	1438(3)	5189(5)	64(2)
C(10)	8233(8)	1915(3)	4743(6)	71(2)
S(11)	5175(1)	4460(1)	3925(1)	41(1)
C(12)	3846(5)	4232(2)	4146(4)	39(1)
N(13)	3704(4)	3774(2)	4464(3)	38(1)
C(14)	4134(5)	3373(2)	4146(3)	35(1)
O(15)	4551(4)	3325(1)	3438(3)	42(1)
N(16)	2948(5)	4518(2)	4108(4)	50(1)
C(17)	3026(6)	5039(2)	3862(5)	55(2)
C(18)	3009(8)	5115(3)	2966(6)	73(2)
C(19)	1816(7)	4333(3)	4285(6)	67(2)
C(20A)	1602(17)	4312(6)	5057(12)	95(5)
C(20B)	1150(30)	4119(9)	3650(20)	95(5)
S(21)	5128(1)	549(1)	1628(1)	45(1)
C(22)	3850(5)	787(2)	1327(3)	37(1)
N(23)	3713(4)	1258(2)	1041(3)	39(1)
C(24)	4159(5)	1646(2)	1375(3)	35(1)
O(25)	4602(4)	1685(1)	2063(2)	43(1)

N(26)	2945(4)	497(2)	1269(3)	39(1)
C(27)	3003(6)	-31(2)	1454(4)	46(2)
C(28)	3296(8)	-339(3)	750(5)	70(2)
C(29)	1836(6)	676(2)	986(4)	48(1)
C(30)	1087(7)	821(3)	1647(6)	71(2)
S(31)	5974(2)	4460(1)	1705(1)	50(1)
C(32)	6567(5)	4007(2)	1109(3)	36(1)
N(33)	5887(4)	3649(2)	771(3)	37(1)
C(34)	5419(5)	3310(2)	1210(3)	32(1)
O(35)	5520(4)	3261(1)	1977(2)	36(1)
N(36)	7635(5)	4000(2)	910(3)	44(1)
C(37)	8444(6)	4382(3)	1140(5)	56(2)
C(38)	9348(9)	4218(3)	1715(6)	78(2)
C(39)	8074(6)	3590(3)	412(4)	55(2)
C(40)	8298(7)	3119(3)	851(6)	63(2)
C(41)	4111(5)	2917(2)	4664(3)	32(1)
C(42)	3694(6)	2914(2)	5426(4)	41(1)
C(43)	3781(5)	2488(3)	5878(3)	46(1)
C(44)	4290(6)	2077(2)	5550(4)	41(1)
C(45)	4705(5)	2107(2)	4775(3)	32(1)
N(46)	4599(3)	2519(2)	4335(2)	34(1)
C(51)	4772(5)	2917(2)	794(3)	32(1)
C(52)	4350(5)	2963(2)	20(3)	37(1)
C(53)	3816(5)	2571(2)	-319(3)	44(2)
C(54)	3723(6)	2126(2)	104(4)	41(1)
C(55)	4153(5)	2113(2)	876(3)	34(1)
N(56)	4646(3)	2500(2)	1227(2)	32(1)
O(61)	7126(4)	1348(2)	2453(3)	50(1)
C(62)	7445(5)	1762(2)	2251(3)	40(1)
O(63)	6811(4)	2139(2)	2172(3)	52(1)
C(64)	8683(7)	1837(3)	2093(6)	71(2)
O(71)	7260(4)	3653(2)	3111(3)	54(1)
C(72)	7498(5)	3217(2)	3318(4)	45(1)
O(73)	6791(4)	2884(2)	3427(3)	51(1)
C(74)	8728(7)	3089(4)	3448(7)	84(3)
O(91)	3516(5)	1107(2)	3133(4)	69(2)
C(92)	2916(12)	871(6)	3714(8)	155(7)

O(93)	3382(18)	3945(5)	2171(16)	326(2)

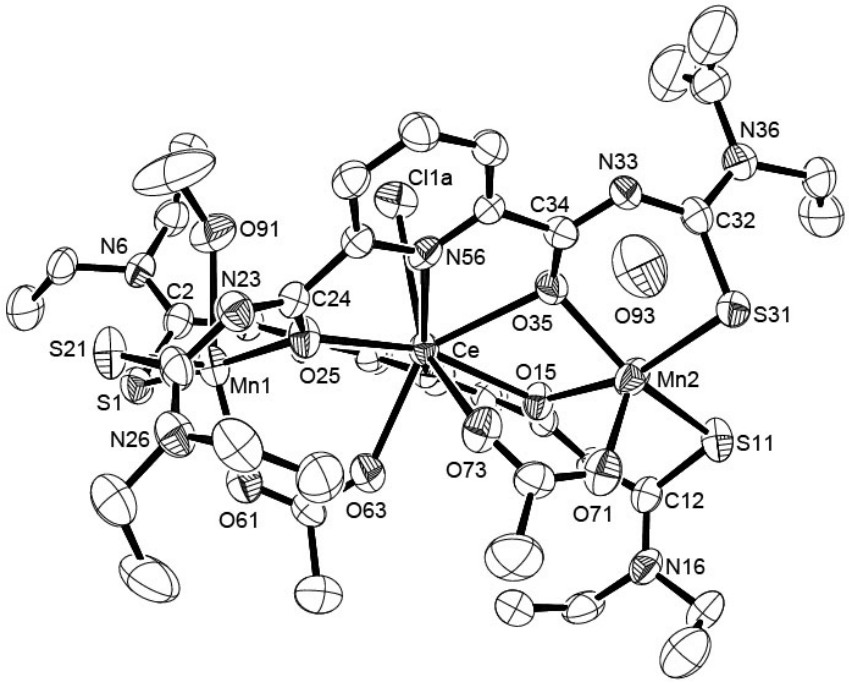

Fig A14 Ellipsoid plot (50% probability) of $[CeMn_2(L^a)_2(\mu\text{-}OAc)_2(Cl)(CH_3OH)]\cdot H_2O$

15) $[CeCu_2(L^a)_2Cl_3]\cdot H_2O$

Table 29 Crystal data and structure refinement for $[CeCu_2(L^a)_2Cl_3]\cdot H_2O$.

Empirical formula	$C_{34}H_{46}CeCl_3Cu_2N_{10}O_5S_4$	
Formula weight	1176.60	
Temperature	200(2) K	
Wavelength	0.71073 Å	
Crystal system	Monoclinic	
Space group	C2/c	
Unit cell dimensions	a = 19.182(5) Å	α = 90°
	b = 16.241(4) Å	β = 109.19(2)°
	c = 17.100(4) Å	γ = 90°
Volume	5031(2) $Å^3$	
Z	4	
Density (calculated)	1.553 g/cm^3	
Absorption coefficient	2.099 mm^{-1}	
F(000)	2364	
Crystal description	Prism	
Crystal color	Green	
Crystal size	0.21 x 0.17 x 0.14 mm^3	
Theta range for data collection	1.68 to 29.40	
Index ranges	-26<=h<=26, -19<=k<=22, -18<=l<=23	
Reflections collected	15647	
Independent reflections	6777 [R(int) = 0.3799]	
Completeness to theta = 29.40°	97.2 %	
Absorption correction	Integration	
Max. and min. transmission	0.9459 and 0.7892	
Refinement method	Full-matrix least-squares on F^2	
Data / restraints / parameters	6777 / 0 / 272	
Goodness-of-fit on F^2	0.728	
Final R indices [I>2sigma(I)]	R1 = 0.0880, wR2 = 0.1843	
R indices (all data)	R1 = 0.3784, wR2 = 0.3317	
Largest diff. peak and hole	1.204 and -3.286 $e.Å^{-3}$	

Table A30 Atomic coordinates (x 10^4) and equivalent isotropic displacement parameters ($Å^2$x 10^3) for $[CeCu_2(L^a)_2Cl_3]\cdot H_2O$. U(eq) is defined as one third of the trace of the orthogonalized U^{ij} tensor.

	x	y	z	U(eq)
Ce	0	9252(1)	7500	38(1)
Cl(1)	0	7522(6)	7500	69(3)
Cl(2)	923(2)	10700(4)	7603(3)	53(2)
Cu(1)	1915(1)	9605(2)	8364(2)	48(1)
S(1)	2567(3)	10171(5)	9608(4)	67(2)
C(2)	2426(9)	9421(13)	10220(13)	45(6)
N(3)	1726(7)	9193(13)	10226(9)	48(5)
C(4)	1147(9)	9151(14)	9564(11)	41(5)
O(5)	1115(6)	9219(11)	8810(8)	55(4)
N(6)	2959(7)	9062(13)	10844(12)	62(6)
C(7)	3766(9)	9210(20)	10861(18)	93(1)
C(8)	4064(11)	9920(20)	11490(20)	109(1)
C(9)	2838(12)	8525(17)	11452(17)	75(9)
C(10)	2763(16)	7690(19)	11220(20)	94(1)
S(11)	2953(3)	9621(5)	8016(5)	81(2)
C(12)	2767(11)	8835(16)	7311(15)	57(7)
N(13)	-2109(8)	8771(12)	8367(12)	56(5)
C(14)	-1455(10)	8887(13)	8242(15)	44(6)
O(15)	-1311(6)	8933(8)	7583(9)	42(4)
N(16)	3255(10)	8273(17)	7266(15)	93(8)
C(17)	4063(15)	8370(30)	7870(20)	133(2)
C(18)	4193(19)	7890(20)	8540(30)	180(2)
C(19)	3091(16)	7564(19)	6630(30)	125(1)
C(20)	3380(30)	7730(30)	5960(30)	190(2)
C(41)	392(9)	9032(11)	9695(11)	33(5)
C(42)	354(9)	8968(14)	10479(13)	47(6)
C(43)	-340(9)	8846(15)	10558(12)	55(7)
C(44)	-922(10)	8812(15)	9823(15)	56(7)
C(45)	-840(9)	8895(15)	9057(13)	50(6)
N(46)	-165(8)	9009(11)	8972(10)	48(5)
O(91)	4120(20)	8330(30)	13900(40)	200(3)

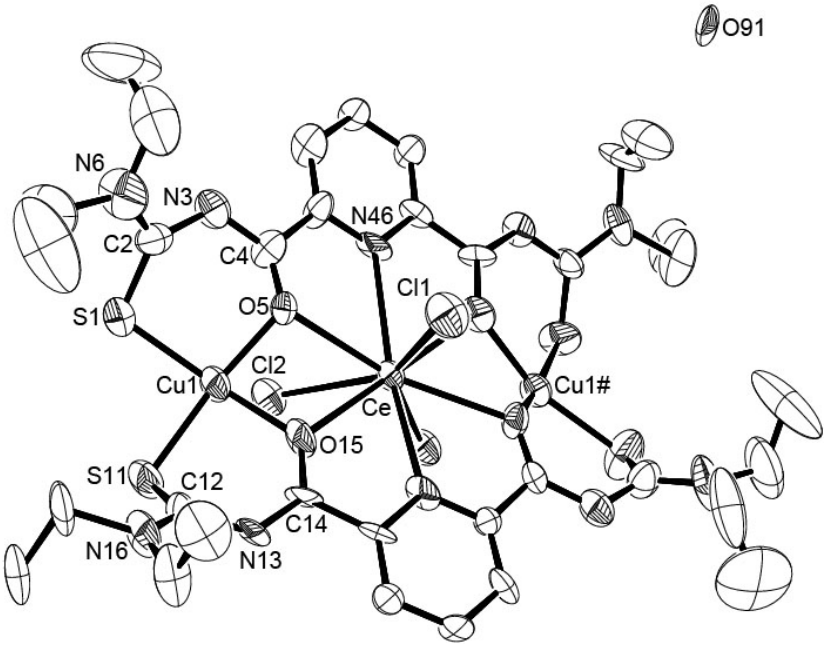

Fig A15 Ellipsoid plot (50% probability) of $[CeCu_2(L^a)_2Cl_3]\cdot H_2O$

16) [$GdZn_2(L^a)_2(\mu\text{-}OAc)_2(OAc)$]

Table A31 Crystal data and structure refinement for [$GdZn_2(L^a)_2(\mu\text{-}OAc)_2(OAc)$].

Empirical formula	$C_{40}H_{55}GdN_{10}O_{10}S_4Zn_2$	
Formula weight	1251.76	
Temperature	200(2) K	
Wavelength	0.71073 Å	
Crystal system	Monoclinic	
Space group	C2/c	
Unit cell dimensions	a = 30.505(3) Å	α = 90°
	b = 9.634(1) Å	β = 130.86(1)°
	c = 22.452(2) Å	γ = 90°
Volume	4990.4(11) $Å^3$	
Z	4	
Density (calculated)	1.666 g/cm^3	
Absorption coefficient	2.498 mm^{-1}	
F(000)	2532	
Crystal description	Prism	
Crystal color	Colorless	
Crystal size	0.38 x 0.32 x 0.26 mm^3	
Theta range for data collection	1.82 to 29.36	
Index ranges	-41<=h<=41, -13<=k<=13, -30<=l<=30	
Reflections collected	25848	
Independent reflections	6742 [R(int) = 0.0894]	
Completeness to theta = 29.36°	98.3 %	
Absorption correction	Integration	
Max. and min. transmission	0.8742 and 0.7438	
Refinement method	Full-matrix least-squares on F^2	
Data / restraints / parameters	6742 / 0 / 305	
Goodness-of-fit on F^2	0.943	
Final R indices [I>2sigma(I)]	R1 = 0.0527, wR2 = 0.1196	
R indices (all data)	R1 = 0.0829, wR2 = 0.1396	
Largest diff. peak and hole	1.065 and -1.732 e.$Å^{-3}$	

Table A32 Atomic coordinates (x 10^4) and equivalent isotropic displacement parameters ($Å^2$x 10^3) for [$GdZn_2(L^a)_2(\mu\text{-}OAc)_2(OAc)$]. U(eq) is defined as one third of the trace of the orthogonalized U^{ij} tensor.

	x	y	z	U(eq)
Gd	0	1724(1)	2500	31(1)
Zn(1)	863(1)	2740(1)	1993(1)	34(1)
S(1)	1580(1)	1408(2)	2164(1)	44(1)
C(2)	1945(2)	497(6)	3036(3)	36(1)
N(3)	1896(2)	676(5)	3589(2)	36(1)
C(4)	1414(2)	1020(5)	3428(3)	34(1)
O(5)	904(2)	1117(4)	2760(2)	36(1)
N(6)	2352(2)	-402(5)	3227(3)	39(1)
C(7)	2484(3)	-708(6)	2723(4)	46(1)
C(8)	2948(3)	224(7)	2882(5)	56(2)
C(9)	2714(3)	-1105(7)	3998(4)	52(2)
C(10)	2433(4)	-2407(10)	3975(6)	82(3)
S(11)	-564(1)	4028(2)	4111(1)	41(1)
C(12)	-51(2)	2860(5)	4805(3)	34(1)
N(13)	414(2)	2440(5)	4890(3)	38(1)
C(14)	413(2)	2257(5)	4321(3)	33(1)
O(15)	-22(2)	2217(4)	3571(2)	38(1)
N(16)	-56(2)	2394(5)	5360(3)	38(1)
C(17)	-495(3)	2799(7)	5405(4)	49(2)
C(18)	-966(3)	1728(9)	5032(5)	64(2)
C(19)	404(3)	1470(6)	6002(3)	46(1)
C(20)	902(3)	2299(8)	6704(4)	62(2)
C(41)	1475(2)	1332(6)	4138(3)	35(1)
C(42)	2002(3)	1307(6)	4905(3)	42(1)
C(43)	2013(2)	1653(7)	5513(3)	46(1)
C(44)	1504(3)	1993(6)	5344(3)	41(1)
C(45)	988(2)	1962(5)	4558(3)	33(1)
N(46)	978(2)	1651(5)	3969(2)	33(1)
O(61)	-1280(2)	4094(5)	2124(2)	47(1)
C(62)	-1038(3)	4321(6)	1840(3)	39(1)
O(63)	-569(2)	3826(4)	2103(2)	45(1)

C(64)	-1363(4)	5211(9)	1115(5)	72(2)
O(81)	183(2)	-555(4)	3113(2)	42(1)
C(82)	0	-1214(9)	2500	40(2)
C(84)	0	-2761(12)	2500	101(6)

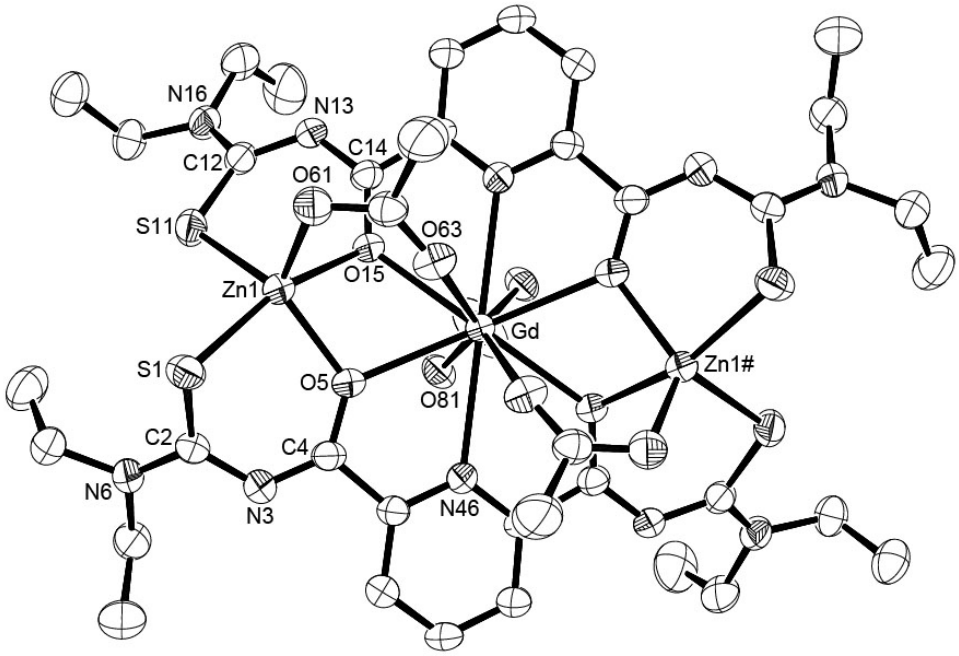

Fig A16 Ellipsoid plot (50% probability) of $[GdZn_2(L^a)_2(\mu\text{-}OAc)_2(OAc)]$

17) $[SrMn_2(L^b)_3]\cdot 3CH_2Cl_2\cdot 3H_2O$

Table A33 Crystal data and structure refinement for $[SrMn_2(L^b)_3]\cdot 3CH_2Cl_2\cdot 3H_2O$.

Empirical formula	$C_{54}H_{63}Cl_6Mn_2N_{15}O_{15}S_6Sr$	
Formula weight	1764.75	
Temperature	200(2) K	
Wavelength	0.71073 Å	
Crystal system	Trigonal	
Space group	$P\overline{3}$	
Unit cell dimensions	a = 15.780(1) Å	α = 90°
	b = 15.780(1) Å	β = 90°
	c = 17.464(1) Å	γ = 120°
Volume	3766.1(4) $Å^3$	
Z	2	
Density (calculated)	1.556 g/cm^3	
Absorption coefficient	1.484 mm^{-1}	
F(000)	1796	
Crystal description	Block	
Crystal color	Orange	
Crystal size	0.540 x 0.380 x 0.240 mm^3	
Theta range for data collection	2.77 to 29.34	
Index ranges	-21<=h<=14, -21<=k<=21, -22<=l<=23	
Reflections collected	39188	
Independent reflections	6833 [R(int) = 0.1794]	
Completeness to theta = 29.34°	98.7 %	
Absorption correction	Integration	
Max. and min. transmission	0.8847 and 0.8184	
Refinement method	Full-matrix least-squares on F^2	
Data / restraints / parameters	6833 / 0 / 298	
Goodness-of-fit on F^2	1.032	
Final R indices [I>2sigma(I)]	R1 = 0.1018, wR2 = 0.2349	
R indices (all data)	R1 = 0.1785, wR2 = 0.2729	
Largest diff. peak and hole	1.530 and -1.210 $e.Å^{-3}$	

Table A34 Atomic coordinates (x 10^4) and equivalent isotropic displacement parameters ($Å^2$x 10^3) for $[SrMn_2(L^b)_3]\cdot 3CH_2Cl_2\cdot 3H_2O$. U(eq) is defined as one third of the trace of the orthogonalized U^{ij} tensor.

	x	y	z	U(eq)
Sr	6667	3333	2172(1)	21(1)
Mn(1)	6667	3333	111(1)	26(1)
Mn(2)	6667	3333	4226(1)	22(1)
S(1)	5127(2)	2619(1)	-700(1)	34(1)
C(2)	4357(6)	1473(6)	-339(5)	36(2)
N(3)	4523(5)	1037(5)	261(4)	35(2)
C(4)	5100(5)	1509(5)	836(4)	26(1)
O(5)	5576(4)	2429(3)	964(3)	28(1)
N(6)	3514(6)	889(6)	-698(5)	61(3)
C(7)	3141(10)	1212(10)	-1328(9)	90(5)
C(8)	2583(12)	524(12)	-1831(11)	125(8)
C(9)	2811(11)	-77(10)	-429(9)	105(6)
C(10)	2270(14)	-731(11)	-957(12)	137(9)
O(10)	1864(7)	-404(7)	-1536(6)	95(3)
S(11)	5627(1)	1849(1)	5082(1)	29(1)
C(12)	6076(5)	1130(5)	4741(4)	24(1)
N(13)	5903(5)	775(4)	4010(4)	30(1)
C(14)	6052(5)	1328(5)	3409(4)	24(1)
O(15)	6522(4)	2261(3)	3371(3)	27(1)
N(16)	6514(5)	793(5)	5193(4)	30(1)
C(17)	6696(7)	1002(7)	6010(5)	42(2)
C(18)	7785(7)	1488(8)	6147(6)	49(2)
C(19)	6913(6)	179(5)	4919(6)	38(2)
C(20)	8009(7)	720(7)	5091(7)	54(3)
O(20)	8178(5)	914(5)	5886(5)	58(2)
C(21)	5615(5)	777(5)	2684(4)	26(1)
C(22)	5203(6)	-231(5)	2632(5)	33(2)
C(23)	4773(7)	-685(6)	1950(5)	44(2)
C(24)	4731(6)	-134(6)	1351(5)	39(2)
C(25)	5154(5)	866(5)	1450(4)	27(1)
N(26)	5605(4)	1326(4)	2094(4)	25(1)

Cl(31)	2707(5)	2892(6)	7854(4)	164(2)
C(32)	1818(16)	2595(17)	7170(12)	128(7)
Cl(33)	2034(10)	3685(8)	6798(6)	249(6)
O(31)	3333	-3333	2891(16)	184(1)
O(32)	10000	0	4200(20)	159(1)
O(34)	0	0	7320(16)	143(9)

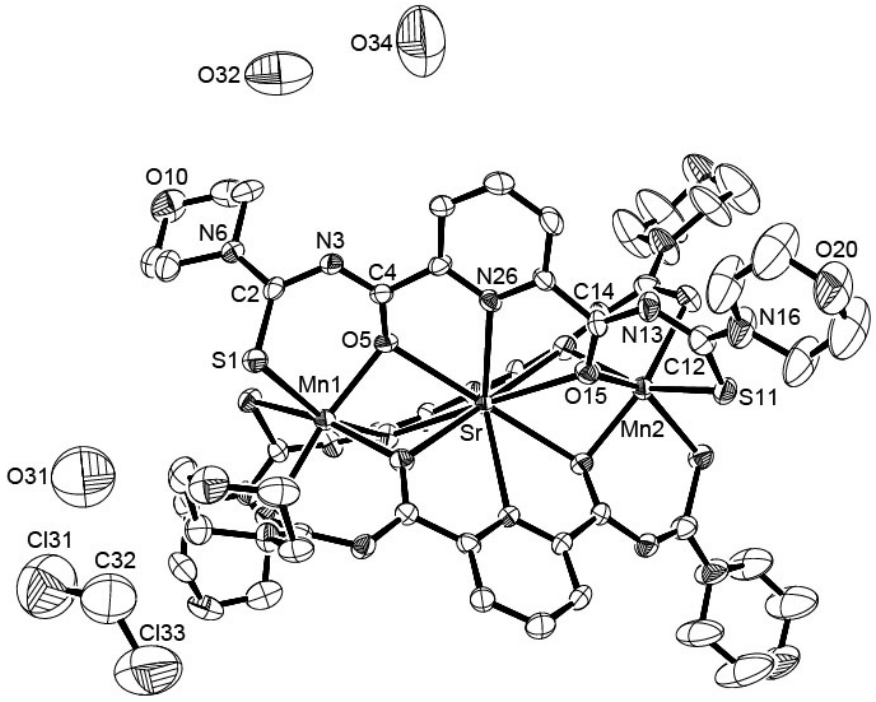

Fig A17 Ellipsoid plot (50% probability) of $[SrMn_2(L^b)_3]\cdot 3CH_2Cl_2\cdot 3H_2O$

18) $[SrMn_2(L^b)_3(THF)]\cdot 0.5C_4H_8O_2$

Table A35 Crystal data and structure refinement for $[SrMn_2(L^b)_3(THF)]\cdot 0.5C_4H_8O_2$.

Empirical formula	$C_{57}H_{69}Mn_2N_{15}O_{14}S_6Sr$	
Formula weight	1578.13	
Temperature	200(2) K	
Wavelength	0.71073 Å	
Crystal system	Triclinic	
Space group	$P\bar{1}$	
Unit cell dimensions	a = 10.210(3) Å	α = 97.82(2)°
	b = 17.374(5) Å	β = 90.49(2)°
	c = 19.449(5) Å	γ = 100.46(2)°
Volume	3359.2(2) $Å^3$	
Z	2	
Density (calculated)	1.560 g/cm^3	
Absorption coefficient	1.422 mm^{-1}	
F(000)	1624	
Crystal description	Prism	
Crystal color	Orange	
Crystal size	0.240 x 0.200 x 0.160 mm^3	
Theta range for data collection	3.39 to 29.41	
Index ranges	-11<=h<=14, -23<=k<=23, -26<=l<=26	
Reflections collected	40558	
Independent reflections	17996 [R(int) = 0.1091]	
Completeness to theta = 29.41°	97.0 %	
Absorption correction	Integration	
Max. and min. transmission	0.8479 and 0.7555	
Refinement method	Full-matrix least-squares on F^2	
Data / restraints / parameters	17996 / 0 / 856	
Goodness-of-fit on F^2	0.855	
Final R indices [I>2sigma(I)]	R1 = 0.0564, wR2 = 0.1022	
R indices (all data)	R1 = 0.1400, wR2 = 0.1253	
Largest diff. peak and hole	0.604 and -1.043 e.$Å^{-3}$	

Table A36 Atomic coordinates (x 10^4) and equivalent isotropic displacement parameters ($Å^2$x 10^3) for $[SrMn_2(L^b)_3THF]\cdot 0.5C_4H_8O_2$. U(eq) is defined as one third of the trace of the orthogonalized U^{ij} tensor.

	x	y	z	U(eq)
Sr(1)	9958(1)	4533(1)	2459(1)	27(1)
Mn(1)	10355(1)	2447(1)	1936(1)	29(1)
Mn(2)	9574(1)	6629(1)	2974(1)	29(1)
S(1)	8713(1)	1288(1)	1272(1)	40(1)
C(2)	8579(5)	1798(2)	581(2)	32(1)
N(3)	7910(4)	2418(2)	647(2)	36(1)
C(4)	8257(4)	3042(2)	1116(2)	28(1)
O(5)	9328(3)	3245(2)	1475(1)	30(1)
N(6)	9002(4)	1577(2)	-50(2)	41(1)
C(7)	9542(6)	860(3)	-245(3)	55(2)
C(8)	10905(6)	1060(3)	-551(3)	58(2)
C(9)	9012(6)	2053(3)	-625(2)	47(1)
C(10)	10413(6)	2213(4)	-878(3)	60(2)
O(10)	10881(4)	1507(3)	-1104(2)	66(1)
S(11)	7574(1)	7251(1)	2933(1)	39(1)
C(12)	6902(5)	6930(2)	2106(2)	36(1)
N(13)	6733(4)	6183(2)	1771(2)	36(1)
C(14)	7507(5)	5670(2)	1854(2)	29(1)
O(15)	8660(3)	5773(2)	2122(1)	33(1)
N(16)	6373(5)	7431(2)	1770(2)	50(1)
C(17)	6466(6)	8273(3)	2030(3)	55(2)
C(18)	5152(7)	8483(4)	1995(3)	68(2)
C(19)	5723(7)	7213(3)	1070(3)	61(2)
C(20)	4434(7)	7489(4)	1080(3)	70(2)
O(20)	4564(5)	8304(2)	1313(2)	70(1)
S(21)	12396(1)	2253(1)	1175(1)	39(1)
C(22)	13469(5)	2442(2)	1892(2)	37(1)
N(23)	13729(4)	3124(2)	2340(2)	36(1)
C(24)	12916(5)	3638(2)	2442(2)	31(1)
O(25)	11688(3)	3536(2)	2293(2)	33(1)
N(26)	14255(5)	1928(2)	2003(2)	49(1)

C(27)	14195(7)	1161(3)	1580(3)	55(2)
C(28)	13774(7)	525(3)	2024(3)	65(2)
C(29)	15111(7)	2017(3)	2625(3)	70(2)
C(30)	14608(8)	1357(4)	3032(3)	73(2)
O(30)	14624(5)	612(2)	2625(2)	67(1)
S(31)	11237(1)	7661(1)	2429(1)	40(1)
C(32)	12441(5)	7672(2)	3054(2)	34(1)
N(33)	12987(4)	7051(2)	3176(2)	32(1)
C(34)	12404(5)	6299(2)	2988(2)	29(1)
O(35)	11223(3)	6018(2)	2801(1)	31(1)
N(36)	12993(4)	8359(2)	3440(2)	37(1)
C(37)	12735(6)	9124(3)	3312(3)	50(1)
C(38)	12554(6)	9624(3)	3990(3)	56(2)
C(39)	14061(5)	8415(3)	3962(2)	42(1)
C(40)	13814(6)	8957(3)	4603(2)	45(1)
O(40)	13677(4)	9712(2)	4450(2)	52(1)
S(41)	10964(1)	1622(1)	2833(1)	39(1)
C(42)	9405(5)	1484(2)	3185(2)	35(1)
N(43)	8865(4)	2065(2)	3543(2)	37(1)
C(44)	8971(5)	2778(2)	3369(2)	30(1)
O(45)	9304(3)	3008(2)	2795(1)	37(1)
N(46)	8712(4)	751(2)	3188(2)	41(1)
C(47)	9118(6)	32(3)	2846(3)	53(1)
C(48)	9014(6)	-565(3)	3343(3)	58(2)
C(49)	7402(6)	589(3)	3500(3)	53(1)
C(50)	7411(7)	-20(3)	3976(3)	66(2)
O(50)	7740(4)	-720(2)	3616(2)	61(1)
S(51)	10130(1)	7359(1)	4196(1)	36(1)
C(52)	8905(5)	6846(2)	4655(2)	34(1)
N(53)	8645(4)	6052(2)	4652(2)	34(1)
C(54)	8788(4)	5515(2)	4121(2)	30(1)
O(55)	9011(3)	5586(2)	3491(1)	33(1)
N(56)	8210(4)	7241(2)	5113(2)	41(1)
C(57)	8234(6)	8093(3)	5164(3)	45(1)
C(58)	6874(6)	8212(3)	4949(3)	57(2)
C(59)	7181(6)	6868(3)	5543(3)	50(1)
C(60)	5849(6)	7021(4)	5314(3)	64(2)

O(60)	5842(4)	7847(3)	5360(2)	67(1)
C(61)	7269(4)	3582(2)	1185(2)	28(1)
C(62)	5979(5)	3340(2)	909(2)	34(1)
C(63)	5138(5)	3879(3)	947(2)	37(1)
C(64)	5630(5)	4644(3)	1249(2)	36(1)
C(65)	6923(5)	4838(2)	1528(2)	29(1)
N(66)	7719(4)	4312(2)	1518(2)	28(1)
C(71)	13556(5)	4434(2)	2798(2)	31(1)
C(72)	14857(5)	4613(3)	3036(2)	42(1)
C(73)	15398(5)	5381(3)	3291(3)	47(1)
C(74)	14614(5)	5951(3)	3290(2)	39(1)
C(75)	13311(5)	5721(2)	3048(2)	29(1)
N(76)	12762(4)	4970(2)	2817(2)	29(1)
C(81)	8597(4)	3380(2)	3930(2)	27(1)
C(82)	8032(5)	3168(3)	4543(2)	34(1)
C(83)	7759(5)	3742(3)	5054(2)	40(1)
C(84)	8029(5)	4514(3)	4935(2)	38(1)
C(85)	8548(4)	4689(2)	4298(2)	28(1)
N(86)	8836(4)	4130(2)	3798(2)	27(1)
O(91)	11056(4)	4899(2)	1290(2)	46(1)
C(93)	12195(8)	4777(4)	236(3)	77(2)
C(92)	11562(10)	4371(4)	797(4)	105(3)
C(94)	11956(9)	5591(4)	403(3)	93(3)
C(95)	11368(11)	5645(4)	1094(4)	121(4)
O(96)	4286(8)	9414(4)	172(4)	140(2)
C(97)	5728(8)	9641(6)	291(4)	97(3)
C(98)	3527(9)	10001(5)	134(5)	101(3)

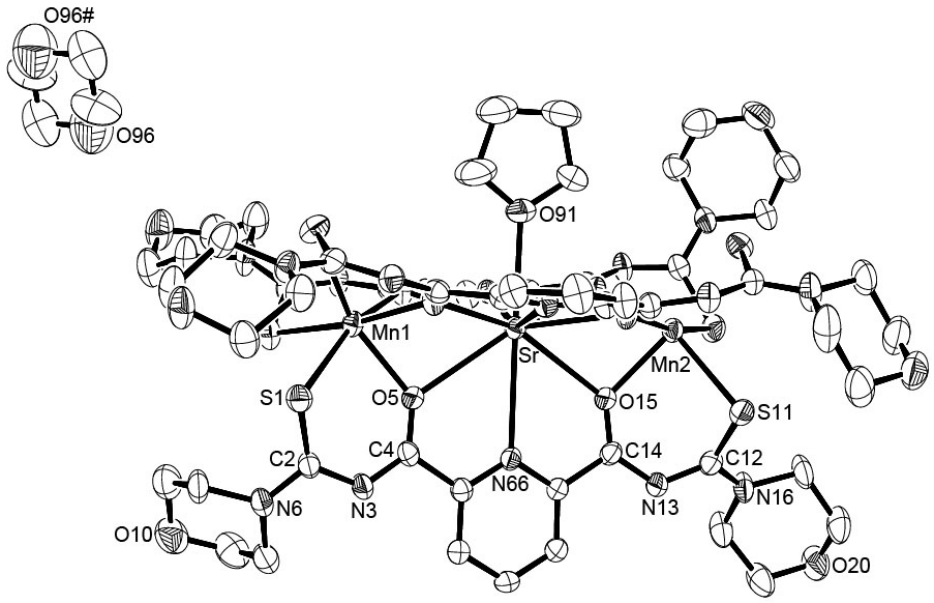

Fig A18 Ellipsoid plot (50% probability) of $[SrMn_2(L^b)_3(THF)]\cdot 0.5C_4H_8O_2$

19) $[BaMn_2(L^a)_3]\cdot 2H_2O$

Table A37 Crystal data and structure refinement for $[BaMn(L^a)_3]\cdot 2H_2O$.

Empirical formula	$C_{51}H_{69}BaMn_2N_{15}O_8S_6$	
Formula weight	1459.79	
Temperature	200(2) K	
Wavelength	0.71073 Å	
Crystal system	Monoclinic	
Space group	$P2_1/c$	
Unit cell dimensions	a = 17.321(1) Å	α = 90°
	b = 18.991(1) Å	β = 92.98(1)°
	c = 20.151(1) Å	γ = 90°
Volume	6619.6(6) $Å^3$	
Z	4	
Density (calculated)	1.465 g/cm^3	
Absorption coefficient	1.212 mm^{-1}	
F(000)	2984	
Crystal description	Plate	
Crystal color	Orange	
Crystal size	0.210 x 0.120 x 0.030 mm^3	
Theta range for data collection	1.85 to 29.28	
Index ranges	-22<=h<=23, -21<=k<=26, -27<=l<=27	
Reflections collected	51956	
Independent reflections	17776 [R(int) = 0.1124]	
Completeness to theta = 29.28°	98.4 %	
Absorption correction	Integration	
Max. and min. transmission	0.7172 and 0.4528	
Refinement method	Full-matrix least-squares on F^2	
Data / restraints / parameters	17776 / 0 / 749	
Goodness-of-fit on F^2	1.129	
Final R indices [I>2sigma(I)]	R1 = 0.0750, wR2 = 0.2000	
R indices (all data)	R1 = 0.0855, wR2 = 0.2087	
Largest diff. peak and hole	2.407 and -2.371 $e.Å^{-3}$	

Table A38 Atomic coordinates (x 10^4) and equivalent isotropic displacement parameters ($Å^2$x 10^3) for $[BaMn_2(L^a)_3]\cdot 2H_2O$. U(eq) is defined as one third of the trace of the orthogonalized U^{ij} tensor.

	x	y	z	U(eq)
Ba	944(1)	7406(1)	3220(1)	36(1)
Mn(1)	-1145(1)	7545(1)	3595(1)	35(1)
Mn(2)	3035(1)	7192(1)	2860(1)	39(1)
S(1)	-1933(1)	6536(1)	4096(1)	51(1)
C(2)	-1452(3)	6534(3)	4859(3)	45(1)
N(3)	-685(2)	6368(2)	4964(2)	43(1)
C(4)	-141(3)	6555(3)	4566(2)	38(1)
O(5)	-163(2)	7033(2)	4125(2)	40(1)
N(6)	-1823(3)	6605(3)	5421(2)	54(1)
C(7)	-2666(4)	6661(5)	5425(4)	76(2)
C(8)	-2920(6)	7427(5)	5526(5)	94(3)
C(9)	-1412(4)	6599(4)	6077(3)	60(2)
C(10)	-1362(5)	5878(5)	6388(4)	77(2)
S(11)	4089(1)	6767(1)	3701(1)	54(1)
C(12)	3792(3)	5912(3)	3794(3)	46(1)
N(13)	3089(2)	5715(3)	3993(2)	45(1)
C(14)	2439(3)	6080(3)	3868(2)	41(1)
O(15)	2285(2)	6516(2)	3415(2)	41(1)
N(16)	4294(3)	5385(3)	3739(3)	57(1)
C(17)	5115(3)	5504(4)	3591(4)	69(2)
C(18)	5623(4)	5592(6)	4205(5)	96(3)
C(19)	4068(4)	4651(4)	3821(4)	68(2)
C(20)	3748(7)	4327(6)	3186(5)	113(4)
S(21)	-1788(1)	8424(1)	4356(1)	43(1)
C(22)	-1455(3)	9186(3)	4014(2)	40(1)
N(23)	-696(2)	9362(2)	4023(2)	42(1)
C(24)	-154(3)	8923(2)	3837(2)	36(1)
O(25)	-232(2)	8342(2)	3548(2)	41(1)
N(26)	-1943(2)	9686(2)	3783(2)	44(1)
C(27)	-2787(3)	9597(3)	3743(3)	49(1)
C(28)	-3154(3)	9860(4)	4356(3)	62(2)
C(29)	-1652(3)	10367(3)	3543(3)	53(1)

C(30)	-1504(5)	10336(4)	2811(4)	76(2)
S(31)	3877(1)	8239(1)	2567(1)	51(1)
C(32)	3903(3)	8669(3)	3319(2)	42(1)
N(33)	3275(2)	8910(2)	3621(2)	42(1)
C(34)	2596(3)	8591(3)	3601(2)	40(1)
O(35)	2415(2)	7981(2)	3416(2)	44(1)
N(36)	4581(2)	8859(3)	3620(2)	47(1)
C(37)	5340(3)	8669(4)	3377(3)	59(2)
C(38)	5755(4)	8122(4)	3795(4)	74(2)
C(39)	4600(3)	9333(3)	4199(3)	52(1)
C(40)	4559(4)	10093(4)	3988(4)	69(2)
S(41)	-2239(1)	7788(1)	2701(1)	47(1)
C(42)	-2143(3)	6962(3)	2371(2)	45(1)
N(43)	-1532(2)	6785(3)	2003(2)	46(1)
C(44)	-815(3)	6941(3)	2191(2)	39(1)
O(45)	-552(2)	7109(2)	2764(2)	40(1)
N(46)	-2700(2)	6480(3)	2406(2)	54(1)
C(47)	-3433(3)	6633(4)	2722(3)	65(2)
C(48)	-4038(4)	6928(5)	2231(4)	78(2)
C(49)	-2616(4)	5763(4)	2135(4)	70(2)
C(50)	-2524(11)	5222(6)	2641(6)	152(6)
S(51)	3520(1)	6485(1)	1867(1)	49(1)
C(52)	3129(3)	7093(3)	1305(2)	49(1)
N(53)	2356(2)	7144(3)	1163(2)	53(1)
C(54)	1850(3)	7165(3)	1623(2)	41(1)
O(55)	1976(2)	7268(2)	2235(2)	42(1)
N(56)	3575(3)	7505(3)	948(3)	57(1)
C(57)	4434(4)	7440(5)	989(4)	71(2)
C(58)	4692(5)	6960(6)	480(5)	100(3)
C(59)	3250(5)	8075(5)	510(4)	82(2)
C(60)	3295(9)	8774(7)	868(7)	153(6)
C(61)	601(3)	6160(3)	4681(2)	39(1)
C(62)	685(3)	5671(3)	5202(3)	47(1)
C(63)	1357(3)	5282(3)	5268(3)	52(1)
C(64)	1923(3)	5390(3)	4828(3)	50(1)
C(65)	1812(3)	5903(3)	4339(2)	40(1)
N(66)	1155(2)	6278(2)	4255(2)	39(1)

C(71)	656(3)	9205(2)	3976(2)	37(1)
C(72)	784(3)	9857(3)	4284(3)	45(1)
C(73)	1530(3)	10101(3)	4379(3)	48(1)
C(74)	2131(3)	9690(3)	4168(3)	45(1)
C(75)	1960(3)	9043(3)	3866(2)	38(1)
N(76)	1235(2)	8799(2)	3781(2)	37(1)
C(81)	-246(2)	6910(3)	1646(2)	37(1)
C(82)	-485(3)	6803(3)	988(2)	43(1)
C(83)	57(3)	6844(3)	503(2)	46(1)
C(84)	821(3)	6974(3)	701(2)	44(1)
C(85)	1018(3)	7054(3)	1370(2)	40(1)
N(86)	501(2)	7028(2)	1840(2)	38(1)
O(91)	-359(5)	5267(4)	3136(4)	121(3)
O(93)	749(5)	6057(7)	7101(4)	163(5)

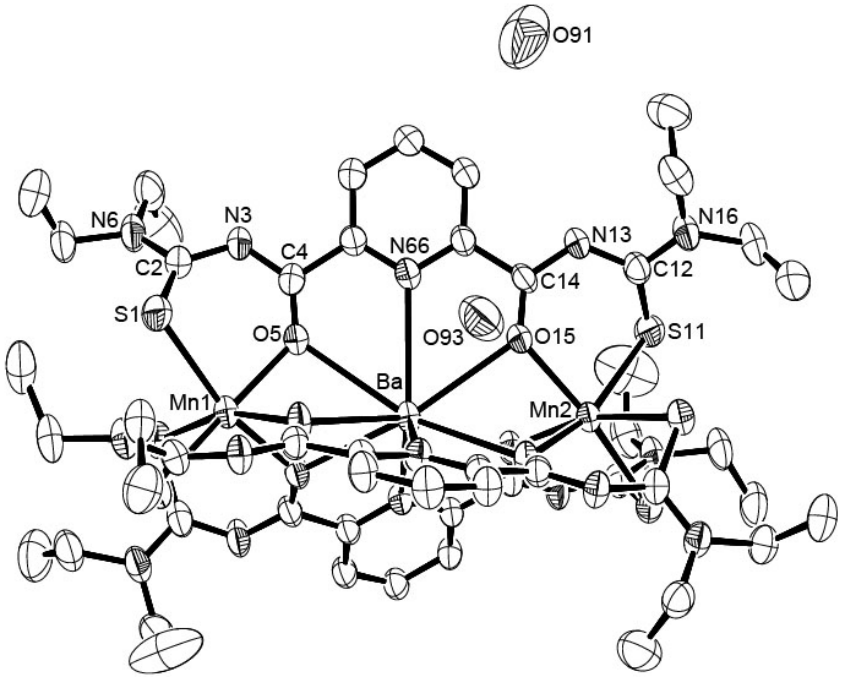

Fig A19 Ellipsoid plot (50% probability) of $[BaMn_2(L^a)_3]\cdot 2H_2O$

20) $[BaMn_2(L^b)_3CH_3OH)]_2 \cdot 4CH_2Cl_2 \cdot 3CH_3OH \cdot 10H_2O$

Table A39 Crystal data and structure refinement for $[BaMn_2(L^b)_3(CH_3OH)]_2 \cdot 4CH_2Cl_2 \cdot 2CH_3OH \cdot 10H_2O$.

Empirical formula	$C_{110}H_{138}Ba_2Cl_8Mn_4N_{30}O_{38}S_{12}$	
Formula weight	3651.26	
Temperature	200(2) K	
Wavelength	0.71073 Å	
Crystal system	Triclinic	
Space group	$P\bar{1}$	
Unit cell dimensions	a = 17.382(1) Å	α = 108.26(1)°
	b = 22.190(2) Å	β = 97.94(1)°
	c = 22.462(2) Å	γ = 93.57(1)°
Volume	8097.1(11) $Å^3$	
Z	2	
Density (calculated)	1.498 g/cm^3	
Absorption coefficient	1.145 mm^{-1}	
F(000)	3704	
Crystal description	Prism	
Crystal color	Orange	
Crystal size	0.340 x 0.280 x 0.220 mm^3	
Theta range for data collection	1.65 to 29.36	
Index ranges	-23<=h<=23, -30<=k<=30, -30<=l<=30	
Reflections collected	64496	
Independent reflections	39899 [R(int) = 0.1891]	
Completeness to theta = 29.36°	89.6 %	
Absorption correction	None	
Refinement method	Full-matrix least-squares on F^2	
Data / restraints / parameters	39899 / 0 / 1841	
Goodness-of-fit on F^2	0.747	
Final R indices [I>2sigma(I)]	R1 = 0.0862, wR2 = 0.1977	
R indices (all data)	R1 = 0.2823, wR2 = 0.3134	
Largest diff. peak and hole	1.613 and -1.943 $e.Å^{-3}$	

Table A40 Atomic coordinates (x 10^4) and equivalent isotropic displacement parameters ($Å^2$x 10^3) for $[BaMn_2(L^b)_3(CH_3OH)]_2 \cdot 4CH_2Cl_2 \cdot 2CH_3OH \cdot 10H_2O$. U(eq) is defined as one third of the trace of the orthogonalized U^{ij} tensor.

	x	y	z	U(eq)
Ba(1)	9211(1)	2324(1)	8289(1)	30(1)
Mn(1)	7054(1)	1897(1)	8080(1)	35(1)
Mn(2)	11352(1)	2759(1)	8540(1)	32(1)
S(1)	12339(2)	1941(2)	8447(2)	45(1)
C(2)	12226(8)	1756(6)	9133(8)	41(4)
N(3)	11541(6)	1489(6)	9223(6)	42(3)
C(4)	10833(8)	1622(6)	9038(6)	33(3)
O(5)	10681(5)	2114(4)	8847(4)	33(2)
N(6)	12824(7)	1789(8)	9554(7)	59(4)
C(7)	13629(9)	2025(10)	9541(10)	66(5)
C(8)	13878(11)	2598(10)	10080(12)	81(6)
C(9)	12778(10)	1663(9)	10133(10)	71(6)
C(10)	13041(12)	2262(11)	10666(13)	89(7)
O(10)	13849(8)	2493(9)	10680(7)	100(5)
S(11)	6450(2)	1804(2)	9051(2)	53(1)
C(12)	6742(9)	1061(8)	8981(8)	48(4)
N(13)	7480(7)	901(6)	9025(6)	46(3)
C(14)	8065(8)	1208(7)	8879(6)	34(3)
O(15)	8032(5)	1604(4)	8588(5)	37(2)
N(16)	6187(7)	580(7)	8917(8)	65(5)
C(17)	5349(10)	627(10)	8906(13)	86(8)
C(18)	5039(13)	300(15)	9323(18)	131(13)
C(19)	6360(11)	-91(9)	8753(12)	81(7)
C(20)	6032(15)	-403(14)	9151(15)	113(9)
O(20)	5178(9)	-362(9)	9123(10)	115(6)
S(21)	12019(2)	3575(2)	9591(2)	41(1)
C(22)	11718(7)	4234(6)	9403(6)	32(3)
N(23)	10996(6)	4365(5)	9286(6)	40(3)
C(24)	10401(7)	3919(6)	9037(7)	36(3)
O(25)	10399(5)	3323(4)	8752(4)	39(2)
N(26)	12272(6)	4709(5)	9436(6)	37(3)

C(27)	13110(8)	4660(7)	9529(8)	44(4)
C(28)	13452(9)	4785(7)	8997(9)	52(4)
C(29)	12082(9)	5293(7)	9346(9)	50(4)
C(30)	12462(10)	5402(10)	8851(12)	79(6)
O(30)	13270(7)	5385(6)	8933(6)	69(4)
S(31)	6087(2)	2606(2)	7730(2)	46(1)
C(32)	6251(8)	3124(6)	8502(8)	38(3)
N(33)	6913(6)	3526(5)	8751(6)	40(3)
C(34)	7595(8)	3356(7)	8675(8)	47(4)
O(35)	7785(4)	2779(4)	8505(5)	36(2)
N(36)	5705(6)	3163(6)	8864(6)	41(3)
C(37)	4920(8)	2821(7)	8657(7)	42(4)
C(38)	4329(8)	3297(7)	8817(7)	41(3)
C(39)	5841(8)	3558(7)	9547(8)	47(4)
C(40)	5223(8)	3993(8)	9670(9)	54(4)
O(40)	4444(6)	3658(5)	9471(6)	54(3)
S(41)	11881(2)	3358(2)	7849(2)	46(1)
C(42)	11764(9)	2728(8)	7134(7)	44(4)
N(43)	11102(7)	2364(6)	6825(6)	43(3)
C(44)	10527(8)	2219(6)	7096(7)	36(3)
O(45)	10521(5)	2300(4)	7682(5)	34(2)
N(46)	12376(8)	2656(8)	6834(7)	65(4)
C(47)	13148(9)	3025(10)	7050(11)	78(6)
C(48)	13794(11)	2614(11)	6974(11)	79(6)
C(49)	12325(12)	2173(14)	6164(10)	104(9)
C(50)	12972(12)	1763(11)	6138(12)	92(7)
O(50)	13730(8)	2161(7)	6348(8)	80(4)
S(51)	6531(2)	770(2)	7360(2)	48(1)
C(52)	6550(9)	949(7)	6649(8)	48(4)
N(53)	7186(8)	1102(7)	6440(6)	52(3)
C(54)	7787(7)	1482(6)	6817(7)	32(3)
O(55)	7841(5)	1822(4)	7390(5)	39(2)
N(56)	5889(9)	783(12)	6223(8)	109(8)
C(57)	5159(14)	447(12)	6272(13)	99(8)
C(58)	4479(11)	702(12)	6058(16)	106(10)
C(59)	5837(15)	970(20)	5644(14)	190(20)
C(60)	5154(15)	1107(13)	5409(13)	127(12)

O(60)	4428(10)	787(9)	5474(9)	108(6)
C(61)	10209(8)	1223(6)	9106(6)	35(3)
C(62)	10301(8)	687(6)	9289(7)	39(3)
C(63)	9681(8)	309(7)	9342(8)	47(4)
C(64)	8926(8)	456(7)	9209(7)	44(4)
C(65)	8847(8)	1008(7)	9040(7)	37(3)
N(66)	9461(7)	1383(6)	8977(6)	41(3)
C(71)	9601(7)	4159(6)	9029(6)	31(3)
C(72)	9509(8)	4801(6)	9170(8)	42(4)
C(73)	8762(8)	4994(7)	9147(8)	46(4)
C(74)	8139(7)	4521(6)	8982(8)	40(4)
C(75)	8265(7)	3888(6)	8859(7)	35(3)
N(76)	8991(6)	3707(5)	8867(5)	30(2)
C(81)	9790(7)	1892(5)	6636(6)	28(3)
C(82)	9783(9)	1669(6)	5991(7)	40(3)
C(83)	9099(8)	1349(7)	5576(7)	40(3)
C(84)	8440(10)	1293(7)	5844(7)	48(4)
C(85)	8480(7)	1535(6)	6491(6)	30(3)
N(86)	9146(7)	1823(5)	6883(5)	39(3)
O(91)	9202(16)	2865(10)	9722(8)	171(12)
C(92)	9210(40)	3354(17)	10115(10)	440(50)
Ba(1A)	9102(1)	-3286(1)	6772(1)	32(1)
Mn(2A)	10370(1)	-1782(1)	6962(1)	38(1)
O(5A)	7709(6)	-4030(5)	6031(5)	44(3)
S(11A)	10323(2)	-1145(2)	6170(2)	48(1)
C(12A)	9424(9)	-887(6)	6336(6)	37(3)
N(13A)	8770(7)	-1293(5)	6152(6)	42(3)
C(14A)	8682(9)	-1849(6)	6244(6)	36(3)
O(15A)	9136(5)	-2063(4)	6603(5)	38(2)
N(16A)	9361(7)	-272(6)	6612(6)	47(3)
C(17A)	9990(10)	246(7)	6745(8)	51(4)
C(18A)	10068(11)	701(8)	7437(8)	62(5)
C(19A)	8610(8)	-50(6)	6770(7)	46(4)
C(20A)	8757(10)	386(8)	7434(8)	55(4)
O(20A)	9320(7)	908(5)	7564(5)	55(3)
S(31A)	11861(2)	-1764(2)	7131(2)	54(1)
C(32A)	11874(9)	-2243(8)	6325(9)	54(4)

N(33A)	11614(7)	-2837(6)	6078(6)	46(3)
O(35A)	10395(5)	-2792(4)	6399(5)	41(2)
N(36A)	12249(9)	-1941(6)	5976(7)	63(4)
C(37A)	12536(15)	-1267(10)	6116(13)	102(8)
C(38A)	13221(14)	-1178(11)	5870(11)	91(7)
C(39A)	12256(17)	-2253(13)	5261(11)	108(9)
C(40A)	12915(15)	-2191(11)	5060(12)	99(8)
O(40A)	13140(8)	-1489(7)	5244(7)	86(4)
O(45A)	8092(6)	-3863(5)	7341(5)	42(2)
S(51A)	10398(2)	-743(2)	7890(2)	48(1)
C(52A)	10840(8)	-1037(8)	8463(8)	48(4)
N(53A)	10520(7)	-1485(6)	8640(6)	43(3)
C(54A)	10074(8)	-2005(6)	8236(7)	35(3)
O(55A)	10035(5)	-2225(5)	7638(5)	41(2)
N(56A)	11525(8)	-742(7)	8801(8)	64(4)
C(57A)	11974(13)	-205(12)	8717(16)	119(11)
C(58A)	12722(16)	-170(20)	8790(19)	220(30)
C(59A)	11966(12)	-993(12)	9261(14)	122(12)
C(60A)	12751(17)	-890(30)	9303(18)	190(20)
O(60A)	13159(8)	-419(11)	9198(9)	117(7)
C(61A)	7249(7)	-3247(6)	5575(7)	38(3)
C(62A)	6683(9)	-3090(7)	5168(8)	55(5)
C(63A)	6744(10)	-2515(8)	5140(9)	56(4)
C(64A)	7412(9)	-2083(7)	5483(8)	49(4)
C(65A)	7946(8)	-2282(6)	5865(6)	31(3)
N(66A)	7877(7)	-2865(5)	5920(6)	39(3)
C(85A)	9621(7)	-2384(6)	8536(7)	33(3)
N(86A)	9081(7)	-2852(6)	8130(5)	39(3)
O(91A)	10265(9)	-3716(8)	7535(6)	96(5)
C(92A)	10247(15)	-4148(13)	7883(11)	107(9)
Cl(1C)	4271(8)	7996(8)	9286(10)	287(10)
C(1D)	4390(20)	7305(18)	8620(17)	169(17)
Cl(1E)	4052(4)	6597(5)	8700(5)	153(4)
Cl(2C)	4464(7)	7125(4)	4354(5)	169(4)
C(2D)	4325(16)	6501(10)	3638(13)	112(10)
Cl(2E)	5192(4)	6159(4)	3540(4)	122(2)
Cl(3C)	2318(4)	988(4)	2371(4)	110(2)

C(3D)	1642(13)	1348(12)	1991(12)	94(8)
Cl(3E)	1758(4)	1230(3)	1213(3)	91(2)
Cl(4C)	6716(9)	7433(6)	7253(8)	238(6)
C(4D)	6070(20)	6740(15)	6988(15)	152(13)
Cl(4E)	5840(10)	6584(9)	7640(7)	275(9)
O(1B)	1655(11)	6970(9)	7626(10)	116(6)
C(1B)	2330(20)	6700(20)	7460(16)	210(20)
O(2B)	9767(16)	2870(11)	5169(9)	159(10)
C(2B)	10582(16)	2730(20)	5085(14)	220(30)
O(1F)	3039(14)	4822(8)	7239(8)	139(8)
O(2F)	4257(13)	9287(7)	7502(7)	134(8)
O(4F)	7712(16)	9645(12)	3100(20)	370(30)
O(5F)	1984(13)	7286(13)	9310(20)	270(20)
O(6F)	2340(8)	4005(6)	6039(6)	74(4)
O(7F)	7760(30)	9753(11)	4830(20)	440(40)
O(8F)	4390(20)	8069(13)	7423(15)	251(18)
O(9F)	8907(19)	9541(14)	4771(19)	310(20)
O(10F)	5197(7)	8175(7)	5959(8)	88(4)
Mn(1A)	7732(1)	-4744(1)	6502(1)	36(1)
S(21A)	7808(2)	-5914(2)	5776(2)	39(1)
S(41A)	7466(3)	-5247(2)	7329(2)	52(1)
S(1A)	6255(2)	-4934(2)	6081(3)	60(1)
O(25A)	8943(6)	-4597(5)	6392(5)	48(3)
N(23A)	9400(7)	-5576(5)	6066(5)	35(3)
N(26A)	8899(7)	-6352(5)	6454(5)	39(3)
C(74A)	10609(8)	-5096(7)	5637(7)	39(3)
N(43A)	7678(7)	-4061(6)	8216(6)	46(3)
N(46A)	6638(7)	-4733(6)	8211(7)	52(3)
C(75A)	10115(8)	-4708(6)	5955(7)	33(3)
C(82A)	8750(9)	-3095(7)	9035(7)	42(3)
C(71A)	10814(9)	-3822(7)	5954(7)	37(3)
N(6A)	5950(9)	-5319(7)	4824(9)	71(5)
C(72A)	11340(8)	-4172(7)	5604(7)	41(3)
N(76A)	10201(8)	-4056(7)	6099(6)	55(4)
C(84A)	9725(9)	-2245(7)	9198(7)	47(4)
C(81A)	8664(8)	-3192(6)	8391(7)	35(3)
C(42A)	7235(9)	-4628(8)	7924(7)	44(4)

C(24A)	9394(9)	-4986(8)	6149(6)	43(4)
C(22A)	8749(8)	-5946(5)	6123(6)	32(3)
C(83A)	9270(10)	-2624(8)	9439(7)	57(5)
C(34A)	10934(8)	-3086(6)	6169(7)	40(4)
C(44A)	8108(8)	-3764(7)	7934(7)	39(3)
C(2A)	6301(9)	-4854(7)	5358(9)	57(5)
O(30A)	9131(6)	-6788(4)	7503(5)	45(3)
C(28A)	8362(9)	-6710(8)	7232(8)	47(4)
C(30A)	9650(10)	-6323(8)	7437(8)	54(4)
C(29A)	9703(9)	-6376(8)	6765(8)	52(4)
C(27A)	8316(10)	-6796(7)	6533(8)	49(4)
C(48A)	5333(12)	-5271(12)	8176(13)	95(8)
C(9A)	5944(13)	-5243(11)	4189(10)	83(7)
C(73A)	11221(12)	-4826(10)	5447(8)	76(7)
C(47A)	6152(11)	-5308(9)	8061(10)	74(6)
C(50A)	5709(12)	-4265(11)	8907(14)	101(8)
C(7A)	5594(15)	-5908(9)	4796(14)	103(9)
C(49A)	6493(14)	-4285(13)	8832(11)	107(9)
C(8A)	5870(20)	-6468(14)	4386(17)	145(14)
C(10A)	6168(19)	-5830(20)	3778(18)	152(13)
N(3A)	6572(7)	-4297(5)	5277(7)	48(3)
O(50A)	5307(9)	-4858(8)	8779(8)	96(5)
C(4A)	7175(9)	-3922(7)	5646(8)	49(4)
O(10A)	5824(16)	-6414(9)	3754(14)	164(11)
O(3F)	6386(10)	9174(8)	6075(14)	257(19)

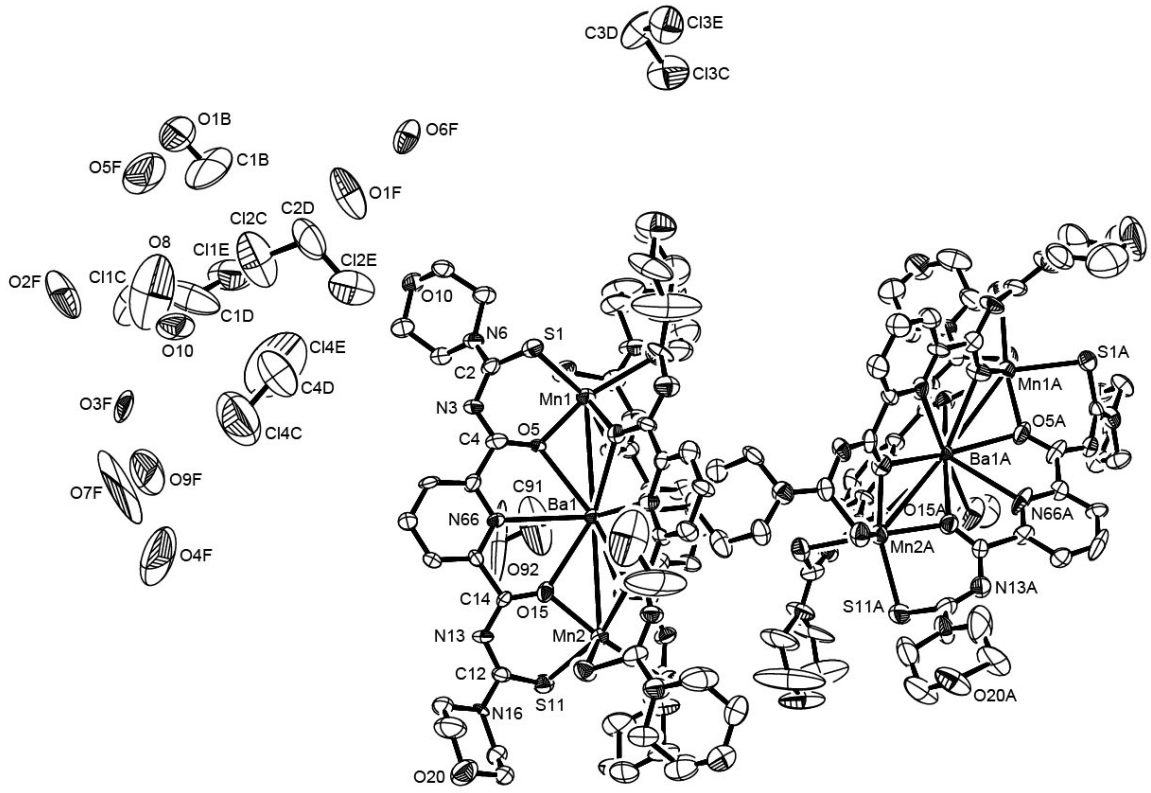

Fig A20 Ellipsoid plot (50% probability) of $[BaMn_2(L^b)_3(CH_3OH)]_2 \cdot 4CH_2Cl_2 \cdot 2CH_3OH \cdot 10H_2O$.

21) $[BaCo_2(L^a)_3(CH_3OH)]\cdot CH_3OH$

Table A41 Crystal data and structure refinement for $[BaCo_2(L^a)_3(CH_3OH)]\cdot CH_3OH$

Empirical formula	$C_{53}H_{77}BaCo_2N_{15}O_8S_6$	
Formula weight	1499.86	
Temperature	200(2) K	
Wavelength	0.71073 Å	
Crystal system	Triclinic	
Space group	$P\bar{1}$	
Unit cell dimensions	a = 10.364(1) Å	α = 72.99(1)°
	b = 17.934(1) Å	β = 86.04(1)°
	c = 19.168(1) Å	γ = 78.65(1)°
Volume	3340.0(4) $Å^3$	
Z	2	
Density (calculated)	1.491 g/cm^3	
Absorption coefficient	1.322 mm^{-1}	
F(000)	1540	
Crystal description	Plate	
Crystal color	Brown	
Crystal size	0.620 x 0.290 x 0.010 mm^3	
Theta range for data collection	3.21 to 29.24	
Index ranges	-14<=h<=12, -23<=k<=24, -26<=l<=26	
Reflections collected	38107	
Independent reflections	17924 [R(int) = 0.0560]	
Completeness to theta = 29.24°	98.7 %	
Absorption correction	Integration	
Max. and min. transmission	0.9293 and 0.7043	
Refinement method	Full-matrix least-squares on F^2	
Data / restraints / parameters	17924 / 0 / 783	
Goodness-of-fit on F^2	0.875	
Final R indices [I>2sigma(I)]	R1 = 0.0472, wR2 = 0.1068	
R indices (all data)	R1 = 0.1005, wR2 = 0.1273	
Largest diff. peak and hole	1.115 and -1.085 $e.Å^{-3}$	

Table A42 Atomic coordinates (x 10^4) and equivalent isotropic displacement parameters ($Å^2$x 10^3) for $[BaCo_2(L^a)_3(CH_3OH)]\cdot CH_3OH$. U(eq) is defined as one third of the trace of the orthogonalized U^{ij} tensor.

	x	y	z	U(eq)
Ba(1)	1095(1)	709(1)	2541(1)	33(1)
Co(1)	747(1)	-1394(1)	3014(1)	37(1)
Co(2)	1380(1)	2817(1)	2161(1)	38(1)
S(1)	2255(1)	-2507(1)	3868(1)	43(1)
C(2)	3553(4)	-2493(2)	3266(2)	40(1)
N(3)	4193(3)	-1871(2)	3006(2)	39(1)
C(4)	3602(4)	-1128(2)	2914(2)	35(1)
O(5)	2390(3)	-842(2)	2875(2)	38(1)
N(6)	4076(4)	-3144(2)	3062(2)	53(1)
C(7)	3538(7)	-3875(3)	3320(3)	71(2)
C(8)	4203(8)	-4434(4)	3988(5)	114(3)
C(9)	5166(6)	-3137(3)	2526(3)	65(2)
C(10)	4680(7)	-2883(4)	1746(3)	78(2)
S(11)	3180(1)	3349(1)	1332(1)	46(1)
C(12)	4493(5)	2910(3)	1914(2)	46(1)
N(13)	4843(4)	2121(2)	2228(2)	48(1)
C(14)	4027(4)	1609(2)	2382(2)	41(1)
O(15)	2786(3)	1748(2)	2417(2)	40(1)
N(16)	5308(4)	3337(2)	2058(2)	53(1)
C(17)	5210(6)	4185(3)	1714(3)	60(1)
C(18)	4693(9)	4664(4)	2221(4)	101(3)
C(19)	6424(6)	2940(3)	2563(3)	69(2)
C(20)	5970(8)	2712(5)	3350(4)	101(3)
S(21)	-1038(1)	-2046(1)	3525(1)	55(1)
C(22)	-1782(5)	-1656(3)	4202(3)	55(1)
N(23)	-1695(4)	-968(2)	4331(2)	46(1)
C(24)	-880(4)	-491(3)	4017(2)	39(1)
O(25)	67(3)	-560(2)	3576(1)	39(1)
N(26)	-2593(6)	-2063(3)	4673(3)	89(2)
C(27A)	-2556(12)	-2910(6)	4834(6)	67(2)
C(27B)	-3231(15)	-2678(8)	4363(8)	67(2)

C(28A)	-3804(19)	-2973(9)	4529(9)	121(5)
C(28B)	-2450(20)	-3482(11)	4823(10)	121(5)
C(29)	-3247(8)	-1772(4)	5268(4)	101(3)
C(30)	-4465(8)	-1177(5)	5009(5)	119(3)
S(31)	1911(1)	3432(1)	3047(1)	53(1)
C(32)	534(5)	3400(3)	3594(2)	51(1)
N(33)	-55(4)	2766(2)	3879(2)	49(1)
C(34)	-49(4)	2181(3)	3589(2)	40(1)
O(35)	339(3)	2120(2)	2966(2)	43(1)
N(36)	8(6)	4018(3)	3841(3)	78(2)
C(37A)	720(20)	4697(9)	3722(10)	87(4)
C(37B)	130(20)	4874(11)	3375(12)	87(4)
C(38A)	-70(20)	5410(11)	3413(14)	179(8)
C(38B)	900(30)	5104(13)	3939(17)	179(8)
C(39)	-1117(9)	3966(4)	4371(4)	102(3)
C(40)	-2392(10)	4111(7)	4008(7)	163(5)
S(41)	1098(1)	-2126(1)	2109(1)	53(1)
C(42)	-216(5)	-1660(3)	1556(2)	49(1)
N(43)	-577(4)	-872(2)	1238(2)	42(1)
C(44)	-391(4)	-319(2)	1521(2)	37(1)
O(45)	-14(3)	-388(2)	2157(1)	38(1)
N(46)	-960(5)	-2088(3)	1336(3)	71(1)
C(47)	-1091(10)	-3017(6)	1809(5)	129(4)
C(48)	-207(10)	-3307(8)	1384(4)	150(5)
C(49)	-1963(6)	-1707(3)	779(3)	65(2)
C(50)	-3229(6)	-1306(4)	1067(3)	76(2)
S(51)	-249(1)	3989(1)	1657(1)	49(1)
C(52)	-957(4)	3880(2)	921(2)	41(1)
N(53)	-1041(4)	3193(2)	777(2)	46(1)
C(54)	-373(4)	2486(2)	1084(2)	38(1)
O(55)	585(3)	2255(2)	1522(2)	41(1)
N(56)	-1575(4)	4532(2)	423(2)	49(1)
C(57)	-1544(5)	5343(3)	433(2)	47(1)
C(58)	-2749(5)	5728(3)	765(3)	63(1)
C(59)	-2159(7)	4453(3)	-239(4)	85(2)
C(60)	-3380(8)	4216(5)	-81(4)	106(3)
C(61)	4517(4)	-546(2)	2803(2)	35(1)

C(62)	5872(4)	-790(3)	2809(2)	44(1)
C(63)	6665(5)	-226(3)	2690(3)	50(1)
C(64)	6081(5)	560(3)	2557(3)	50(1)
C(65)	4717(4)	763(2)	2558(2)	39(1)
N(66)	3938(3)	219(2)	2692(2)	35(1)
C(71)	-1115(4)	265(3)	4255(2)	40(1)
C(72)	-1858(5)	309(3)	4876(2)	47(1)
C(73)	-1950(5)	978(3)	5108(2)	49(1)
C(74)	-1344(5)	1587(3)	4705(2)	45(1)
C(75)	-644(4)	1505(3)	4076(2)	39(1)
N(76)	-521(3)	852(2)	3853(2)	37(1)
C(81)	-772(4)	511(2)	1032(2)	36(1)
C(82)	-1357(4)	652(3)	362(2)	43(1)
C(83)	-1713(5)	1426(3)	-63(2)	47(1)
C(84)	-1447(5)	2035(3)	173(2)	43(1)
C(85)	-802(4)	1846(2)	834(2)	39(1)
N(86)	-492(3)	1097(2)	1262(2)	35(1)
O(91)	2484(3)	585(2)	1206(2)	59(1)
C(92)	3279(6)	-70(4)	1049(3)	72(2)
O(93)	3647(4)	1902(3)	595(2)	74(1)
C(94)	5015(7)	1842(5)	455(4)	89(2)

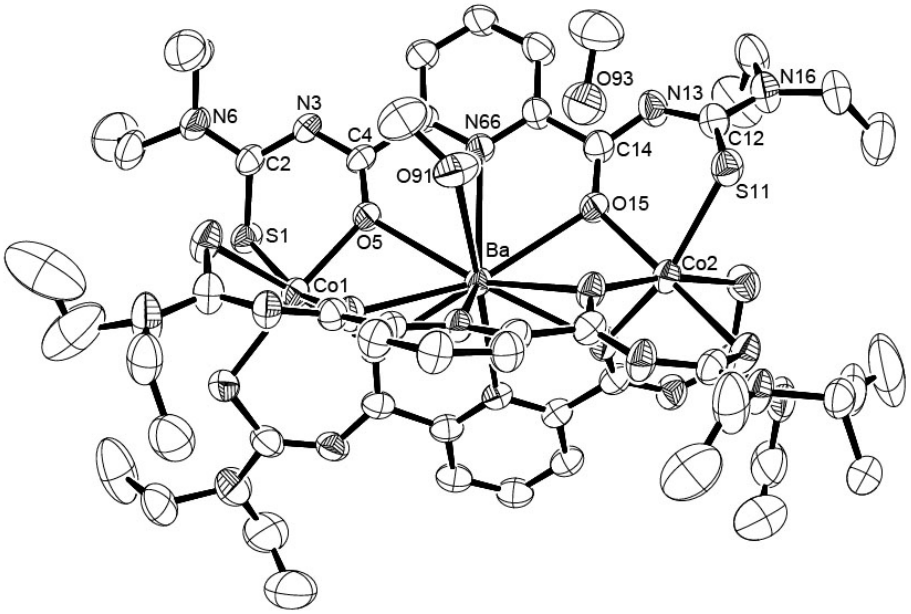

Fig A21 Ellipsoid plot (50% probability) of $[BaCo_2(L^a)_3(CH_3OH)]\cdot CH_3OH$.

22) $[BaCo_2(L^b)_3]\cdot 8H_2O$

Table A43 Crystal data and structure refinement for $[BaCo_2(L^b)_3]\cdot 8H_2O$.

Empirical formula	$C_{51}H_{57}BaCo_2N_{15}O_{20}S_6$	
Formula weight	1647.48	
Temperature	200(2) K	
Wavelength	0.71073 Å	
Crystal system	Tetragonal	
Space group	$I4_1/a$	
Unit cell dimensions	a = 43.450(2) Å	α = 90°
	b = 43.450(2) Å	β = 90°
	c = 18.621(1) Å	γ = 90°
Volume	35155(3) $Å^3$	
Z	16	
Density (calculated)	1.245 g/cm^3	
Absorption coefficient	1.021 mm^{-1}	
F(000)	13344	
Crystal description	Prism	
Crystal color	Brown	
Crystal size	0.600 x 0.347 x 0.200 mm^3	
Theta range for data collection	1.51 to 29.32	
Index ranges	-59<=h<=59, -59<=k<=59, -25<=l<=23	
Reflections collected	328129	
Independent reflections	23866 [R(int) = 0.1458]	
Completeness to theta = 29.32°	99.1 %	
Absorption correction	None	
Refinement method	Full-matrix least-squares on F^2	
Data / restraints / parameters	23866 / 0 / 875	
Goodness-of-fit on F^2	1.012	
Final R indices [I>2sigma(I)]	R1 = 0.0914, wR2 = 0.2405	
R indices (all data)	R1 = 0.1524, wR2 = 0.2761	
Largest diff. peak and hole	2.362 and -1.171 $e.Å^{-3}$	

Table A44 Atomic coordinates (x 10^4) and equivalent isotropic displacement parameters ($Å^2$x 10^3) for $[BaCo_2(L^b)_3]\cdot 8H_2O$. U(eq) is defined as one third of the trace of the orthogonalized U^{ij} tensor.

	x	y	z	U(eq)
Ba	1603(1)	1550(1)	5237(1)	50(1)
Co(1)	1533(1)	2041(1)	6834(1)	53(1)
Co(2)	1661(1)	1077(1)	3617(1)	57(1)
S(1)	1026(1)	2218(1)	7282(1)	61(1)
C(2)	965(2)	2492(2)	6640(4)	56(2)
N(3)	944(1)	2433(1)	5929(4)	58(2)
C(4)	1101(2)	2227(2)	5579(4)	54(2)
O(5)	1339(1)	2073(1)	5804(3)	57(1)
N(6)	913(2)	2785(1)	6815(4)	60(2)
C(7)	944(2)	2913(2)	7544(5)	69(2)
C(8)	1172(2)	3179(2)	7517(6)	79(2)
C(9)	834(2)	3030(2)	6288(5)	77(2)
C(10)	1049(2)	3282(2)	6304(6)	83(3)
O(10)	1076(2)	3416(1)	7005(4)	79(2)
S(11)	1174(1)	859(1)	3150(2)	80(1)
C(12)	1065(2)	1178(2)	2668(5)	78(2)
N(13)	1021(2)	1466(2)	2948(4)	76(2)
C(14)	1164(2)	1567(2)	3527(4)	60(2)
O(15)	1388(1)	1456(1)	3853(3)	60(1)
N(16)	989(3)	1148(2)	1993(5)	71(2)
C(17)	1017(5)	874(4)	1558(10)	86(3)
C(19)	908(7)	1417(4)	1549(10)	87(3)
C(18)	852(14)	870(20)	840(20)	146(6)
C(20)	794(9)	1305(6)	821(11)	115(4)
O(20)	736(6)	991(7)	786(18)	121(3)
S(21)	1710(1)	2544(1)	7068(1)	68(1)
C(22)	2089(2)	2575(2)	6788(4)	57(2)
N(23)	2221(1)	2429(1)	6261(4)	61(2)
C(24)	2126(2)	2166(2)	5958(4)	57(2)
O(25)	1931(1)	1973(1)	6176(3)	56(1)
N(26)	2263(2)	2790(1)	7134(4)	64(2)
C(27)	2155(2)	3000(2)	7682(5)	73(2)

C(28)	2124(2)	3320(2)	7374(6)	87(3)
C(29)	2560(2)	2891(2)	6843(6)	77(2)
C(30)	2516(2)	3225(2)	6551(6)	85(3)
O(30)	2408(2)	3426(1)	7096(5)	92(2)
S(31)	1829(1)	1243(1)	2444(1)	79(1)
C(32)	2196(3)	1360(3)	2576(6)	96(3)
N(33)	2302(2)	1544(2)	3127(5)	92(3)
C(34)	2179(2)	1560(2)	3771(5)	65(2)
O(35)	1984(1)	1385(1)	4062(3)	59(1)
N(36)	2408(3)	1319(4)	2066(7)	115(3)
C(37)	2707(4)	1458(6)	2173(15)	177(8)
C(38)	2910(4)	1283(5)	1867(10)	163(7)
C(39)	2354(4)	1143(7)	1397(11)	241(1)
C(40)	2573(5)	979(6)	1206(12)	218(1)
O(40)	2881(3)	1084(3)	1232(7)	168(5)
S(41)	1659(1)	1897(1)	8102(1)	67(1)
C(42)	1382(2)	1618(2)	8194(4)	58(2)
N(43)	1372(2)	1359(1)	7805(3)	58(1)
C(44)	1451(2)	1350(2)	7127(4)	52(2)
O(45)	1496(1)	1564(1)	6691(3)	52(1)
N(46)	1174(2)	1635(2)	8717(4)	72(2)
C(47)	1153(3)	1883(2)	9251(6)	88(3)
C(48)	823(4)	2001(4)	9256(8)	151(7)
C(49)	945(2)	1393(3)	8847(6)	86(3)
C(50)	633(3)	1556(4)	8867(9)	129(5)
O(50)	606(2)	1778(3)	9401(5)	119(3)
S(51)	1958(1)	605(1)	3550(1)	67(1)
C(52)	1739(2)	370(2)	4094(4)	56(2)
N(53)	1650(1)	437(1)	4766(3)	58(1)
C(54)	1599(2)	715(2)	5018(4)	53(2)
O(55)	1575(1)	964(1)	4685(3)	57(1)
N(56)	1666(2)	85(1)	3873(4)	63(2)
C(57)	1736(2)	-37(2)	3162(5)	67(2)
C(58)	1435(2)	-123(2)	2785(5)	75(2)
C(59)	1479(2)	-127(2)	4298(5)	66(2)
C(60)	1193(2)	-207(2)	3894(5)	70(2)
O(60)	1261(1)	-337(1)	3210(3)	72(2)

C(61)	1012(2)	2173(2)	4824(4)	59(2)
C(62)	800(2)	2370(2)	4499(5)	73(2)
C(63)	720(3)	2312(2)	3792(6)	93(3)
C(64)	834(2)	2045(2)	3447(5)	84(3)
C(65)	1036(2)	1860(2)	3828(4)	61(2)
N(66)	1136(1)	1931(1)	4504(4)	58(1)
C(71)	1473(2)	1024(2)	6823(4)	56(2)
C(72)	1455(2)	765(2)	7264(5)	76(2)
C(73)	1484(3)	486(2)	6965(5)	95(3)
C(74)	1530(2)	458(2)	6217(5)	77(2)
C(75)	1545(2)	725(2)	5818(4)	54(2)
N(76)	1519(1)	1004(1)	6104(3)	51(1)
C(81)	2301(2)	2084(2)	5273(5)	71(2)
C(82)	2567(3)	2229(3)	5110(8)	132(6)
C(83)	2694(4)	2184(5)	4456(11)	222(1)
C(84)	2583(3)	1950(4)	4036(9)	161(8)
C(85)	2314(2)	1806(2)	4226(5)	72(2)
N(86)	2174(1)	1873(1)	4846(4)	63(2)
O(91)	697(2)	697(2)	7504(5)	112(3)
O(92)	93(2)	815(2)	8095(8)	164(5)
O(93)	269(2)	2427(2)	8110(10)	175(6)
O(94)	49(3)	2715(2)	5309(8)	155(4)
O(95)	3657(3)	826(3)	2421(7)	163(4)

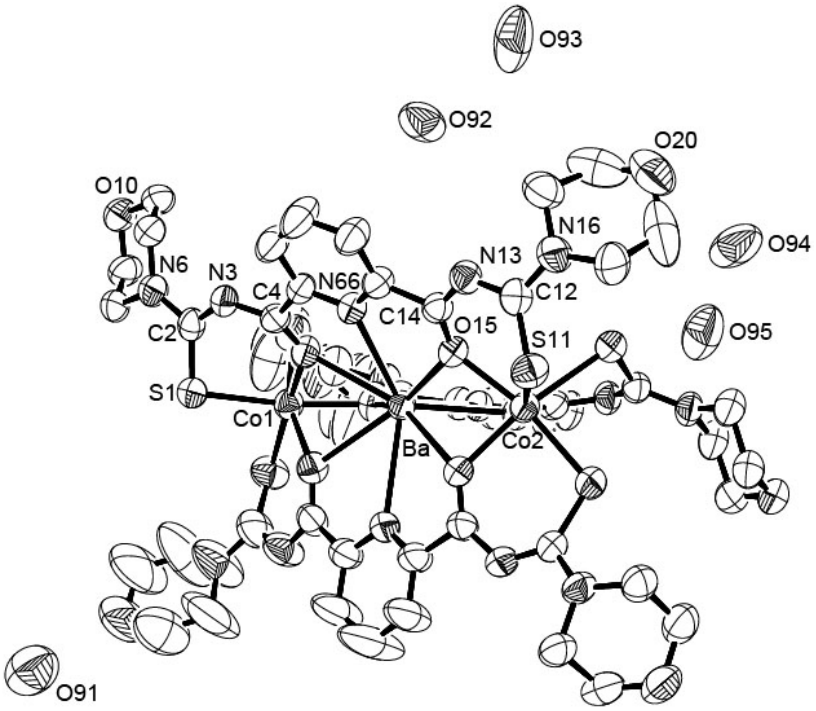

Fig A22 Ellipsoid plot (50% probability) of $[BaCo_2(L^b)_3]\cdot 8H_2O$.

23) $[BaNi_2(L^b)_3]\cdot CH_3OH\cdot CH_2Cl_2\cdot 2H_2O$

Table A45 Crystal data and structure refinement for $[BaNi_2(L^b)_3]\cdot CH_3OH\cdot CH_2Cl_2\cdot 2H_2O$.

Empirical formula	$C_{53}H_{63}BaCl_2N_{15}Ni_2O_{15}S_6$	
Formula weight	1668.20	
Temperature	200(2) K	
Wavelength	0.71073 Å	
Crystal system	Monoclinic	
Space group	$P2_1/c$	
Unit cell dimensions	a = 17.692(1) Å	α = 90°
	b = 18.463(1) Å	β = 95.57(1)°
	c = 20.982(1) Å	γ = 90°
Volume	6821.4(6) $Å^3$	
Z	4	
Density (calculated)	1.624 g/cm^3	
Absorption coefficient	1.452 mm^{-1}	
F(000)	3392	
Crystal description	Prism	
Crystal color	Brown	
Crystal size	0.240 x 0.190 x 0.060 mm^3	
Theta range for data collection	2.61 to 29.35	
Index ranges	-24<=h<=24, -25<=k<=19, -28<=l<=28	
Reflections collected	70490	
Independent reflections	18427 [R(int) = 0.2423]	
Completeness to theta = 29.35°	98.3 %	
Absorption correction	Integration	
Max. and min. transmission	0.9502 and 0.8182	
Refinement method	Full-matrix least-squares on F^2	
Data / restraints / parameters	18427 / 1 / 849	
Goodness-of-fit on F^2	0.744	
Final R indices [I>2sigma(I)]	R1 = 0.0646, wR2 = 0.0940	
R indices (all data)	R1 = 0.2255, wR2 = 0.1276	
Largest diff. peak and hole	1.800 and -0.890 $e.Å^{-3}$	

Table A46 Atomic coordinates (x 10^4) and equivalent isotropic displacement parameters ($Å^2$x 10^3) for $[BaNi_2(L^b)_3]\cdot CH_3OH\cdot CH_2Cl_2\cdot 2H_2O$. U(eq) is defined as one third of the trace of the orthogonalized U^{ij} tensor.

	x	y	z	U(eq)
Ba	5336(1)	1462(1)	2383(1)	18(1)
Ni(1)	3417(1)	1503(1)	2853(1)	21(1)
Ni(2)	7251(1)	1392(1)	1922(1)	20(1)
S(1)	2826(1)	2512(1)	3316(1)	26(1)
C(2)	2719(5)	3094(5)	2664(4)	22(2)
N(3)	3284(4)	3285(4)	2310(3)	22(2)
C(4)	3884(5)	2882(5)	2236(4)	18(2)
O(5)	3995(3)	2220(4)	2318(3)	21(1)
N(6)	2061(4)	3424(4)	2521(3)	23(2)
C(7)	1405(5)	3388(6)	2883(4)	29(2)
C(8)	727(5)	3158(6)	2447(5)	44(3)
C(9)	1930(5)	3902(6)	1946(4)	36(3)
C(10)	1222(5)	3633(8)	1553(4)	45(3)
O(10)	590(3)	3634(5)	1917(3)	48(2)
S(11)	7558(1)	1873(1)	911(1)	27(1)
C(12)	7539(5)	2785(5)	1072(4)	20(2)
N(13)	6985(4)	3144(4)	1344(4)	23(2)
C(14)	6465(5)	2838(5)	1670(4)	18(2)
O(15)	6472(3)	2206(3)	1907(3)	22(1)
N(16)	8092(4)	3214(5)	884(4)	24(2)
C(17)	8666(5)	2961(6)	450(5)	32(2)
C(18)	9422(5)	3304(6)	682(5)	35(3)
C(19)	8108(5)	4006(5)	989(5)	29(2)
C(20)	8897(5)	4252(6)	1169(5)	35(2)
O(20)	9399(3)	4058(4)	706(3)	32(2)
S(21)	2933(1)	674(1)	3610(1)	24(1)
C(22)	3378(5)	1050(5)	4297(4)	25(2)
N(23)	4141(4)	1108(4)	4426(3)	21(2)
C(24)	4602(4)	1252(5)	3980(4)	22(2)
O(25)	4454(3)	1516(4)	3432(2)	22(1)
N(26)	2978(4)	1227(5)	4780(3)	34(2)

C(27)	2145(5)	1155(6)	4758(5)	36(3)
C(28)	1802(6)	1880(7)	4860(5)	48(3)
C(29)	3317(5)	1579(7)	5375(4)	45(3)
C(30)	2924(6)	2300(7)	5467(5)	46(3)
O(30)	2125(4)	2222(5)	5450(3)	53(2)
S(31)	8190(1)	2083(1)	2597(1)	26(1)
C(32)	8384(4)	1394(6)	3159(4)	24(2)
N(33)	7871(4)	1122(4)	3525(3)	21(2)
C(34)	7150(4)	1065(5)	3333(4)	21(2)
O(35)	6822(3)	1101(3)	2779(3)	23(1)
N(36)	9096(4)	1158(4)	3267(3)	27(2)
C(37)	9739(4)	1394(6)	2938(4)	29(2)
C(38)	10394(5)	1586(7)	3423(6)	52(3)
C(39)	9307(5)	570(6)	3729(5)	38(3)
C(40)	9962(5)	812(6)	4183(5)	40(3)
O(40)	10597(4)	999(4)	3848(3)	43(2)
S(41)	2367(1)	1234(1)	2058(1)	29(1)
C(42)	2444(4)	306(5)	2051(4)	25(2)
N(43)	3087(4)	-69(4)	1963(3)	24(2)
C(44)	3794(5)	188(5)	2076(4)	21(2)
O(45)	4006(3)	741(4)	2395(3)	24(2)
N(46)	1838(4)	-104(5)	2093(3)	27(2)
C(47)	1099(5)	165(6)	2198(4)	32(2)
C(48)	483(5)	-174(6)	1730(5)	36(2)
C(49)	1868(5)	-907(5)	2074(5)	31(2)
C(50)	1233(5)	-1181(6)	1595(5)	38(3)
O(50)	504(4)	-944(4)	1755(4)	43(2)
S(51)	8117(1)	427(1)	1878(1)	25(1)
C(52)	7635(5)	-75(5)	1287(4)	21(2)
N(53)	6911(4)	-311(4)	1307(4)	25(2)
C(54)	6348(5)	92(5)	1494(4)	18(2)
O(55)	6333(3)	771(3)	1581(3)	20(1)
N(56)	7984(4)	-318(5)	796(3)	27(2)
C(57)	8744(6)	-112(7)	672(5)	41(3)
C(58)	8723(6)	263(7)	32(5)	51(3)
C(59)	7599(5)	-756(6)	287(4)	40(3)
C(60)	7609(6)	-369(8)	-348(5)	60(4)

O(60)	8377(4)	-203(5)	-465(3)	59(2)
C(61)	4537(5)	3311(5)	1987(4)	21(2)
C(62)	4469(5)	4034(5)	1852(4)	25(2)
C(63)	5090(5)	4397(5)	1653(4)	26(2)
C(64)	5754(5)	4015(5)	1594(4)	21(2)
C(65)	5775(5)	3289(5)	1735(4)	21(2)
N(66)	5181(4)	2935(4)	1941(3)	18(2)
C(81)	4397(5)	-278(5)	1836(4)	19(2)
C(82)	4289(5)	-995(6)	1665(4)	27(2)
C(83)	4871(5)	-1395(6)	1456(4)	30(2)
C(84)	5550(5)	-1059(5)	1397(4)	25(2)
C(85)	5634(5)	-324(5)	1565(4)	21(2)
N(86)	5072(4)	59(4)	1786(3)	19(2)
C(71)	5422(5)	1064(5)	4191(4)	25(2)
C(72)	5668(4)	809(6)	4782(4)	31(2)
C(73)	6418(5)	638(6)	4928(4)	37(3)
C(74)	6906(5)	705(6)	4451(4)	30(2)
C(75)	6629(4)	951(5)	3862(4)	23(2)
N(76)	5902(4)	1114(4)	3708(3)	21(2)
Cl(91)	9957(2)	1553(2)	1211(1)	60(1)
C(92)	10669(6)	1662(7)	686(5)	60(4)
Cl(93)	10268(2)	1753(2)	-114(2)	65(1)
O(94)	6796(5)	2656(5)	3427(4)	62(2)
C(95)	7166(8)	2767(7)	4045(6)	69(4)
O(96)	4549(4)	1462(5)	810(3)	69(3)
O(97)	5378(5)	2425(5)	114(3)	59(2)

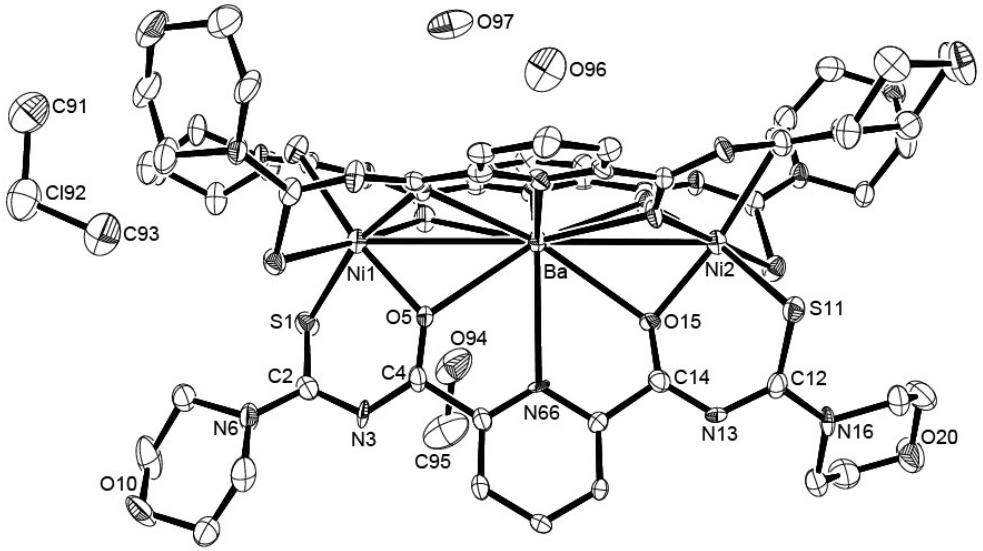

Fig A23 Ellipsoid plot (50% probability) of $[BaNi_2(L^b)_3]\cdot CH_3OH\cdot CH_2Cl_2\cdot 2H_2O$.

24) [K{ReO(OCH$_3$)}$_2$(L^a)$_2$](PF$_6$)

Table A47 Crystal data and structure refinement for [K{ReO(OCH$_3$)}$_2$(L^a)$_2$](PF$_6$).

Empirical formula	$C_{36}H_{52}F_6KN_{10}O_8PRe_2S_4$	
Formula weight	1437.59	
Temperature	200(2) K	
Wavelength	0.71073 Å	
Crystal system	Triclinic	
Space group	$P\bar{1}$	
Unit cell dimensions	a = 9.644(1) Å	α = 76.83(1)°
	b = 15.717(1) Å	β = 86.03(1)°
	c = 17.297(2) Å	γ = 88.12(1)°
Volume	2546.3(4) Å^3	
Z	2	
Density (calculated)	1.875 g/cm^3	
Absorption coefficient	5.105 mm^{-1}	
F(000)	1408	
Crystal description	Prism	
Crystal color	Red	
Crystal size	0.30 x 0.25 x 0.18 mm^3	
Theta range for data collection	3.32 to 29.24	
Index ranges	-13<=h<=13, -21<=k<=21, -19<=l<=23	
Reflections collected	27935	
Independent reflections	13662 [R(int) = 0.0523]	
Completeness to theta = 29.24°	98.7 %	
Absorption correction	Integration	
Max. and min. transmission	0.7134 and 0.4599	
Refinement method	Full-matrix least-squares on F^2	
Data / restraints / parameters	13662 / 3 / 621	
Goodness-of-fit on F^2	0.874	
Final R indices [I>2sigma(I)]	R1 = 0.0525, wR2 = 0.1220	
R indices (all data)	R1 = 0.1016, wR2 = 0.1393	
Largest diff. peak and hole	2.395 and -1.896 e.Å^{-3}	

Table A48 Atomic coordinates (x 10^4) and equivalent isotropic displacement parameters ($Å^2$x 10^3) for $[K\{ReO(OCH_3)\}_2(L^a)_2](PF_6)$. U(eq) is defined as one third of the trace of the orthogonalized U^{ij} tensor.

	x	y	z	U(eq)
K	2011(2)	2672(1)	2797(1)	74(1)
O(1)	2538(5)	911(3)	1266(3)	70(1)
Re(1)	1598(1)	1802(1)	847(1)	49(1)
O(3)	723(5)	2880(3)	513(3)	67(1)
C(62)	764(15)	3774(8)	94(8)	135(5)
O(2)	2521(7)	3264(5)	4937(3)	89(2)
Re(2)	3361(1)	2247(1)	4981(1)	84(1)
O(4)	3956(8)	1237(5)	4765(5)	98(2)
C(72)	3860(20)	845(16)	4023(13)	284(2)
S(1)	2834(2)	1987(1)	-400(1)	64(1)
C(2)	3979(8)	2829(5)	-413(4)	57(2)
N(3)	4643(6)	2938(4)	215(3)	56(1)
C(4)	4225(7)	2763(4)	970(4)	51(2)
O(5)	3015(5)	2565(3)	1294(3)	59(1)
N(6)	4368(9)	3338(4)	-1110(4)	79(2)
C(7)	3760(14)	3336(7)	-1844(5)	102(4)
C(8)	4551(18)	2767(8)	-2308(6)	133(5)
C(9)	5442(14)	4011(6)	-1179(6)	104(4)
C(10)	4810(20)	4866(8)	-1079(9)	156(6)
S(11)	5347(3)	2554(2)	5528(2)	106(1)
C(12)	6254(11)	3282(7)	4766(6)	88(3)
N(13)	6317(7)	3274(5)	3989(4)	71(2)
C(14)	5391(8)	3008(5)	3585(5)	63(2)
O(15)	4131(6)	2793(4)	3786(3)	71(1)
N(16)	7011(9)	3874(6)	4951(5)	96(3)
C(17)	7088(16)	3988(9)	5779(7)	126(4)
C(18A)	8400(30)	3551(15)	6054(12)	153(9)
C(18B)	5880(50)	4660(30)	6030(20)	153(9)
C(19)	7835(13)	4501(8)	4316(8)	115(4)
C(20A)	7000(30)	5280(12)	3842(11)	134(7)
C(20B)	9480(50)	3990(20)	4590(20)	134(7)

S(21)	-41(2)	1058(2)	349(1)	69(1)
C(22)	-1501(7)	958(5)	1010(5)	57(2)
N(23)	-1563(6)	1004(4)	1778(4)	60(2)
C(24)	-691(7)	1321(5)	2170(4)	57(2)
O(25)	407(5)	1761(3)	1928(3)	58(1)
N(26)	-2688(6)	783(4)	729(4)	62(2)
C(27)	-2769(8)	615(7)	-68(6)	79(3)
C(28)	-2995(10)	1445(8)	-688(6)	100(3)
C(29)	-4014(7)	712(5)	1224(5)	66(2)
C(30)	-4292(9)	-224(6)	1657(6)	84(3)
S(31)	2459(3)	1641(2)	6266(1)	100(1)
C(32)	732(13)	1414(8)	6204(6)	104(3)
N(33)	82(9)	1329(6)	5558(4)	95(3)
C(34)	449(10)	1554(6)	4800(5)	75(2)
O(35)	1516(6)	1975(5)	4443(3)	84(2)
N(36)	-103(13)	1233(9)	6895(5)	139(4)
C(37)	449(16)	1290(13)	7692(8)	156(7)
C(38)	177(16)	2183(12)	7804(8)	153(6)
C(39)	-1890(20)	1254(16)	6833(8)	192(9)
C(40)	-1900(30)	307(17)	6875(11)	430(4)
C(41)	5325(7)	2903(4)	1503(4)	51(2)
C(42)	6695(7)	3070(5)	1200(5)	64(2)
C(43)	7669(8)	3210(6)	1713(6)	76(2)
C(44)	7251(8)	3198(5)	2475(5)	69(2)
C(45)	5865(7)	3023(5)	2742(4)	57(2)
N(46)	4911(6)	2860(4)	2261(4)	54(1)
C(51)	-1091(7)	1188(5)	3053(5)	60(2)
C(52)	-2354(10)	791(6)	3346(6)	87(3)
C(53)	-2693(13)	683(8)	4157(7)	113(4)
C(54)	-1781(12)	923(7)	4634(6)	98(3)
C(55)	-553(9)	1303(6)	4288(5)	71(2)
N(56)	-203(6)	1447(4)	3510(4)	61(2)
P(1)	743(4)	4979(2)	2236(3)	119(1)
F(1)	165(10)	4058(6)	2704(8)	195(5)
F(2)	1261(13)	5854(7)	1842(9)	249(7)
F(3)	1250(20)	4610(16)	1575(10)	369(1)
F(4)	2163(12)	4724(9)	2555(9)	254(8)

F(6)	-678(15)	5193(11)	1939(13)	314(1)
F(5)	170(20)	5281(11)	2980(11)	306(1)

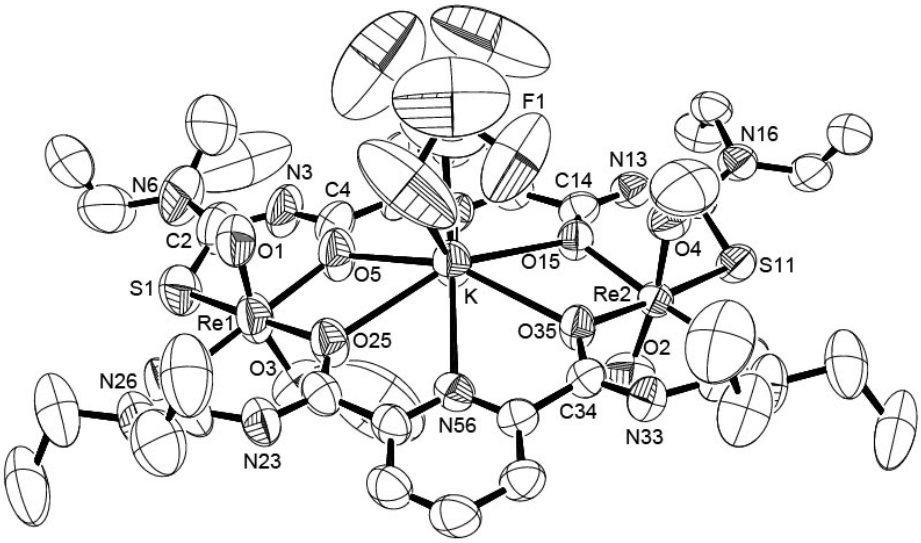

Fig A24 Ellipsoid plot (50% probability) of $[K\{ReO(OCH_3)\}_2(L^a)_2](PF_6)$.

25) [K{ReO(OCH$_3$)}$_2$(L^a)$_2$](ReO$_4$)

Table A49 Crystal data and structure refinement for [K{ReO(OCH$_3$)}$_2$(L^a)$_2$](ReO$_4$).

Empirical formula	$C_{36}H_{52}KN_{10}O_{12}Re_3S_4$	
Formula weight	1542.82	
Temperature	200(2) K	
Wavelength	0.71073 Å	
Crystal system	Triclinic	
Space group	$P\bar{1}$	
Unit cell dimensions	a = 9.387(1) Å	α = 73.97(1)°
	b = 15.691(2) Å	β = 80.02(1)°
	c = 18.372(3) Å	γ = 81.92(1)°
Volume	2549.2(6) Å^3	
Z	2	
Density (calculated)	2.010 g/cm^3	
Absorption coefficient	7.415 mm^{-1}	
F(000)	1484	
Crystal description	Prism	
Crystal color	Red	
Crystal size	0.380 x 0.280 x 0.240 mm^3	
Theta range for data collection	2.00 to 29.37	
Index ranges	-12<=h<=12, -21<=k<=21, -25<=l<=24	
Reflections collected	28410	
Independent reflections	13619 [R(int) = 0.1491]	
Completeness to theta = 29.37°	97.0 %	
Absorption correction	Integration	
Max. and min. transmission	0.6866 and 0.3638	
Refinement method	Full-matrix least-squares on F^2	
Data / restraints / parameters	13619 / 0 / 595	
Goodness-of-fit on F^2	0.854	
Final R indices [I>2sigma(I)]	R1 = 0.0734, wR2 = 0.1484	
R indices (all data)	R1 = 0.2365, wR2 = 0.2111	
Largest diff. peak and hole	1.332 and -2.211 e.Å^{-3}	

Table A50 Atomic coordinates (x 10^4) and equivalent isotropic displacement parameters ($Å^2$x 10^3) for $[K\{ReO(OCH_3)\}_2(L^a)_2](ReO_4)$. U(eq) is defined as one third of the trace of the orthogonalized U^{ij} tensor.

	x	y	z	U(eq)
K(1)	6742(4)	12166(2)	2585(2)	71(1)
Re(1)	5522(1)	14615(1)	2733(1)	61(1)
O(1)	6296(11)	14290(8)	3527(7)	74(3)
O(3)	5041(16)	14684(8)	1888(9)	100(5)
C(5)	5250(30)	14790(20)	1080(20)	162(1)
Re(2)	8460(1)	9700(1)	3343(1)	68(1)
O(2)	8749(11)	10097(8)	4069(7)	80(4)
O(4)	7972(14)	9617(9)	2605(14)	120(9)
C(6)	7550(50)	10000(30)	1930(30)	270(3)
Re(3)	6116(2)	12270(1)	328(1)	167(1)
O(11)	5892(18)	12246(14)	1225(11)	144(7)
O(12)	8050(30)	11710(20)	138(17)	249(1)
O(13)	5160(30)	11509(16)	126(17)	219(1)
O(14)	6300(50)	13247(17)	-240(20)	320(2)
S(1)	3442(5)	15374(3)	3242(4)	92(2)
C(2)	2071(16)	14687(12)	3461(12)	75(6)
N(3)	2154(12)	13772(9)	3579(9)	65(4)
C(4)	3289(15)	13239(11)	3414(10)	56(4)
O(5)	4569(10)	13382(6)	3035(7)	64(3)
N(6)	710(13)	15086(10)	3519(11)	87(5)
C(7)	380(20)	16060(14)	3543(18)	109(9)
C(8)	140(30)	16520(20)	2800(20)	171(1)
C(9)	-556(15)	14557(12)	3727(12)	70(5)
C(10)	-940(20)	14191(13)	4555(13)	91(6)
S(11)	7625(5)	8348(3)	4052(3)	79(2)
C(12)	5744(16)	8510(12)	4268(11)	63(5)
N(13)	4859(14)	9296(11)	4168(9)	76(4)
C(14)	5171(16)	10105(11)	3814(11)	71(5)
O(15)	6340(11)	10405(7)	3442(8)	75(3)
N(16)	5061(13)	7802(9)	4597(9)	71(4)
C(17)	5793(19)	6876(11)	4802(11)	76(5)

C(18)	5940(20)	6432(13)	4203(14)	98(7)
C(19)	3431(19)	7856(12)	4707(14)	97(7)
C(20)	2890(20)	7960(13)	5473(13)	86(6)
S(21)	6530(5)	15972(3)	2271(3)	81(2)
C(22)	8130(20)	15804(14)	1616(11)	75(5)
N(23)	8961(14)	15002(9)	1706(8)	65(4)
C(24)	8674(16)	14196(9)	1990(9)	54(4)
O(25)	7392(11)	13907(7)	2229(7)	67(3)
N(26)	8556(18)	16503(9)	1103(9)	81(5)
C(27)	7680(30)	17373(14)	911(17)	129(1)
C(28)	8110(40)	17933(17)	1310(20)	172(1)
C(29)	10040(30)	16431(18)	644(16)	137(1)
C(30)	9820(40)	16300(20)	-97(18)	190(2)
S(31)	10766(5)	8928(3)	3144(4)	90(2)
C(32)	11645(18)	9657(10)	2328(12)	76(6)
N(33)	11558(14)	10524(9)	2208(9)	77(5)
C(34)	10452(16)	11079(11)	2358(10)	60(4)
O(35)	9141(12)	10939(8)	2608(8)	79(4)
N(36)	12620(20)	9303(10)	1842(12)	122(8)
C(37)	12850(40)	8315(19)	1930(20)	183(2)
C(38)	13980(40)	8002(19)	2300(30)	260(3)
C(41)	3896(15)	10794(11)	3877(11)	64(5)
C(42)	2486(16)	10533(11)	4155(10)	66(5)
C(43)	1358(17)	11151(12)	4198(12)	78(6)
C(44)	1572(15)	12023(11)	3992(11)	67(5)
C(45)	2983(17)	12287(11)	3682(11)	67(5)
N(46)	4141(12)	11646(8)	3627(8)	59(4)
C(51)	9910(18)	13546(11)	1974(11)	68(5)
C(52)	11310(20)	13746(13)	1779(13)	86(6)
C(53)	12460(20)	13141(13)	1762(12)	77(5)
C(54)	12203(19)	12288(13)	1920(12)	80(6)
C(55)	10765(15)	12034(12)	2149(10)	67(5)
N(56)	9644(12)	12660(9)	2186(8)	61(4)
C(39)	13390(40)	9920(20)	1140(30)	270(3)
C(40)	12270(90)	10210(30)	440(30)	440(6)

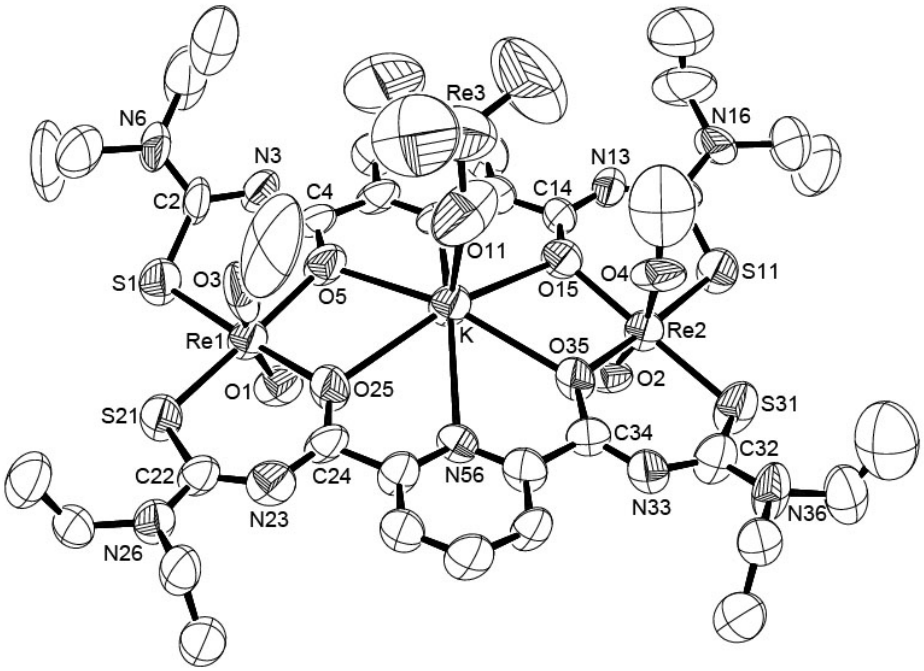

Fig A25 Ellipsoid plot (50% probability) of $[K\{ReO(OCH_3)\}_2(L^a)_2](ReO_4)$.

26) [Cs{ReO(OCH$_3$)}$_2$(L^a)$_2$](PF$_6$)

Table A51 Crystal data and structure refinement for [Cs{ReO(OCH$_3$)}$_2$(L^a)$_2$](PF$_6$).

Empirical formula	$C_{36}H_{52}CsF_6N_{10}O_8PRe_2S_4$	
Formula weight	1531.40	
Temperature	200(2) K	
Wavelength	0.71073 Å	
Crystal system	Triclinic	
Space group	$P\bar{1}$	
Unit cell dimensions	a = 9.682(2) Å	α = 78.01(2)°
	b = 15.651(4) Å	β = 85.75(2)°
	c = 17.313(3) Å	γ = 89.17(1)°
Volume	2559.2(1) Å^3	
Z	2	
Density (calculated)	1.987 g/cm^3	
Absorption coefficient	5.699 mm^{-1}	
F(000)	1480	
Crystal description	Prism	
Crystal color	Orange	
Crystal size	0.140 x 0.117 x 0.070 mm^3	
Theta range for data collection	3.20 to 29.37	
Index ranges	-13<=h<=13, -21<=k<=21, -23<=l<=22	
Reflections collected	29499	
Independent reflections	13730 [R(int) = 0.0703]	
Completeness to theta = 29.37°	97.3 %	
Absorption correction	Integration	
Max. and min. transmission	0.6840 and 0.4498	
Refinement method	Full-matrix least-squares on F^2	
Data / restraints / parameters	13730 / 4 / 614	
Goodness-of-fit on F^2	1.020	
Final R indices [I>2sigma(I)]	R1 = 0.0732, wR2 = 0.1799	
R indices (all data)	R1 = 0.1324, wR2 = 0.2101	
Largest diff. peak and hole	1.980 and -1.800 e.Å^{-3}	

Table A52 Atomic coordinates (x 10^4) and equivalent isotropic displacement parameters ($Å^2$x 10^3) for $[Cs\{ReO(OCH_3)\}_2(L^a)_2](PF_6)$. U(eq) is defined as one third of the trace of the orthogonalized U^{ij} tensor.

	x	y	z	U(eq)
Cs(1)	1792(1)	3096(1)	2743(1)	76(1)
O(1)	2530(8)	943(6)	1287(6)	84(2)
Re(1)	1629(1)	1826(1)	849(1)	63(1)
O(3)	874(9)	2874(7)	549(5)	86(3)
C(61)	1110(20)	3818(18)	251(13)	154(9)
O(2)	2630(12)	3316(8)	4945(6)	104(3)
Re(2)	3379(1)	2288(1)	4958(1)	87(1)
O(4)	3865(12)	1322(9)	4687(6)	118(4)
C(62)	3750(20)	919(17)	3907(17)	163(1)
S(1)	2871(3)	1988(2)	-385(2)	74(1)
C(2)	4050(12)	2812(8)	-405(7)	69(3)
N(3)	4750(9)	2957(6)	213(5)	63(2)
C(4)	4320(11)	2780(8)	957(6)	66(3)
O(5)	3113(7)	2580(6)	1274(4)	75(2)
N(6)	4442(11)	3321(7)	-1113(5)	76(3)
C(7)	3800(16)	3295(12)	-1841(7)	97(5)
C(8)	4572(18)	2698(12)	-2317(8)	109(5)
C(9)	5532(19)	3992(10)	-1207(9)	97(5)
C(10)	4980(30)	4838(13)	-1109(12)	144(8)
S(11)	5376(4)	2549(3)	5512(2)	99(1)
C(12)	6317(13)	3269(9)	4770(7)	81(4)
N(13)	6416(11)	3277(8)	3997(6)	81(3)
C(14)	5476(10)	3016(8)	3569(6)	66(3)
O(15)	4220(9)	2833(7)	3778(4)	86(3)
N(16)	7055(13)	3899(9)	5003(7)	104(4)
C(17)	7080(20)	3980(15)	5825(10)	115(6)
C(18)	5960(40)	4608(17)	6016(13)	194(1)
C(19)	7937(19)	4509(15)	4399(11)	127(7)
C(20)	9450(40)	4070(20)	4473(19)	231(2)
S(21)	-31(3)	1097(2)	335(2)	73(1)
C(22)	-1536(11)	1007(8)	1003(6)	62(3)

N(23)	-1602(8)	1057(6)	1765(5)	62(2)
C(24)	-698(10)	1352(7)	2163(6)	60(2)
O(25)	417(7)	1795(6)	1932(4)	73(2)
N(26)	-2693(9)	824(7)	702(5)	68(2)
C(27)	-2725(11)	652(10)	-100(7)	80(4)
C(28)	-2898(16)	1480(12)	-715(8)	103(5)
C(29)	-4031(10)	762(9)	1180(7)	71(3)
C(30)	-4376(13)	-172(9)	1607(8)	85(4)
S(31)	2495(4)	1650(3)	6229(2)	96(1)
C(32)	758(17)	1467(16)	6181(7)	129(8)
N(33)	119(13)	1354(11)	5552(6)	117(5)
C(34)	481(14)	1588(11)	4792(7)	89(4)
O(35)	1522(9)	2014(8)	4429(5)	100(3)
N(36)	20(20)	1530(30)	6865(10)	290(2)
C(37)	390(30)	1938(13)	7550(12)	139(8)
C(38)	580(20)	1061(15)	7938(17)	170(1)
C(39)	-1410(30)	1630(20)	6786(13)	340(3)
C(40)	-1890(30)	720(20)	6937(12)	230(2)
C(41)	5421(11)	2951(8)	1488(6)	65(3)
C(42)	6786(11)	3126(9)	1185(7)	73(3)
C(43)	7770(11)	3268(9)	1682(8)	82(4)
C(44)	7339(12)	3273(9)	2463(8)	77(3)
C(45)	5964(12)	3060(8)	2736(7)	69(3)
N(46)	5019(9)	2895(6)	2241(5)	64(2)
C(51)	-1092(10)	1194(7)	3036(6)	61(3)
C(52)	-2342(13)	795(11)	3346(7)	91(4)
C(53)	-2661(18)	638(12)	4145(8)	112(6)
C(54)	-1759(16)	894(12)	4633(8)	107(6)
C(55)	-527(13)	1285(10)	4290(7)	78(3)
N(56)	-196(9)	1457(7)	3492(5)	68(2)
P(1)	570(6)	5543(4)	2226(4)	123(2)
F(1)	1785(19)	5089(10)	2659(13)	235(1)
F(2)	-239(16)	4692(11)	2462(16)	244(1)
F(3)	1460(20)	6378(11)	2014(18)	307(2)
F(4)	-180(30)	5897(13)	2914(16)	289(1)
F(5)	1210(20)	5217(14)	1552(10)	223(8)
F(6)	-550(30)	6000(20)	1765(15)	315(1)

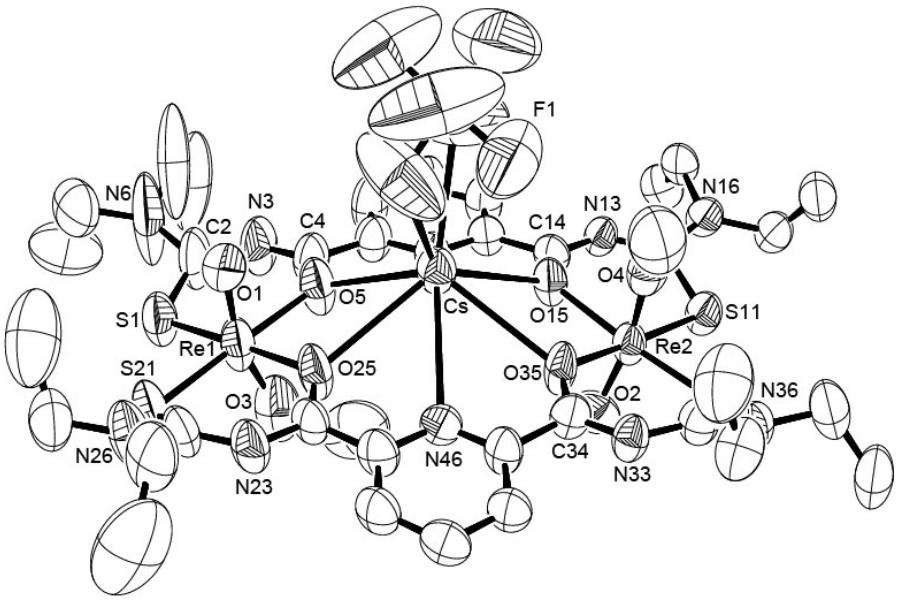

Fig A26 Ellipsoid plot (50% probability) of $[Cs\{ReO(OCH_3)\}_2(L^a)_2](PF_6)$.

27) [Cs{ReO(OCH$_3$)}$_2$(L^a)$_2$](ReO$_4$)

Table A53 Crystal data and structure refinement for [Cs{ReO(OCH$_3$)}$_2$(L^a)$_2$](ReO$_4$).

Empirical formula	$C_{36}H_{52}CsN_{10}O_{12}Re_3S_4$	
Formula weight	1636.63	
Temperature	200(2) K	
Wavelength	0.71073 Å	
Crystal system	Triclinic	
Space group	$P\bar{1}$	
Unit cell dimensions	a = 9.729(1) Å	α = 79.38(1)°
	b = 15.624(1) Å	β = 85.07(1)°
	c = 17.199(1) Å	γ = 87.89(1)°
Volume	2559.5(3) Å^3	
Z	2	
Density (calculated)	2.124 g/cm^3	
Absorption coefficient	8.005 mm^{-1}	
F(000)	1556	
Crystal description	Plate	
Crystal color	Orange	
Crystal size	0.350 x 0.197 x 0.040 mm^3	
Theta range for data collection	2.51 to 25.00	
Index ranges	-11<=h<=11, -18<=k<=18, -18<=l<=20	
Reflections collected	17719	
Independent reflections	8902 [R(int) = 0.0577]	
Completeness to theta = 25.00°	98.6 %	
Absorption correction	Integration	
Max. and min. transmission	0.7104 and 0.1309	
Refinement method	Full-matrix least-squares on F^2	
Data / restraints / parameters	8902 / 0 / 600	
Goodness-of-fit on F^2	1.002	
Final R indices [I>2sigma(I)]	R1 = 0.0589, wR2 = 0.1531	
R indices (all data)	R1 = 0.0791, wR2 = 0.1648	
Largest diff. peak and hole	2.591 and -2.041 e.Å^{-3}	

Table A54 Atomic coordinates (x 10^4) and equivalent isotropic displacement parameters ($Å^2$x 10^3) for $[Cs\{ReO(OCH_3)\}_2(L^a)_2](ReO_4)$. U(eq) is defined as one third of the trace of the orthogonalized U^{ij} tensor.

	x	y	z	U(eq)
Re(1)	1580(1)	1844(1)	865(1)	41(1)
Cs(1)	1750(1)	3119(1)	2791(1)	53(1)
Re(2)	3365(1)	2329(1)	4990(1)	53(1)
S(21)	-107(3)	1170(2)	338(2)	52(1)
S(1)	2780(3)	2037(2)	-394(2)	56(1)
S(31)	2539(4)	1655(3)	6261(2)	67(1)
S(11)	5403(4)	2537(3)	5538(2)	68(1)
O(25)	396(7)	1806(6)	1966(4)	50(2)
O(15)	4177(8)	2871(6)	3804(5)	54(2)
O(35)	1514(8)	2074(6)	4473(5)	59(2)
N(23)	-1608(8)	1082(6)	1806(5)	42(2)
N(3)	4638(9)	2975(6)	217(5)	42(2)
O(5)	3080(8)	2544(6)	1328(5)	60(2)
N(46)	4954(8)	2893(6)	2264(5)	40(2)
N(13)	6408(9)	3251(7)	4019(6)	51(2)
N(56)	-175(9)	1491(6)	3539(5)	45(2)
C(24)	-700(10)	1378(8)	2208(7)	44(2)
C(22)	-1542(10)	1021(7)	1033(7)	40(2)
C(45)	5344(10)	2928(7)	1510(6)	42(2)
C(41)	5909(10)	3048(7)	2756(7)	44(2)
C(34)	504(12)	1631(10)	4824(6)	55(3)
C(12)	6308(12)	3267(9)	4789(7)	56(3)
C(55)	-1063(10)	1206(7)	3089(6)	42(2)
C(14)	5451(11)	3023(8)	3595(7)	51(3)
N(33)	120(12)	1443(10)	5586(6)	76(4)
C(4)	4251(11)	2801(7)	972(7)	44(2)
C(51)	-493(11)	1329(9)	4318(7)	52(3)
C(2)	3965(11)	2851(8)	-401(6)	45(2)
C(32)	789(16)	1568(13)	6210(8)	84(5)
N(26)	-2706(8)	806(6)	770(5)	41(2)
N(6)	4326(12)	3344(7)	-1090(7)	62(3)

N(16)	7012(11)	3881(7)	5020(6)	59(3)
C(27)	-2744(11)	613(8)	-47(7)	50(3)
C(44)	6686(11)	3079(9)	1182(7)	53(3)
C(29)	-4018(10)	737(8)	1257(7)	49(3)
C(42)	7301(11)	3230(9)	2464(7)	54(3)
C(43)	7683(11)	3233(9)	1705(8)	59(3)
C(54)	-2280(13)	778(10)	3416(8)	64(4)
C(17)	6993(14)	4014(11)	5866(8)	69(4)
C(52)	-1666(14)	892(12)	4690(8)	79(5)
C(7)	3699(18)	3302(10)	-1832(8)	73(4)
C(28)	-3065(15)	1397(11)	-643(8)	74(4)
C(9)	5458(19)	3969(10)	-1151(10)	80(5)
C(19)	7920(14)	4481(11)	4454(9)	73(4)
C(8)	4530(20)	2744(14)	-2302(9)	104(7)
C(53)	-2570(15)	620(13)	4216(8)	83(5)
C(30)	-4315(14)	-160(11)	1663(11)	77(4)
C(18)	5850(20)	4657(12)	6042(11)	96(5)
C(20)	9378(18)	4056(15)	4461(12)	103(6)
C(10)	4820(30)	4839(14)	-1077(16)	151(1)
O(2)	2622(10)	3307(7)	5015(5)	67(2)
O(3)	801(9)	2955(6)	628(5)	58(2)
O(4)	3946(9)	1280(6)	4659(5)	60(2)
O(1)	2490(8)	936(5)	1274(6)	59(2)
N(36)	-41(15)	1670(13)	6865(8)	105(6)
C(39)	-1710(20)	1635(18)	6838(11)	112(7)
C(5)	3774(17)	896(12)	3971(10)	82(4)
C(37)	450(20)	1837(14)	7642(10)	93(5)
C(38)	590(20)	1020(16)	8099(17)	129(9)
C(40)	-2000(30)	770(20)	6989(14)	179(2)
C(3)	1060(20)	3879(13)	363(15)	114(7)
O(11)	796(12)	6478(7)	1205(7)	83(3)
O(12)	-469(18)	6192(9)	3184(8)	123(5)
O(13)	2100(16)	5186(11)	2563(10)	130(6)
O(14)	-500(20)	4840(12)	2109(13)	158(7)
Re(3)	539(1)	5598(1)	2282(1)	90(1)
Re(4)	1495(8)	5672(4)	1766(5)	90(1)

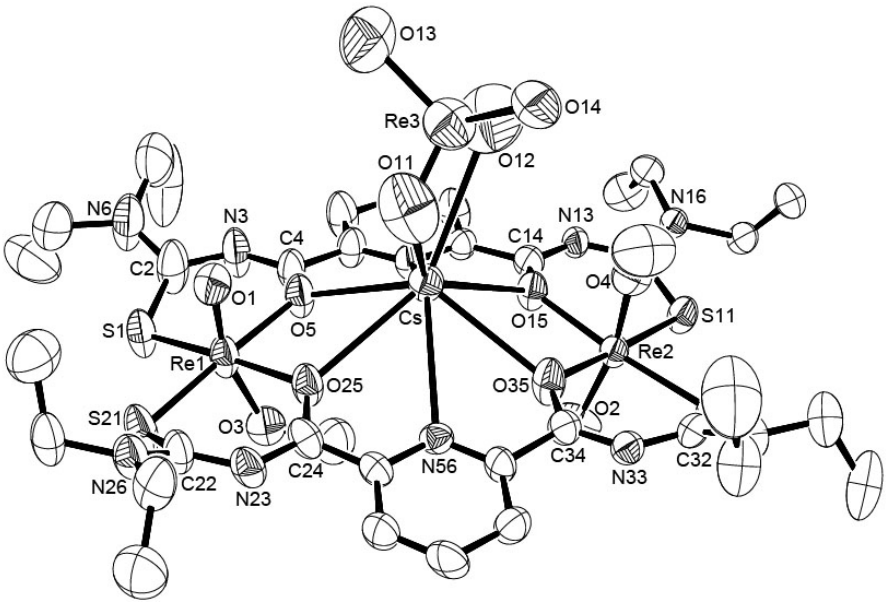

Fig A27 Ellipsoid plot (50% probability) of $[Cs\{ReO(OCH_3)\}_2(L^a)_2](ReO_4)$.

28) $[K(Re_2O_3)_2(L^a)_4](PF_6)\cdot 5CH_3CN$

Table A55 Crystal data and structure refinement for $[K(Re_2O_3)_2(L^a)_4](PF_6)\cdot 5CH_3CN$.

Empirical formula	$C_{78}H_{107}F_6KN_{25}O_{14}PRe_4S_8$	
Formula weight	2804.24	
Temperature	200(2) K	
Wavelength	0.71073 Å	
Crystal system	Monoclinic	
Space group	C2/c	
Unit cell dimensions	a = 25.783(1) Å	α = 90°
	b = 16.410(1) Å	β = 91.16(1)°
	c = 24.227(1) Å	γ = 90°
Volume	10248.3(9) $Å^3$	
Z	4	
Density (calculated)	1.817 g/cm^3	
Absorption coefficient	5.009 mm^{-1}	
F(000)	5512	
Crystal description	Prism	
Crystal color	Brown	
Crystal size	0.310 x 0.153 x 0.070 mm^3	
Theta range for data collection	1.68 to 29.28	
Index ranges	-35<=h<=35, -22<=k<=17, -33<=l<=33	
Reflections collected	63193	
Independent reflections	13829 [R(int) = 0.2138]	
Completeness to theta = 29.28°	98.9 %	
Absorption correction	Integration	
Max. and min. transmission	0.7228 and 0.2811	
Refinement method	Full-matrix least-squares on F^2	
Data / restraints / parameters	13829 / 0 / 625	
Goodness-of-fit on F^2	0.876	
Final R indices [I>2sigma(I)]	R1 = 0.0635, wR2 = 0.1408	
R indices (all data)	R1 = 0.1046, wR2 = 0.1638	
Largest diff. peak and hole	4.774 and -2.654 $e.Å^{-3}$	

Table A56 Atomic coordinates (x 10^4) and equivalent isotropic displacement parameters ($Å^2$x 10^3) for $[K(Re_2O_3)_2(L^a)_4](PF_6)\cdot 5CH_3CN$. U(eq) is defined as one third of the trace of the orthogonalized U^{ij} tensor.

	x	y	z	U(eq)
K(1)	2500	2500	0	45(1)
O(1)	3649(3)	456(4)	823(3)	43(2)
Re(1)	3237(1)	201(1)	294(1)	30(1)
O(3)	2736(2)	209(3)	-300(2)	33(1)
Re(2)	2248(1)	262(1)	-897(1)	32(1)
O(2)	1804(3)	533(4)	-1387(3)	47(2)
S(1)	2953(1)	-1041(1)	631(1)	38(1)
C(2)	2458(3)	-833(4)	1097(4)	34(2)
N(3)	2318(3)	-105(4)	1319(3)	32(1)
C(4)	2430(3)	625(5)	1136(3)	30(2)
O(5)	2653(2)	882(3)	703(2)	35(1)
N(6)	2202(3)	-1468(4)	1304(3)	36(2)
C(7)	2314(4)	-2318(5)	1157(4)	43(2)
C(8)	2002(5)	-2600(6)	669(5)	56(3)
C(9)	1774(4)	-1355(6)	1690(4)	44(2)
C(10)	1957(5)	-1372(7)	2282(4)	56(3)
S(11)	3820(1)	-531(1)	-221(1)	40(1)
C(12)	4137(3)	136(5)	-657(4)	38(2)
N(13)	4067(3)	946(4)	-726(3)	36(2)
C(14)	3753(3)	1445(5)	-448(3)	30(2)
O(15)	3446(2)	1328(3)	-75(2)	35(1)
N(16)	4511(3)	-181(4)	-973(3)	40(2)
C(17)	4663(4)	-1053(6)	-934(5)	50(2)
C(18)	5070(5)	-1190(8)	-492(6)	72(4)
C(19)	4804(4)	328(6)	-1359(5)	52(2)
C(20)	5230(5)	771(9)	-1083(7)	77(4)
S(21)	1867(1)	-955(1)	-635(1)	47(1)
C(22)	1372(4)	-732(5)	-184(4)	44(2)
N(23)	1291(3)	-21(5)	99(4)	40(2)
C(24)	1498(3)	694(5)	26(4)	34(2)
O(25)	1833(2)	957(3)	-328(2)	32(1)

N(26)	1027(4)	-1312(5)	-97(5)	63(3)
C(27)	1060(5)	-2128(7)	-368(6)	70(4)
C(28)	851(9)	-2128(13)	-938(9)	146(1)
C(29)	469(18)	-1080(20)	167(17)	260(3)
C(30)	618(8)	-1334(16)	590(20)	300(4)
S(31)	2781(1)	-495(1)	-1466(1)	45(1)
C(32)	3183(3)	195(5)	-1798(3)	33(2)
N(33)	3123(3)	1011(4)	-1845(3)	35(2)
C(34)	2865(3)	1506(4)	-1513(3)	31(2)
O(35)	2639(2)	1373(3)	-1070(2)	33(1)
N(36)	3573(3)	-95(4)	-2092(3)	39(2)
C(37)	3720(4)	-968(6)	-2085(5)	50(2)
C(38)	3504(6)	-1429(8)	-2563(6)	81(4)
C(39)	3862(4)	448(6)	-2462(4)	45(2)
C(40)	3577(5)	650(8)	-2988(4)	59(3)
C(41)	2248(3)	1266(4)	1524(3)	33(2)
C(42)	2036(5)	1043(5)	2033(4)	51(3)
C(43)	1865(5)	1633(6)	2378(4)	57(3)
C(44)	1884(4)	2442(6)	2220(4)	46(2)
C(45)	2097(3)	2618(5)	1698(3)	33(2)
N(46)	2281(3)	2050(4)	1359(3)	33(1)
C(51)	1306(3)	1319(5)	427(4)	35(2)
C(52)	1055(4)	1075(6)	902(4)	47(2)
C(53)	858(4)	1655(6)	1247(4)	49(2)
C(54)	913(4)	2472(6)	1109(4)	45(2)
C(55)	1186(3)	2669(5)	630(4)	33(2)
N(56)	1385(3)	2107(4)	296(3)	33(1)
P(1)	0	7439(2)	7500	33(1)
F(1)	0	6426(7)	7500	109(5)
F(2)	0	8363(7)	7500	119(5)
F(3)	-617(3)	7394(6)	7538(4)	82(2)
F(4)	-50(4)	7410(8)	6853(3)	106(3)
C(61)	1426(5)	2495(7)	8895(5)	62(3)
C(62)	915(9)	2191(16)	8802(10)	135(9)
N(63)	493(10)	1970(20)	8706(16)	290(2)
C(64)	9354(8)	9804(14)	6876(10)	124(8)
C(65)	9286(7)	10032(11)	7484(12)	99(6)

N(66)	9253(9)	10212(13)	7907(11)	149(9)
C(67)	5000	7020(20)	7500	360(5)
C(68)	5000	7859(19)	7500	125(1)
N(69)	5000	8581(14)	7500	112(8)

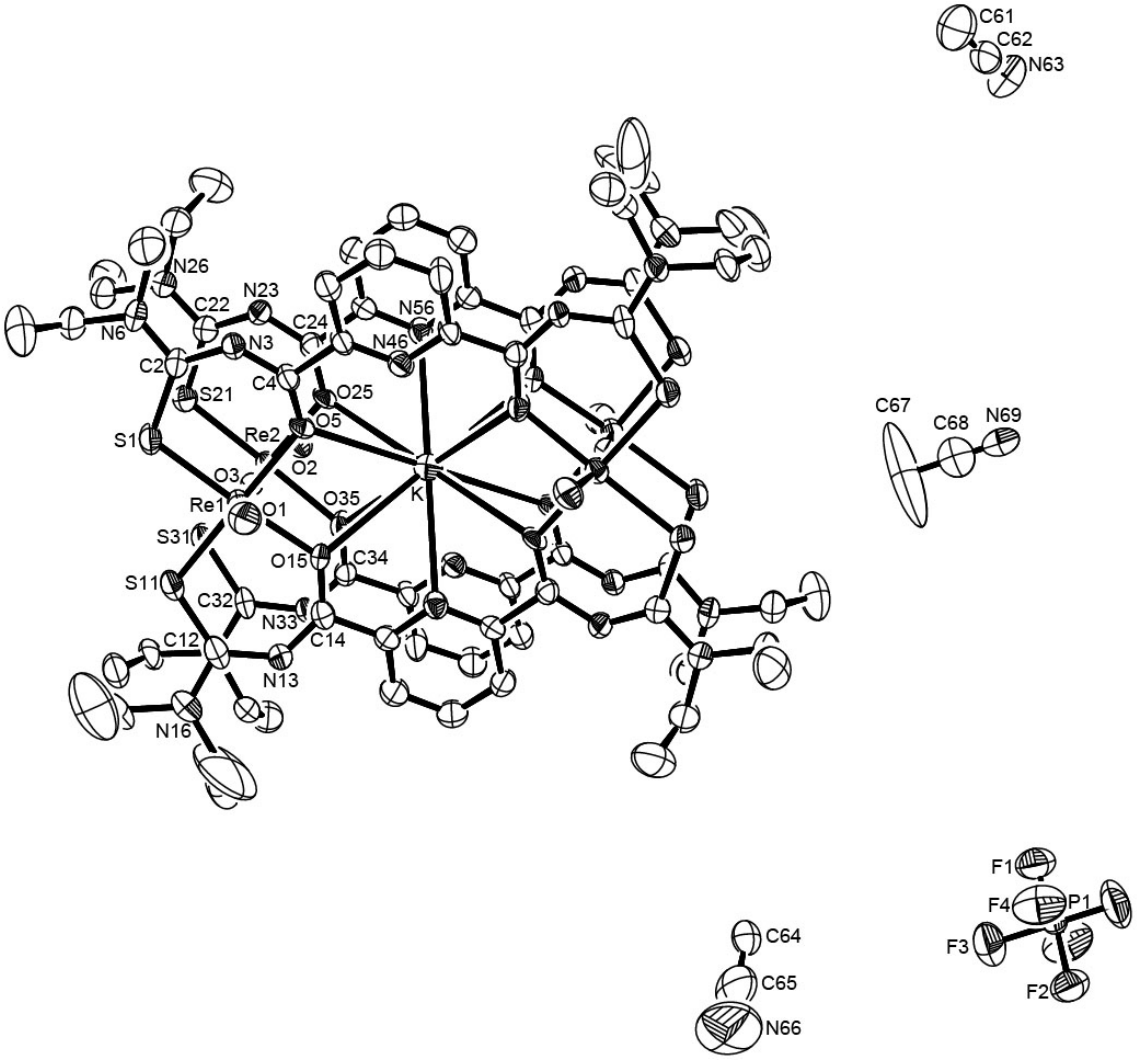

Fig A28 Ellipsoid plot (50% probability) of $[K(Re_2O_3)_2(L^a)_4](PF_6)\cdot 5CH_3CN$.

29) $[Rb(Re_2O_3)_2(L^a)_4](PF_6)\cdot 2CH_3CN\cdot 3H_2O$

Table A57 Crystal data and structure refinement for $[Rb(Re_2O_3)_2(L^a)_4](PF_6)\cdot 2CH_3CN\cdot 3H_2O$.

Empirical formula	$C_{72}H_{98}F_6N_{22}O_{17}PRbRe_4S_8$	
Formula weight	2775.44	
Temperature	200(2) K	
Wavelength	0.71073 Å	
Crystal system	Monoclinic	
Space group	C2/c	
Unit cell dimensions	a = 25.719(1) Å	α = 90°
	b = 16.430(1) Å	β = 91.68(1)°
	c = 24.261(1) Å	γ = 90°
Volume	10247.4(9) $Å^3$	
Z	4	
Density (calculated)	1.799 g/cm^3	
Absorption coefficient	5.439 mm^{-1}	
F(000)	5416	
Crystal description	Plate	
Crystal color	Brown	
Crystal size	0.330 x 0.163 x 0.060 mm^3	
Theta range for data collection	3.17 to 26.81	
Index ranges	-32<=h<=32, -19<=k<=20, -30<=l<=30	
Reflections collected	45320	
Independent reflections	10870 [R(int) = 0.0468]	
Completeness to theta = 26.81°	99.0 %	
Absorption correction	Empirical	
Max. and min. transmission	0.790707 and 0.390869	
Refinement method	Full-matrix least-squares on F^2	
Data / restraints / parameters	10870 / 2 / 595	
Goodness-of-fit on F^2	0.945	
Final R indices [I>2sigma(I)]	R1 = 0.0403, wR2 = 0.0931	
R indices (all data)	R1 = 0.0663, wR2 = 0.1009	
Largest diff. peak and hole	1.078 and -0.992 e.$Å^{-3}$	

Table A58 Atomic coordinates (x 10^4) and equivalent isotropic displacement parameters ($Å^2$x 10^3) for $[Rb(Re_2O_3)_2(L^a)_4](PF_6)\cdot 2CH_3CN\cdot 3H_2O$. U(eq) is defined as one third of the trace of the orthogonalized U^{ij} tensor.

	x	y	z	U(eq)
Rb(1)	2500	2500	5000	52(1)
O(1)	1801(2)	4485(3)	3605(2)	62(1)
Re(1)	2243(1)	4739(1)	4099(1)	43(1)
O(3)	2733(2)	4765(2)	4704(2)	46(1)
Re(2)	3238(1)	4785(1)	5296(1)	41(1)
O(2)	3642(2)	4534(3)	5823(2)	55(1)
S(1)	1869(1)	5959(1)	4367(1)	59(1)
C(2)	1354(3)	5732(4)	4780(3)	61(2)
N(3)	1266(2)	5027(4)	5059(3)	63(2)
C(4)	1486(2)	4315(4)	5007(3)	47(1)
O(5)	1810(2)	4047(2)	4669(2)	45(1)
N(6)	1021(3)	6328(4)	4866(4)	91(2)
C(7)	1058(4)	7146(5)	4607(4)	90(3)
C(8)	832(5)	7114(10)	4066(6)	158(6)
S(11)	2787(1)	5494(1)	3541(1)	58(1)
C(12)	3170(3)	4804(4)	3197(3)	49(2)
N(13)	3120(2)	3992(3)	3164(2)	47(1)
C(14)	2877(2)	3496(4)	3487(2)	43(1)
O(15)	2629(2)	3617(2)	3923(2)	44(1)
N(16)	3553(2)	5107(3)	2896(2)	57(1)
C(17)	3697(4)	5982(5)	2900(4)	79(2)
C(18)	3443(5)	6409(7)	2447(4)	110(4)
C(19)	3850(3)	4578(4)	2536(3)	58(2)
C(20)	3553(4)	4358(5)	2002(3)	75(2)
S(21)	2947(1)	6027(1)	5626(1)	48(1)
C(22)	2452(2)	5828(3)	6090(2)	43(1)
N(23)	2310(2)	5101(3)	6297(2)	45(1)
C(24)	2420(2)	4361(4)	6134(3)	44(1)
O(25)	2649(2)	4104(2)	5706(2)	46(1)
N(26)	2199(2)	6468(3)	6281(2)	50(1)
C(27)	2321(3)	7311(4)	6145(3)	54(2)

C(28)	1998(3)	7586(5)	5662(3)	67(2)
C(29)	1777(3)	6353(4)	6670(3)	57(2)
C(30)	1966(4)	6369(5)	7269(3)	74(2)
S(31)	3822(1)	5517(1)	4783(1)	52(1)
C(32)	4139(2)	4846(4)	4348(3)	44(1)
N(33)	4072(2)	4038(3)	4287(2)	46(1)
C(34)	3779(2)	3540(4)	4560(2)	41(1)
O(35)	3456(2)	3652(2)	4934(2)	45(1)
N(36)	4500(2)	5175(3)	4035(2)	52(1)
C(37)	4655(3)	6044(4)	4079(3)	60(2)
C(38)	5061(4)	6197(5)	4510(4)	82(3)
C(39)	4789(3)	4667(4)	3643(3)	64(2)
C(40)	5241(4)	4247(7)	3898(4)	101(3)
C(41)	3839(2)	2657(4)	4391(3)	43(1)
C(42)	4096(3)	2464(4)	3919(3)	53(2)
C(43)	4152(3)	1650(4)	3779(3)	62(2)
C(44)	3967(3)	1068(4)	4129(3)	57(2)
C(45)	1287(2)	3696(4)	5404(3)	45(1)
N(46)	3642(2)	2093(3)	4724(2)	41(1)
C(51)	2916(2)	2617(4)	3309(2)	45(1)
C(52)	3132(3)	2444(4)	2804(3)	61(2)
C(53)	3155(4)	1629(4)	2646(3)	75(2)
C(54)	2987(3)	1046(4)	2987(3)	61(2)
C(55)	2226(2)	3719(4)	6511(3)	45(1)
N(56)	2732(2)	2054(3)	3646(2)	41(1)
P(1)	0	7558(2)	2500	50(1)
F(1)	608(2)	7612(5)	2479(3)	116(2)
F(2)	0	8557(6)	2500	143(4)
F(3)	-37(3)	7601(6)	1858(2)	138(3)
F(4)	0	6654(6)	2500	167(5)
C(9)	605(5)	6273(8)	5355(12)	233(1)
C(10)	246(11)	6070(20)	5046(14)	321(2)
C(65)	572(14)	5200(30)	3229(11)	400(3)
C(66)	694(9)	4994(14)	2638(12)	680(7)
N(67)	691(13)	4740(20)	2209(13)	380(2)
O(63)	3693(7)	7552(7)	1164(4)	239(8)
O(61)	5000	6470(20)	2500	277(1)

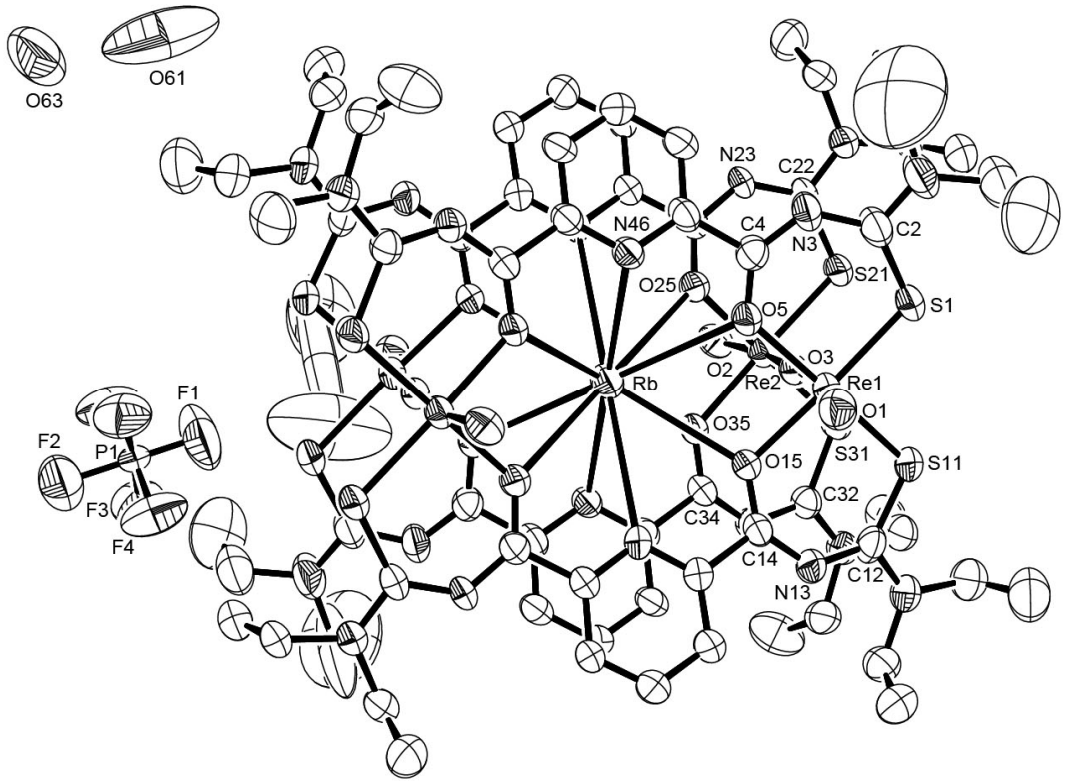

Fig A29 Ellipsoid plot (50% probability) of $[Rb(Re_2O_3)_2(L^a)_4](PF_6)\cdot 2CH_3CN\cdot 3H_2O$.

30) $[Cs(Re_2O_3)_2(L^a)_4]Cl \cdot CsCl \cdot 3H_2O$

Table A59 Crystal data and structure refinement for $[Cs(Re_2O_3)_2(L^a)_4]Cl \cdot CsCl \cdot 3H_2O$.

Empirical formula	$C_{68}H_{92}Cl_2Cs_2N_{20}O_{17}Re_4S_8$	
Formula weight	2799.62	
Temperature	200(2) K	
Wavelength	0.71073 Å	
Crystal system	Triclinic	
Space group	$P\bar{1}$	
Unit cell dimensions	a = 11.700(1) Å	α = 85.35(1)°
	b = 15.261(1) Å	β = 87.96(1)°
	c = 28.588(2) Å	γ = 86.81(1)°
Volume	5077.3(7) $Å^3$	
Z	2	
Density (calculated)	1.831 g/cm^3	
Absorption coefficient	5.741 mm^{-1}	
F(000)	2696	
Crystal description	Prism	
Crystal color	Red	
Crystal size	0.580 x 0.370 x 0.180 mm^3	
Theta range for data collection	3.25 to 29.31	
Index ranges	-13<=h<=16, -20<=k<=20, -39<=l<=39	
Reflections collected	60246	
Independent reflections	27188 [R(int) = 0.1080]	
Completeness to theta = 29.31°	97.9 %	
Absorption correction	Integration	
Max. and min. transmission	0.6764 and 0.3455	
Refinement method	Full-matrix least-squares on F^2	
Data / restraints / parameters	27188 / 0 / 1091	
Goodness-of-fit on F^2	0.863	
Final R indices [I>2sigma(I)]	R1 = 0.0715, wR2 = 0.1789	
R indices (all data)	R1 = 0.1524, wR2 = 0.2101	
Largest diff. peak and hole	2.828 and -3.458 $e.Å^{-3}$	

Table A60 Atomic coordinates (x 10^4) and equivalent isotropic displacement parameters ($Å^2$x 10^3) for $[Cs(Re_2O_3)_2(L^a)_4]Cl \cdot CsCl \cdot 3H_2O$. U(eq) is defined as one third of the trace of the orthogonalized U^{ij} tensor.

	x	y	z	U(eq)
Cs(1)	9882(1)	-2588(1)	7447(1)	45(1)
O(1)	12362(9)	-405(6)	8118(4)	60(3)
Re(1)	11435(1)	-1042(1)	8437(1)	43(1)
O(6)	10415(8)	-1925(6)	8660(3)	48(2)
Re(2)	10565(1)	-2528(1)	5965(1)	41(1)
O(2)	11578(9)	-1797(6)	5868(3)	60(3)
O(3)	8441(9)	-3563(6)	9049(3)	57(3)
Re(3)	9418(1)	-2785(1)	8937(1)	44(1)
O(7)	9381(8)	-3244(6)	6244(3)	47(2)
Re(4)	8170(1)	-3966(1)	6450(1)	44(1)
O(4)	7150(9)	-4534(7)	6751(4)	64(3)
S(1)	10531(4)	13(2)	8896(1)	56(1)
C(2)	9839(12)	774(9)	8490(5)	49(3)
N(3)	9314(11)	554(7)	8090(4)	52(3)
C(4)	9495(12)	-145(9)	7855(5)	48(3)
O(5)	10241(7)	-778(5)	7898(3)	41(2)
N(6)	9728(11)	1602(6)	8578(4)	56(3)
C(7)	10292(17)	1915(10)	8980(5)	69(5)
C(8)	9472(19)	1927(14)	9400(6)	94(6)
C(9)	9089(16)	2234(9)	8257(6)	68(5)
C(10)	9920(30)	2624(15)	7891(8)	124(9)
S(11)	9456(4)	-2043(2)	5330(1)	56(1)
C(12)	8579(13)	-1149(9)	5488(4)	50(3)
N(13)	8377(10)	-853(7)	5918(3)	48(3)
C(14)	8913(11)	-1080(7)	6300(4)	40(3)
O(15)	9759(9)	-1602(5)	6399(3)	48(2)
N(16)	7997(13)	-713(9)	5147(4)	72(4)
C(17)	8067(18)	-983(11)	4649(5)	76(6)
C(18)	8970(20)	-496(14)	4367(7)	112(8)
C(19)	7199(17)	59(11)	5238(6)	79(6)
C(20)	7760(20)	829(12)	5276(6)	107(9)

S(21)	12646(4)	-1450(2)	9055(1)	57(1)
C(22)	13386(13)	-2409(9)	8918(5)	51(3)
N(23)	13495(11)	-2762(8)	8503(4)	57(3)
C(24)	12903(12)	-2574(8)	8122(4)	45(3)
O(25)	12069(8)	-2070(6)	8030(3)	45(2)
N(26)	13923(12)	-2866(9)	9264(4)	68(4)
C(27)	13970(17)	-2547(12)	9752(5)	79(6)
C(28)	14859(19)	-1884(15)	9773(8)	111(8)
C(29)	14583(17)	-3779(12)	9197(6)	78(5)
C(30)	15745(18)	-3645(18)	9052(8)	112(8)
S(31)	11340(3)	-3626(2)	5513(1)	53(1)
C(32)	12365(12)	-4266(8)	5854(4)	45(3)
N(33)	12793(9)	-4099(7)	6253(3)	45(2)
C(34)	12394(12)	-3526(9)	6562(4)	43(3)
O(35)	11476(7)	-3043(5)	6566(3)	40(2)
N(36)	12803(10)	-5000(7)	5680(4)	50(3)
C(37)	12514(13)	-5266(9)	5206(5)	53(3)
C(38)	11491(13)	-5868(9)	5242(5)	57(4)
C(39)	13632(15)	-5562(10)	5927(5)	64(4)
C(40)	14865(15)	-5335(14)	5809(6)	83(6)
S(41)	8639(4)	-1807(3)	9461(1)	58(1)
C(42)	7696(13)	-1076(10)	9150(5)	56(4)
N(43)	7210(11)	-1164(8)	8739(4)	58(3)
C(44)	7514(13)	-1718(9)	8417(5)	53(3)
O(45)	8381(8)	-2253(6)	8379(3)	46(2)
N(46)	7366(15)	-350(11)	9358(5)	98(7)
C(47)	7755(15)	-150(12)	9806(6)	77(6)
C(48)	7100(17)	-563(13)	10231(7)	89(6)
C(49)	6050(40)	230(30)	9190(11)	230(3)
C(50)	6750(20)	630(20)	8956(12)	163(2)
S(51)	7029(3)	-3369(3)	5840(1)	64(1)
C(52)	6164(13)	-2525(9)	6047(5)	54(3)
N(53)	6041(11)	-2260(8)	6490(4)	57(3)
C(54)	6761(12)	-2434(8)	6847(4)	45(3)
O(55)	7673(8)	-2903(5)	6875(3)	44(2)
N(56)	5452(15)	-2110(10)	5746(5)	91(6)
C(57)	5460(20)	-2264(13)	5238(6)	96(7)

C(58)	4600(20)	-2961(14)	5147(6)	96(7)
C(59)	4228(17)	-1568(16)	5963(6)	90(6)
C(60)	4670(40)	-810(30)	5915(10)	240(3)
S(61)	10703(4)	-3308(2)	9510(1)	56(1)
C(62)	11355(13)	-4274(9)	9318(5)	52(3)
N(63)	11514(11)	-4513(7)	8881(4)	52(3)
C(64)	10991(13)	-4199(8)	8501(4)	47(3)
O(65)	10237(8)	-3603(5)	8435(3)	46(2)
N(66)	11758(12)	-4855(8)	9656(4)	61(3)
C(67)	11532(17)	-4775(10)	10162(5)	71(5)
C(68)	12450(20)	-4326(14)	10372(6)	108(8)
C(69)	12482(17)	-5642(11)	9539(6)	78(5)
C(70)	11760(20)	-6420(13)	9466(8)	110(8)
S(71)	8830(4)	-5056(2)	5970(1)	58(1)
C(72)	9593(13)	-5828(9)	6329(5)	54(3)
N(73)	10173(11)	-5700(7)	6706(4)	52(3)
C(74)	10096(12)	-5041(9)	6977(4)	44(3)
O(75)	9322(8)	-4387(5)	6982(3)	44(2)
N(76)	9617(12)	-6685(7)	6215(4)	57(3)
C(77)	9029(16)	-6934(11)	5806(6)	75(5)
C(78)	7810(20)	-7082(14)	5874(9)	119(8)
C(79)	10220(20)	-7376(11)	6489(6)	95(7)
C(80)	9470(40)	-8110(20)	6721(12)	220(2)
C(81)	8704(12)	-137(8)	7452(4)	43(3)
C(82)	7644(12)	346(9)	7450(5)	53(3)
C(83)	7031(14)	362(10)	7065(5)	62(4)
C(84)	7401(13)	-80(9)	6677(5)	55(4)
C(85)	8429(12)	-557(8)	6712(4)	44(3)
N(86)	9075(10)	-612(6)	7097(3)	42(2)
C(91)	13383(11)	-3093(8)	7712(4)	41(3)
C(92)	14471(12)	-3531(10)	7737(5)	57(4)
C(93)	14885(13)	-3953(10)	7364(5)	60(4)
C(94)	14218(12)	-3969(9)	6964(4)	50(3)
C(95)	13148(11)	-3524(8)	6982(4)	41(3)
N(96)	12758(9)	-3082(7)	7341(3)	41(2)
C(101)	6696(11)	-1639(8)	8013(4)	42(3)
C(102)	5637(12)	-1183(9)	8052(5)	53(3)

C(103)	4943(13)	-1145(10)	7681(5)	60(4)
C(104)	5294(13)	-1522(10)	7286(5)	59(4)
C(105)	6353(11)	-1977(8)	7271(4)	44(3)
N(106)	7040(9)	-2037(7)	7631(3)	43(2)
C(111)	11399(11)	-4666(7)	8078(4)	40(3)
C(112)	12424(13)	-5171(9)	8067(5)	56(4)
C(113)	12700(13)	-5614(10)	7685(5)	61(4)
C(114)	11961(14)	-5583(10)	7314(5)	57(4)
C(115)	10944(12)	-5067(8)	7348(4)	45(3)
N(116)	10703(10)	-4598(7)	7708(4)	44(2)
Cs(2)	15290(2)	-6532(2)	8842(1)	143(1)
Cl(2)	5402(3)	-1486(3)	3859(1)	55(1)
Cl(1)	4367(5)	1853(3)	6387(2)	83(2)
O(10)	17860(19)	-4470(20)	8059(9)	187(1)
O(9)	11290(30)	-4590(20)	11552(10)	254(2)
O(8)	1870(20)	-290(40)	6985(7)	570(5)

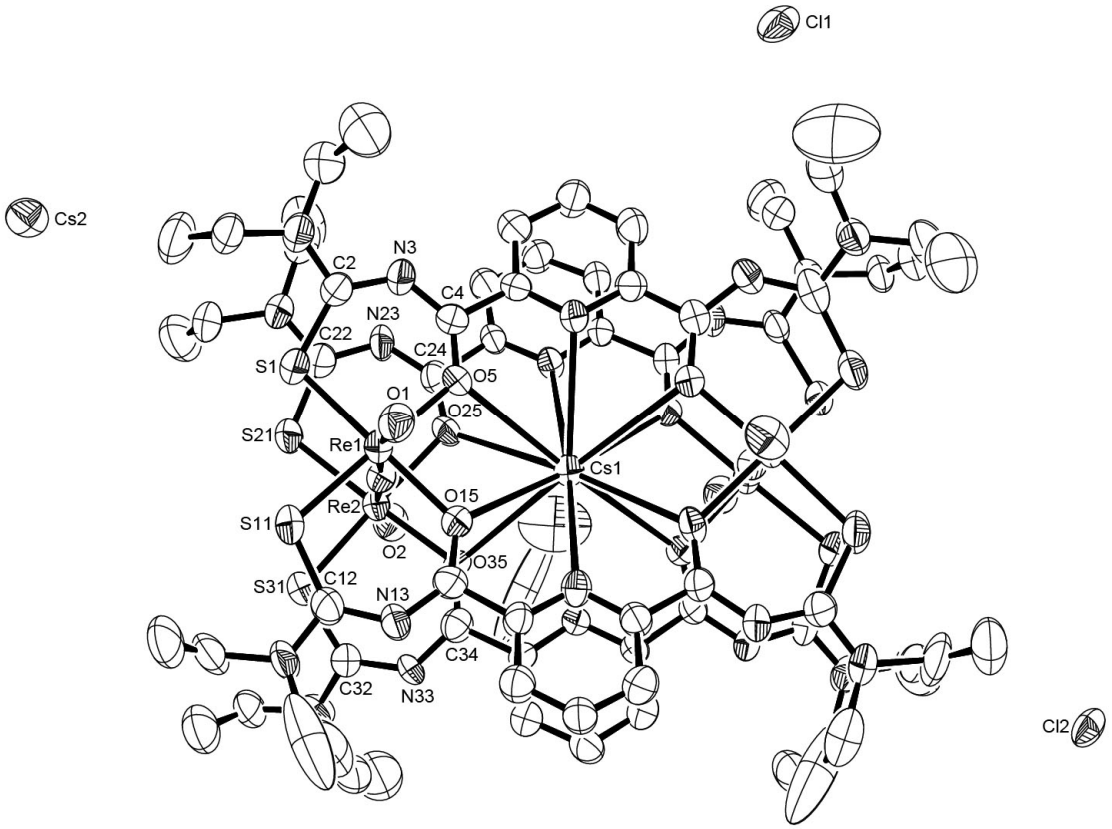

Fig A30 Ellipsoid plot (50% probability) of $[Cs(Re_2O_3)_2(L^a)_4]Cl \cdot CsCl \cdot 3H_2O$.

31) $[Tl(Re_2O_3)_2(L^a)_4](PF_6)\cdot 2CH_3CN)\cdot 3CH_3OH)$

Table A61 Crystal data and structure refinement for $[Tl(Re_2O_3)_2(L^a)_4](PF_6)\cdot 2CH_3CN\cdot 3CH_3OH$.

Empirical formula	$C_{75}H_{110}F_6N_{22}O_{17}PRe_4S_8Tl$	
Formula weight	2942.47	
Temperature	293(2) K	
Wavelength	0.71073 Å	
Crystal system	Monoclinic	
Space group	C2/c	
Unit cell dimensions	a = 25.816(2) Å	α = 90°
	b = 16.4122(7) Å	β = 91.183(5)°
	c = 24.215(1) Å	γ = 90°
Volume	10257.8(1) $Å^3$	
Z	4	
Density (calculated)	1.905 g/cm^3	
Absorption coefficient	6.527 mm^{-1}	
F(000)	5712	
Crystal description	block	
Crystal color	orange	
Crystal size	0.140 x 0.090 x 0.060 mm^3	
Theta range for data collection	3.37 to 29.23	
Index ranges	-35<=h<=35, -22<=k<=22, -33<=l<=32	
Reflections collected	40597	
Independent reflections	13790 [R(int) = 0.0715]	
Completeness to theta = 29.23°	99.1 %	
Absorption correction	Integration	
Max. and min. transmission	0.7231 and 0.4748	
Refinement method	Full-matrix least-squares on F^2	
Data / restraints / parameters	13790 / 2 / 612	
Goodness-of-fit on F^2	1.025	
Final R indices [I>2sigma(I)]	R1 = 0.0643, wR2 = 0.1626	
R indices (all data)	R1 = 0.0994, wR2 = 0.1803	
Largest diff. peak and hole	4.280 and -1.576 $e.Å^{-3}$	

Table A62 Atomic coordinates (x 10^4) and equivalent isotropic displacement parameters ($Å^2$x 10^3) for $[Tl(Re_2O_3)_2(L^a)_4](PF_6)\cdot 2CH_3CN\cdot 3CH_3OH$. U(eq) is defined as one third of the trace of the orthogonalized U^{ij} tensor.

	x	y	z	U(eq)
Tl(1)	2500	7500	5000	46(1)
O(1)	3651(3)	5451(4)	5818(3)	48(2)
Re(1)	3243(1)	5204(1)	5297(1)	34(1)
O(3)	2736(2)	5229(4)	4702(3)	39(1)
Re(2)	2252(1)	5261(1)	4102(1)	35(1)
O(2)	1808(3)	5516(5)	3608(3)	52(2)
S(1)	2952(1)	3964(1)	5626(1)	41(1)
C(2)	2450(3)	4171(5)	6102(4)	36(2)
N(3)	2325(3)	4901(5)	6322(3)	38(2)
C(4)	2444(3)	5625(5)	6142(4)	32(2)
O(5)	2663(2)	5879(4)	5712(3)	36(1)
N(6)	2207(3)	3536(5)	6294(4)	41(2)
C(7)	2320(4)	2684(5)	6152(4)	44(2)
C(8)	2002(5)	2405(7)	5657(5)	58(3)
C(9)	1779(4)	3635(6)	6690(5)	47(2)
C(10)	1969(5)	3619(8)	7285(5)	61(3)
S(11)	3822(1)	4475(1)	4776(1)	43(1)
C(12)	4147(4)	5150(5)	4339(4)	38(2)
N(13)	4065(3)	5957(4)	4266(3)	36(2)
C(14)	3762(3)	6447(5)	4554(4)	34(2)
O(15)	3459(2)	6336(4)	4936(3)	37(1)
N(16)	4512(3)	4838(5)	4030(4)	44(2)
C(17)	4661(4)	3951(6)	4068(5)	49(2)
C(18)	5081(6)	3814(9)	4521(7)	73(4)
C(19)	4797(4)	5328(7)	3637(5)	53(3)
C(20)	5245(5)	5786(10)	3916(6)	73(4)
S(21)	1878(1)	4044(2)	4371(1)	50(1)
C(22)	1367(4)	4276(6)	4809(5)	47(2)
N(23)	1284(4)	4973(5)	5089(4)	48(2)
C(24)	1507(4)	5687(6)	5016(4)	38(2)
O(25)	1822(2)	5950(4)	4671(3)	38(1)

N(26)	1030(4)	3677(6)	4893(5)	65(3)
C(27)	1076(6)	2870(8)	4621(6)	67(4)
C(28)	821(10)	2880(16)	4078(11)	150(1)
C(29)	605(6)	3798(11)	5302(12)	138(1)
C(30)	167(14)	3990(40)	5020(20)	340(4)
S(31)	2795(1)	4510(1)	3541(1)	48(1)
C(32)	3194(4)	5193(5)	3204(4)	37(2)
N(33)	3123(3)	6016(4)	3159(3)	36(2)
C(34)	2130(4)	8498(5)	6519(4)	35(2)
O(35)	2637(2)	6384(4)	3923(3)	39(1)
N(36)	3583(3)	4904(5)	2913(4)	43(2)
C(37)	3716(4)	4030(6)	2916(5)	51(3)
C(38)	3511(7)	3573(9)	2449(8)	90(5)
C(39)	3869(4)	5445(7)	2534(5)	49(2)
C(40)	3564(5)	5645(9)	2012(5)	63(3)
C(41)	3821(3)	7332(5)	4370(4)	34(2)
C(42)	4080(4)	7526(6)	3888(5)	48(2)
C(43)	4131(5)	8346(7)	3755(5)	55(3)
C(44)	3942(4)	8935(6)	4097(5)	50(3)
C(45)	1308(4)	6313(6)	5420(4)	41(2)
N(46)	3622(3)	7898(4)	4707(3)	33(2)
C(51)	2097(3)	7622(5)	6703(4)	37(2)
C(52)	1883(5)	7438(6)	7216(5)	53(3)
C(53)	1873(5)	6628(7)	7392(4)	53(3)
C(54)	2042(5)	6036(6)	7034(5)	53(3)
C(55)	2243(3)	6269(5)	6524(4)	37(2)
N(56)	2279(3)	7054(5)	6365(3)	37(2)
P(1)	5000	7468(2)	2500	30(1)
F(1)	5000	6449(9)	2500	125(6)
F(2)	5000	8373(8)	2500	131(7)
F(3)	5050(4)	7416(10)	3140(4)	125(5)
F(4)	4389(3)	7406(6)	2539(4)	89(3)
O(61)	3554(5)	2510(8)	1102(6)	91(3)
C(62)	4073(9)	2166(18)	1202(11)	230(2)
O(63)	5000	3510(30)	2500	190(2)
C(64)	5000	2590(30)	2500	340(7)
C(67)	5692(7)	64(13)	2534(16)	126(1)

C(68)	5653(9)	-218(19)	3138(10)	133(1)
N(66)	5734(9)	249(18)	2084(13)	170(1)

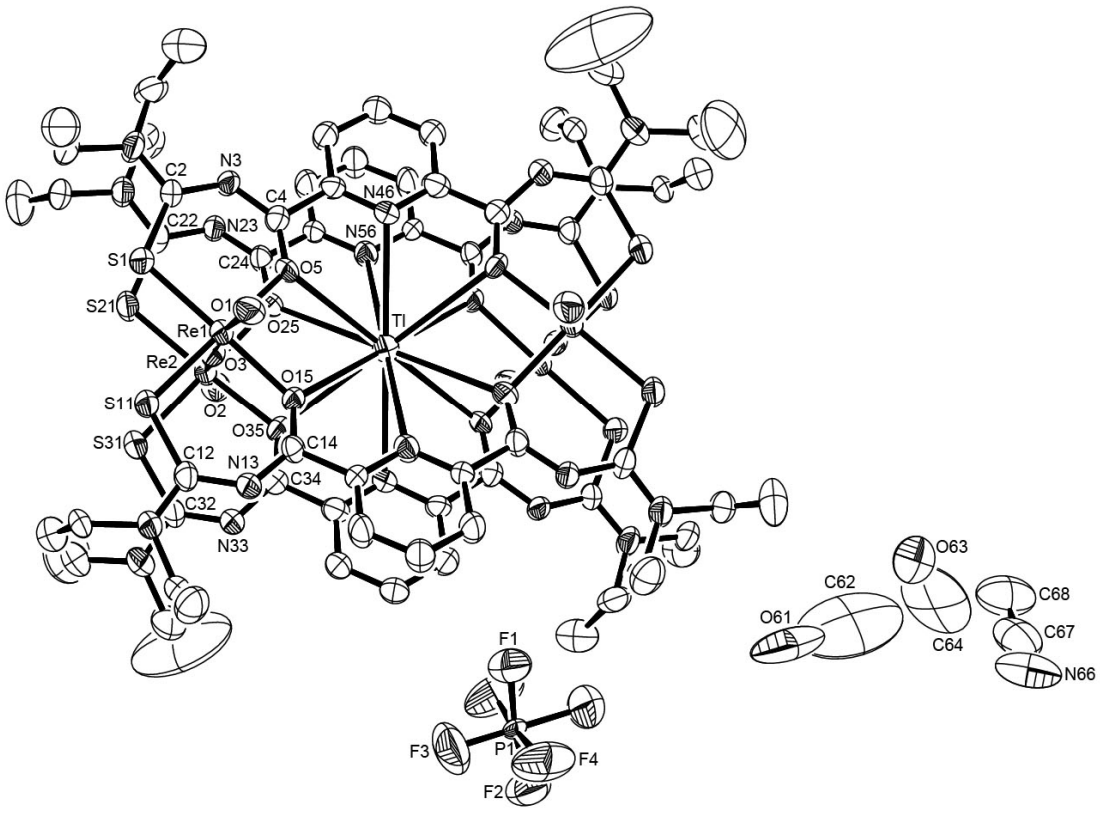

Fig A31 Ellipsoid plot (50% probability) of $[Tl(Re_2O_3)_2(L^a)_4](PF_6)\cdot 2CH_3CN\cdot 3CH_3OH$.

32) $[Na_2(H_2O)_2(Re_2O_3)_2(L^a)_4][B(C_6H_5)_4]_2 \cdot 2CH_2Cl_2$.

Table A63 Crystal data and structure refinement for $[Na_2(H_2O)_2(Re_2O_3)_2(L^a)_4][B(C_6H_5)_4]_2 \cdot 2CH_2Cl_2$.

Empirical formula	$C_{118}H_{136}B_2Cl_4N_{20}Na_2O_{16}Re_4S_8$	
Formula weight	3301.15	
Temperature	200(2) K	
Wavelength	0.71073 Å	
Crystal system	Triclinic	
Space group	$P\bar{1}$	
Unit cell dimensions	a = 12.085(1) Å	α = 98.75(1)°
	b = 16.078(1) Å	β = 99.47(1)°
	c = 18.882(1) Å	γ = 98.17(1)°
Volume	3523.7(4) $Å^3$	
Z	1	
Density (calculated)	1.556 g/cm^3	
Absorption coefficient	3.688 mm^{-1}	
F(000)	1640	
Crystal description	Block	
Crystal color	Red	
Crystal size	0.570 x 0.507 x 0.410 mm^3	
Theta range for data collection	3.34 to 29.24	
Index ranges	-16<=h<=16, -22<=k<=22, -25<=l<=24	
Reflections collected	37600	
Independent reflections	18836 [R(int) = 0.0705]	
Completeness to theta = 29.24°	98.2 %	
Absorption correction	Integration	
Max. and min. transmission	0.2960 and 0.1493	
Refinement method	Full-matrix least-squares on F^2	
Data / restraints / parameters	18836 / 4 / 813	
Goodness-of-fit on F^2	1.090	
Final R indices [I>2sigma(I)]	R1 = 0.0529, wR2 = 0.1485	
R indices (all data)	R1 = 0.0595, wR2 = 0.1536	
Largest diff. peak and hole	2.117 and -3.515 $e.Å^{-3}$	

Table A64 Atomic coordinates (x 10^4) and equivalent isotropic displacement parameters ($Å^2$x 10^3) for $[Na_2(H_2O)_2(Re_2O_3)_2(L^a)_4][B(C_6H_5)_4]_2 \cdot 2CH_2Cl_2$. U(eq) is defined as one third of the trace of the orthogonalized U^{ij} tensor.

	x	y	z	U(eq)
Na(1)	9266(3)	10102(2)	5130(1)	35(1)
O(4)	9266(3)	10102(2)	5130(1)	35(1)
O(5)	7677(9)	9592(5)	5199(5)	147(3)
Na(2)	7677(9)	9592(5)	5199(5)	147(3)
O(1)	7628(4)	7745(3)	4885(2)	43(1)
Re(1)	8885(1)	7577(1)	4645(1)	28(1)
O(3)	10396(3)	7748(2)	4456(2)	30(1)
Re(2)	11921(1)	7861(1)	4287(1)	29(1)
O(2)	13290(4)	8142(3)	4195(3)	53(1)
S(1)	8185(1)	6526(1)	3628(1)	35(1)
C(2)	8008(4)	7022(3)	2863(3)	30(1)
N(3)	7979(4)	7855(3)	2850(2)	33(1)
C(4)	8243(4)	8511(3)	3387(3)	30(1)
O(5)	8752(3)	8592(2)	4049(2)	33(1)
N(6)	7810(4)	6509(3)	2216(2)	33(1)
C(7)	7581(5)	6853(4)	1529(3)	40(1)
C(8)	8669(6)	7243(5)	1326(4)	51(1)
C(9)	7827(5)	5586(3)	2121(3)	39(1)
C(10)	6659(7)	5075(4)	2073(5)	61(2)
S(11)	9220(1)	6470(1)	5259(1)	35(1)
C(12)	10129(4)	6948(3)	6083(2)	28(1)
N(13)	10131(4)	7727(3)	6456(2)	34(1)
C(14)	9797(4)	8398(3)	6217(3)	30(1)
O(15)	9635(3)	8563(2)	5577(2)	32(1)
N(16)	10814(4)	6477(3)	6403(2)	32(1)
C(17)	10765(5)	5566(3)	6096(3)	35(1)
C(18)	9766(5)	4973(4)	6231(3)	42(1)
C(19)	11589(5)	6829(4)	7102(3)	40(1)
C(20)	11104(7)	6598(5)	7748(3)	54(2)
S(21)	11376(2)	6851(1)	3217(1)	43(1)
C(22)	11444(5)	7436(3)	2519(3)	32(1)

N(23)	8738(4)	11765(3)	7491(2)	34(1)
C(24)	8777(5)	11172(3)	6945(3)	31(1)
O(25)	8535(4)	11152(2)	6257(2)	38(1)
N(26)	11643(4)	7016(3)	1896(2)	33(1)
C(27)	11622(6)	7413(4)	1240(3)	41(1)
C(28)	12765(7)	7861(6)	1193(5)	66(2)
C(29)	11882(5)	6134(3)	1822(3)	37(1)
C(30)	10811(6)	5471(4)	1644(4)	48(1)
S(31)	12291(1)	6758(1)	4933(1)	38(1)
C(32)	13289(5)	7357(4)	5685(3)	39(1)
N(33)	13144(4)	8072(3)	6106(3)	37(1)
C(34)	7380(4)	11320(3)	4106(3)	32(1)
O(35)	7747(3)	11203(2)	4748(2)	33(1)
N(36)	14221(4)	7037(3)	5902(3)	42(1)
C(37)	15091(6)	7510(5)	6532(4)	56(2)
C(38)	15955(10)	8121(8)	6292(8)	100(4)
C(39)	14492(6)	6249(4)	5516(4)	51(2)
C(40)	13975(9)	5465(5)	5787(6)	75(2)
C(41)	9140(5)	10383(3)	7164(3)	32(1)
C(42)	9277(7)	10290(4)	7890(3)	46(2)
C(43)	9567(8)	9531(4)	8074(3)	53(2)
C(44)	9791(6)	8927(4)	7542(3)	43(1)
C(45)	9641(5)	9070(3)	6819(3)	31(1)
N(46)	9311(4)	9782(3)	6635(2)	31(1)
C(51)	7478(5)	10642(3)	3495(3)	32(1)
C(52)	7154(6)	10725(4)	2774(3)	45(1)
C(53)	7272(7)	10082(4)	2224(3)	52(2)
C(54)	7652(6)	9359(4)	2409(3)	43(1)
C(55)	7928(5)	9312(3)	3150(3)	32(1)
N(56)	7872(4)	9947(3)	3690(2)	31(1)
B(1)	7248(5)	6683(4)	8987(3)	36(1)
C(61)	8380(5)	7419(4)	9318(3)	39(1)
C(62)	9465(5)	7280(4)	9204(4)	47(1)
C(63)	10453(6)	7893(5)	9492(4)	57(2)
C(64)	10381(7)	8664(5)	9884(4)	62(2)
C(65)	9352(7)	8828(4)	9994(4)	58(2)
C(66)	8359(6)	8219(4)	9721(3)	46(1)

C(71)	7260(5)	5859(3)	9418(3)	36(1)
C(72)	6258(6)	5314(4)	9407(4)	50(1)
C(73)	6217(7)	4587(5)	9719(5)	58(2)
C(74)	7185(6)	4359(4)	10060(4)	49(1)
C(75)	8226(6)	4882(4)	10091(3)	46(1)
C(76)	8239(5)	5619(4)	9780(3)	41(1)
C(81)	7240(5)	6345(4)	8115(3)	39(1)
C(82)	7701(5)	6899(5)	7685(3)	48(1)
C(83)	7673(5)	6645(6)	6940(4)	54(2)
C(84)	7152(6)	5809(6)	6596(4)	63(2)
C(85)	6684(8)	5263(5)	7000(4)	63(2)
C(86)	6739(6)	5525(4)	7746(4)	49(1)
C(91)	6080(5)	7072(3)	9070(3)	38(1)
C(92)	5804(6)	7307(5)	9753(4)	51(1)
C(93)	4856(7)	7660(5)	9855(5)	61(2)
C(94)	4103(6)	7781(5)	9255(5)	64(2)
C(95)	4337(6)	7547(5)	8557(5)	61(2)
C(96)	5307(5)	7188(4)	8477(4)	47(1)
Cl(67)	4967(3)	6822(3)	2463(4)	87(2)
C(68)	5188(15)	7551(10)	3335(11)	180(2)
Cl(69)	5061(6)	8571(5)	3053(5)	129(3)
Cl(77)	3526(6)	9896(3)	257(5)	134(4)
C(78)	3510(16)	10525(9)	1093(9)	131(1)
Cl(79)	4105(7)	10305(4)	1913(6)	151(4)

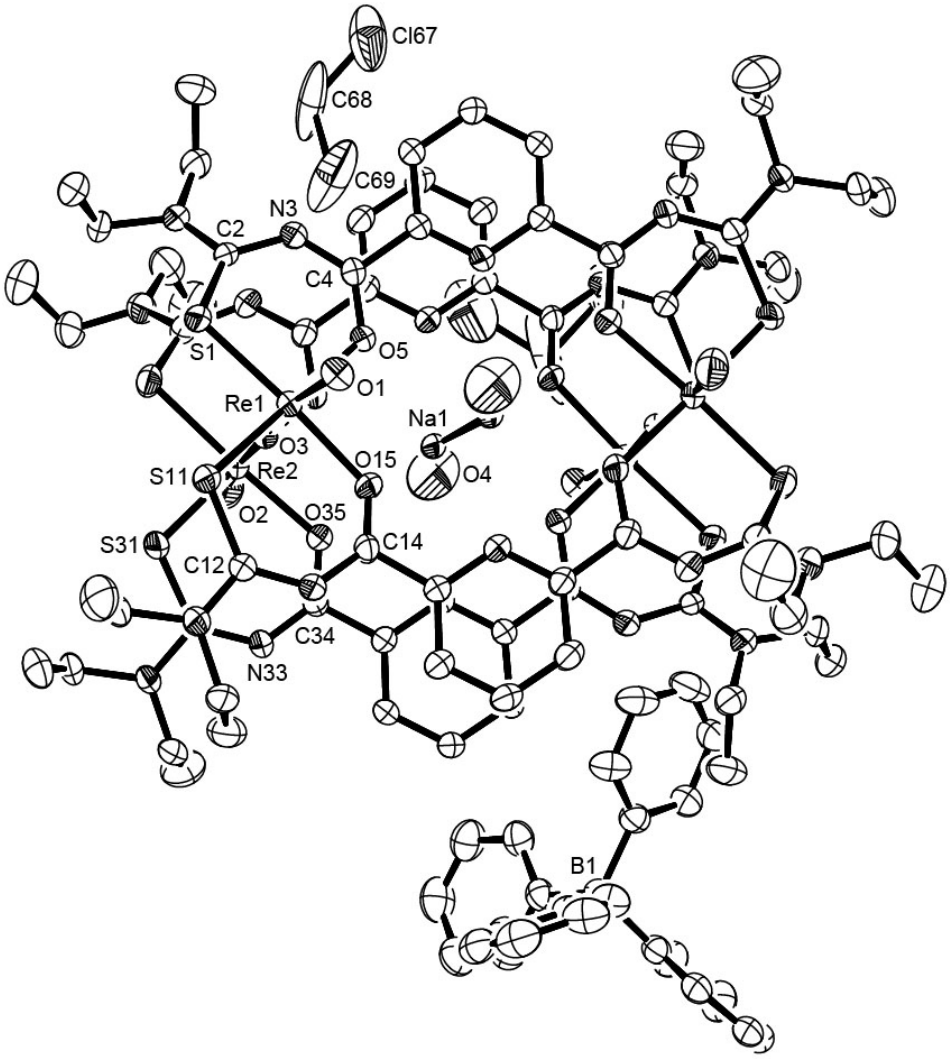

Fig A32 Ellipsoid plot (50% probability) of $[Na_2(H_2O)_2(Re_2O_3)_2(L^a)_4][B(C_6H_5)_4]_2 \cdot 2CH_2Cl_2$.

33) $[Na_2(H_2O)_2(Re_2O_3)_2(L^a)_4][B(C_6H_5)_4]_2$.

Table A65 Crystal data and structure refinement for $[Na_2(H_2O)_2(Re_2O_3)_2(L^a)_4][B(C_6H_5)_4]_2$.

Empirical formula	$C_{116}H_{132}B_2N_{20}Na_2O_{16}Re_4S_8$	
Formula weight	3131.30	
Temperature	200(2) K	
Wavelength	0.71073 Å	
Radiation	MoK	
Crystal system	Triclinic	
Space group	$P\bar{1}$	
Unit cell dimensions	a = 12.059(1) Å	α = 98.52(1)°
	b = 16.077(1) Å	β = 99.61(1)°
	c = 18.968(1) Å	γ = 98.28(1)°
Volume	3531.7(4) $Å^3$	
Z	1	
Density (calculated)	1.472 g/cm^3	
Absorption coefficient	3.603 mm^{-1}	
F(000)	1556	
Crystal description	Prism	
Crystal color	Red	
Crystal size	0.320 x 0.280 x 0.230 mm^3	
Theta range for data collection	3.29 to 29.36	
Index ranges	-16<=h<=16, -22<=k<=22, -25<=l<=20	
Reflections collected	39477	
Independent reflections	18928 [R(int) = 0.0758]	
Completeness to theta = 29.36°	97.4 %	
Absorption correction	Integration	
Max. and min. transmission	0.7124 and 0.5274	
Refinement method	Full-matrix least-squares on F^2	
Data / restraints / parameters	18928 / 0 / 757	
Goodness-of-fit on F^2	0.939	
Final R indices [I>2sigma(I)]	R1 = 0.0569, wR2 = 0.1335	
R indices (all data)	R1 = 0.1106, wR2 = 0.1534	
Largest diff. peak and hole	2.063 and -2.533 $e.Å^{-3}$	

Table A66 Atomic coordinates (x 10^4) and equivalent isotropic displacement parameters ($Å^2$x 10^3) for $[Na_2(H_2O)_2(Re_2O_3)_2(L^a)_4][B(C_6H_5)_4]_2$. U(eq) is defined as one third of the trace of the orthogonalized U^{ij} tensor.

	x	y	z	U(eq)
Na(1)	821(4)	9903(2)	4845(2)	35(1)
O(7)	821(4)	9903(2)	4845(2)	35(1)
O(8)	2240(5)	10382(3)	4812(2)	47(1)
Na(2)	2240(5)	10382(3)	4812(2)	47(1)
O(1)	3280(6)	8124(4)	4141(4)	54(2)
Re(1)	1940(1)	7857(1)	4262(1)	31(1)
O(6)	421(5)	7769(3)	4457(3)	34(1)
Re(3)	-1086(1)	7595(1)	4652(1)	30(1)
O(3)	2323(5)	12234(4)	5101(3)	43(1)
S(1)	2303(2)	6744(1)	4894(1)	42(1)
C(2)	3259(8)	7299(5)	5641(5)	40(2)
N(3)	3147(6)	8031(4)	6065(4)	40(2)
C(4)	2649(7)	8651(5)	5856(5)	33(2)
O(5)	2315(5)	8789(3)	5219(3)	37(1)
N(6)	4194(7)	6966(5)	5878(4)	46(2)
S(11)	1312(2)	6852(1)	3196(1)	48(1)
C(12)	1424(7)	7447(5)	2509(5)	35(2)
N(13)	1250(7)	8255(4)	2503(4)	40(2)
C(14)	1219(8)	8839(5)	3060(5)	35(2)
O(15)	1476(6)	8863(3)	3745(3)	40(1)
N(16)	1646(7)	7035(4)	1902(4)	45(2)
S(21)	-754(2)	6477(1)	5258(1)	37(1)
C(22)	154(7)	6952(5)	6089(4)	30(2)
N(23)	164(6)	7731(4)	6450(4)	37(2)
C(24)	-171(7)	8407(4)	6216(4)	32(2)
O(25)	-310(5)	8577(3)	5576(3)	34(1)
N(26)	835(6)	6479(4)	6406(4)	35(2)
S(31)	-1814(2)	6551(1)	3636(1)	38(1)
C(32)	-1989(7)	7057(5)	2882(5)	37(2)
N(33)	-2031(6)	7888(4)	2872(4)	38(2)
C(34)	-1772(7)	8541(5)	3411(4)	32(2)
O(35)	-1228(5)	8625(3)	4061(3)	35(1)

N(36)	-2189(6)	6555(4)	2239(4)	39(2)
C(41)	2558(7)	9337(5)	6471(5)	35(2)
C(45)	2098(7)	10653(5)	6816(4)	33(2)
N(46)	2145(6)	10021(4)	6284(4)	33(1)
C(51)	836(8)	9633(5)	2837(5)	38(2)
C(55)	333(8)	10937(5)	3181(5)	36(2)
N(56)	673(6)	10227(4)	3371(4)	31(1)
C(44)	2376(10)	10600(6)	7552(5)	51(3)
C(39)	-2441(9)	6906(6)	1548(5)	46(2)
C(29)	1626(8)	6826(5)	7108(5)	42(2)
C(42)	2901(9)	9248(5)	7194(5)	50(2)
C(37)	-2174(8)	5638(5)	2132(5)	45(2)
C(43)	2758(12)	9877(6)	7725(5)	67(4)
C(54)	177(10)	11090(6)	2471(5)	52(3)
C(52)	687(11)	9722(6)	2112(5)	57(3)
C(27)	793(8)	5568(5)	6099(5)	39(2)
C(53)	356(13)	10473(7)	1924(6)	75(4)
C(7)	4458(8)	6185(6)	5500(6)	50(2)
C(17)	1903(8)	6152(5)	1831(5)	43(2)
C(28)	-213(8)	4976(5)	6226(5)	43(2)
C(9)	5044(9)	7404(8)	6520(6)	61(3)
C(38)	-3323(10)	5112(6)	2086(7)	66(3)
C(30)	1145(10)	6579(7)	7739(6)	61(3)
C(19)	1662(13)	7436(7)	1261(6)	72(4)
C(40)	-1354(11)	7279(7)	1343(6)	64(3)
C(18)	853(10)	5501(6)	1647(6)	61(3)
C(20)	2790(15)	7866(11)	1213(10)	111(6)
C(8)	3937(11)	5405(7)	5738(7)	72(3)
C(10)	5962(14)	8022(9)	6337(10)	109(6)
C(81)	2719(8)	4154(5)	580(5)	41(2)
C(91)	1583(8)	2593(6)	691(5)	44(2)
C(92)	1602(10)	1793(6)	298(6)	55(2)
C(61)	2765(8)	3672(6)	1884(5)	43(2)
C(85)	1770(10)	5114(6)	-106(5)	55(3)
C(71)	3881(8)	2934(6)	939(6)	47(2)
C(86)	1732(8)	4379(6)	203(5)	46(2)
C(82)	3715(8)	4698(6)	579(6)	53(2)

C(63)	2317(8)	3425(8)	3053(6)	58(3)
C(84)	2795(10)	5629(6)	-80(6)	55(2)
C(64)	2860(10)	4246(9)	3391(6)	70(4)
C(83)	3746(10)	5411(7)	259(7)	64(3)
C(66)	3308(9)	4488(6)	2242(6)	53(2)
C(76)	4212(10)	2738(7)	268(6)	61(3)
C(96)	504(9)	2745(7)	804(6)	57(3)
B(1)	2729(9)	3336(6)	1024(6)	43(2)
C(62)	2273(9)	3153(8)	2321(6)	58(3)
C(72)	4631(9)	2772(7)	1519(7)	62(3)
C(95)	-469(10)	2127(7)	531(7)	64(3)
C(65)	3347(12)	4759(8)	2985(7)	72(3)
C(93)	613(12)	1190(7)	29(6)	66(3)
C(94)	-420(12)	1375(8)	136(7)	71(3)
C(75)	5134(12)	2383(8)	170(7)	75(3)
C(73)	5614(11)	2419(9)	1427(9)	81(4)
C(74)	5865(10)	2220(8)	768(9)	75(4)

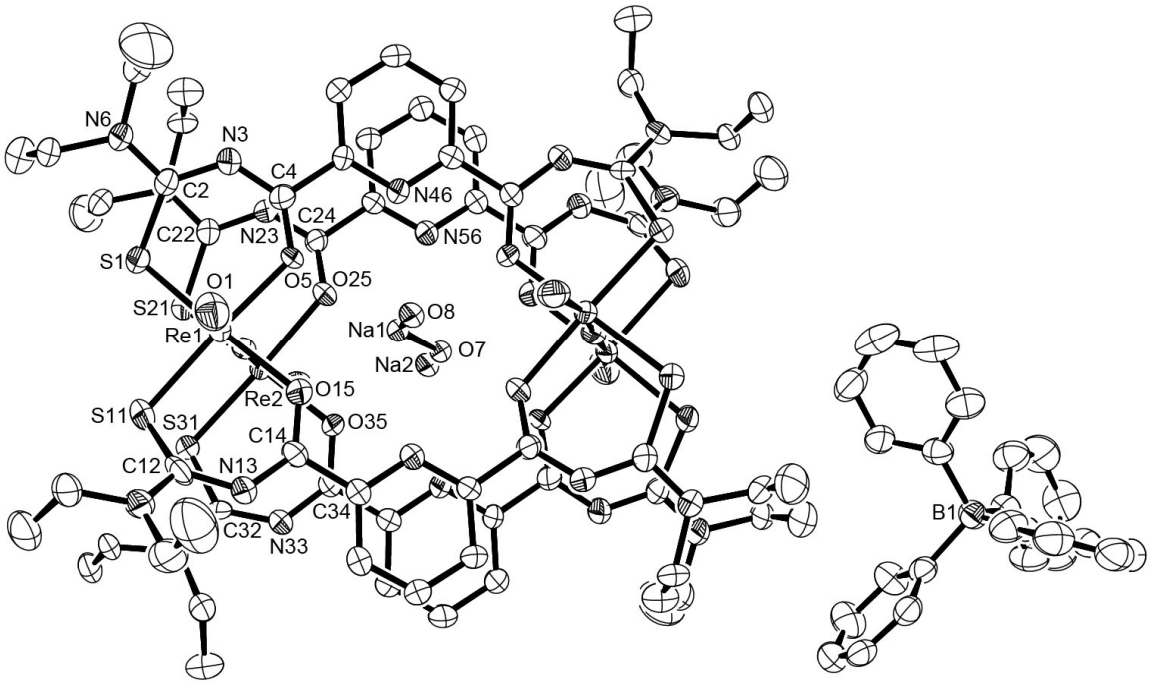

Fig A33 Ellipsoid plot (50% probability) of $[Na_2(H_2O)_2(Re_2O_3)_2(L^a)_4][B(C_6H_5)_4]_2$.